DISSERTATION

ALTERATION OF DIFFERENTIATION AND GROWTH OF NORMAL HUMAN EPIDERMAL KERATINOCYTES BY BENZO[*A*]PYRENE AND ARSENIC

Submitted by

Damon Scott Perez

Department of Environmental and Radiological Health Sciences

In partial fulfillment of the requirements
For the Degree of Doctor of Philosophy
Colorado State University
Fort Collins, Colorado
Spring 2005

COLORADO STATE UNIVERSITY

December 14th, 2004

WE HEREBY RECOMMEND THAT THE DISSERTATION PREPARED UNDER OUR SUPERVISION BY DAMON SCOTT PEREZ ENTITLED ALTERATION OF DIFFERENTIATION AND GROWTH OF NORMAL HUMAN EPIDERMAL KERATINOCYTES BY BENZO[A]PYRENE AND ARSENIC BE ACCEPTED AS FULFULLING IN PART REQUIREMENTS FOR THE DEGREE OF DOCTOR OF PHILOSOPHY

Committee on Graduate Work

_____

_____

_____

_____

_____
Co-Advisor

_____
Advisor

_____
Department Head

ABSTRACT OF DISSERTATION

ALTERATION OF DIFFERENTIATION AND GROWTH OF NORMAL HUMAN EPIDERMAL KERATINOCYTES BY BENZO[*A*]PYRENE AND ARSENIC

Normal human epidermal keratinocytes (NHEK) were chosen as an *in vitro* model for mechanistic studies into how altered regulation of differentiation may play a role in the malignant transformation process in human cells. Initially, the cytotoxicity of four petroleum-derived hydrocarbons [benzo[*a*]pyrene (BaP), carbazole, dibenzothiophene, and isoquinoline] was investigated using the MTT assay; however, the research direction changed to focusing on examining the cellular effects, in NHEK, of BaP, the most toxic and carcinogenic polycyclic aromatic hydrocarbon among the four, and arsenic, another high priority skin carcinogen. This work demonstrates that BaP and arsenic inhibit terminal differentiation in NHEK. Arsenic also decreases proliferation in a manner suggestive of a G2 block. In contrast, BaP increases proliferation rates and induces rapid progression through the cell cycle, possibly by a shortened G2 phase. Differentiation is more sensitive to chemically-mediated perturbations than is proliferation, indicating that the former process may be the initial target at environmentally prevalent concentrations. To identify molecular alterations that are responsible for the observed chemical-specific effects, microarray analysis was carried out on NHEK treated with each carcinogen. From this analysis, BaP and arsenic altered 103 and 122 genes respectively. More sensitive real-time PCR revealed that BaP-treatment perturbed the expression of genes involved in cellular differentiation and growth. Altered genes include; α-integrin binding

protein-63, interleukin-1α, interleukin-1β, Ras guanyl releasing protein-1, retinoic acid- and interferon-inducible protein, and YY1-associated factor-2. Arsenic altered the expression of genes involved in cell cycle checkpoint regulation. These genes include; MAX binding protein, RAD50, retinoblastoma-1, retinoblastoma-binding protein-1, and transforming growth factor β-stimulated protein. Gene expression results suggest that BaP and arsenic target different steps in the pathways to growth and differentiation in this cell type and provide mechanistic clues as to how these chemicals favor transformation in target cells. Moreover, a quantitative biologically-based computer model of NHEK was developed providing an *in silico* experimental platform with which one can test chemical-mediated effects on cell cycle kinetics and differentiation. A clearer understanding of cellular growth and differentiation, both from a normal standpoint and from alterations induced by chemical exposure, will greatly aid the risk assessment process for environmental contaminants.

Damon Scott Perez
Environmental and Radiological Health Science Department
Colorado State University
Fort Collins, CO 80523
Spring 2005

ACKNOWLEGDEMENTS

I would like to thank my advisors Drs. Julie Campain and Raymond Yang for providing me the unique opportunity to work on a research project in which I gained invaluable scientific experience utilizing various experimental techniques and technologies. I also thank my advisors and members of my committee (Drs. Michael Fox, Rajinder Ranu, and Marie Legare) for their support and guidance during my time at the Center for Environmental Toxicology and Technology at Colorado State University.

In addition, I wish to thank all the graduate students, post-doctoral fellows, and laboratory technicians I have worked with over the years. Specifically, I would like to thank Dr. Dong-Soon Bae for her guidance and instruction which aided me in my experimental research. I also cherish the close friendships I have developed with Drs. Ivan Dobrev, Ty Higuchi, and Ken Liao. If I didn't attend graduate school at Colorado State University, I would have never met such wonderful, genuine people.

DEDICATION

I dedicate this work to my loving parents, Gilbert and Myra Perez, and to my brother and best friend, Darryl Perez. They have been my support, motivation, and joy during graduate school and throughout my entire life. The ones whose company I enjoy, laugh with, and love.

TABLE OF CONTENTS

Chapter 1

Introduction

1.1. Goals and Specific Aims

The overall objective of studies in our laboratory is development of predictive tools for detecting potentially carcinogenic chemicals and chemical mixtures. Toward this end, normal human epidermal keratinocytes (NHEK) have been chosen as an *in vitro* model for mechanistic studies into how altered regulation of differentiation may play a role in the transformation process in human cells. The epidermis is characterized by a highly regulated balance between epithelial cell growth and squamous differentiation. Although the exact mechanisms involved have not been completely elucidated, an imbalance between two such important and opposing processes has been strongly linked to the onset of carcinogenesis in this cell type. The studies described in this dissertation are aimed at developing a mechanistic understanding of how two diverse skin carcinogens may alter the normal balance between growth and differentiation such that they favor malignant transformation. Through this work, I will also clarify whether signaling pathways involved in keratinocyte differentiation and proliferation are disrupted by different carcinogens or whether only chemical-specific effects are evident. **My hypothesis is that dermal carcinogens interfere with cellular differentiation and growth through dysregulation of controlling signal transduction pathways for terminal differentiation and cell proliferation.** It is my belief that integrating cell and

molecular biology information with computational modeling will improve our understanding of keratinocyte growth and differentiation, and help predict chemically-induced cell kinetic changes due to carcinogen exposure. Developing a quantitative biologically-based computer model for the differentiation of human keratinocytes will provide an *in silico* experimental platform which may test this hypothesis much more efficiently. The effects of chemical exposures may then be simulated as perturbations of critical biological processes in an otherwise normal state.

My hypothesis will be tested in the following **Specific Aims**:

- **Aim 1.** To characterize the time- and dose-dependent effects of two mechanistically diverse skin carcinogens, benzo[*a*]pyrene (BaP) and arsenic, on growth rate, cell cycle distribution, and squamous differentiation in human keratinocytes.
- **Aim 2.** To select chemically-altered genes which, based upon their known or putative function, are involved in the switch between growth and differentiation in keratinocytes.
- **Aim 3.** To develop, and refine a biologically-based computer model for the process of squamous differentiation using the data in the literature and from Aims 1 and 2.

1.2. Overview

In the research presented herein, I will present how BaP and arsenic, through altered NHEK differentiation and proliferation, produce conditions that support cellular transformation. To better understand the process of cellular transformation, the Literature Review in Chapter 2 provides essential background information regarding the importance

of maintaining proper balance between cell growth and squamous differentiation in the skin. Also discussed is the linkage between phenotypic changes in keratinocytes and initiation of cell transformation that eventually lead to the onset of cancer. Relevant information concerning the chemicals of interest is presented along with their effects in skin as demonstrated in previously published work. To accomplish my goals and approach the Specific Aims listed above, these studies were organized in the following way: (1) Perform cytotoxicity studies, (2) examine chemically-induced phenotypic alterations (i.e. alterations in NHEK growth and differentiation), (3) Attempt to correlate gene expression alterations to the chemically-altered phenotype(s), and (4) construct a mathematical model to aid in understanding NHEK cell cycle kinetics and cellular differentiation perturbations induced by chemical exposure.

Cytotoxicity studies on four petroleum-derived hydrocarbons in NHEK (Chapter 3) were conducted to gather critical data for selecting reasonable concentrations to use in later studies examining chemical effects on NHEK differentiation, proliferation, and gene expression. Rather than continuing experimentation on each hydrocarbon, the research focus switched to specifically investigate the effects of the most cytotoxic hydrocarbon, BaP, and a commonly known skin carcinogen, arsenic, on NHEK differentiation and proliferation. Phenotypic changes produced due to chemical exposure were examined and is explained in detail throughout Chapter 4. More specifically, BaP- and arsenic-induced alterations of NHEK morphology, differentiation, cell cycle distribution, and potential doubling time were investigated. Subsequently, gene expression analyses under different chemical exposure scenarios were completed and documented in Chapter 5. In this chapter, the mechanisms and/or pathways that may have been involved in the chemically-

induced changes of growth and differentiation observed in Chapter 4 were examined. In the end, two mathematical models were constructed that illustrate keratinocyte behavior in terms of cell cycle kinetics and differentiation abilities (Chapter 6). The NHEK models used flow cytometry results displayed in Chapter 4 and other essential parameters from the literature as explained in detail throughout Chapter 6. Lastly, Chapter 7 explains the significance of this body of work and what conclusions are deduced from the resulting data. Also in this chapter, I will discuss future studies that could potentially branch off from many points within these experiments. Taken together, my results give a better understanding of how carcinogens modulate keratinocyte growth and squamous differentiation in NHEK and the molecular mechanism(s) behind their effects.

Chapter 2

Literature Review: The Relationship between Altered Keratinocyte Differentiation and Cancer

2.1. The Differentiation Process in the Epidermis

All mammals are continually challenged by a variety of environmental hazards, and the first line of protection is provided by the epidermis. The mammalian epidermis is a highly organized tissue that forms an essential barrier between the organism and the surrounding environment. This protective function arises from finely regulated proliferation and differentiation processes. The integumentary system consists of the skin, sweat glands, oil glands, hair, and nails. The skin itself is made up of two layers, which are the epidermis and the dermis. Some consider the layer just below the skin, the hypodermis (subcutaneous layer or superficial fascia), as a third skin layer; however, this region is not technically part of the integumentary system. The studies presented within this dissertation utilized an *in vitro* keratinocyte model system which is representative of the outer most layer of the skin, the epidermis. Keratinocytes comprise approximately 95% of the cells in the epidermis (Eckert 1989; Green 1977; Green *et al.* 1982). Other major cell types which reside in the epidermis are melanocytes, Langerhans' cells, and Merkel cells.

The epidermis has a thickness which varies from 0.075-0.15 mm over the body to 0.8 mm on the palms of the hands and 1.4 mm on the soles of the feet (Plewig 1970). The epidermis itself is divided into five layers, which are, from the inner to the outer most, the stratum basale or stratum germinativum (basal), stratum spinosum (spinous), stratum granulosum (granular), stratum lucidum (only found in thickened areas of the epidermis), and the stratum corneum (cornified) (Figure 2.1). Keratinocyte differentiation is a process whereby a relatively undifferentiated keratinocyte is converted into a fully mature keratinocyte termed a corneocyte. Only the deepest or inner-most basal layer of the epidermis has the capacity for DNA synthesis and mitosis (Fuchs 1993). This layer provides a continuous supply of cells that repopulate the epidermis (Lavker *et al.* 1993; Yang *et al.* 1993). Cell regeneration is thought to be achieved by a hierarchy of proliferative cells within the basal layer consisting of stem cells and transit-amplifying cells (Lajtha 1979).

In the early stages of epidermal differentiation, basal cells detach from the basement membrane and migrate to suprabasal layers, where they progress through an intricate series of stage-specific morphological and biochemical changes. The spinous layer, the second epidermal cell layer is characterized by dense desmosomes. Early markers of keratinocyte differentiation, including involucrin, and transglutaminase 1, are first expressed in this layer and becomes more prominent in the granular layer (Holbrook and Wolff 1987). The next layer, the stratum granulosum, is rich in granules. These granules contain products of keratinocyte differentiation that are used to assemble various terminal keratinocyte structures, including the corneocyte cornified envelope (Elias *et al.* 1988; Steven *et al.* 1990; Takahashi *et al.* 1992). The stratum lucidum is considered the

'transition zone' and is the layer that separates the dead from living epidermal layers. This is a region of systematic destruction of cellular organelles and nucleic acids that coincides with assembly of the keratin intermediate filament bundles and the cornified envelope. These cornified cells are the terminal product of keratinocyte differentiation. Corneocytes are dead, flattened polyhedron-shaped cells that occupy the stratum corneum and are uniquely adapted to provide a protective surface.

Corneocytes consist of a stabilized array of keratin filaments contained within a covalently cross-linked protein envelope (Matoltsy and Matoltsy 1966). Keratin intermediate filament bundles course through their interior and connect at various points to the surrounding marginal band (i.e., the cornified envelope). The marginal band is a thick band that forms beneath the inner leaflet of the plasma membrane and is composed of a variety of proteins that are covalently connected by ε-(γ-glutamyl)lysine protein-protein crosslinks (Holbrook and Wolff 1987; Rice and Green 1977). These crosslinks are formed by the enzyme transglutaminase (Abernethy *et al.* 1977; Polakowska *et al.* 1991; Thacher and Rice 1985). Adjacent corneocytes are held together by modified desmosomes and by an interlocking system of ridges and grooves (Holbrook and Wolff 1987). The composite of billions of terminal keratinocytes (cornified envelopes) forms the protective layer on top of the epidermal surface; the dead cells that make up this layer eventually slough off into the environment. A typical cornified envelope is 12.0 μm in diameter and is chemically resistant to boiling detergents, chaotrophic salts, and reducing agents (Matoltsy and Matoltsy 1966; Sun and Green 1976). This chemical resistance is due to the presence of isodipeptide bonds, i.e., ε-(γ-glutamyl)lysine (Figure 2.2).

Turnover time for the corneocyte compartment has been determined to be 14 days in humans (Bergstresser and Taylor 1977). The average time required for a newly differentiated basal cell to become a corneocyte is 31 days (Bergstresser and Taylor 1977). Thus, according to these results, the entire epidermal differentiation process takes an average of 45 days. A more recent study confirmed these results with a calculated epidermal turnover rate of 47 or 48 days (Iizuka 1994).

2.2. Regulation of Keratinocyte Differentiation

The transition from basal cell to corneocyte is a complex process that requires the simultaneous activation and inactivation of a wide variety of proteins and genes. In order for differentiation to produce a normal epidermal surface, these genes must be expressed at the correct time and location. A major goal of keratinocyte- and/or skin-related research is to identify the mechanisms that regulate this complex process.

2.2.1. Differentiation Markers

The cytokeratins, cornified envelope precursor proteins, and transglutaminase are useful markers of gene expression in keratinocytes, both *in vitro* and *in vivo* (Fuchs 1990; Rice and Green 1977; Stoler *et al.* 1988; Yuspa 1994). The cytokeratins are a family of over thirty proteins that are assembled to form the intermediate filaments in epithelial cells (Steinert *et al.* 1985). Based on sequence homology and expression pattern, the keratins can be divided into acidic and neutral-basic families (Albers and Fuchs 1992; Steinert *et al.* 1985; Woodcock-Mitchell *et al.* 1982). Keratins are expressed in pairs to assure the presence of a neutral-basic and acidic partner to permit filament assembly (Woodcock-Mitchell *et al.* 1982). Specifically in the epidermis, cytokeratins 5 (K5) and

14 (K14) are expressed in the basal cells and form an intermediate filament network that is suitable for cells that are proliferating (Fuchs and Green 1980). In contrast, cytokeratins 1 (K1) and 10 (K10) are expressed in suprabasal cells (Woodcock-Mitchell *et al.* 1982). These keratins are involved in the formation of the intermediate filament bundles that are present in differentiating keratinocytes (Aebi *et al.* 1983). The keratin bundles are stabilized by disulfide bonds and occupy the interior volume of the cytoplasm in terminally differentiated cells (Aebi *et al.* 1983). These bundles provide structural stability to the corneocyte. Profilaggrin, the precursor of filaggrin, is expressed in the suprabasal layers and is converted to filaggrin, which packages the keratin filaments into fibrils (Takahashi *et al.* 1992).

Involucrin and loricrin are envelope precursor proteins that are expressed in the epidermal suprabasal layers (Hohl *et al.* 1991; Mehrel *et al.* 1990; Rice and Green 1977; Takahashi *et al.* 1992; Thacher and Rice 1985). These proteins are crosslinked to form the cornified envelope by the enzyme transglutaminase which catalyzes the formation of inter-protein ε-(γ-glutamyl)lysine bonds. Thus the cornified envelope is a structure comprised of covalently crosslinked proteins that is assembled beneath the deteriorating plasma membrane during the final stages of keratinocyte differentiation.

2.2.2. The Switch between Growth and Differentiation in Keratinocytes

The onset of keratinocyte differentiation can be triggered by several distinct signals. These signals include activation of: (1) an extracellular Ca^{2+} receptor mechanism, (2) increase in cell-cell adhesions, and (3) detachment from the substratum (Dotto 1999).

Compartmentalization and differential expression of signaling molecules in the skin and cultured keratinocytes have provided clues to the regulatory pathways which are

involved during epidermal differentiation. Mouse and human basal keratinocytes with a high growth fraction can be cultured in medium with a calcium (Ca^{2+}) concentration of 0.05 mM or less, whereas media with 0.1 mM Ca^{2+} has been shown to induce terminal differentiation (Boyce and Ham 1983; Hawley-Nelson *et al.* 1980; Hennings *et al.* 1980a; Hennings *et al.* 1980b; Shipley and Pittelkow 1987). These findings have facilitated the analysis of the regulation of keratinocyte growth and differentiation. In culture, Ca^{2+}-induced maturing keratinocytes cease proliferation, stratify, express the suprabasal markers of differentiation, activate transglutaminase, cornify, and slough (desquamate) as a sheet of matured squames (Hennings *et al.* 1980b; Yuspa *et al.* 1989). As seen *in vitro*, a key regulator for keratinocyte maturation *in vivo* is a gradient of extracellular Ca^{2+} across the epidermis that is low in the basal compartment and increases in concentration within each outer epidermal layer (Elias *et al.* 1998; Malmquist *et al.* 1984; Menon *et al.* 1985). The binding of Ca^{2+} and/or other divalent or trivalent cations to transmembrane Ca^{2+} receptors initiates downstream signaling pathways which include phospholipase C (PLC) activation and increased intracellular Ca^{2+} (Filvaroff *et al.* 1994; McNeil *et al.* 1998; Xie and Bikle 1999). 1-α,25dihydroxy vitamin D3 ($1,25(OH)_2D$) also promotes differentiation, by inducing involucrin and transglutaminase expression, via many of the same pathways as Ca^{2+}, although in the absence of Ca^{2+} $1,25(OH)_2D$ stimulated differentiation is not as complete (Bikle and Pillai 1993; Bikle *et al.* 2003; Gibson *et al.* 1996; Hosomi *et al.* 1983; Johansen *et al.* 2000; Su *et al.* 1994). An opposing vitamin A gradient may also contribute to the regulation of keratinocyte gene expression and differentiation (Regnier and Darmon 1991).

Ca^{2+} has also been shown to trigger keratinocyte differentiation through a more indirect mechanism, such as by promoting close cell-cell adhesion. One of the earliest, and most important, changes associated with Ca^{2+}-induced differentiation is the establishment of close intercellular contacts, through adherens junctions and desmosome formation (Lewis *et al.* 1994; O'Keefe *et al.* 1987). Cadherin-mediated adherens junctions may play a role in cell signaling events associated with growth and differentiation. Moreover, transmembrane tyrosine kinase receptors, src kinase family members, cell-surface tyrosine phosphatases, and protein kinase C (PKC) family members have all been found to be associated with specific adherens junction components and/or to be present at the adherens junction (Fagotto and Gumbiner 1996).

The addition of Ca^{2+} to cultured keratinocytes induces stratification (i.e. sliding of cells over each other with a simultaneous loss of adhesion to the substrate) (Calautti *et al.* 1995). Induced detachment of keratinocytes from the matrix is associated with the induction of biochemical markers of differentiation, as well as growth arrest (Di Cunto *et al.* 1998; Li *et al.* 1996; Watt *et al.* 1988). Keratinocyte attachment to the underlying extracellular matrix is mediated by integrin based structures, and these structures are thought to function as important signaling centers controlling the switch among keratinocyte growth, differentiation, and apoptosis (Frisch and Ruoslahti 1997; Giancotti 1997). The down regulation of integrin expression parallels that of increasing Ca^{2+} concentrations in keratinocytes (Tennenbaum *et al.* 1996). Studies have demonstrated that attachment via the $\alpha_4\beta_6$ integrin receptor (found only in basal layers) may serve as a positive determinant of keratinocyte proliferation, while the loss of $\alpha_4\beta_6$ and $\alpha_3\beta_1$ integrin receptor (involved in focal contacts) attachment may trigger signaling events contributing

to differentiation (Alt *et al.* 2001; Fuchs *et al.* 1997; Levy *et al.* 2000; Tennenbaum *et al.* 1996). These events may be controlled by Ras and MAPK-dependent pathways (Mainiero *et al.* 1997).

2.2.3. Intermediate Pathways involved in Keratinocyte Differentiation

PLC- and PKC-dependent pathways, as well as induction of tyrosine phosphorylation, play an important role in the switch between growth and differentiation. Intracellular PLC activation has been reported to occur within 30 seconds to one minute after Ca^{2+} treatment, in association with a very early increase in intracellular Ca^{2+} concentrations (Jaken and Yuspa 1988; Tang *et al.* 1988). Direct functional studies indicate that both PLC-γ activation and a rise in free intracellular Ca^{2+} are required for late aspects of keratinocyte differentiation (Li *et al.* 1995; Xie and Bikle 1999). Phosphatidyl inositol bis phosphate (PIP_2) breakdown results in inositol 1,4,5-triphosphate (IP_3) production, which in turn triggers the increase in free intracellular Ca^{2+} by mobilization from intracellular stores. Diacylglycerol (DAG), the other product of PIP_2 break-down, is also increased at very early stages following Ca^{2+} treatment (Jaken and Yuspa 1988). DAG is known to directly activate PKC. Among the 11 PKC isoforms, PKC-α, -δ, and -ε are activated upon Ca^{2+}-induced differentiation (Alt *et al.* 2001; Denning *et al.* 1995a; Denning *et al.* 1995b; Yang *et al.* 2003). Down regulation of these same isoforms are associated with decreased induction of late keratinocyte differentiation markers such as loricrin, filaggrin, and small proline rich protein (SPR-1) (Stanwell *et al.* 1996; Tesfagaigzi and Carlson 1999). Studies also show the possible involvement of other PKC isoforms (η, and ζ) in keratinocyte differentiation (Kashiwagi *et al.* 2002; Kashiwagi *et al.* 2000; Ohba *et al.* 1998; Osada *et al.* 1993; Osada *et al.* 1990).

The induction of tyrosine phosphorylation occurs as an early and specific event in keratinocyte differentiation in response to Ca^{2+} (Filvaroff *et al.* 1994; Filvaroff *et al.* 1990). Tyrosine phosphorylation of p62, and other similar proteins, causes the protein to associate with Ras-GTPase Activating Protein (Ras-GAP) in response to increased intracellular Ca^{2+}, thus inhibiting the activation of Ras-GRP (Filvaroff *et al.* 1992). In keratinocytes, p62 tyrosine phosphorylation is induced specifically in response to increased extracellular Ca^{2+} (Filvaroff *et al.* 1992; Filvaroff *et al.* 1994). It has been suggested that tyrosine phosphorylation may serve as a negative feedback mechanism to inactivate PKC-δ during late stages of differentiation (Denning *et al.* 1996). The tyrosine kinase, Fyn, is activated a few hours after Ca^{2+}-induced differentiation and may be responsible for several phosphorylating events (Calautti *et al.* 1995). Also, essential adherens junction components such as β-catenin, γ-catenin/plakoglobin, and p120-Cas (binds to E-cadherin) all become tyrosine phosphorylated by Fyn in cultured mouse keratinocytes within nine hours of Ca^{2+} treatment (Calautti *et al.* 1998). Interestingly, adherens junction formation has been recently reported to depend on a second signaling pathway involving the Rho and Rac GTPases, which control actin/cytoskeleton organization and cell motility (Braga *et al.* 1997).

2.2.4. Transcription and Cell Cycle Regulation of Keratinocyte Differentiation

There are distinct signaling pathways connected with transcription and cell-cycle control in keratinocyte differentiation. Evidence indicates that the two signaling pathways triggered by increased extracellular Ca^{2+} remain distinct even at the nuclear level. One of these pathways is specifically initiated by increased extracellular Ca^{2+}, leading to p62

tyrosine phosphorylation and, further downstream, to $p21^{WAF1}$ promoter activation (Missero *et al.* 1995; Prowse *et al.* 1997). Cyclin-dependent kinase inhibitor $p21^{WAF1}$ generally plays a role in the inhibition of cell growth and its expression is typically increased in post-mitotic cells immediately adjacent to the proliferative compartment (Di Cunto *et al.* 1998). Guanine and cytosine binding factors (GC rich repeats) such as Sp3, as well as the transcriptional co-activator p300, appear to be involved (Ogryzko *et al.* 1996; Prowse *et al.* 1997). Tyrosine phosphorylation is a critical step in the activation of the signal transducters and activators of transcription (STAT) family of transcription factors, which regulate inducibility of the *p21* promoter in response to epidermal growth factor (EGF) and interferon-γ (IFNγ) (Hauser *et al.* 1998; Look *et al.* 1995). The myc family has also been shown to be implicated in the control of keratinocyte growth and differentiation (Gandarillas *et al.* 2000; Gandarillas and Watt 1997; Hurlin *et al.* 1995; Pelengaris *et al.* 1999; Vastrik *et al.* 1995). Other key regulatory factors which could bind to the *p21* promoter and with which Sp3 may interact include E2F family members (Hiyama *et al.* 1997). In addition, studies also indicate E2F-1 promotes the expression of keratinocyte proliferation-specific marker genes and suppresses differentiation-specific marker genes (Dicker *et al.* 2000; Paramio *et al.* 2000a).

The other pathway that is activated in response to Ca^{2+} leads to PKC and Fyn activation, AP-1 factor modulation, and differentiation marker expression (Eckert *et al.* 1997; Rossi *et al.* 1998; Rutberg *et al.* 1996; Rutberg *et al.* 1997; Whitmarsh and Davis 1996). The product of the *Whn* gene functions as a specific suppressor of this pathway (repressing involucrin and transglutaminase), while it does not affect the pathway leading to *p21* promoter activation (Brissette *et al.* 1996; Jessen *et al.* 2000). Several other

transcription factors, such as those in the NF-κB/rel family (induced by PKC activation), as well as nuclear hormone receptors, are likely to play an important role in the balance between keratinocyte growth and differentiation (Hu *et al.* 2001; Li *et al.* 2000; Nehls *et al.* 1996; Qin *et al.* 1999; Seitz *et al.* 1998). Unfortunately, the interconnections between activation of these factors and the specific signaling pathways involved in keratinocyte differentiation remain to be established. Other signaling pathways and/or genes not mentioned here are also involved in the regulation of keratinocyte differentiation, however, this literature review focused on the most highly characterized pathways and signals which are thought to control this cellular process. Figure 2.3 depicts numerous factors and genes involved in regulating the switch between differentiation and proliferation in keratinocytes.

2.3. Altered Differentiation and Cancer in the Skin

2.3.1. The Carcinogenesis Process

Cancer can be characterized as uncontrolled cell growth which eventually leads to tumor formation. Cancer may develop due to the disruption of the normally well-controlled balance between cell division, death, and differentiation in living organisms. Ultimately cancer is a disease of abnormal gene expression which can occur through direct DNA insults (gene mutations, translocations, or amplifications) and abnormal gene transcription or translation. The process of carcinogenesis can be divided into three stages: initiation, promotion, and progression. Initiation is an irreversible stage involving a permanent heritable change in gene expression caused by direct DNA damage (somatic mutations) or epigenic events. Promotion is a reversible stage that requires multiple and

frequent exposures over a substantial period of time. Within the promotion stage there are two operational stages, conversion and propagation. Conversion is a limiting step which allows cells to override local growth restraints or proliferative latency. Propagation is characterized by chronic mitogenic stimulation during which time initiated cell populations expand. Finally, progression is an irreversible stage that is characterized by gross structural changes to chromosomes and genetic instability. Most chemicals work at distinct stages in this process and, therefore, must combine with other chemicals or other types of carcinogens to induce the development of malignant tumors. There are chemicals that, at high enough concentrations and/or prolonged exposures, can cause cancer by themselves, and are termed complete carcinogens. For example, BaP has been termed a complete carcinogen as shown in previous rodent skin research (Ashurst *et al.* 1983; Iskander *et al.* 2004; Jensen *et al.* 1993).

Somatic mutations leading to uncontrolled growth of cancer may be categorized as affecting two classes of genes: proto-oncogenes and tumor suppressor genes. Proto-oncogenes, such as *ras* and *myc*, encode proteins involved in the cascade of events leading to cellular proliferation including growth factors, growth factor receptors, and transcription factors. An activating mutation of a single copy of a proto-oncogene can lead to unrestricted cell growth. In contrast, tumor suppressor genes, such as *p53* and *retinoblastoma (RB)*, are genes that normally control critical checkpoints in cell growth and division. Typically, inactivation of both copies of tumor suppressor genes is required for unrestricted cell growth.

2.3.1.1. Skin Cancer

In general, there are two common types of nonmelanoma skin cancers: basal cell and squamous cell carcinomas. Basal cell carcinoma (BCC) is the most common form of skin cancer. It is a malignant neoplasm of basal cells of the epidermis. Ultraviolet (UV) irradiation has been a common culprit of many BCC cases. Less often, BCC may result from exposure to arsenic or certain industrial pollutants. Squamous cell carcinoma (SCC) is a malignant neoplasm of the keratinizing (transit-amplifying) cells within the epidermis and is the second most common skin cancer in humans. SCC usually occurs later in life than BCC. Although most cases of SCC are related to sun exposure, a smaller number develop in skin that has been injured or exposed to carcinogens. Subsequent sections will further discuss the events that drive the carcinogenic process in skin.

2.3.2. Initiation in the Skin

Initiating agents, such as the potent mutagen and carcinogen BaP, can potentially trigger the onset of carcinogenesis by causing mutations which can produce subtle changes in keratinocyte phenotype, unrecognizable in the context of the intact epidermis. Initiated keratinocytes *in vitro* display an altered response to signals for terminal differentiation, a characteristic which provides a selective growth advantage under culture conditions favoring differentiation (Kilkenny *et al.* 1985; Kulesz-Martin *et al.* 1980; Yuspa and Morgan 1981). Exploitation of this difference has been particularly helpful in isolating keratinocytes of mouse and human origin *in vitro* (Hennings *et al.* 1987b; Kilkenny *et al.* 1985; Kulesz-Martin *et al.* 1983; Yuspa *et al.* 1986).

Important insights into the genetic alterations associated with the initiated phenotype have surfaced from the identification of mutations in the cellular Harvey *ras*

gene (c-*ras*^{Ha}) associated with papilloma formation (Balmain *et al.* 1984; Bizub *et al.* 1986; Harper *et al.* 1987). These genetic studies indicate that: (1) c-*ras*^{Ha} gene mutations were frequently heterozygous in papillomas and could be detected in initiated skin prior to tumor formation (Nelson *et al.* 1992); (2) the initiating agent determined the existence, nature, and site of the c-*ras*^{Ha} mutation (Brown *et al.* 1990; Harper *et al.* 1986); and (3) many human benign and malignant skin tumors, probably induced by UV light, also contain *ras* gene mutations (Ananthaswamy *et al.* 1989; Ananthaswamy *et al.* 1988; Corominas *et al.* 1989; Daya-Grosjean *et al.* 1993; Leon *et al.* 1988; Suarez *et al.* 1989).

2.3.3. Promotion in the Skin

Application of tumor promoters to initiated epidermis causes the selective clonal outgrowth of a percentage of the chemically-mutated cells to produce multiple benign squamous cell papillomas; each lesion represents an expanded clone of a single initiated cell (Boutwell 1974; Deamant and Iannaccone 1987; Iannaccone *et al.* 1987). In skin carcinogenesis, selective clonal expansion of the initiated population may result from differential sensitivity of initiated and normal keratinocytes to either cytotoxicity or growth stimulatory affects of exogenous tumor promoters (Finzi *et al.* 1987; Hartley *et al.* 1987). Phorbol esters, such as 12-O-tetradeanoylphorbol-13-acetate (TPA), are both potent exogenous tumor promoters in initiated cells that activate PKC and accelerates terminal differentiation in normal keratinocytes (Dlugosz and Yuspa 1993; Yuspa *et al.* 1980, 1982). In contrast to normal cells, initiated keratinocytes are resistant to terminal differentiation induced by PKC activators such as TPA (Hennings *et al.* 1987a; Hennings *et al.* 1990a; Yuspa *et al.* 1983a). The differential response of normal and initiated cells favors the growth of a neoplastic subpopulation, enhancing clonal outgrowth and

producing papillomas. Therefore, the process of tumor promotion by phorbol esters *in vivo* recapitulates the clonal selection of initiated cells by differentiation-inducing agents in keratinocyte culture (Hennings *et al.* 1992; Hennings *et al.* 1990a; Strickland *et al.* 1992).

In skin, squamous papillomas are characterized by a high rate of proliferation and by delayed expression of differentiation markers, properties which are analogous to the phenotype of individual initiated cells *in vivo* (Glick *et al.* 1993; Roop *et al.* 1988). The mechanisms of exogenous promotion is likely to be epigenetic in most cases since: (1) papillomas are diploid when they first emerge (Aldaz *et al.* 1988a; Aldaz *et al.* 1988b); (2) a single genetic change in normal keratinocytes is sufficient to produce a papilloma phenotype (Bailleul *et al.* 1990; Greenhalgh *et al.* 1993); and (3) most promoting agents are not mutagens (Yuspa and Dlugosz 1991). In the absence of exposures to exogenous tumor promoters, initiated skin rarely develops into tumors. Thus, exogenous promotion in general is a rate-limiting early event in carcinogenesis, but the actual tumor yield is determined by additional hereditary factors influencing both the initiation and promotion stages (DiGiovanni *et al.* 1991). The genes which determine hereditary susceptibility to initiators and promoters in mouse skin remain largely to be defined, and susceptibility appears to be multigenic (Bangrazi *et al.* 1990; Naito *et al.* 1988).

2.3.4. Progression and Tumor Formation in the Skin

Premalignant progression of a papilloma to a carcinoma in mouse skin is generally a spontaneous process that is not enhanced by most exogenous tumor promoters (Hennings *et al.* 1983; Hennings *et al.* 1990b). Genetic studies indicate that nonrandom, sequential chromosomal aberrations are associated with premalignant progression of

mouse papillomas; particularly prominent are trisomies of chromosomes 6 and 7 (Aldaz *et al.* 1987; Aldaz *et al.* 1988a; Aldaz *et al.* 1989; Bianchi *et al.* 1990; Conti *et al.* 1986). Premalignant progression and malignant conversion can be enhanced and accelerated by exposing animals bearing papillomas to mutagens (Hennings *et al.* 1983; Hennings *et al.* 1990b; O'Connell *et al.* 1986).

Malignant conversion of benign tumors is a relatively rare occurrence since less than 5% of squamous papillomas spontaneously convert to clinically detectable cancers (Hennings *et al.* 1983; Hennings *et al.* 1990b). Squamous papilloma cell lines *in vitro* can be converted to squamous carcinoma cells by introducing the following oncogenes: *c-ras*^{HA} (mut), v-*ras*^{HA}, v-*fos*, c-*myc*, *E1A*, TGFα, *p53* (mut), *neu*, and v-*jun* (Dotto *et al.* 1988; Finzi *et al.* 1988; Greenhalgh *et al.* 1989; Greenhalgh and Yuspa 1988; Harper *et al.* 1986). In particular, changes in two cellular genes, c-*ras*^{HA} and *p53*, have been identified with malignant conversion in skin tumors. The mutated *ras*^{HA} oncogene, which is heterozygous in papillomas, is frequently homozygous in carcinomas (Bianchi *et al.* 1990; Quintanilla *et al.* 1986). An oncogenic *ras*^{HA} gene can cause malignant conversion of papilloma cells with a heterozygous c-*ras*^{HA} gene mutation (Greenhalgh *et al.* 1989; Harper *et al.* 1986). Mutations in the *p53* tumor suppressor gene are rarely found in chemically induced papillomas, but are frequently detected in squamous carcinomas, particularly those induced by benzo[*a*]pyrene (Burns *et al.* 1991; Kress *et al.* 1992; Ruggeri *et al.* 1991; Ruggeri *et al.* 1993). In addition, topical administration of initiators and promoters to mice lacking an intact *p53* gene results in rapid progression of papillomas to the carcinoma stage (Kemp *et al.* 1993). Also, mutations in the *p53* gene are frequently detected in human squamous and basal cell carcinomas of the skin (Brash

et al. 1991; Kanjilal *et al.* 1993; Rady *et al.* 1992; Ziegler *et al.* 1993). Overall, it seems multiple mechanisms may influence this late stage of carcinogenesis.

2.3.5. The Altered Phenotype of Initiated Keratinocytes

A subpopulation of keratinocytes isolated from carcinogen-initiated skin or normal basal keratinocytes exposed to carcinogens *in vitro* resists the Ca^{2+}-mediated induction of terminal differentiation and evolves as multiple foci which continue to grow in medium with >0.1 mM Ca^{2+}. These foci show properties consistent with the initiated phenotype. Ca^{2+} resistant foci: (1) develop from keratinocytes initiated *in vivo* or *in vitro* (Kawamura *et al.* 1985; Kulesz-Martin *et al.* 1980; Yuspa and Morgan 1981); (2) are more frequent with exposure to strong initiators and higher initiator doses (Kilkenny *et al.* 1985); (3) develop even if a delay of 10 weeks is interposed between initiation *in vivo* and Ca^{2+} selection *in vitro* (Kawamura *et al.* 1985); and (4) develop into cell lines which produce papillomas or carcinomas when grafted into nude mice (Kulesz-Martin *et al.* 1983; Strickland *et al.* 1988).

Phenotypic alterations such as increased proliferation rates and blocks to differentiation are commonly seen in initiated keratinocytes. The oncogenic activation of c-ras^{HA} is thought to play a key role in facilitating the development of the initiated phenotype in skin. When v-ras^{HA} oncogene is introduced into cultured normal keratinocytes, recipient cells form papillomas when grafted into nude mice, indicating that this single genetic change is sufficient to produce the initiated phenotype (Roop *et al.* 1986). However, other changes, in addition to *ras* mutations, are thought to be required to fully transform human keratinocytes (Kawamura *et al.* 1985). *In vitro*, mouse

keratinocytes expressing v-*ras*^{HA} have a high proliferation rate and fail to terminally differentiate in response to medium with >0.1 Ca^{2+} (Cheng *et al.* 1990; Roop *et al.* 1987; Yuspa *et al.* 1985; Yuspa *et al.* 1983b). This hyperproliferation induced by v-*ras*^{HA} transduction is caused by overexpression of and autocrine response to TGFα, a growth factor known to be elevated in papillomas (Glick *et al.* 1991; Imamoto *et al.* 1991; Lee *et al.* 1992). When basal cells are cultured in 0.05 mM Ca^{2+} medium, v-*ras*^{HA} keratinocytes express a phenotype with a striking similarity to normal keratinocytes exposed to activators of PKC, such as phorbol esters and DAG (Dlugosz and Yuspa 1993; Roop *et al.* 1987; Toftgard *et al.* 1985; Yuspa *et al.* 1983a). When v-*ras*^{HA} keratinocytes are exposed to medium with >0.1 mM Ca^{2+}, they share similar features with phorbol ester-treated epidermal cells; Cytokeratins K1 and K10 are not induced, while loricrin and filaggrin are overexpressed (Dlugosz and Yuspa 1993). However, transglutaminase mRNA decreases in Ca^{2+}-treated v-*ras*^{HA} keratinocytes, and terminal differentiation is blocked (Yuspa *et al.* 1985). An essential role for PKC activation in the v-*ras*^{HA} keratinocyte phenotype is supported by studies with the functional PKC inhibitor, bryostatin (Sako *et al.* 1987). This report suggests that qualitative and quantitative changes in keratinocyte PKC isoforms might be a consequence of v-*ras*^{HA} oncogene expression. Differential modification of isoforms, particularly activation of PKC-α and inhibition of PKC-δ, produce keratinocytes with enhanced proliferative capacity and reduced sensitivity to signals for terminal differentiation (Denning *et al.* 1993; Denning *et al.* 1995b; Deucher *et al.* 2002; Dlugosz and Yuspa 1991).

In later stages of carcinogenesis, TGFβ, *p53*, *fos*, *p21*^{WAF1} and integrin alterations seem to play critical roles in keratinocyte transformation. TGFβs are potent growth

inhibitors for cultured keratinocytes, and TGFβ-1 regulates basal cell proliferation *in vivo*. The absence of TGFβ-1 in normal epidermis of TGFβ-1 knockout mice causes basal cell hyperproliferation (Dahler *et al.* 2001; Glick *et al.* 1993). TGFβ isoforms are differentially expressed in increasingly malignant grades of keratinocytes (Gold *et al.* 2000). Tumor suppressor *p53* has been shown to promote differentiation in keratinocytes (Paramio *et al.* 2000b). Several laboratories have reported that the introduction of a mutant *p53* gene into neoplastic epithelial cells with endogenous wild-type *p53* conveys resistance to the growth-inhibitory effects of TGFβ (Gerwin *et al.* 1992; Reiss and Sartorelli 1987). This suggests a link between mutations in *p53*, TGFβ, and premalignant progression. Squamous cancers produced by v-*fos* oncogene-mediated conversion are highly invasive and vascular, do not express K1 or K10, and have disseminated expression of $\alpha_4\beta_6$ integrin throughout the tumor mass (Tennenbaum *et al.* 1996; Tennenbaum *et al.* 1992). Changes in integrin distribution could have profound effects on the neoplastic phenotype since integrins are important mediators of cell-cell and cell-extracellular matrix interactions (Hynes 1992; Owens and Watt 2001; Ruoslahti 1991). Other oncogenes which modify gene transcription, such as c-*myc*, *EIA*, or v-*jun*, do not cause phenotypic progression when transduced into papilloma cell suggesting the *fos*-related changes in genetic regulation are specific for malignant conversion. It is also interesting to note that $p21^{WAF1}$ enhances papilloma formation but not malignant conversion in mouse skin (Weinberg *et al.* 1999). In addition, $p21^{WAF1}$ successfully inhibits the growth of skin cancers, even those with alterations in *p53*, $p21^{ras}$, *RB* gene product, and telomerase activity (Kallassy *et al.* 1998).

The initiated phenotype results from mutational events producing intrinsic changes in intracellular signaling pathways, particularly those related to terminal differentiation. However, initiated cells remain responsive to extrinsic restraints imposed by surrounding normal cells and the microenvironment. Nevertheless, defects in the control of proliferation, differentiation, and apoptosis can lead to a disturbance of epidermal homeostasis and have been implicated in cancer, as well as other skin diseases.

2.4. Chemicals of Interest

2.4.1. Arsenic

Arsenic is widely distributed, at low concentrations, in food, water, air and soil (Bettley and O'Shea 1975; Chappell *et al.* 1997; Knowles and Benson 1984). Arsenic combined with oxygen, chlorine, and sulfur is called inorganic arsenic, which represents the most common form of either arsenate or arsenite in the environment (Bettley and O'Shea 1975; Knowles and Benson 1984; Landolph 1994). Studies indicate that arsenite is considerably more toxic and carcinogenic than arsenate (Tsuda *et al.* 1995). Inorganic arsenic species have been ranked highest in priority on the list of Top 20 Hazardous Substances by the ATSDR and USEPA (ATSDR 1999a, 2003a). Exposure to arsenic occurs through arsenic-rich geological soil, nonferrous smelters, pesticide manufacturing and use, microelectronics, burning of fossil fuels, or from consumption of contaminated drinking water (Basu *et al.* 2001; Jessen *et al.* 2001). Although arsenic is a known human carcinogen, it is only slightly mutagenic during chronic exposure or at very high concentrations (Jha *et al.* 1992; Mure *et al.* 2003; Rossman 1981; Rossman *et al.* 1980).

Thus, arsenic has been characterized as a promoting, progressing, and/or co-mutagenic agent (Lee *et al.* 1988; Maier *et al.* 2002; Rossman *et al.* 2001; Rudel *et al.* 1996).

Potential carcinogenic actions for arsenic include oxidative stress, genotoxic damage, inhibition of DNA repair, epigenetic effects such as altered methylation, and activation of certain signal transduction pathways leading to aberrant gene expression. Unlike many carcinogens, arsenic fails to behave as a mutagen and cause point mutations in standard assays (Rossman and Goncharova 1998), but has been shown to induce large deletion mutations instead (Hu *et al.* 1998). There are numerous reports showing that arsenic exposure induces chromosome aberrations (Rossman *et al.* 2001), aneuploidy and micronuclei formation (Gurr *et al.* 1993; Wang and Huang 1994), DNA-protein cross-linking and sister chromatid exchange in animal and human cells (Dong and Luo 1993). Both nucleotide-excision-repair (NER) and base-excision repair (BER) of DNA are inhibited by very low, non-cytotoxic concentrations of arsenic (Hartwig *et al.* 2002). Arsenic inhibits the completion of DNA excision repair, perhaps via effects on DNA ligase, which is especially sensitive to arsenite in cells (Li and Rossman 1989). The activation of NADH oxidase by arsenic may produce O_2^- radicals. The clastogenic activity of arsenic is likely mediated through O_2^- and its secondary radicals (Hei *et al.* 1998; Lynn *et al.* 2000). Gene amplification induced by arsenic may also play a role in its carcinogenic effects (Hughes 2002).

2.4.1.1. Arsenic-Induced Alterations in the Epidermis

Although arsenic is a potent human skin carcinogen, the exact mechanism of arsenic induced carcinogenesis is currently unclear. Arsenic accumulates in the skin and is associated with hyperkeratosis (hypertrophy of the corneous layer of the skin) and

acanthosis (an increase in the thickness of the stratum spinosum of the epidermis), pigmentation disorders, and keratinocyte tumors including basal cell carcinomas and squamous cell carcinomas (Chen *et al.* 1985; Shi *et al.* 2004). Due to arsenic-contaminated drinking water in many countries, development of neoplastic skin lesions has become a health problem of global proportions (Chowdhury *et al.* 2000; Tseng 1977; Wong *et al.* 1998). Hence, ingested arsenic can be absorbed and accumulated in the skin (Lansdown 1995). Many cases of nonmelanoma skin cancer have been reported among people exposed to arsenic through dietary, occupational, or medicinal means (Germolec *et al.* 1998; Saha 1996; Schwartz 1997; Tseng 1977). The toxicity of arsenic has been related to its high reactivity with vicinal sulfhydryl groups on macromolecules such as glutathione (GSH) and cysteine (Scott *et al.* 1993). The reason that the skin is unusually sensitive to arsenic toxicity may be due to its richness in sulfhydryl-containing molecules, such as keratin (Lindgren *et al.* 1982; Yamauchi and Yamamura 1983).

Arsenic (arsenite in particular) has been shown to be a potent differentiation inhibitor in keratinocytes by decreasing cornified envelope formation or by altering differentiation-associated markers (Jessen *et al.* 2001; Kachinskas *et al.* 1994; Perez *et al.* 2003). These studies demonstrate that involucrin, transglutaminase, SPR-1, and filaggrin expression are suppressed by arsenic exposure in various keratinocyte cell lines. In addition, arsenic has been shown to have dose-dependent effects on cell proliferation and to affect expression of a variety of growth regulatory factors in keratinocytes (Germolec *et al.* 1996; Monzon *et al.* 1996; Vega *et al.* 2001). In particular, non-cytotoxic to slightly toxic concentrations of arsenic have been shown to increase cell proliferation (hormesis), while toxic concentrations inhibit cell growth (Chen *et al.* 2000; Liao *et al.* 2004; Styblo

et al. 2002; Vega *et al.* 2001). These phenotypic changes due to arsenic exposure may be related to altered expression of genes which modulate signal transduction pathways known to regulate keratinocyte proliferation and differentiation. Arsenic has been reported to be a potent stimulator of proto-oncogenes c-*fos* and c-*jun* expression and AP-1 transactivational activity (Cavigelli *et al.* 1996; Liao *et al.* 2004). The requirement of AP-1 for tumor promotion has been demonstrated in various cell models (Angel and Karin 1991). The induction of AP-1 activity by arsenic appears to be mediated by activation of PKC and MAPK family members (Huang *et al.* 2001a). NFκB activation is thought to be associated with initiation and accelerated tumorigenesis (Gilmore 1997). Studies also observed the activation of NFκB following arsenic exposure in keratinocytes (Huang *et al.* 2001b; Liao *et al.* 2004). TGFα overexpression has been associated with the neoplastic transformation in the skin, and arsenic has been shown to induce TGFα in human skin (Simeonova and Luster 2000). There are conflicting reports on arsenic-induced effects on tumor suppressor *p53*. One report failed to demonstrate an effect of arsenic on *p53*-dependent transcription (Huang *et al.* 1999); however, other reports show arsenic decreasing *p53* expression (Hamadeh *et al.* 1999), or inducing *p53* phosphorylation and accumulation (Salazar *et al.* 1997; Yih and Lee 2000).

2.4.2. Benzo[a]pyrene

Benzo[*a*]pyrene (BaP) is a ubiquitous environmental pollutant and has been proven to be a potent mutagen and carcinogen in both humans and animals. The polycyclic aromatic hydrocarbon (PAH) is also among the Superfund Top 10 Priority Hazardous Substances and is a common constituent in petroleum products (ATSDR 1999b, 2003b). BaP is also a constituent of many soots, oils, tars, tobacco smoke,

overcooked foods, and air pollutants formed by incomplete pyrolysis of combustible organic material (Hanelt *et al.* 1997; Miller *et al.* 2000; Parkinson and Newbold 1980).

BaP must be bioactivated in order to induce its adverse effects in an organism or target tissue. In the cell, BaP is metabolized mostly by cytochromes P450 1A1 and 1B1, as well as epoxide hydrolase, yielding *syn*- and *anti*-BaP-7,8-diol-9,10-epoxides (BPDE) (Guengerich *et al.* 1996; Guengerich and Shimada 1998; Hartwig *et al.* 2003). BDPE can then react and bind to DNA at the 2-amino group of guanine (BPDE-N^2-dG) in the minor groove, as well as N^7 of guanine in the major groove. The majority of BPDE forms stable adducts at the N^2 positions of guanine, which is considered to be the critical event in carcinogenicity (Sage and Haseltine 1984). If left unrepaired, mutation can occur, typified by a G to T transversion in the DNA (Figure 2.4) (Tran *et al.* 2002). This transversion predominates in many *ras* and *p53* mutations found in a variety of cancers, including skin cancer (Amstad and Cerutti 1995; Cherpillod and Amstad 1995; Colapietro *et al.* 1993; Hattori *et al.* 1996). If DNA repair mechanisms are not functioning properly to repair adduct-induced transversions produced by BPDE, these mutations are likely to be inherited by daughter cells.

2.4.2.1. Benzo[*a*]pyrene-Induced Alterations in the Skin

There is potential for either environmental or occupational dermal exposure to BaP. The most likely source of dermal contact with toxic BaP levels would be in workers in the petroleum industry. Bioactivated BaP is a known skin carcinogen, acting as a mutagen and an initiating agent during transformation (Ashurst *et al.* 1983; Mager *et al.* 1977). When applied dermally, BaP induces cytokinetic abnormalities and inflammation, followed by skin tumors (Albert *et al.* 1991; Albert *et al.* 1996). Many of the earliest

studies of BaP were carried out using the murine skin system (Lee and O'Neill 1971; Turusov *et al.* 1987). The chemical alters differentiation in multiple cell types (Edmondson and Mossman 1991; Reiners *et al.* 1991). This activity is likely due to mutagenesis of proteins in crucial signal transduction paths. Clearly, much work remains to be done to clarify the relationship between BaP exposure, abnormalities in proliferation and differentiation, and development of neoplastic skin lesions.

Although there have been limited studies on BaP-mediated effects on keratinocyte proliferation and differentiation, the data which are available support BaP's ability to alter these cellular processes. BaP has been proven to suppress keratinocyte differentiation in cultured squamous carcinoma cells by inhibiting retinoid-induced transglutaminase and by inhibiting the expression of involucrin and transglutaminase in the absence of a differentiation inducing agent (Rice *et al.* 1988; Rubin and Rice 1988). In related studies, BaP exposure was also shown to alter the expression of differentiation-related cytokeratins in tracheal and bladder epithelial cells (Edmondson and Mossman 1991; Summerhayes *et al.* 1981). The fact that BaP is capable of altering the differentiation program of committed cells may explain, in part, why exposures of the tracheal epithelium to BaP lead to squamous metaplasia and potentially squamous cell carcinoma (Benfield *et al.* 1981; Chopra and Joiakim 1991; Saffiotti *et al.* 1964; Yoshimoto *et al.* 1980). BaP is known to interfere with other cellular transduction pathways within the cell, namely those involving Ca^{2+} and epidermal growth factor (EGF) in lymphocytes. These cells exhibit glutathione (GSH) depletion and an elevation of intracellular Ca^{2+} upon BPDE treatment, possibly as a result of sulfhydryl damage produced by this BaP metabolite (Romero *et al.* 1997). As a result, alterations in Ca^{2+}

homeostasis, cell activation, and proliferation in these cells can be compromised (Romero *et al.* 1997). In support of this interpretation, cultures of epidermal keratinocytes exhibit an increase in overall metabolism of BaP upon pre-incubation in high Ca^{2+} medium prior to BaP treatment (DiGiovanni *et al.* 1989). These results indicate that the expression and inducibility of enzymes involved in BaP metabolism can be regulated by Ca^{2+}, a factor which is extremely important in keratinocyte differentiation (DiGiovanni *et al.* 1989).

2.4.2.2. Benzo[*a*]pyrene-Mediated Perturbation in Genes Potentially Involved in Proliferation and Differentiation Regulation

BaP also exerts profound effects on genes that have been shown to play crucial roles in keratinocyte proliferation, apoptosis, differentiation, and carcinogenesis. Evidence indicates that the *p53* and *ras* genes are selective targets of metabolically activated BaP. More specifically, reports show a link between BaP exposure, G to T transversion mutation in *p53*, and skin carcinoma formation (Puisieux *et al.* 1991; Ruggeri *et al.* 1993). Activation of the c-ras^{HA} proto-oncogene by BaP has been reported previously (Marshall *et al.* 1984). Studies also demonstrate that BaP initiated papillomas exhibit a high incidence of specific *ras* mutations and that PKC levels constitutively decreased in these papillomas, indicating that activated *ras* gene is associated with and may contribute to the observed decrease in PKC levels (Colapietro *et al.* 1993). If this effect of *ras* and PKC were seen in BaP treated keratinocytes, inhibited differentiation and increased proliferation would be the most likely phenotypic alterations. BaP-mediated interference in PKC-related signal transduction in vascular smooth muscle cells has also been reported (Ou and Ramos 1994; Ou *et al.* 1995). BaP-induced alterations in function of p53, Ras, and PKC have been shown to have an impact on cell growth and

carcinogenesis, however, whether these changes correlate with perturbed differentiation awaits clarification. In related studies done in hepatocytes, the time- and dose-dependent effects of BaP on c-*fos*, c-*jun*, c-*myc*, and c-ras^{HA} expression were evaluated (Zhao and Ramos 1998). Upstream from these and other genes, BaP can also mimic growth factor signaling pathways leading to alterations in cell growth and proliferation. This is best exemplified by BaP interfering with EGF signaling cascades which activate Ras-MAPK signaling pathways (Guyda *et al.* 1990; Ivanovic and Weinstein 1982). BaP has also demonstrated the ability to activate insulin-like growth factor (IGF-1) signaling pathways under insulin-deficient conditions in human mammary epithelial cells (Zhang *et al.* 1995). From all these studies, one can begin to acquire a sense of how BaP might alter various cellular processes; however, many more molecular studies are required to better understand and describe the mechanisms behind the alterations produced by BaP, especially in the skin. Although a plethora of data exist on BaP, much work remains to be done to clarify the relationship between BaP exposure, abnormalities in cells proliferation and differentiation, alterations in cell signaling pathways, and the development of neoplastic skin lesions.

2.5. Mathematical Models Describing Keratinocyte Differentiation

In general, numerous mathematical cell-cycle models have been developed to describe the cell cycle kinetics and growth rates of various tumor and normal cell lines and tissues (Basse *et al.* 2003; Bertuzzi *et al.* 2002; Bertuzzi *et al.* 1997; Clairambault *et al.* 2003; Kimmel *et al.* 1985; Kimmel *et al.* 1983; Ubezio 1993; Willnow 1979).

However, there are very few mathematical models that depict and incorporate skin differentiation. Modeling studies presented in this dissertation are largely based on the cell kinetic theories developed by Gordon G. Steel (Steel 1977). In subsequent sections, I review literature that was used to formulate and construct keratinocyte differentiation and cell cycle kinetics models presented in Chapter 6. The conceptual keratinocyte model (simple version) that was developed is depicted in Figure 2.5 and the schematic of the more complex version is shown in Figure 2.6.

2.5.1. Modeling the Cell Cycle

In order to mathematically describe the cell cycle one must understand the dynamics and kinetics that are involved. The cell cycle is separated into four main phases: G1 (Gap 1), S-phase (DNA synthesis), G2 (Gap 2), and M (Mitosis). After cell division occurs in mitosis, daughter cells re-enter the cycle at G1. It is at this point where cells, keratinocytes for example, have a 'choice'. Cells can either: (1) continue through the cell cycle and enter into S-phase, (2) differentiate into a phenotypically new cell type, or (3) enter into a state of cell arrest in G0 called quiescence. This 'decision' depends on various endogenous and exogenous signals and growth factor availability. To consider all the factors which control the cell cycle in a model is a very difficult task because the cell cycle is a very complex system to describe mathematically. In order to better understand this process, it is sometimes required to first build a simplistic model (thus, following the Law of Parsimony) which describes the basic cell cycle and differentiation process in the cell type of interest. Cell cycle data are often obtained by various flow cytometric methods and other cell kinetic methods. This data can aid in producing computer

simulations of the cell population with respect to various factors such as time, confluence, or chemical exposure.

Germinative cell production is determined by three parameters: (1) the cell cycle time, (2) the loss of cycling cells by programmed cell death (Laporte *et al.* 1996), and (3) the proportion of keratinocytes actively engaged in the cell cycle (or growth fraction). The term growth fraction (GF) is used to describe the proportion of proliferative cells in a given tissue or population and can be described by the following equation (Heenen and Galand 1997; Lamerton and Steel 1968; Mendelsohn 1960; Steel 1977):

$$GF = \frac{new\_proliferating\_cells}{all\_new\_cells} = \alpha - 1 \qquad \text{(Steel 1977)} \qquad (2\text{-}1)$$

where α is the average number of proliferating daughter cells produced at each division. The variable α realistically lies between 1 and 2: α = 1 when all daughter cells do not continue to proliferate and α = 2 if all daughter cells continue to proliferate. GF can be measured by flow cytometry using proliferation-associated antigens such as proliferating cell nuclear antigen (PCNA) and Ki-67 (Darzynkiewicz *et al.* 2001; Gorisse *et al.* 1999; Wilson 1998).

Flow cytometry can be used to gather data on the cell distribution and/or potential doubling time (T_{pot}) of cells. Cell distribution data displays the fraction of cells in each phase of the cell cycle based on DNA content: G1+G0 cells = n, G2+M cells = 2n, and n < S-phase cells < 2n; where n = DNA content in a normal diploid cell. T_{pot} is the turnover time in tissue, and is defined as the time within which a cell population would double its number if cell loss does not occur (Steel 1977). T_{pot} can be measured by pulse-labeling cells with bromodeoxyuridine (BrdU) and then detecting its incorporation into DNA synthesizing cells by the use of fluorescent antibodies. Cells are counterstained with

propidium iodide to measure DNA content. From the flow cytometry data, T_{pot} can be estimated using the following equation:

$$T_{POT} = \lambda \times \frac{T_S}{LI} \qquad \text{(Steel 1977)} \qquad (2\text{-}2)$$

where T_S is the period of DNA synthesis, LI (labeling index) is the fraction of cells synthesizing DNA and labeled with BrdU, and λ is a correction factor for the nonlinear distribution of cells through the cell cycle (Steel 1977; Wilson 1994b). Correction factor λ ranges from 0.693 to 1.386 depending on where the S period occurs within the cell cycle (i.e., a lower value represents S-phase occurring toward the end of the cell cycle and a higher value denotes S-phase occurring toward the beginning of the cell cycle) (Lamerton and Steel 1968; Steel 1977). Typically, λ is set to 0.8 when dealing with human tumor cells according to previous reports (Bertuzzi *et al.* 1997; Steel and Bensted 1965; Terry *et al.* 1991; Willnow 1979). However, 0.75 is also a common value often used for λ (Bassukas *et al.* 1991; Steel 1977; Willnow 1979). T_S can be measured by the relative movement of BrdU labeled S-phase cells through a certain region of the bivariate histogram produced during flow cytometric analysis as demonstrated in Chapter 4 and described in a previous study (Begg *et al.* 1985). After the T_{pot}, cell cycle distribution, and GF data have been collected, it is possible to calculate the parameters which are required for quantitative description of a relatively simple cell cycle model.

With the data collected above, cell kinetic parameters can be calculated. In order to calculate phase times for cells in each cell cycle phase, the cell cycle time (T_C) must first be determined. T_C is the interval within which one group of cells complete a mitotic cycle, i.e. from birth at mitosis to eventual splitting to form two progeny at the next

mitosis (Wilson 1994a). T_C can be calculated from the following equation if T_{pot} and α are known:

$$T_{POT} = \frac{\ln 2}{\ln \alpha} T_C \qquad \text{(Steel 1977)} \qquad (2\text{-}3)$$

Some modelers assume T_C equals T_{pot} (Basse *et al.* 2003); however, by doing this an inaccurate assumption is made that after undergoing mitosis all cells continue to divide and no cells enter G0. Hence, GF is not being considered in this scheme (Steel 1977; Ubezio 1993). T_C is always shorter in time than T_{pot} since T_{pot} takes the cell population as a whole under consideration (cells dividing and in G0) and T_C is simply the time interval of a dividing cell from one mitosis to the subsequent one (Wilson 1994a). Now that we know T_C, we can calculate cell phase times using the following equation:

$$T_i = -\frac{T_C}{\ln \alpha} \ln\left\{ e^{-\left(\frac{T_{i-1}}{T_C}\right)\ln \alpha} - \frac{\alpha - 1}{\alpha} P_i \right\} \qquad \text{(Steel 1977)} \qquad (2\text{-}4)$$

where T_i = cumulative time including the phase of interest (i.e., $T_1 = T_{G1}$, $T_2 = T_{G1}+T_S$, and $T_3 = T_{G1}+T_S+T_{G2/M} = T_C$). P_i = fraction of cells in phase i. As discussed above, α can be calculated from measuring the GF in a population. In our keratinocyte models G2 and M were lumped into one compartment (G2+M) and the same was done regarding G0 and G1 cells (G1+G0). Once the average time in each cell cycle phase is computed, rate constants (k) can be calculated from the following equation:

$$T_i = \frac{1}{k_i + \mu_i} \qquad \text{(Basse *et al.* 2003)} \qquad (2\text{-}5)$$

where μ_i is the death rate parameter of a particular cell cycle phase.

Cell death rates can also be measured by the flow cytometer as described in previous studies (Ormerod *et al.* 1994). Basically, this is a time-course study using flow cytometric

analysis which measures propidium iodide uptake in dead cells. By setting a gate on forward angle light scatter (FALS), which is an indicator of cell size, debris and cell clumps can be partially excluded from analysis, thus making this a more accurate estimation of the death rates of the population of interest. However, these measurements are problematic in that the death rate in healthy cell cultures has been demonstrated to be very low and difficult to measure accurately in many populations. For these studies, death rates in keratinocytes are negligible and uniform and that the majority of death in untreated populations will be due to terminal differentiation of granular cells.

By utilizing all the results obtained from the flow cytometer and data calculated from the equations mentioned in this section, a fairly simple mathematical model of the cell cycle can be constructed. Once the model is complete, it is relatively easy to replace control data with data from chemically-exposed cells to examine any changes that may occur in the kinetics of the cell cycle.

2.5.2. Modeling Keratinocyte Differentiation

The cell types in keratinocyte populations are categorized as either stem, transit-amplifying, or post-mitotic. Stem cells can divide indefinitely (Potten and Loeffler 1990), and are the source of interfollicular keratinocytes in normal epidermis. A stem cell can be in a resting state (G0) or a proliferative state. Given an appropriate signal, stem cells differentiate into transit-amplifying (TA) cells. These cells are in the first stages of terminal differentiation. TA cells are thought to divide between three to five times (Heenen and Galand 1997; Jones *et al.* 1995; Jones and Watt 1993; Perez-Losada and Balmain 2003; Potten 1981). Once they stop dividing they are categorized as post-mitotic. Post-mitotic cells migrate from the germinative compartment and eventually

desquamate at the skin surface. The cell type distribution in the skin is estimated to be approximately 10% stem cells, 50% TA cells, and 40% post-mitotic cells (Heenen and Galand 1997). Other reports demonstrate a similar cell type population distribution of 40-50% proliferating cells, 10% of which are stem cells (Jensen *et al.* 1999; Jones *et al.* 1995; Moles and Watt 1997).

Although the required methods may be difficult to perform and the resulting data are not entirely precise, it is theoretically possible to distinguish between cycling, quiescent, and differentiating keratinocytes. Presently, the capability exists to estimate and discriminate between cycling verses non-cycling cells (G0) by labeling cells with a proliferation-associated antigen such as Ki-67 (Endl *et al.* 2001; Gorisse *et al.* 1999; van Erp *et al.* 1994). It is also possible to distinguish differentiating cells from other non-cycling cells with the use of markers such as involucrin and β_1 integrin (Dover and Watt 1987; Jensen *et al.* 1999; Jones *et al.* 1995; Jones and Watt 1993; van Erp *et al.* 1994), and also by stathmokinetic procedures (Kimmel *et al.* 1986; Staiano-Coico *et al.* 1989; Staiano-Coico *et al.* 1986). Most studies indicate about 40-55% of G1+G0 keratinocytes differentiate into post-mitotic cells (Dover and Watt 1987; Kimmel *et al.* 1986; Thorud *et al.* 1988; van Erp *et al.* 1994); however, the initiation of differentiation and the faction of differentiating cells depend on many factors such as cell confluency, Ca^{2+} concentration, cell size, and cell age (Loeffler *et al.* 1987; Savill 2003; van Erp *et al.* 1994; van Ruissen *et al.* 1994; Watt *et al.* 1988). Dover and Watt (1987) measured the differentiation rate of a normal keratinocyte to be approximately 0.017 hr^{-1}. This rate is very comparable to the differentiation rate calculated from the stathmokinetic data presented by Kimmel *et al.* (1986).

Another challenge is to discern between stem and TA cells within the epidermis. Although proliferation occurs less frequently in stem than in TA cells, both populations are dividing, thus many methods cannot separate these two cells types. One major difference between these two cell types is the amount of RNA content within the cell. In general, cells that cycle faster have a higher RNA content (Kimmel *et al.* 1986; Staiano-Coico *et al.* 1986). Therefore, basal keratinocytes (slow cycling cells) are regarded as low-RNA cells and TA cells (fast cycling cells) are deemed high-RNA cells. Kimmel *et al.* and Staino-Coico *et al.* (1986) are the only groups who have attempted to separate the two populations based on this type of analysis in keratinocytes. Their stathmokinetic studies in keratinocytes have been used to derive the most complete model which describes the behavior of this cell type in culture. Nevertheless, the model has its uncertainties as well. It is still not possible to accurately measure how often keratinocyte stem cells divide, how many times TA cells divide before differentiating, or the probability with which a daughter cell from a divided stem cell will remain a stem cell or differentiate into a TA cell. Researchers have developed fitted estimates for these unknown variables and, in most cases, these estimates seem to fit well with the cell cycle data used in their keratinocyte models. Figure 2.5 depicts a more complex differentiation model similar to the model presented in Kimmel *et al.* (1986). This model will be presented in more detail in Chapter 6.

2.6. References

Abernethy, J. L., Hill, R. L., and Goldsmith, L. A. (1977). Epsilon-(gamma-glutamyl)lysine cross-links in human stratum corneum. *J.Biol.Chem.* **252**, 1837-1839.

Aebi, U., Fowler, W. E., Rew, P., and Sun, T. T. (1983). The fibrillar substructure of keratin filaments unraveled. *J.Cell Biol.* **97**, 1131-1143.

Albers, K., and Fuchs, E. (1992). The molecular biology of intermediate filament proteins. *Int.Rev.Cytol.* **134**, 243-279.

Albert, R. E., Miller, M. L., Cody, T., Andringa, A., Shukla, R., and Baxter, C. S. (1991). Benzo[a]pyrene-induced skin damage and tumor promotion in the mouse. *Carcinogenesis* **12**, 1273-1280.

Albert, R. E., Miller, M. L., Cody, T. E., Talaska, G., Underwood, P., and Andringa, A. (1996). Epidermal cytokinetics, DNA adducts, and dermal inflammation in the mouse skin in response to repeated benzo[a]pyrene exposures. *Toxicology & Applied Pharmacology* **136**, 67-74.

Aldaz, C. M., Conti, C. J., Klein-Szanto, A. J., and Slaga, T. J. (1987). Progressive dysplasia and aneuploidy are hallmarks of mouse skin papillomas: relevance to malignancy. *Proc.Natl.Acad.Sci.U.S.A* **84**, 2029-2032.

Aldaz, C. M., Conti, C. J., Larcher, F., Trono, D., Roop, D. R., Chesner, J., Whitehead, T., and Slaga, T. J. (1988a). Sequential development of aneuploidy, keratin modifications, and gamma-glutamyltransferase expression in mouse skin papillomas. *Cancer Res.* **48**, 3253-3257.

Aldaz, C. M., Conti, C. J., Yuspa, S. H., and Slaga, T. J. (1988b). Cytogenetic profile of mouse skin tumors induced by the viral Harvey-ras gene. *Carcinogenesis* **9**, 1503-1505.

Aldaz, C. M., Trono, D., Larcher, F., Slaga, T. J., and Conti, C. J. (1989). Sequential trisomization of chromosomes 6 and 7 in mouse skin premalignant lesions. *Mol.Carcinog.* **2**, 22-26.

Alt, A., Ohba, M., Li, L., Gartsbein, M., Belanger, A., Denning, M. F., Kuroki, T., Yuspa, S. H., and Tennenbaum, T. (2001). Protein kinase Cdelta-mediated phosphorylation of alpha6beta4 is associated with reduced integrin localization to the hemidesmosome and decreased keratinocyte attachment. *Cancer Res.* **61**, 4591-4598.

Amstad, P. A., and Cerutti, P. A. (1995). Ultraviolet-B-light-induced mutagenesis of C-H-ras codons 11 and 12 in human skin fibroblasts. *Int.J.Cancer* **63**, 136-139.

Ananthaswamy, H. N., Applegate, L. A., Goldberg, L. H., and Bales, E. S. (1989). Deletion of the c-Ha-ras-1 allele in human skin cancers. *Mol.Carcinog.* **2**, 298-301.

Ananthaswamy, H. N., Price, J. E., Goldberg, L. H., and Bales, E. S. (1988). Detection and identification of activated oncogenes in human skin cancers occurring on sun-exposed body sites. *Cancer Res.* **48**, 3341-3346.

Angel, P., and Karin, M. (1991). The role of Jun, Fos and the AP-1 complex in cell-proliferation and transformation. *Biochim.Biophys.Acta* **1072**, 129-157.

Ashurst, S. W., Cohen, G. M., Nesnow, S., DiGiovanni, J., and Slaga, T. J. (1983). Formation of benzo(a)pyrene/DNA adducts and their relationship to tumor initiation in mouse epidermis. *Cancer Res.* **43**, 1024-1029.

ATSDR (1999a). Toxicological profile for arsenic. *Agency for Toxic Substance and Disease Registry* **Atlanta**.

ATSDR (1999b). Toxicological profile for polycyclic aromatic hydrocarbons (PAHs). *Agency for Toxic Substance and Disease Registry* **Atlanta**.

ATSDR (2003a). Toxicological profile for arsenic. *Agency for Toxic Substance and Disease Registry* **Atlanta**.

ATSDR (2003b). Toxicological profile for polycyclic aromatic hydrocarbons (PAHs). *Agency for Toxic Substance and Disease Registry* **Atlanta**.

Bailleul, B., Surani, M. A., White, S., Barton, S. C., Brown, K., Blessing, M., Jorcano, J., and Balmain, A. (1990). Skin hyperkeratosis and papilloma formation in transgenic mice expressing a ras oncogene from a suprabasal keratin promoter. *Cell* **62**, 697-708.

Balmain, A., Ramsden, M., Bowden, G. T., and Smith, J. (1984). Activation of the mouse cellular Harvey-ras gene in chemically induced benign skin papillomas. *Nature* **307**, 658-660.

Bangrazi, C., Mouton, D., Neveu, T., Saran, A., Covelli, V., Doria, G., and Biozzi, G. (1990). Genetics of chemical carcinogenesis. 1. Bidirectional selective breeding of susceptible and resistant lines of mice to two-stage skin carcinogenesis. *Carcinogenesis* **11**, 1711-1719.

Basse, B., Baguley, B. C., Marshall, E. S., Joseph, W. R., Van Brunt, B., Wake, G., and Wall, D. J. (2003). A mathematical model for analysis of the cell cycle in cell lines derived from human tumors. *J.Math.Biol.* **47**, 295-312.

Bassukas, I. D., Arai, A., Schell, H., and Hornstein, O. P. (1991). Growth and cell kinetics of human hair papilla cells in vitro. An autoradiographic and flow cytometric study. *Cell Prolif.* **24**, 367-374.

Basu, A., Mahata, J., Gupta, S., and Giri, A. K. (2001). Genetic toxicology of a paradoxical human carcinogen, arsenic: a review. [Review] [183 refs]. *Mutation Research* **488**, 171-194.

Begg, A. C., McNally, N. J., Shrieve, D. C., and Karcher, H. (1985). A method to measure the duration of DNA synthesis and the potential doubling time from a single sample. *Cytometry* **6**, 620-626.

Benfield, J. R., Shors, E. C., Hammond, W. G., Paladugu, R. R., Cohen, A. H., Jensen, T., Fu, P. C., Pak, H. Y., and Teplitz, R. L. (1981). A clinically relevant canine lung cancer model. *Ann.Thorac.Surg.* **32**, 592-601.

Bergstresser, P. R., and Taylor, J. R. (1977). Epidermal 'turnover time'--a new examination. *Br.J.Dermatol.* **96**, 503-509.

Bertuzzi, A., Faretta, M., Gandolfi, A., Sinisgalli, C., Starace, G., Valoti, G., and Ubezio, P. (2002). Kinetic heterogeneity of an experimental tumour revealed by BrdUrd incorporation and mathematical modelling. *Bull.Math.Biol.* **64**, 355-384.

Bertuzzi, A., Gandolfi, A., Sinisgalli, C., Starace, G., and Ubezio, P. (1997). Cell loss and the concept of potential doubling time. *Cytometry* **29**, 34-40.

Bettley, F. R., and O'Shea, J. A. (1975). The absorption of arsenic and its relation to carcinoma. *Br.J.Dermatol.* **92**, 563-568.

Bianchi, A. B., Aldaz, C. M., and Conti, C. J. (1990). Nonrandom duplication of the chromosome bearing a mutated Ha-ras-1 allele in mouse skin tumors. *Proc.Natl.Acad.Sci.U.S.A* **87**, 6902-6906.

Bikle, D. D., and Pillai, S. (1993). Vitamin D, calcium, and epidermal differentiation. *Endocr.Rev.* **14**, 3-19.

Bikle, D. D., Tu, C. L., Xie, Z., and Oda, Y. (2003). Vitamin D regulated keratinocyte differentiation: role of coactivators. *J.Cell Biochem.* **88**, 290-295.

Bizub, D., Wood, A. W., and Skalka, A. M. (1986). Mutagenesis of the Ha-ras oncogene in mouse skin tumors induced by polycyclic aromatic hydrocarbons. *Proc.Natl.Acad.Sci.U.S.A* **83**, 6048-6052.

Boutwell, R. K. (1974). The function and mechanism of promoters of carcinogenesis. *CRC Crit Rev.Toxicol.* **2**, 419-443.

Boyce, S. T., and Ham, R. G. (1983). Calcium-regulated differentiation of normal human epidermal keratinocytes in chemically defined clonal culture and serum-free serial culture. *J.Invest Dermatol.* **81**, 33s-40s.

Braga, V. M., Machesky, L. M., Hall, A., and Hotchin, N. A. (1997). The small GTPases Rho and Rac are required for the establishment of cadherin-dependent cell-cell contacts. *J.Cell Biol.* **137**, 1421-1431.

Brash, D. E., Rudolph, J. A., Simon, J. A., Lin, A., McKenna, G. J., Baden, H. P., Halperin, A. J., and Ponten, J. (1991). A role for sunlight in skin cancer: UV-induced p53 mutations in squamous cell carcinoma. *Proc.Natl.Acad.Sci.U.S.A* **88**, 10124-10128.

Brissette, J. L., Li, J., Kamimura, J., Lee, D., and Dotto, G. P. (1996). The product of the mouse nude locus, Whn, regulates the balance between epithelial cell growth and differentiation. *Genes Dev.* **10**, 2212-2221.

Brown, K., Buchmann, A., and Balmain, A. (1990). Carcinogen-induced mutations in the mouse c-Ha-ras gene provide evidence of multiple pathways for tumor progression. *Proc.Natl.Acad.Sci.U.S.A* **87**, 538-542.

Burns, P. A., Kemp, C. J., Gannon, J. V., Lane, D. P., Bremner, R., and Balmain, A. (1991). Loss of heterozygosity and mutational alterations of the p53 gene in skin tumours of interspecific hybrid mice. *Oncogene* **6**, 2363-2369.

Calautti, E., Cabodi, S., Stein, P. L., Hatzfeld, M., Kedersha, N., and Paolo, D. G. (1998). Tyrosine phosphorylation and src family kinases control keratinocyte cell-cell adhesion. *J.Cell Biol.* **141**, 1449-1465.

Calautti, E., Missero, C., Stein, P. L., Ezzell, R. M., and Dotto, G. P. (1995). Fyn tyrosine kinase is involved in keratinocyte differentiation control. *Genes Dev.* **9**, 2279-2291.

Cavigelli, M., Li, W. W., Lin, A., Su, B., Yoshioka, K., and Karin, M. (1996). The tumor promoter arsenite stimulates AP-1 activity by inhibiting a JNK phosphatase. *EMBO J* **15**, 6269-6279.

Chappell, W. R., Beck, B. D., Brown, K. G., Chaney, R., Cothern, R., Cothern, C. R., Irgolic, K. J., North, D. W., Thornton, I., and Tsongas, T. A. (1997). Inorganic arsenic: a need and an opportunity to improve risk assessment. *Environ.Health Perspect.* **105**, 1060-1067.

Chen, C. J., Chuang, Y. C., Lin, T. M., and Wu, H. Y. (1985). Malignant neoplasms among residents of a blackfoot disease-endemic area in Taiwan: high-arsenic artesian well water and cancers. *Cancer Res.* **45**, 5895-5899.

Chen, N. Y., Ma, W. Y., Yang, C. S., and Dong, Z. (2000). Inhibition of arsenite-induced apoptosis and AP-1 activity by epigallocatechin-3-gallate and theaflavins. *J.Environ.Pathol.Toxicol.Oncol.* **19**, 287-295.

Cheng, C., Kilkenny, A. E., Roop, D., and Yuspa, S. H. (1990). The v-ras oncogene inhibits the expression of differentiation markers and facilitates expression of cytokeratins 8 and 18 in mouse keratinocytes. *Mol.Carcinog.* **3**, 363-373.

Cherpillod, P., and Amstad, P. A. (1995). Benzo[a]pyrene-induced mutagenesis of p53 hot-spot codons 248 and 249 in human hepatocytes. *Mol.Carcinog.* **13**, 15-20.

Chopra, D. P., and Joiakim, A. P. (1991). Alterations in sugar residues in squamous metaplasia in hamster tracheal explants induced by benzo(a)pyrene and its reversal by retinoic acid. *In Vitro Cell Dev.Biol* **27A**, 229-233.

Chowdhury, U. K., Biswas, B. K., Chowdhury, T. R., Samanta, G., Mandal, B. K., Basu, G. C., Chanda, C. R., Lodh, D., Saha, K. C., Mukherjee, S. K., Roy, S., Kabir, S., Quamruzzaman, Q., and Chakraborti, D. (2000). Groundwater arsenic contamination in Bangladesh and West Bengal, India. *Environ.Health Perspect.* **108**, 393-397.

Clairambault, J., Laroche, B., Mischler, S., and Perthame, B. (2003). A mathematical model of the cell cycle and its control. *Institut National de Recherche en Infomatique et en Automatique (INRIA)* **4892**, 3-17.

Colapietro, A. M., Goodell, A. L., and Smart, R. C. (1993). Characterization of benzo[a]pyrene-initiated mouse skin papillomas for Ha-ras mutations and protein kinase C levels. *Carcinogenesis* **14**, 2289-2295.

Conti, C. J., Aldaz, C. M., O'Connell, J., Klein-Szanto, A. J., and Slaga, T. J. (1986). Aneuploidy, an early event in mouse skin tumor development. *Carcinogenesis* **7**, 1845-1848.

Corominas, M., Kamino, H., Leon, J., and Pellicer, A. (1989). Oncogene activation in human benign tumors of the skin (keratoacanthomas): is HRAS involved in differentiation as well as proliferation? *Proc.Natl.Acad.Sci.U.S.A* **86**, 6372-6376.

Dahler, A. L., Cavanagh, L. L., and Saunders, N. A. (2001). Suppression of keratinocyte growth and differentiation by transforming growth factor beta1 involves multiple signaling pathways. *J Invest Dermatol.* **116**, 266-274.

Darzynkiewicz, Z., Bedner, E., and Smolewski, P. (2001). Flow cytometry in analysis of cell cycle and apoptosis. *Semin.Hematol.* **38**, 179-193.

Daya-Grosjean, L., Robert, C., Drougard, C., Suarez, H., and Sarasin, A. (1993). High mutation frequency in ras genes of skin tumors isolated from DNA repair deficient xeroderma pigmentosum patients. *Cancer Res.* **53**, 1625-1629.

Deamant, F. D., and Iannaccone, P. M. (1987). Clonal origin of chemically induced papillomas: separate analysis of epidermal and dermal components. *J.Cell Sci.* **88 (Pt 3)**, 305-312.

Denning, M. F., Dlugosz, A. A., Howett, M. K., and Yuspa, S. H. (1993). Expression of an oncogenic rasHa gene in murine keratinocytes induces tyrosine phosphorylation and reduced activity of protein kinase C delta. *J.Biol.Chem.* **268**, 26079-26081.

Denning, M. F., Dlugosz, A. A., Threadgill, D. W., Magnuson, T., and Yuspa, S. H. (1996). Activation of the epidermal growth factor receptor signal transduction pathway stimulates tyrosine phosphorylation of protein kinase C delta. *J.Biol.Chem.* **271**, 5325-5331.

Denning, M. F., Dlugosz, A. A., Williams, E. K., Szallasi, Z., Blumberg, P. M., and Yuspa, S. H. (1995a). Specific protein kinase C isozymes mediate the induction of keratinocyte differentiation markers by calcium. *Cell Growth Differ.* **6**, 149-157.

Denning, M. F., Kazanietz, M. G., Blumberg, P. M., and Yuspa, S. H. (1995b). Cholesterol sulfate activates multiple protein kinase C isoenzymes and induces granular cell differentiation in cultured murine keratinocytes. *Cell Growth Differ.* **6**, 1619-1626.

Deucher, A., Efimova, T., and Eckert, R. L. (2002). Calcium-dependent involucrin expression is inversely regulated by protein kinase C (PKC)alpha and PKCdelta. *J.Biol.Chem.* **277**, 17032-17040.

Di Cunto, F., Topley, G., Calautti, E., Hsiao, J., Ong, L., Seth, P. K., and Dotto, G. P. (1998). Inhibitory function of p21Cip1/WAF1 in differentiation of primary mouse keratinocytes independent of cell cycle control. [see comments.]. *Science* **280**, 1069-1072.

Dicker, A. J., Popa, C., Dahler, A. L., Serewko, M. M., Hilditch-Maguire, P. A., Frazer, I., and Saunders, N. A. (2000). E2F-1 induces proliferation-specific genes and suppresses squamous differentiation-specific genes in human epidermal keratinocytes. *Oncogene* **19**, 2887-2894.

DiGiovanni, J., Gill, R. D., Nettikumara, A. N., Colby, A. B., and Reiners, J. J., Jr. (1989). Effect of extracellular calcium concentration on the metabolism of polycyclic aromatic hydrocarbons by cultured mouse keratinocytes. *Cancer Res.* **49**, 5567-5574.

DiGiovanni, J., Walker, S. C., Beltran, L., Naito, M., and Eastin, W. C., Jr. (1991). Evidence for a common genetic pathway controlling susceptibility to mouse skin tumor promotion by diverse classes of promoting agents. *Cancer Res.* **51**, 1398-1405.

Dlugosz, A. A., and Yuspa, S. H. (1991). Staurosporine induces protein kinase C agonist effects and maturation of normal and neoplastic mouse keratinocytes in vitro. *Cancer Res.* **51**, 4677-4684.

Dlugosz, A. A., and Yuspa, S. H. (1993). Coordinate changes in gene expression which mark the spinous to granular cell transition in epidermis are regulated by protein kinase C. *J.Cell Biol.* **120**, 217-225.

Dong, J. T., and Luo, X. M. (1993). Arsenic-induced DNA-strand breaks associated with DNA-protein crosslinks in human fetal lung fibroblasts. *Mutat.Res.* **302**, 97-102.

Dotto, G. P. (1999). Signal transduction pathways controlling the switch between keratinocyte growth and differentiation. *Crit Rev Oral Biol Med* **10**, 442-457.

Dotto, G. P., O'Connell, J., Patskan, G., Conti, C., Ariza, A., and Slaga, T. J. (1988). Malignant progression of papilloma-derived keratinocytes: differential effects of the ras, neu, and p53 oncogenes. *Mol.Carcinog.* **1**, 171-179.

Dover, R., and Watt, F. M. (1987). Measurement of the rate of epidermal terminal differentiation: expression of involucrin by S-phase keratinocytes in culture and in psoriatic plaques. *J.Invest Dermatol.* **89**, 349-352.

Eckert, R. L. (1989). Structure, function, and differentiation of the keratinocyte. *Physiol Rev.* **69**, 1316-1346.

Eckert, R. L., Crish, J. F., and Saunders, N. A. (1997). The epidermal keratinocyte as a model for the study of gene regulation and cell differentiation. *Physiological Reviews* **77**, 397-424.

Edmondson, S. W., and Mossman, B. T. (1991). Alterations in keratin expression in hamster tracheal epithelial cells exposed to benzo[a]pyrene. *Carcinogenesis* **12**, 679-684.

Elias, P. M., Menon, G. K., Grayson, S., and Brown, B. E. (1988). Membrane structural alterations in murine stratum corneum: relationship to the localization of polar lipids and phospholipases. *J.Invest Dermatol.* **91**, 3-10.

Elias, P. M., Nau, P., Hanley, K., Cullander, C., Crumrine, D., Bench, G., Sideras-Haddad, E., Mauro, T., Williams, M. L., and Feingold, K. R. (1998). Formation of the epidermal calcium gradient coincides with key milestones of barrier ontogenesis in the rodent. *J.Invest Dermatol.* **110**, 399-404.

Endl, E., Kausch, I., Baack, M., Knippers, R., Gerdes, J., and Scholzen, T. (2001). The expression of Ki-67, MCM3, and p27 defines distinct subsets of proliferating, resting, and differentiated cells. *J.Pathol.* **195**, 457-462.

Fagotto, F., and Gumbiner, B. M. (1996). Cell contact-dependent signaling. *Dev.Biol.* **180**, 445-454.

Filvaroff, E., Calautti, E., McCormick, F., and Dotto, G. P. (1992). Specific changes of Ras GTPase-activating protein (GAP) and a GAP-associated p62 protein during calcium-induced keratinocyte differentiation. *Mol.Cell Biol.* **12**, 5319-5328.

Filvaroff, E., Calautti, E., Reiss, M., and Dotto, G. P. (1994). Functional evidence for an extracellular calcium receptor mechanism triggering tyrosine kinase activation associated with mouse keratinocyte differentiation. *Journal of Biological Chemistry* **269**, 21735-21740.

Filvaroff, E., Stern, D. F., and Dotto, G. P. (1990). Tyrosine phosphorylation is an early and specific event involved in primary keratinocyte differentiation. *Mol.Cell Biol.* **10**, 1164-1173.

Finzi, E., Fleming, T., Segatto, O., Pennington, C. Y., Bringman, T. S., Derynck, R., and Aaronson, S. A. (1987). The human transforming growth factor type alpha coding sequence is not a direct-acting oncogene when overexpressed in NIH 3T3 cells. *Proc.Natl.Acad.Sci.U.S.A* **84**, 3733-3737.

Finzi, E., Kilkenny, A., Strickland, J. E., Balaschak, M., Bringman, T., Derynck, R., Aaronson, S., and Yuspa, S. H. (1988). TGF alpha stimulates growth of skin papillomas by autocrine and paracrine mechanisms but does not cause neoplastic progression. *Mol.Carcinog.* **1**, 7-12.

Frisch, S. M., and Ruoslahti, E. (1997). Integrins and anoikis. *Curr.Opin.Cell Biol.* **9**, 701-706.

Fuchs, E. (1990). Epidermal differentiation: the bare essentials. *J.Cell Biol.* **111**, 2807-2814.

Fuchs, E. (1993). Epidermal Differentiation and Keratin Gene Expression. *Journal of Cell Science* **Supplement 17**, 197-208.

Fuchs, E., Dowling, J., Segre, J., Lo, S. H., and Yu, Q. C. (1997). Integrators of epidermal growth and differentiation: distinct functions for beta 1 and beta 4 integrins. *Curr.Opin.Genet.Dev.* **7**, 672-682.

Fuchs, E., and Green, H. (1980). Changes in keratin gene expression during terminal differentiation of the keratinocyte. *Cell* **19**, 1033-1042.

Gandarillas, A., Davies, D., and Blanchard, J. M. (2000). Normal and c-Myc-promoted human keratinocyte differentiation both occur via a novel cell cycle involving cellular growth and endoreplication. *Oncogene* **19**, 3278-3289.

Gandarillas, A., and Watt, F. M. (1997). c-Myc promotes differentiation of human epidermal stem cells. *Genes Dev.* **11**, 2869-2882.

Germolec, D. R., Spalding, J., Yu, H. S., Chen, G. S., Simeonova, P. P., Humble, M. C., Bruccoleri, A., Boorman, G. A., Foley, J. F., Yoshida, T., and Luster, M. I. (1998). Arsenic enhancement of skin neoplasia by chronic stimulation of growth factors. *Am.J Pathol.* **153**, 1775-1785.

Germolec, D. R., Yoshida, T., Gaido, K., Wilmer, J. L., Simeonova, P. P., Kayama, F., Burleson, F., Dong, W., Lange, R. W., and Luster, M. I. (1996). Arsenic induces overexpression of growth factors in human keratinocytes. *Toxicology and Applied Pharmacology* **141**, 308-318.

Gerwin, B. I., Spillare, E., Forrester, K., Lehman, T. A., Kispert, J., Welsh, J. A., Pfeifer, A. M., Lechner, J. F., Baker, S. J., Vogelstein, B., and . (1992). Mutant p53 can induce tumorigenic conversion of human bronchial epithelial cells and reduce their responsiveness to a negative growth factor, transforming growth factor beta 1. *Proc.Natl.Acad.Sci.U.S.A* **89**, 2759-2763.

Giancotti, F. G. (1997). Integrin signaling: specificity and control of cell survival and cell cycle progression. *Curr.Opin.Cell Biol.* **9**, 691-700.

Gibson, D. F., Ratnam, A. V., and Bikle, D. D. (1996). Evidence for separate control mechanisms at the message, protein, and enzyme activation levels for transglutaminase during calcium-induced differentiation of normal and transformed human keratinocytes. *J.Invest Dermatol.* **106**, 154-161.

Gilmore, T. D. (1997). Clinically relevant findings. *J.Clin.Invest.* **100**, 2935-2936.

Glick, A. B., Kulkarni, A. B., Tennenbaum, T., Hennings, H., Flanders, K. C., O'Reilly, M., Sporn, M. B., Karlsson, S., and Yuspa, S. H. (1993). Loss of expression of

transforming growth factor beta in skin and skin tumors is associated with hyperproliferation and a high risk for malignant conversion. *Proc.Natl.Acad.Sci.U.S.A* **90**, 6076-6080.

Glick, A. B., Sporn, M. B., and Yuspa, S. H. (1991). Altered regulation of TGF-beta 1 and TGF-alpha in primary keratinocytes and papillomas expressing v-Ha-ras. *Mol.Carcinog.* **4**, 210-219.

Gold, L. I., Jussila, T., Fusenig, N. E., and Stenback, F. (2000). TGF-beta isoforms are differentially expressed in increasing malignant grades of HaCaT keratinocytes, suggesting separate roles in skin carcinogenesis. *J Pathol.* **190**, 579-588.

Gorisse, M. C., Venteo, L., and Pluot, M. (1999). A method for simultaneous quantification of monoclonal antibody Ki-67 and DNA content by flow cytometry. Application to breast carcinomas. *Anal.Quant.Cytol.Histol.* **21**, 8-16.

Green, H. (1977). Terminal differentiation of cultured human epidermal cells. *Cell* **11**, 405-416.

Green, H., Fuchs, E., and Watt, F. (1982). Differentiated structural components of the keratinocyte. *Cold Spring Harb.Symp.Quant.Biol.* **46 Pt 1**, 293-301.

Greenhalgh, D. A., Rothnagel, J. A., Quintanilla, M. I., Orengo, C. C., Gagne, T. A., Bundman, D. S., Longley, M. A., and Roop, D. R. (1993). Induction of epidermal hyperplasia, hyperkeratosis, and papillomas in transgenic mice by a targeted v-Ha-ras oncogene. *Mol.Carcinog.* **7**, 99-110.

Greenhalgh, D. A., Welty, D. J., Strickland, J. E., and Yuspa, S. H. (1989). Spontaneous Ha-ras gene activation in cultured primary murine keratinocytes: consequences of Ha-ras gene activation in malignant conversion and malignant progression. *Mol.Carcinog.* **2**, 199-207.

Greenhalgh, D. A., and Yuspa, S. H. (1988). Malignant conversion of murine squamous papilloma cell lines by transfection with the fos oncogene. *Mol.Carcinog.* **1**, 134-143.

Guengerich, F. P., Johnson, W. W., Ueng, Y. F., Yamazaki, H., and Shimada, T. (1996). Involvement of cytochrome P450, glutathione S-transferase, and epoxide hydrolase in the metabolism of aflatoxin B1 and relevance to risk of human liver cancer. *Environ.Health Perspect.* **104 Suppl 3**, 557-562.

Guengerich, F. P., and Shimada, T. (1998). Activation of procarcinogens by human cytochrome P450 enzymes. *Mutat.Res.* **400**, 201-213.

Gurr, J. R., Lin, Y. C., Ho, I. C., Jan, K. Y., and Lee, T. C. (1993). Induction of chromatid breaks and tetraploidy in Chinese hamster ovary cells by treatment with sodium arsenite during the G2 phase. *Mutat.Res.* **319**, 135-142.

Guyda, H. J., Mathieu, L., Lai, W., Manchester, D., Wang, S. L., Ogilvie, S., and Shiverick, K. T. (1990). Benzo(a)pyrene inhibits epidermal growth factor binding and receptor autophosphorylation in human placental cell cultures. *Mol.Pharmacol.* **37**, 137-143.

Hamadeh, H. K., Vargas, M., Lee, E., and Menzel, D. B. (1999). Arsenic disrupts cellular levels of p53 and mdm2: a potential mechanism of carcinogenesis. *Biochemical & Biophysical Research Communications* **263**, 446-449.

Hanelt, S., Helbig, R., Hartmann, A., Lang, M., Seidel, A., and Speit, G. (1997). A comparative investigation of DNA adducts, DNA strand breaks and gene mutations induced by benzo[a]pyrene and (+/-)-*anti*-benzo[a]pyrene-7,8-diol 9,10-oxide in cultured human cells. *Mutation Research* **390**, 179-188.

Harper, J. R., Reynolds, S. H., Greenhalgh, D. A., Strickland, J. E., Lacal, J. C., and Yuspa, S. H. (1987). Analysis of the rasH oncogene and its p21 product in chemically induced skin tumors and tumor-derived cell lines. *Carcinogenesis* **8**, 1821-1825.

Harper, J. R., Roop, D. R., and Yuspa, S. H. (1986). Transfection of the EJ rasHa gene into keratinocytes derived from carcinogen-induced mouse papillomas causes malignant progression. *Mol.Cell Biol.* **6**, 3144-3149.

Hartley, J. A., Gibson, N. W., Kilkenny, A., and Yuspa, S. H. (1987). Mouse keratinocytes derived from initiated skin or papillomas are resistant to DNA strand breakage by benzoyl peroxide: a possible mechanism for tumor promotion mediated by benzoyl peroxide. *Carcinogenesis* **8**, 1827-1830.

Hartwig, A., Asmuss, M., Ehleben, I., Herzer, U., Kostelac, D., Pelzer, A., Schwerdtle, T., and Burkle, A. (2002). Interference by toxic metal ions with DNA repair processes and cell cycle control: molecular mechanisms. *Environ.Health Perspect.* **110 Suppl 5**, 797-799.

Hartwig, A., Blessing, H., Schwerdtle, T., and Walter, I. (2003). Modulation of DNA repair processes by arsenic and selenium compounds. *Toxicology* **193**, 161-169.

Hattori, Y., Nishigori, C., Tanaka, T., Uchida, K., Nikaido, O., Osawa, T., Hiai, H., Imamura, S., and Toyokuni, S. (1996). 8-hydroxy-2'-deoxyguanosine is increased in epidermal cells of hairless mice after chronic ultraviolet B exposure. *J.Invest Dermatol.* **107**, 733-737.

Hauser, P. J., Agrawal, D., Hackney, J., and Pledger, W. J. (1998). STAT3 activation accompanies keratinocyte differentiation. *Cell Growth Differ.* **9**, 847-855.

Hawley-Nelson, P., Sullivan, J. E., Kung, M., Hennings, H., and Yuspa, S. H. (1980). Optimized conditions for the growth of human epidermal cells in culture. *J.Invest Dermatol.* **75**, 176-182.

Heenen, M., and Galand, P. (1997). The growth fraction of normal human epidermis. *Dermatology* **194**, 313-317.

Hei, T. K., Liu, S. X., and Waldren, C. (1998). Mutagenicity of arsenic in mammalian cells: role of reactive oxygen species. *Proc.Natl.Acad.Sci.U.S.A* **95**, 8103-8107.

Hennings, H., Blumberg, P. M., Pettit, G. R., Herald, C. L., Shores, R., and Yuspa, S. H. (1987a). Bryostatin 1, an activator of protein kinase C, inhibits tumor promotion by phorbol esters in SENCAR mouse skin. *Carcinogenesis* **8**, 1343-1346.

Hennings, H., Holbrook, K., Steinert, P., and Yuspa, S. (1980a). Growth and differentiation of mouse epidermal cells in culture: effects of extracellular calcium. *Curr.Probl.Dermatol.* **10**, 3-25.

Hennings, H., Lowry, D. T., Robinson, V. A., Morgan, D. L., Fujiki, H., and Yuspa, S. H. (1992). Activity of diverse tumor promoters in a keratinocyte co-culture model of initiated epidermis. *Carcinogenesis* **13**, 2145-2151.

Hennings, H., Michael, D., Cheng, C., Steinert, P., Holbrook, K., and Yuspa, S. H. (1980b). Calcium regulation of growth and differentiation of mouse epidermal cells in culture. *Cell* **19**, 245-254.

Hennings, H., Michael, D., Lichti, U., and Yuspa, S. H. (1987b). Response of carcinogen-altered mouse epidermal cells to phorbol ester tumor promoters and calcium. *J.Invest Dermatol.* **88**, 60-65.

Hennings, H., Robinson, V. A., Michael, D. M., Pettit, G. R., Jung, R., and Yuspa, S. H. (1990a). Development of an in vitro analogue of initiated mouse epidermis to study tumor promoters and antipromoters. *Cancer Res.* **50**, 4794-4800.

Hennings, H., Shores, R., Wenk, M. L., Spangler, E. F., Tarone, R., and Yuspa, S. H. (1983). Malignant conversion of mouse skin tumours is increased by tumour initiators and unaffected by tumour promoters. *Nature* **304**, 67-69.

Hennings, H., Shores, R. A., Poirier, M. C., Reed, E., Tarone, R. E., and Yuspa, S. H. (1990b). Enhanced malignant conversion of benign mouse skin tumors by cisplatin. *J.Natl.Cancer Inst.* **82**, 836-840.

Hiyama, H., Iavarone, A., LaBaer, J., and Reeves, S. A. (1997). Regulated ectopic expression of cyclin D1 induces transcriptional activation of the cdk inhibitor p21 gene without altering cell cycle progression. *Oncogene* **14**, 2533-2542.

Hohl, D., Mehrel, T., Lichti, U., Turner, M. L., Roop, D. R., and Steinert, P. M. (1991). Characterization of human loricrin. Structure and function of a new class of epidermal cell envelope proteins. *J.Biol.Chem.* **266**, 6626-6636.

Holbrook, K. A., and Wolff, K. (1987). *Dermatology in General Medicine*. McGraw Hill, New York.

Hosomi, J., Hosoi, J., Abe, E., Suda, T., and Kuroki, T. (1983). Regulation of terminal differentiation of cultured mouse epidermal cells by 1 alpha,25-dihydroxyvitamin D3. *Endocrinology* **113**, 1950-1957.

Hu, Y., Baud, V., Oga, T., Kim, K. I., Yoshida, K., and Karin, M. (2001). IKKalpha controls formation of the epidermis independently of NF-kappaB. *Nature* **410**, 710-714.

Hu, Y., Su, L., and Snow, E. T. (1998). Arsenic toxicity is enzyme specific and its affects on ligation are not caused by the direct inhibition of DNA repair enzymes. *Mutat.Res.* **408**, 203-218.

Huang, C., Bode, A. M., Chen, N. Y., Ma, W. Y., Li, J., Nomura, M., and Dong, Z. (2001a). Transactivation of AP-1 in AP-1-luciferase reporter transgenic mice by arsenite and arsenate. *Anticancer Res.* **21**, 261-267.

Huang, C., Li, J., Ding, M., Wang, L., Shi, X., Castranova, V., Vallyathan, V., Ju, G., and Costa, M. (2001b). Arsenic-induced NFkappaB transactivation through Erks- and JNKs-dependent pathways in mouse epidermal JB6 cells. *Mol.Cell Biochem.* **222**, 29-34.

Huang, C., Ma, W. Y., Li, J., and Dong, Z. (1999). Arsenic induces apoptosis through a c-Jun NH2-terminal kinase-dependent, p53-independent pathway. *Cancer Res.* **59**, 3053-3058.

Hughes, M. F. (2002). Arsenic toxicity and potential mechanisms of action. *Toxicol.Lett.* **133**, 1-16.

Hurlin, P. J., Foley, K. P., Ayer, D. E., Eisenman, R. N., Hanahan, D., and Arbeit, J. M. (1995). Regulation of Myc and Mad during epidermal differentiation and HPV-associated tumorigenesis. *Oncogene* **11**, 2487-2501.

Hynes, R. O. (1992). Integrins: versatility, modulation, and signaling in cell adhesion. *Cell* **69**, 11-25.

Iannaccone, P. M., Weinberg, W. C., and Deamant, F. D. (1987). On the clonal origin of tumors: a review of experimental models. *Int.J.Cancer* **39**, 778-784.

Iizuka, H. (1994). Epidermal turnover time. *J.Dermatol.Sci.* **8**, 215-217.

Imamoto, A., Beltran, L. M., and DiGiovanni, J. (1991). Evidence for autocrine/paracrine growth stimulation by transforming growth factor-alpha during the process of skin tumor promotion. *Mol.Carcinog.* **4**, 52-60.

Iskander, K., Paquet, M., Brayton, C., and Jaiswal, A. K. (2004). Deficiency of NRH:quinone oxidoreductase 2 increases susceptibility to 7,12-dimethylbenz(a)anthracene and benzo(a)pyrene-induced skin carcinogenesis. *Cancer Res.* **64**, 5925-5928.

Ivanovic, V., and Weinstein, I. B. (1982). Benzo[a]pyrene and other inducers of cytochrome P1-450 inhibit binding of epidermal growth factor to cell surface receptors. *Carcinogenesis* **3**, 505-510.

Jaken, S., and Yuspa, S. H. (1988). Early signals for keratinocyte differentiation: role of Ca2+-mediated inositol lipid metabolism in normal and neoplastic epidermal cells. *Carcinogenesis* **9**, 1033-1038.

Jensen, K. G., Onfelt, A., Poulsen, H. E., Doehmer, J., and Loft, S. (1993). Effects of benzo[a]pyrene and (+-)-trans-7,8-dihydroxy-7,8-dihydrobenzo[a]pyrene on mitosis in Chinese hamster V79 cells with stable expression of rat cytochrome P4501A1 or 1A2. *Carcinogenesis* **14**, 2115-2118.

Jensen, U. B., Lowell, S., and Watt, F. M. (1999). The spatial relationship between stem cells and their progeny in the basal layer of human epidermis: a new view based on whole-mount labelling and lineage analysis. *Development* **126**, 2409-2418.

Jessen, B. A., Qin, Q., Phillips, M. A., Phillips, D. L., and Rice, R. H. (2001). Keratinocyte differentiation marker suppression by arsenic: mediation by AP1 response elements and antagonism by tetradecanoylphorbol acetate. *Toxicology & Applied Pharmacology* **174**, 302-311.

Jessen, B. A., Qin, Q., and Rice, R. H. (2000). Functional AP1 and CRE response elements in the human keratinocyte transglutaminase promoter mediating Whn suppression. *Gene* **254**, 77-85.

Jha, A. N., Noditi, M., Nilsson, R., and Natarajan, A. T. (1992). Genotoxic effects of sodium arsenite on human cells. *Mutation Research* **284**, 215-221.

Johansen, C., Iversen, L., Ryborg, A., and Kragballe, K. (2000). 1alpha,25-dihydroxyvitamin D3 induced differentiation of cultured human keratinocytes is accompanied by a PKC-independent regulation of AP-1 DNA binding activity. *J Invest Dermatol.* **114**, 1174-1179.

Jones, P. H., Harper, S., and Watt, F. M. (1995). Stem cell patterning and fate in human epidermis. *Cell* **80**, 83-93.

Jones, P. H., and Watt, F. M. (1993). Separation of human epidermal stem cells from transit amplifying cells on the basis of differences in integrin function and expression. *Cell* **73**, 713-724.

Kachinskas, D. J., Phillips, M. A., Qin, Q., Strokes, J. D., and Rice, R. H. (1994). Arsenate perturbation of human keratinocyte differentiation. *Cell Growth Differ.* **5**, 12235-1241.

Kallassy, M., Martel, N., Damour, O., Yamasaki, H., and Nakazawa, H. (1998). Growth arrest of immortalized human keratinocytes and suppression of telomerase activity by p21WAF1 gene expression. *Mol.Carcinog.* **21**, 26-36.

Kanjilal, S., Pierceall, W. E., Cummings, K. K., Kripke, M. L., and Ananthaswamy, H. N. (1993). High frequency of p53 mutations in ultraviolet radiation-induced murine skin tumors: evidence for strand bias and tumor heterogeneity. *Cancer Res.* **53**, 2961-2964.

Kashiwagi, M., Ohba, M., Chida, K., and Kuroki, T. (2002). Protein kinase C eta (PKC eta): its involvement in keratinocyte differentiation. *J.Biochem.(Tokyo)* **132**, 853-857.

Kashiwagi, M., Ohba, M., Watanabe, H., Ishino, K., Kasahara, K., Sanai, Y., Taya, Y., and Kuroki, T. (2000). PKCeta associates with cyclin E/cdk2/p21 complex, phosphorylates p21 and inhibits cdk2 kinase in keratinocytes. *Oncogene* **19**, 6334-6341.

Kawamura, H., Strickland, J. E., and Yuspa, S. H. (1985). Association of resistance to terminal differentiation with initiation of carcinogenesis in adult mouse epidermal cells. *Cancer Res.* **45**, 2748-2752.

Kemp, C. J., Donehower, L. A., Bradley, A., and Balmain, A. (1993). Reduction of p53 gene dosage does not increase initiation or promotion but enhances malignant progression of chemically induced skin tumors. *Cell* **74**, 813-822.

Kilkenny, A. E., Morgan, D., Spangler, E. F., and Yuspa, S. H. (1985). Correlation of initiating potency of skin carcinogens with potency to induce resistance to terminal differentiation in cultured mouse keratinocytes. *Cancer Res.* **45**, 2219-2225.

Kimmel, M., Bajkowska, K., and Rytwinski, K. (1985). A simple model of cell cycle dynamics with application to estimation of cell cycle parameters. *Acta Haematol.Pol.* **16**, 1-6.

Kimmel, M., Darzynkiewicz, Z., and Staiano-Coico, L. (1986). Stathmokinetic analysis of human epidermal cells *in vitro*. *Cell Tissues Kinet.* **19**, 289-304.

Kimmel, M., Traganos, F., and Darzynkiewicz, Z. (1983). Do all daughter cells enter the "indeterminate" ("A") state of the cell cycle? Analysis of stathmokinetic experiments on L1210 cells. *Cytometry* **4**, 191-201.

Knowles, F. C., and Benson, A. A. (1984). The enzyme inhibitory form of inorganic arsenic. *Z.Gesamte Hyg.* **30**, 625-626.

Kress, S., Sutter, C., Strickland, P. T., Mukhtar, H., Schweizer, J., and Schwarz, M. (1992). Carcinogen-specific mutational pattern in the p53 gene in ultraviolet B radiation-induced squamous cell carcinomas of mouse skin. *Cancer Res.* **52**, 6400-6403.

Kulesz-Martin, M., Kilkenny, A. E., Holbrook, K. A., Digernes, V., and Yuspa, S. H. (1983). Properties of carcinogen altered mouse epidermal cells resistant to calcium-induced terminal differentiation. *Carcinogenesis* **4**, 1367-1377.

Kulesz-Martin, M. F., Koehler, B., Hennings, H., and Yuspa, S. H. (1980). Quantitative assay for carcinogen altered differentiation in mouse epidermal cells. *Carcinogenesis* **1**, 995-1006.

Lajtha, L. G. (1979). Stem cell concepts. *Differentiation* **14**, 23-34.

Lamerton, L. F., and Steel, G. G. (1968). Cell population kinetics in normal and malignant tissues. *Prog.Biophys.Mol.Biol.* **18**, 245-283.

Landolph, J. R. (1994). Molecular mechanisms of transformation of C3H/10T1/2 C1 8 mouse embryo cells and diploid human fibroblasts by carcinogenic metal compounds. *Environ.Health Perspect.* **102 Suppl 3**, 119-125.

Lansdown, A. B. (1995). Physiological and toxicological changes in the skin resulting from the action and interaction of metal ions. *Crit Rev.Toxicol.* **25**, 397-462.

Laporte, M., Galand, P., Fokan, D., Degraef, C., and Heenen, M. (1996). Apoptosis in normal skin, psoriasis and regressing psoriasis. *J.Invest.Dermatol.* **106**, 865.

Lavker, R. M., Miller, S. J., and Sun, T. T. (1993). Epithelial stem cells, hair follicles, and tumor formation. *Recent Results Cancer Res.* **128**, 31-43.

Lee, E., Punnonen, K., Cheng, C., Glick, A., Dlugosz, A., and Yuspa, S. H. (1992). Analysis of phospholipid metabolism in murine keratinocytes transformed by the v-ras oncogene: relationship of phosphatidylinositol turnover and cytokine stimulation to the transformed phenotype. *Carcinogenesis* **13**, 2367-2373.

Lee, P. N., and O'Neill, J. A. (1971). The effect both of time and dose applied on tumour incidence rate in benzopyrene skin painting experiments. *Br.J Cancer* **25**, 759-770.

Lee, T. C., Tanaka, N., Lamb, P. W., Gilmer, T. M., and Barrett, J. C. (1988). Induction of gene amplification by arsenic. *Science* **241**, 79-81.

Leon, J., Kamino, H., Steinberg, J. J., and Pellicer, A. (1988). H-ras activation in benign and self-regressing skin tumors (keratoacanthomas) in both humans and an animal model system. *Mol.Cell Biol.* **8**, 786-793.

Levy, L., Broad, S., Diekmann, D., Evans, R. D., and Watt, F. M. (2000). beta1 integrins regulate keratinocyte adhesion and differentiation by distinct mechanisms. *Mol.Biol.Cell* **11**, 453-466.

Lewis, J. E., Jensen, P. J., Johnson, K. R., and Wheelock, M. J. (1994). E-cadherin mediates adherens junction organization through protein kinase C. *J.Cell Sci.* **107 (Pt 12)**, 3615-3621.

Li, J. H., and Rossman, T. G. (1989). Mechanism of comutagenesis of sodium arsenite with n-methyl-n-nitrosourea. *Biol.Trace Elem.Res.* **21**, 373-381.

Li, J. J., Cao, Y., Young, M. R., and Colburn, N. H. (2000). Induced expression of dominant-negative *c-jun* downregulates NFkB and AP-1 target genes and suppresses tumor phenotype in human keratinocytes. *Molecular Carcinogenesis* **29**, 159-169.

Li, L., Tennenbaum, T., and Yuspa, S. H. (1996). Suspension-induced murine keratinocyte differentiation is mediated by calcium. *J.Invest Dermatol.* **106**, 254-260.

Li, L., Tucker, R. W., Hennings, H., and Yuspa, S. H. (1995). Chelation of intracellular Ca2+ inhibits murine keratinocyte differentiation in vitro. *J.Cell Physiol* **163**, 105-114.

Liao, W. T., Chang, K. L., Yu, C. L., Chen, G. S., Chang, L. W., and Yu, H. S. (2004). Arsenic induces human keratinocyte apoptosis by the FAS/FAS ligand pathway, which correlates with alterations in nuclear factor-kappa B and activator protein-1 activity. *J.Invest Dermatol.* **122**, 125-129.

Lindgren, A., Vahter, M., and Dencker, L. (1982). Autoradiographic studies on the distribution of arsenic in mice and hamsters administered 74As-arsenite or -arsenate. *Acta Pharmacol.Toxicol.(Copenh)* **51**, 253-265.

Loeffler, M., Potten, C. S., and Wichmann, H. E. (1987). Epidermal Cell Proliferation: A Comprehensive Mathematical Model of Cell Proliferation and Migration in the Basal Layer predicts some Unusual Properties of Epidermal Stem Cells. *Virchows Arch B* **53**, 286-300.

Look, D. C., Pelletier, M. R., Tidwell, R. M., Roswit, W. T., and Holtzman, M. J. (1995). Stat1 depends on transcriptional synergy with Sp1. *J.Biol.Chem.* **270**, 30264-30267.

Lynn, S., Gurr, J. R., Lai, H. T., and Jan, K. Y. (2000). NADH oxidase activation is involved in arsenite-induced oxidative DNA damage in human vascular smooth muscle cells. *Circ.Res.* **86**, 514-519.

Mager, R., Huberman, E., Yang, S. K., Gelboin, H. V., and Sachs, L. (1977). Transformation of normal hamster cells by benzo(a)pyrene diol-epoxide. *Int.J.Cancer* **19**, 814-817.

Maier, A., Schumann, B. L., Chang, X., Talaska, G., and Puga, A. (2002). Arsenic co-exposure potentiates benzo[a]pyrene genotoxicity. *Mutat.Res.* **517**, 101-111.

Mainiero, F., Murgia, C., Wary, K. K., Curatola, A. M., Pepe, A., Blumemberg, M., Westwick, J. K., Der, C. J., and Giancotti, F. G. (1997). The coupling of alpha6beta4 integrin to Ras-MAP kinase pathways mediated by Shc controls keratinocyte proliferation. *EMBO J.* **16**, 2365-2375.

Malmquist, K. G., Carlsson, L.-E., Forslind, B., Roomans, G. M., and Akselsson, K. R. (1984). Proton and electron microprobe analysis of human skin. *Nucl.Instr.Met.Physics.Res.* **3**, 611-617.

Marshall, C. J., Vousden, K. H., and Phillips, D. H. (1984). Activation of c-Ha-ras-1 proto-oncogene by in vitro modification with a chemical carcinogen, benzo(a)pyrene diol-epoxide. *Nature* **310**, 586-589.

Matoltsy, A. G., and Matoltsy, M. N. (1966). The membrane protein of horny cells. *J.Invest Dermatol.* **46**, 127-129.

McNeil, S. E., Hobson, S. A., Nipper, V., and Rodland, K. D. (1998). Functional calcium-sensing receptors in rat fibroblasts are required for activation of SRC kinase and mitogen-activated protein kinase in response to extracellular calcium. *J.Biol.Chem.* **273**, 1114-1120.

Mehrel, T., Hohl, D., Rothnagel, J. A., Longley, M. A., Bundman, D., Cheng, C., Lichti, U., Bisher, M. E., Steven, A. C., Steinert, P. M., and . (1990). Identification of a major keratinocyte cell envelope protein, loricrin. *Cell* **61**, 1103-1112.

Mendelsohn, M. L. (1960). The growth fraction: a new concept applied to tumours. *Science* **132**, 1496.

Menon, G. K., Grayson, S., and Elias, P. M. (1985). Ionic calcium reservoirs in mammalian epidermis: ultrastructural localization by ion-capture cytochemistry. *J.Invest Dermatol.* **84**, 508-512.

Miller, M. L., Vasunia, K., Talaska, G., Andringa, A., de Boer, J., and Dixon, K. (2000). The tumor promoter TPA enhances benzo[a]pyrene and benzo[a]pyrene diolepoxide mutagenesis in Big Blue mouse skin. *Environ.Mol.Mutagen.* **35**, 319-327.

Missero, C., Calautti, E., Eckner, R., Chin, J., Tsai, L. H., Livingston, D. M., and Dotto, G. P. (1995). Involvement of the cell-cycle inhibitor Cip1/WAF1 and the E1A-associated p300 protein in terminal differentiation. *Proceedings of the National Academy of Sciences of the United States of America* **92**, 5451-5455.

Moles, J. P., and Watt, F. M. (1997). The epidermal stem cell compartment: variation in expression levels of E-cadherin and catenins within the basal layer of human epidermis. *J.Histochem.Cytochem.* **45**, 867-874.

Monzon, R. I., McWilliams, N., and Hudson, L. G. (1996). Suppression of cornified envelope formation and type 1 transglutaminase by epidermal growth factor in neoplastic keratinocytes. *Endocrinology* **137**, 1727-1734.

Mure, K., Uddin, A. N., Lopez, L. C., Styblo, M., and Rossman, T. G. (2003). Arsenite induces delayed mutagenesis and transformation in human osteosarcoma cells at extremely low concentrations. *Environ.Mol.Mutagen.* **41**, 322-331.

Naito, M., Chenicek, K. J., Naito, Y., and DiGiovanni, J. (1988). Susceptibility to phorbol ester skin tumor promotion in (C57BL/6 x DBA/2) F1 mice is inherited as an incomplete dominant trait: evidence for multi-locus involvement. *Carcinogenesis* **9**, 639-645.

Nehls, M., Kyewski, B., Messerle, M., Waldschutz, R., Schuddekopf, K., Smith, A. J., and Boehm, T. (1996). Two genetically separable steps in the differentiation of thymic epithelium. *Science* **272**, 886-889.

Nelson, M. A., Futscher, B. W., Kinsella, T., Wymer, J., and Bowden, G. T. (1992). Detection of mutant Ha-ras genes in chemically initiated mouse skin epidermis before the development of benign tumors. *Proc.Natl.Acad.Sci.U.S.A* **89**, 6398-6402.

O'Connell, J. F., Klein-Szanto, A. J., Digiovanni, D. M., Fries, J. W., and Slaga, T. J. (1986). Malignant progression of mouse skin papillomas treated with ethylnitrosourea, N-methyl-N'-nitro-N-nitrosoguanidine, or 12-O-tetradecanoylphorbol-13-acetate. *Cancer Lett.* **30**, 269-274.

Ogryzko, V. V., Schiltz, R. L., Russanova, V., Howard, B. H., and Nakatani, Y. (1996). The transcriptional coactivators p300 and CBP are histone acetyltransferases. *Cell* **87**, 953-959.

Ohba, M., Ishino, K., Kashiwagi, M., Kawabe, S., Chida, K., Huh, N. H., and Kuroki, T. (1998). Induction of differentiation in normal human keratinocytes by adenovirus-mediated introduction of the eta and delta isoforms of protein kinase C. *Mol.Cell Biol.* **18**, 5199-5207.

O'Keefe, E. J., Briggaman, R. A., and Herman, B. (1987). Calcium-induced assembly of adherens junctions in keratinocytes. *J.Cell Biol.* **105**, 807-817.

Ormerod, M. G., Orr, R. M., and Peacock, J. H. (1994). The role of apoptosis in cell killing by cisplatin: a flow cytometric study. *Br.J.Cancer* **69**, 93-100.

Osada, S., Hashimoto, Y., Nomura, S., Kohno, Y., Chida, K., Tajima, O., Kubo, K., Akimoto, K., Koizumi, H., Kitamura, Y., and . (1993). Predominant expression of nPKC eta, a Ca(2+)-independent isoform of protein kinase C in epithelial tissues, in association with epithelial differentiation. *Cell Growth Differ.* **4**, 167-175.

Osada, S., Mizuno, K., Saido, T. C., Akita, Y., Suzuki, K., Kuroki, T., and Ohno, S. (1990). A phorbol ester receptor/protein kinase, nPKC eta, a new member of the protein kinase C family predominantly expressed in lung and skin. *J.Biol.Chem.* **265**, 22434-22440.

Ou, X., and Ramos, K. S. (1994). Benzo[a]pyrene inhibits protein kinase C activity in subcultured rat aortic smooth muscle cells. *Chem.Biol.Interact.* **93**, 29-40.

Ou, X., Weber, T. J., Chapkin, R. S., and Ramos, K. S. (1995). Interference with protein kinase C-related signal transduction in vascular smooth muscle cells by benzo[a]pyrene. *Arch.Biochem.Biophys.* **318**, 122-130.

Owens, D. M., and Watt, F. M. (2001). Influence of beta1 integrins on epidermal squamous cell carcinoma formation in a transgenic mouse model: alpha3beta1, but not alpha2beta1, suppresses malignant conversion. *Cancer Res.* **61**, 5248-5254.

Paramio, J. M., Segrelles, C., Casanova, M. L., and Jorcano, J. L. (2000a). Opposite functions for E2F1 and E2F4 in human epidermal keratinocyte differentiation. *J Biol Chem* **275**, 41219-41226.

Paramio, J. M., Segrelles, C., Lain, S., Gomez-Casero, E., Lane, D. P., Lane, E. B., and Jorcano, J. L. (2000b). p53 is phosphorylated at the carboxyl terminus and promotes the differentiation of human HaCaT keratinocytes. *Mol.Carcinog.* **29**, 251-262.

Parkinson, E. K., and Newbold, R. F. (1980). Benzo(a)pyrene metabolism and DNA adduct formation in serially cultivated strains of human epidermal keratinocytes. *Int.J.Cancer* **26**, 289-299.

Pelengaris, S., Littlewood, T., Khan, M., Elia, G., and Evan, G. (1999). Reversible activation of c-Myc in skin: induction of a complex neoplastic phenotype by a single oncogenic lesion. *Mol.Cell* **3**, 565-577.

Perez, D. S., Armstrong-Lea, L., Fox, M. H., Yang, R. S., and Campain, J. A. (2003). Arsenic and benzo[a]pyrene differentially alter the capacity for differentiation and growth properties of primary human epidermal keratinocytes. *Toxicol.Sci.* **76**, 280-290.

Perez-Losada, J., and Balmain, A. (2003). Stem-cell hierarchy in skin cancer. *Nat.Rev.Cancer* **3**, 434-443.

Plewig, G. (1970). Regional differences of cell sizes in the human stratum corneum. II. Effects of sex and age. *J.Invest Dermatol.* **54**, 19-23.

Polakowska, R., Herting, E., and Goldsmith, L. A. (1991). Isolation of cDNA for human epidermal type I transglutaminase. *J.Invest Dermatol.* **96**, 285-288.

Potten, C. S. (1981). Cell replacement in epidermis (keratopoiesis) via discrete units of proliferation. *Int.Rev.Cytol.* **69**, 271-318.

Potten, C. S., and Loeffler, M. (1990). Stem cells: attributes, cycles, spirals, pitfalls and uncertainties. Lessons for and from the crypt. *Development* **110**, 1001-1020.

Prowse, D. M., Bolgan, L., Molnár, Á., and Dotto, G. P. (1997). Involvement of the Sp3 Transcription Factor in Induction of $p21^{Cip1/WAF1}$ in Keratinocyte Differentiation. *Journal of Biological Chemistry* **272**, 1308-1314.

Puisieux, A., Lim, S., Groopman, J., and Ozturk, M. (1991). Selective targeting of p53 gene mutational hotspots in human cancers by etiologically defined carcinogens. *Cancer Res.* **51**, 6185-6189.

Qin, J. Z., Chaturvedi, V., Denning, M. F., Choubey, D., Diaz, M. O., and Nickoloff, B. J. (1999). Role of NF-kappaB in the apoptotic-resistant phenotype of keratinocytes. *Journal of Biological Chemistry* **274**, 37957-37964.

Quintanilla, M., Brown, K., Ramsden, M., and Balmain, A. (1986). Carcinogen-specific mutation and amplification of Ha-ras during mouse skin carcinogenesis. *Nature* **322**, 78-80.

Rady, P., Scinicariello, F., Wagner, R. F., Jr., and Tyring, S. K. (1992). p53 mutations in basal cell carcinomas. *Cancer Res.* **52**, 3804-3806.

Regnier, M., and Darmon, M. (1991). 1,25-Dihydroxyvitamin D3 stimulates specifically the last steps of epidermal differentiation of cultured human keratinocytes. *Differentiation* **47**, 173-188.

Reiners, J. J., Jr., Cantu, A. R., and Pavone, A. (1991). Distribution of constitutive and polycyclic aromatic hydrocarbon-induced cytochrome P-450 activities in murine epidermal cells that differ in their stages of differentiation. *Prog.Clin.Biol.Res.* **369**, 123-135.

Reiss, M., and Sartorelli, A. C. (1987). Regulation of growth and differentiation of human keratinocytes by type beta transforming growth factor and epidermal growth factor. *Cancer Res.* **47**, 6705-6709.

Rice, R. H., and Green, H. (1977). The cornified envelope of terminally differentiated human epidermal keratinocytes consists of cross-linked protein. *Cell* **11**, 417-422.

Rice, R. H., Rong, X. H., and Chakravarty, R. (1988). Suppression of keratinocyte differentiation in SSC-9 human squamous carcinoma cells by benzo[a]pyrene, 12-O-tetradecanoylphorbol-13-acetate and hydroxyurea. *Carcinogenesis* **9**, 1885-1890.

Romero, D. L., Mounho, B. J., Lauer, F. T., Born, J. L., and Burchiel, S. W. (1997). Depletion of glutathione by benzo(a)pyrene metabolites, ionomycin, thapsigargin, and phorbol myristate in human peripheral blood mononuclear cells. *Toxicol.Appl.Pharmacol.* **144**, 62-69.

Roop, D. R., Huitfeldt, H., Kilkenny, A., and Yuspa, S. H. (1987). Regulated expression of differentiation-associated keratins in cultured epidermal cells detected by monospecific antibodies to unique peptides of mouse epidermal keratins. *Differentiation* **35**, 143-150.

Roop, D. R., Krieg, T. M., Mehrel, T., Cheng, C. K., and Yuspa, S. H. (1988). Transcriptional control of high molecular weight keratin gene expression in multistage mouse skin carcinogenesis. *Cancer Res.* **48**, 3245-3252.

Roop, D. R., Lowy, D. R., Tambourin, P. E., Strickland, J., Harper, J. R., Balaschak, M., Spangler, E. F., and Yuspa, S. H. (1986). An activated Harvey ras oncogene produces benign tumours on mouse epidermal tissue. *Nature* **323**, 822-824.

Rossi, A., Jang, S. I., Ceci, R., Steinert, P. M., and Markova, N. G. (1998). Effect of AP1 transcription factors on the regulation of transcription in normal human epidermal keratinocytes. *J.Invest Dermatol.* **110**, 34-40.

Rossman, T. G. (1981). Enhancement of UV-mutagenesis by low concentrations of arsenite in E. coli. *Mutat.Res.* **91**, 207-211.

Rossman, T. G., and Goncharova, E. I. (1998). Spontaneous mutagenesis in mammalian cells is caused mainly by oxidative events and can be blocked by antioxidants and metallothionein. *Mutat.Res.* **402**, 103-110.

Rossman, T. G., Stone, D., Molina, M., and Troll, W. (1980). Absence of arsenite mutagenicity in E coli and Chinese hamster cells. *Environ.Mutagen.* **2**, 371-379.

Rossman, T. G., Uddin, A. N., Burns, F. J., and Bosland, M. C. (2001). Arsenite is a cocarcinogen with solar ultraviolet radiation for mouse skin: an animal model for arsenic carcinogenesis. *Toxicol.Appl.Pharmacol.* **176**, 64-71.

Rubin, A. L., and Rice, R. H. (1988). 2,3,7,8-Tetrachlorodibenzo-p-dioxin and polycyclic aromatic hydrocarbons suppress retinoid-induced tissue transglutaminase in SCC-4 cultured human squamous carcinoma cells. *Carcinogenesis* **9**, 1067-1070.

Rudel, R., Slayton, T. M., and Beck, B. D. (1996). Implications of arsenic genotoxicity for dose response of carcinogenic effects. [Review] [55 refs]. *Regulatory Toxicology & Pharmacology* **23**, 87-105.

Ruggeri, B., Caamano, J., Goodrow, T., DiRado, M., Bianchi, A., Trono, D., Conti, C. J., and Klein-Szanto, A. J. (1991). Alterations of the p53 tumor suppressor gene during mouse skin tumor progression. *Cancer Res.* **51**, 6615-6621.

Ruggeri, B., DiRado, M., Zhang, S. Y., Bauer, B., Goodrow, T., and Klein-Szanto, A. J. (1993). Benzo[a]pyrene-induced murine skin tumors exhibit frequent and characteristic G to T mutations in the p53 gene. *Proc.Natl.Acad.Sci.U.S.A* **90**, 1013-1017.

Ruoslahti, E. (1991). Integrins. *J.Clin.Invest* **87**, 1-5.

Rutberg, S. E., Saez, E., Glick, A., Dlugosz, A. A., Spiegelman, B. M., and Yuspa, S. H. (1996). Differentiation of mouse keratinocytes is accompanied by PKC-dependent changes in AP-1 proteins. *Oncogene* **13**, 167-176.

Rutberg, S. E., Saez, E., Lo, S., Jang, S. I., Markova, N., Spiegelman, B. M., and Yuspa, S. H. (1997). Opposing activities of c-Fos and Fra-2 on AP-1 regulated transcriptional activity in mouse keratinocytes induced to differentiate by calcium and phorbol esters. *Oncogene* **15**, 1337-1346.

Saffiotti, U., Borg, S. A., Grote, M. I., and Karp, D. B. (1964). Retention rates of particular carcinogens in the lungs. *Chicago Med.School Quart.* **24**, 10-17.

Sage, E., and Haseltine, W. A. (1984). High ratio of alkali-sensitive lesions to total DNA modification induced by benzo(a)pyrene diol epoxide. *J.Biol.Chem.* **259**, 11098-11102.

Saha, D. P. (1996). Arsenic poisoning in West Bengal. *Science* **274**, 1287.

Sako, T., Yuspa, S. H., Herald, C. L., Pettit, G. R., and Blumberg, P. M. (1987). Partial parallelism and partial blockade by bryostatin 1 of effects of phorbol ester tumor promoters on primary mouse epidermal cells. *Cancer Res.* **47**, 5445-5450.

Salazar, A. M., Ostrosky-Wegman, P., Menendez, D., Miranda, E., Garcia-Carranca, A., and Rojas, E. (1997). Induction of p53 protein expression by sodium arsenite. *Mutat.Res.* **381**, 259-265.

Savill, N. J. (2003). Mathematical models of hierarchically structured cell populations under equilibrium with application to the epidermis. *Cell Prolif.* **36**, 1-26.

Schwartz, R. A. (1997). Arsenic and the skin. *Int.J.Dermatol.* **36**, 241-250.

Scott, N., Hatlelid, K. M., MacKenzie, N. E., and Carter, D. E. (1993). Reactions of arsenic(III) and arsenic(V) species with glutathione. *Chem.Res.Toxicol.* **6**, 102-106.

Seitz, C. S., Lin, Q., Deng, H., and Khavari, P. A. (1998). Alterations in NF-kappaB function in transgenic epithelial tissue demonstrate a growth inhibitory role for NF-kappaB. *Proc.Natl.Acad.Sci.U.S.A* **95**, 2307-2312.

Shi, H., Hudson, L. G., Ding, W., Wang, S., Cooper, K. L., Liu, S., Chen, Y., Shi, X., and Liu, K. J. (2004). Arsenite causes DNA damage in keratinocytes via generation of hydroxyl radicals. *Chem.Res.Toxicol.* **17**, 871-878.

Shipley, G. D., and Pittelkow, M. R. (1987). Control of growth and differentiation in vitro of human keratinocytes cultured in serum-free medium. *Archives of Dermatology* **123**, 1541a-1544a.

Simeonova, P. P., and Luster, M. I. (2000). Mechanisms of arsenic carcinogenicity: genetic or epigenetic mechanisms? *J.Environ.Pathol.Toxicol.Oncol.* **19**, 281-286.

Staiano-Coico, L., Darzynkiewicz, Z., and McMahon, C. K. (1989). Cultured human keratinocytes: discrimination of different cell cycle compartments based upon measurement of nuclear RNA or total cellular RNA content. *Cell Tissue Kinet.* **22**, 235-243.

Staiano-Coico, L., Higgins, P. J., Darzynkiewicz, Z., Kimmel, M., Gottlieb, A. B., Pagan-Charry, I., Madden, M. R., Finkelstein, J. L., and Hefton, J. M. (1986). Human keratinocyte culture. Identification and staging of epidermal cell subpopulations. *J.Clin.Invest* **77**, 396-404.

Stanwell, C., Denning, M. F., Rutberg, S. E., Cheng, C., Yuspa, S. H., and Dlugosz, A. A. (1996). Staurosporine induces a sequential program of mouse keratinocyte terminal differentiation through activation of PKC isozymes. *J.Invest Dermatol.* **106**, 482-489.

Steel, G. G. (1977). Growth kinetics of tumors: cell population kinetics in relation to the growth and treatment of cancer. In Basic theory of growing cell populations, pp. 57-85. Clarendon Press, Oxford.

Steel, G. G., and Bensted, J. P. (1965). In vitro studies of cell proliferation in tumours. I. Critical appraisal of methods and theoretical considerations. *Eur.J.Cancer* **1**, 275-279.

Steinert, P. M., Steven, A. C., and Roop, D. R. (1985). The molecular biology of intermediate filaments. *Cell* **42**, 411-420.

Steven, A. C., Bisher, M. E., Roop, D. R., and Steinert, P. M. (1990). Biosynthetic pathways of filaggrin and loricrin--two major proteins expressed by terminally differentiated epidermal keratinocytes. *J.Struct.Biol.* **104**, 150-162.

Stoler, A., Kopan, R., Duvic, M., and Fuchs, E. (1988). Use of monospecific antisera and cRNA probes to localize the major changes in keratin expression during normal and abnormal epidermal differentiation. *J.Cell Biol.* **107**, 427-446.

Strickland, J. E., Greenhalgh, D. A., Koceva-Chyla, A., Hennings, H., Restrepo, C., Balaschak, M., and Yuspa, S. H. (1988). Development of murine epidermal cell lines which contain an activated rasHa oncogene and form papillomas in skin grafts on athymic nude mouse hosts. *Cancer Res.* **48**, 165-169.

Strickland, J. E., Ueda, M., Hennings, H., and Yuspa, S. H. (1992). A model for initiated mouse skin: suppression of papilloma but not carcinoma formation by normal epidermal cells in grafts on athymic nude mice. *Cancer Res.* **52**, 1439-1444.

Styblo, M., Drobna, Z., Jaspers, I., Lin, S., and Thomas, D. J. (2002). The role of biomethylation in toxicity and carcinogenicity of arsenic: a research update. *Environ.Health Perspect.* **110 Suppl 5**, 767-771.

Su, M. J., Bikle, D. D., Mancianti, M. L., and Pillai, S. (1994). 1,25-Dihydroxyvitamin D3 potentiates the keratinocyte response to calcium. *J.Biol.Chem.* **269**, 14723-14729.

Suarez, H. G., Daya-Grosjean, L., Schlaifer, D., Nardeux, P., Renault, G., Bos, J. L., and Sarasin, A. (1989). Activated oncogenes in human skin tumors from a repair-deficient syndrome, xeroderma pigmentosum. *Cancer Res.* **49**, 1223-1228.

Summerhayes, I. C., Cheng, Y. S., Sun, T. T., and Chen, L. B. (1981). Expression of keratin and vimentin intermediate filaments in rabbit bladder epithelial cells at different stages of benzo[a]pyrene-induced neoplastic progression. *J.Cell Biol.* **90**, 63-69.

Sun, T. T., and Green, H. (1976). Differentiation of the epidermal keratinocyte in cell culture: formation of the cornified envelope. *Cell* **9**, 511-521.

Takahashi, M., Tezuka, T., and Katunuma, N. (1992). Phosphorylated cystatin alpha is a natural substrate of epidermal transglutaminase for formation of skin cornified envelope. *FEBS Lett.* **308**, 79-82.

Tang, W., Ziboh, V. A., Isseroff, R., and Martinez, D. (1988). Turnover of inositol phospholipids in cultured murine keratinocytes: possible involvement of inositol triphosphate in cellular differentiation. *J.Invest Dermatol.* **90**, 37-43.

Tennenbaum, T., Li, L., Belanger, A. J., De Luca, L. M., and Yuspa, S. H. (1996). Selective changes in laminin adhesion and alpha 6 beta 4 integrin regulation are associated with the initial steps in keratinocyte maturation. *Cell Growth Differ.* **7**, 615-628.

Tennenbaum, T., Yuspa, S. H., Grover, A., Castronovo, V., Sobel, M. E., Yamada, Y., and De Luca, L. M. (1992). Extracellular matrix receptors and mouse skin carcinogenesis: altered expression linked to appearance of early markers of tumor progression. *Cancer Res.* **52**, 2966-2976.

Terry, N. H., White, R. A., Meistrich, M. L., and Calkins, D. P. (1991). Evaluation of flow cytometric methods for determining population potential doubling times using cultured cells. *Cytometry* **12**, 234-241.

Tesfagaigzi, J., and Carlson, D. M. (1999). Expression, regulation, and function of the SPR family of proteins. *Cell Biochemistry and Biophysics* **30**, 243-265.

Thacher, S. M., and Rice, R. H. (1985). Keratinocyte-specific transglutaminase of cultured human epidermal cells: relation to cross-linked envelope formation and terminal differentiation. *Cell* **40**, 685-695.

Thorud, E., Clausen, O. P., and Aarnaes, E. (1988). Turnover and maturation kinetics in the hairless mouse epidermis. Continuous [3H]TdR labelling and mathematical model analyses. *Cell Tissue Kinet.* **21**, 301-314.

Toftgard, R., Yuspa, S. H., and Roop, D. R. (1985). Keratin gene expression in mouse skin tumors and in mouse skin treated with 12-O-tetradecanoylphorbol-13-acetate. *Cancer Res.* **45**, 5845-5850.

Tran, H. P., Prakash, A. S., Barnard, R., Chiswell, B., and Ng, J. C. (2002). Arsenic inhibits the repair of DNA damage induced by benzo(a)pyrene. *Toxicol.Lett.* **133**, 59-67.

Tseng, W. P. (1977). Effects and dose--response relationships of skin cancer and blackfoot disease with arsenic. *Environ.Health Perspect.* **19**, 109-119.

Tsuda, T., Babazono, A., Yamamoto, E., Kurumatani, N., Mino, Y., Ogawa, T., Kishi, Y., and Aoyama, H. (1995). Ingested arsenic and internal cancer: a historical cohort study followed for 33 years. *Am.J.Epidemiol.* **141**, 198-209.

Turusov, V. S., Kosoi, K. K., and Parfenov, I. (1987). [Benzo(a)pyrene and the carcinogenic effect of coal tar]. *Vopr.Onkol.* **33**, 62-67.

Ubezio, P. (1993). Relationship between flow cytometric data and kinetic parameters. *Eur.J.Histochem.* **37**, 15-28.

van Erp, P. E., de Jongh, G. J., Boezeman, J. B., and Schalkwijk, J. (1994). The growth and differentiation of human keratinocytes in vitro: a combined immunohistochemical and flow cytometric study. *Arch.Dermatol.Res.* **286**, 115-122.

van Ruissen, F., van Erp, P. E., de Jongh, G. J., Boezeman, J. B., van de Kerkhof, P. C., and Schalkwijk, J. (1994). Cell kinetic characterization of growth arrest in cultured human keratinocytes. *J Cell Sci.* **107 (Pt 8)**, 2219-2228.

Vastrik, I., Kaipainen, A., Penttila, T. L., Lymboussakis, A., Alitalo, R., Parvinen, M., and Alitalo, K. (1995). Expression of the mad gene during cell differentiation in vivo and its inhibition of cell growth in vitro. *J.Cell Biol.* **128**, 1197-1208.

Vega, L., Styblo, M., Patterson, R., Cullen, W., Wang, C., and Germolec, D. (2001). Differential effects of trivalent and pentavalent arsenicals on cell proliferation and cytokine secretion in normal human epidermal keratinocytes. *Toxicology & Applied Pharmacology* **172**, 225-232.

Wang, T. S., and Huang, H. (1994). Active oxygen species are involved in the induction of micronuclei by arsenite in XRS-5 cells. *Mutagenesis* **9**, 253-257.

Watt, F. M., Jordan, P. W., and O'Neill, C. H. (1988). Cell shape controls terminal differentiation of human epidermal keratinocytes. *Proc.Natl.Acad.Sci.U.S.A* **85**, 5576-5580.

Weinberg, W. C., Fernandez-Salas, E., Morgan, D. L., Shalizi, A., Mirosh, E., Stanulis, E., Deng, C., Hennings, H., and Yuspa, S. H. (1999). Genetic deletion of p21WAF1 enhances papilloma formation but not malignant conversion in experimental mouse skin carcinogenesis. *Cancer Res.* **59**, 2050-2054.

Whitmarsh, A. J., and Davis, R. J. (1996). Transcription factor AP-1 regulation by mitogen-activated protein kinase signal transduction pathways. *J.Mol.Med.* **74**, 589-607.

Willnow, U. (1979). The kinetics of cell proliferation in neuroblastomas. *Arch.Geschwulstforsch.* **49**, 211-219.

Wilson, G. D. (1994a). Analysis of DNA - measurement of cell kinetics by the bromodeoxyuridine/anti-bromodeoxyuridine method. In Flow cytometry: a practical approach (M.G.Ormerod, ed., pp. 137-156. Oxford University Press, New York.

Wilson, G. D. (1994b). Flow Cytometry: A Practical Approach. In Analysis of DNA-measurement of cell kinetics by the bromodeoxyuridine/anti-bromodeoxyuridine method, pp. 137-156. Oxford University Press, Oxford.

Wilson, G. D. (1998). Flow cytometric detection of proliferation-associated antigens, PCNA and Ki-67. *Methods Mol.Biol.* **80**, 355-363.

Wong, S. S., Tan, K. C., and Goh, C. L. (1998). Cutaneous manifestations of chronic arsenicism: review of seventeen cases. *J.Am.Acad.Dermatol.* **38**, 179-185.

Woodcock-Mitchell, J., Eichner, R., Nelson, W. G., and Sun, T. T. (1982). Immunolocalization of keratin polypeptides in human epidermis using monoclonal antibodies. *J.Cell Biol.* **95**, 580-588.

Xie, Z., and Bikle, D. D. (1999). Phospholipase C-gamma1 is required for calcium-induced keratinocyte differentiation. *J.Biol.Chem.* **274**, 20421-20424.

Yamauchi, H., and Yamamura, Y. (1983). Concentration and chemical species of arsenic in human tissue. *Bull.Environ.Contam Toxicol.* **31**, 267-270.

Yang, J. S., Lavker, R. M., and Sun, T. T. (1993). Upper human hair follicle contains a subpopulation of keratinocytes with superior in vitro proliferative potential. *J.Invest Dermatol.* **101**, 652-659.

Yang, L. C., Ng, D. C., and Bikle, D. D. (2003). Role of protein kinase C alpha in calcium induced keratinocyte differentiation: defective regulation in squamous cell carcinoma. *J.Cell Physiol* **195**, 249-259.

Yih, L. H., and Lee, T. C. (2000). Arsenite induces p53 accumulation through an ATM-dependent pathway in human fibroblasts. *Cancer Res.* **60**, 6346-6352.

Yoshimoto, T., Inoue, T., Iizuka, H., Nishikawa, H., Sakatani, M., Ogura, T., Hirao, F., and Yamamura, Y. (1980). Differential induction of squamous cell carcinomas and adenocarcinomas in mouse lung by intratracheal instillation of benzo(a)pyrene and charcoal powder. *Cancer Res.* **40**, 4301-4307.

Yuspa, S. H. (1994). The pathogenesis of squamous cell cancer: lessons learned from studies of skin carcinogenesis--thirty-third G. H. A. Clowes Memorial Award Lecture. *Cancer Res.* **54**, 1178-1189.

Yuspa, S. H., Ben, T., and Hennings, H. (1983a). The induction of epidermal transglutaminase and terminal differentiation by tumor promoters in cultured epidermal cells. *Carcinogenesis* **4**, 1413-1418.

Yuspa, S. H., Ben, T., Hennings, H., and Lichti, U. (1980). Phorbol ester tumor promoters induce epidermal transglutaminase activity. *Biochem.Biophys.Res.Commun.* **97**, 700-708.

Yuspa, S. H., Ben, T., Hennings, H., and Lichti, U. (1982). Divergent responses in epidermal basal cells exposed to the tumor promoter 12-O-tetradecanoylphorbol-13-acetate. *Cancer Res.* **42**, 2344-2349.

Yuspa, S. H., and Dlugosz, A. A. (1991). Cutaneous carcinogenesis: natural and experimental. In Physiology Biochemistry and Molecular Biology of The Skin, pp. 1365-1402. Oxford University Press, New York.

Yuspa, S. H., Kilkenny, A. E., Stanley, J., and Lichti, U. (1985). Keratinocytes blocked in phorbol ester-responsive early stage of terminal differentiation by sarcoma viruses. *Nature* **314**, 459-462.

Yuspa, S. H., Kilkenny, A. E., Steinert, P. M., and Roop, D. R. (1989). Expression of murine epidermal differentiation markers is tightly regulated by restricted extracellular calcium concentrations in vitro. *J.Cell Biol.* **109**, 1207-1217.

Yuspa, S. H., Morgan, D., Lichti, U., Spangler, E. F., Michael, D., Kilkenny, A., and Hennings, H. (1986). Cultivation and characterization of cells derived from mouse skin papillomas induced by an initiation-promotion protocol. *Carcinogenesis* **7**, 949-958.

Yuspa, S. H., and Morgan, D. L. (1981). Mouse skin cells resistant to terminal differentiation associated with initiation of carcinogenesis. *Nature* **293**, 72-74.

Yuspa, S. H., Vass, W., and Scolnick, E. (1983b). Altered growth and differentiation of cultured mouse epidermal cells infected with oncogenic retrovirus: contrasting effects of viruses and chemicals. *Cancer Res.* **43**, 6021-6030.

Zhang, L., Connor, E. E., Chegini, N., and Shiverick, K. T. (1995). Modulation by benzo[a]pyrene of epidermal growth factor receptors, cell proliferation, and secretion of human chorionic gonadotropin in human placental cell lines. *Biochem.Pharmacol.* **50**, 1171-1180.

Zhao, W., and Ramos, K. S. (1998). Modulation of hepatocyte gene expression by the carcinogen benzo[a]pyrene. *Toxicol.In Vitro* **1998**, 395-402.

Ziegler, A., Leffell, D. J., Kunala, S., Sharma, H. W., Gailani, M., Simon, J. A., Halperin, A. J., Baden, H. P., Shapiro, P. E., Bale, A. E., and . (1993). Mutation hotspots due to sunlight in the p53 gene of nonmelanoma skin cancers. *Proc.Natl.Acad.Sci.U.S.A* **90**, 4216-4220.

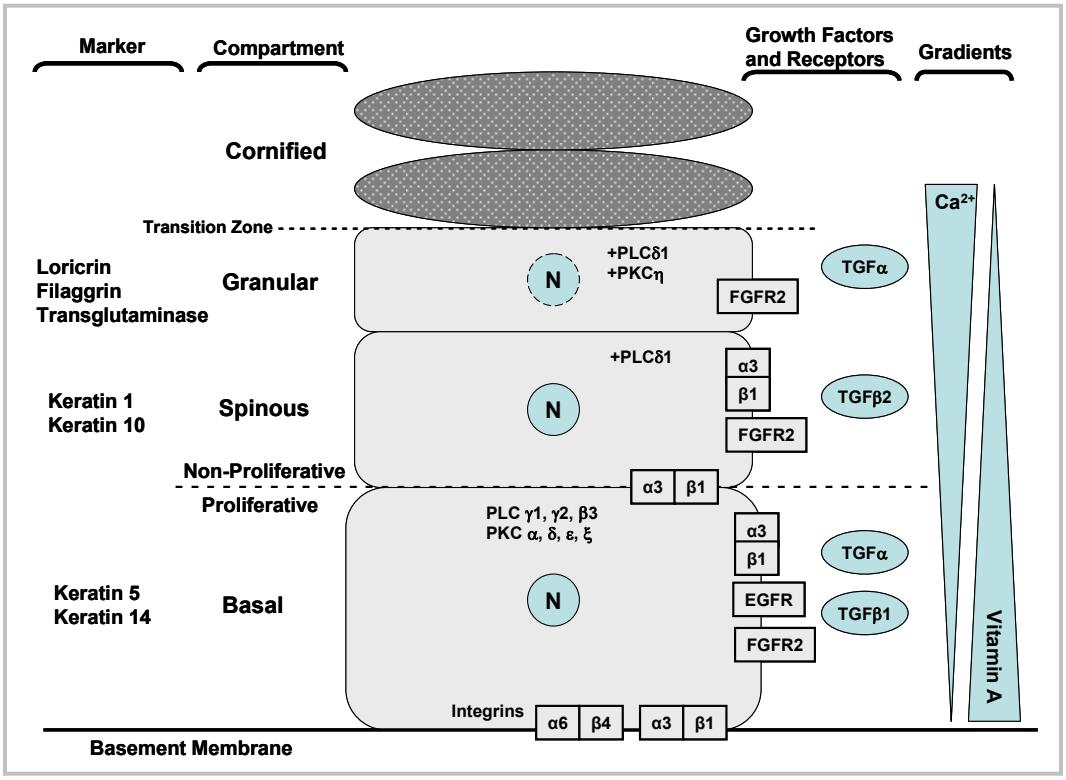

Figure 2.1. **Representation of the stratified epidermis.** This schematic displays the keratinocyte maturation compartments, markers expressed in each compartment, and biochemical pathways which are thought to regulate this phenotype. FGFR2 – fibroblast growth factor receptor 2; EGFR – epidermal growth factor receptor; TGF – transforming growth factor; PKC – protein kinase; PLC – phospholipase C; N – nucleus.

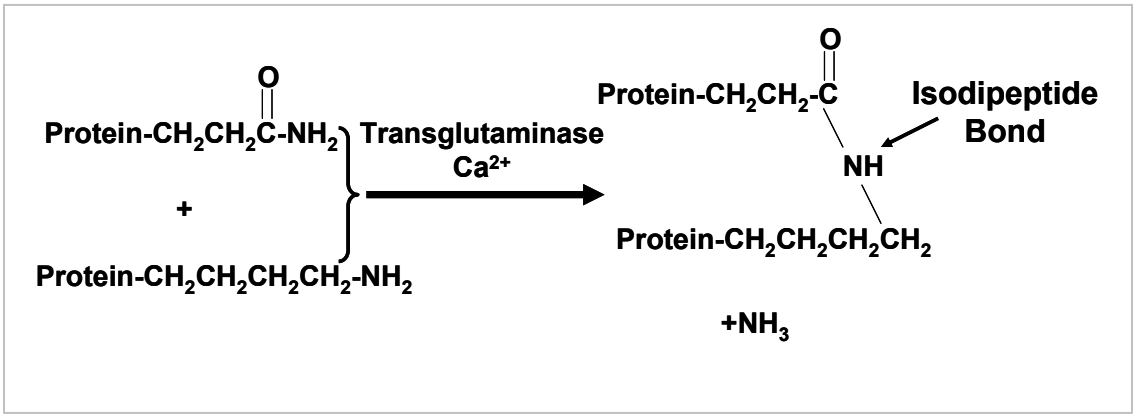

Figure 2.2. **Isodipeptide bond structure in cornified envelopes.** The cornified envelope is a 12.0 μm subplasmalemmal structure. It is extremely chemical resistant (resists boiling in detergents, chaotrophic salts, and reducing agents). Chemical resistance is conferred by the presence of isodipeptide bonds, i.e. ε-(γ-glutamyl)lysine.

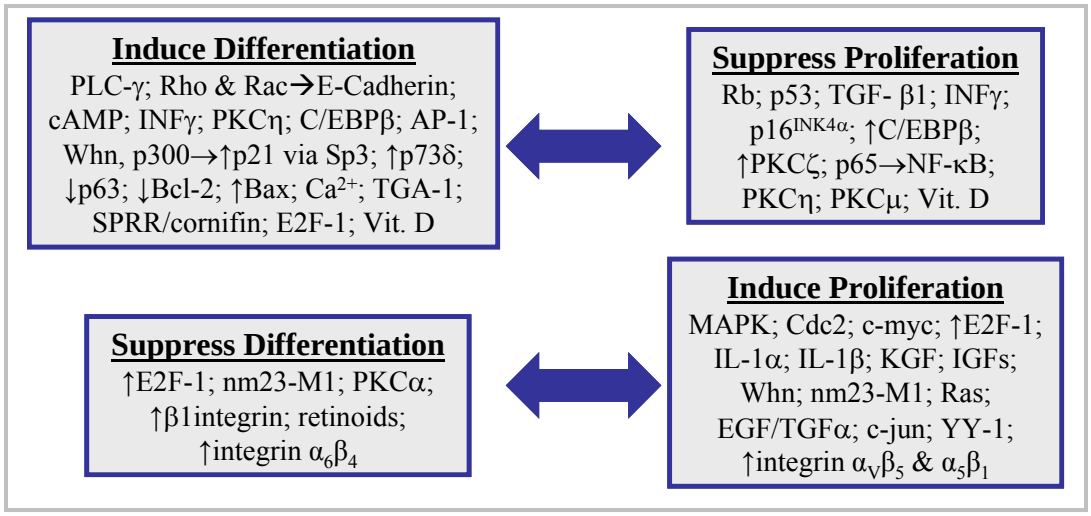

Figure 2.3. **Regulators of keratinocyte proliferation and differentiation.** This diagram summarizes the regulatory roles of keratinocyte differentiation and growth which are involved in maintaining homeostasis within in epidermis. In most cases, induced differentiation is accompanied by decreased proliferation and vice versa.

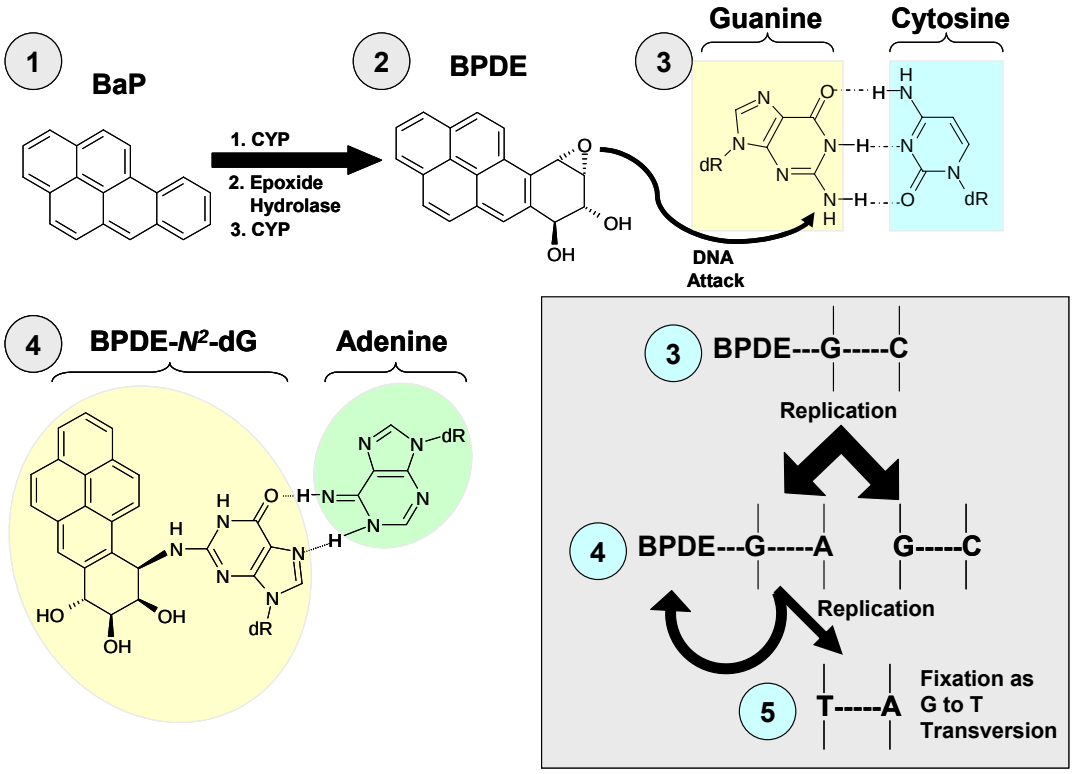

Figure 2.4. **Benzo[*a*]pyrene: Metabolic activation, binding to DNA, and induction of G to T transversion.** (1) Benzo[*a*]pyrene (BaP) is metabolized by cytochrome P450 (CYP), epoxide hydrolase, and again by CYP to produce the ultimate carcinogen (2) BaP-7,8-diol-9,10-epoxide (BPDE). (3) The majority of BPDE forms a stable DNA adduct at the N^2 position of guanine to produce BPDE-N^2-dG. The bulky adduct changes the conformation of guanine in such as way where it can no longer bind to cytosine; however, (4) BPDE-N^2-dG can now bind to adenine. After cell replication, the result is a fixed (5) G to T tranversion mutation which is common in many *ras* and *p53* genes found in a variety of cancers. Nucleic bases: G = guanine; C = cytosine; A = adenine; T = thymine. Note this schematic depicts one of the more common metabolic pathways for BaP, but in reality there are several other bioactivating pathways for BaP to undergo.

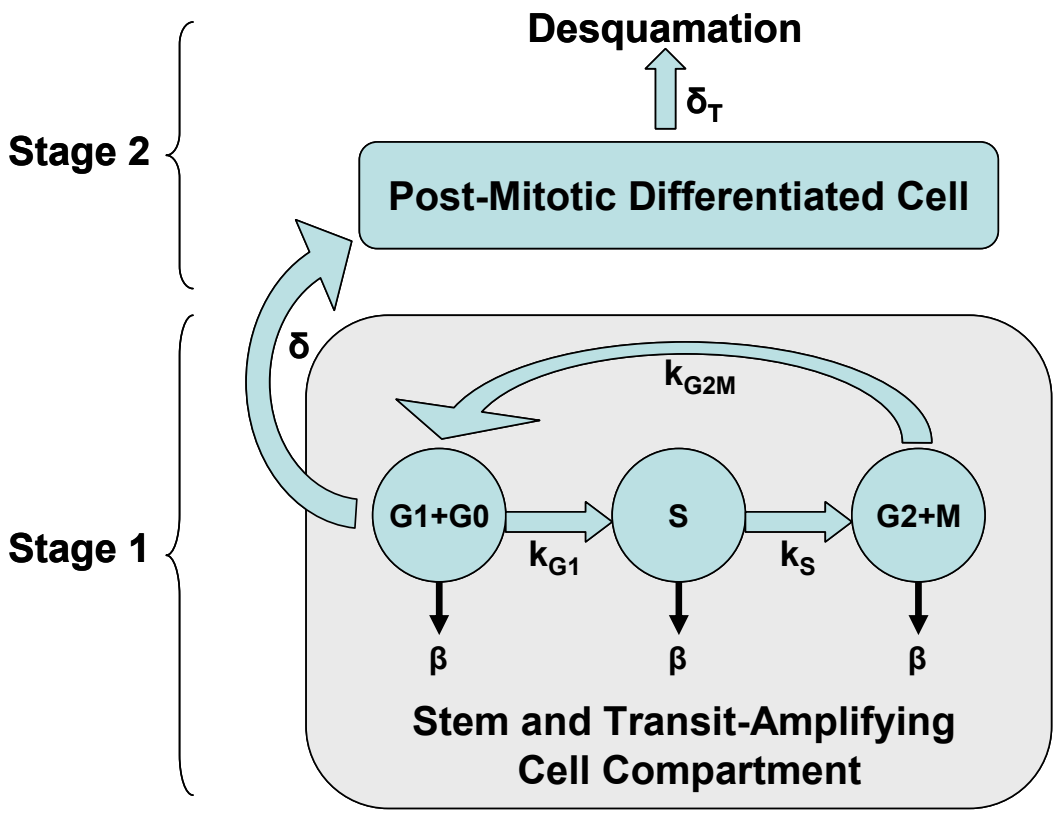

Figure 2.5. **A simple conceptual model for the process of differentiation in normal human epidermal keratinocytes.** This version of the model describes one lumped proliferative population comprised of both stem and transit-amplifying (STA) cells (Stage 1). The model includes three cell cycle compartments (G1+G0, S, and G2+M), and post-mitotic differentiated cells (Stage 2). STA cells leave Stage 1 from the G1+G0 compartment and enter Stage 2, the post-mitotic compartment, according to the differentiation rate δ. Post-mitotic cells eventually terminally differentiate (desquamate) and die at the rate δ_T. Cell death (β) occurs at each compartment. Rates of conversions (k) from one cell phase to the next are also included in the model.

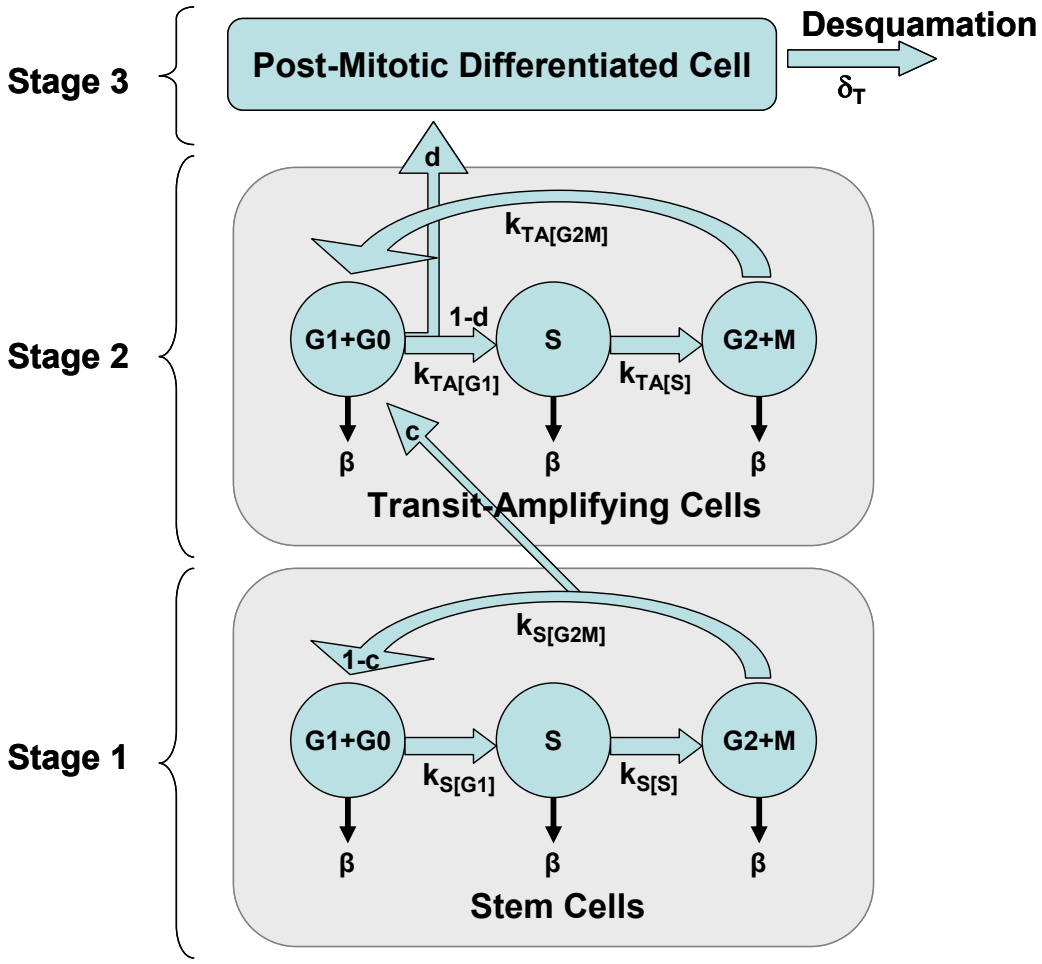

Figure 2.6. **A complex conceptual model for the process of differentiation in normal human epidermal keratinocytes**. Three cell populations are present in this model: stem (S), transit-amplifying (TA), and post-mitotic cells. The overall progression that will be modeled is as follows: Stem cells (Stage 1) can convert to TA cells (Stage 2), which then further undergo multiple cycles of division before converting into post-mitotic (Stage 3) (i.e., granular and cornified) cells expressing the differentiated phenotype. Of these three populations, only stem and TA cells are capable of cycling. The model includes three cell cycle compartments (G1+G0, S, and G2+M), for both stem and TA cells, and a post-mitotic differentiated cell compartment. After stem cell division, a fraction c of daughter cells begin to differentiate and enter G1+G0 phase of the TA compartment. The remaining cells (fraction 1 – c) re-enter the cycle within the same stem cell compartment. Fraction d of TA cells within G1+G0 differentiate further entering the post-mitotic compartment, while the remainder cell fraction (1 – d) continues to cycle within the TA cell population. Post-mitotic cells eventually die as a result of terminal differentiation (desquamatation) at the rate δ_T. Cell death (β) occurs at each compartment. Rates of conversions (k) from one cell phase to the next are also included in the model.

Chapter 3

Cytotoxic Effects of Benzo[*a*]pyrene, Carbazole, Dibenzothiophene, and Isoquinoline in Normal Human Epidermal Keratinocytes

3.1. Introduction

Exposures to petroleum-based hydrocarbons are of significant toxicological concern, both from an occupational and environmental standpoint. Petroleum products find their way into most people's lives, refined or derivatized as a variety of fuels, lubricants, household and industrial products, medicines, and plastics (Seymour and Henry 2001). There are many studies which suggest a link between the components of petroleum and human carcinogenesis; however, there are data gaps on the mechanisms related to the toxicity and/or carcinogenicity of some individual petroleum-based hydrocarbons (Mehlman 1992). Risk analysis is complicated by the fact that these chemicals occur in highly complex mixtures and they are most often derivatized by alkylation with groups of various size, number, and configuration. Little is known about the toxicity and/or carcinogenicity of these derivatives as compared to the parental compounds. In order to examine the effects of chemical mixtures, it is necessary to first study the cytotoxic effects of each chemical singly.

Four common compounds were selected (benzo[*a*]pyrene, dibenzothiophene, carbazole, and isoquinoline) which represent four prevalent classes of hydrocarbons in

marine diesel fuel and heavy distillates from petroleum. In addition to being common constituents in crude petroleum and refined petroleum products, these compounds also represent the major classes of heavy fraction hydrocarbons in such mixtures as pitch, coal tar, smoke, soot, and/or solvents. The polycyclic aromatic hydrocarbon (PAH), benzo[*a*]pyrene (BaP), and its reactive metabolites have been well studied regarding carcinogenicity and mutagenicity in a number of cell systems (Maher *et al.* 1987; Wislocki *et al.* 1976a; Wislocki *et al.* 1976b; Wood *et al.* 1976) Literature regarding BaP and its carcinogenic properties are discussed at length in Chapter 2. In the cell, BaP is metabolized by cytochromes P450 (CYP) 1A1 and 1B1, as well as epoxide hydrolase, yielding *syn*- and *anti*-BaP-7,8-diol-9,10-epoxides (BPDE). It is the dihydrodiol epoxide of BaP that is responsible for the formation of genotoxic DNA lesions that can potentially become carcinogenic (See section 2.4.2 of Chapter 2 and Figure 2.4 for more details) (Cai *et al.* 1997; Hartwig *et al.* 2002; Wislocki *et al.* 1976b). Contrary to the vast amounts of work carried out on BaP, limited information is available on the other three hydrocarbons. Dibenzothiophene (DBT) is a representative sulfur-containing hydrocarbon, which has been studied in terms of general toxicity in rodents as well as its effects on liver regeneration in partially hepatectomized rats (Gershbein 1975; Poon *et al.* 1997). Carbazole (CZ) and isoquinoline (IQ) are representative nitrogen-containing hydrocarbons. CZ has not been well studied; however the *N*-methyl derivative (*N*-methylcarbazole) has been extensively investigated due to the fact it is a known mutagen present in tobacco smoke (Yang *et al.* 1991). Results from studies focusing on CZ and *N*-methylcarbazole have shown that CZ itself is less toxic to hepatocytes than the *N*-methyl form, however CZ does elicit some toxicity to hepatocytes as measured by neutral red

uptake (Yang *et al.* 1991). Studies with IQ have shown that it can induce phase II drug metabolizing enzymes without inducing phase I enzymes such as cytochrome P450 in rats (La Voie *et al.* 1983). Metabolism of IQ has been studied in rat liver homogenates and it has been proposed that the differences in toxicities of quinoline and IQ can be attributed to the formation of a dihydrodiol (La Voie *et al.* 1983). This early study also reported that IQ is not genotoxic.

In an industrial setting, petroleum products are normally stored and handled in systems which, for the most part, are 'closed'. Hence, for most of the time, risks of exposure and resulting toxicity are very low. However, during certain operations, such as loading or unloading, workers are required to take special care to avoid skin contact and excessive inhalation of vapor. Dermal exposure of industrial workers to petroleum and some petroleum products can cause defatting of the skin and gives rise to the characteristic signs of dryness and irritancy – erythema, edema, and fissuring (Henry 1998; Seymour and Henry 2001). Hydrocarbons may also reduce the effectiveness of the skin's protective layer, making the skin susceptible to irritation and other insults (Henry 1998). In addition, material containing significant concentrations of PAHs can potentially produce skin tumors by genotoxic mechanisms (Henry 1998). Studies dating back to the early 1920s demonstrated that the use of unrefined or poorly refined petroleum was associated with the development of skin cancer in humans when exposure was coincident with poor personal hygiene and the lack of personal protective equipment (Mackerer *et al.* 2003). Thus, the skin is a relevant target tissue for the variety of toxic effects induced by petroleum-based hydrocarbons.

For this study, normal human epidermal keratinocytes (NHEK) were chosen as an *in vitro* model for measuring the toxic and carcinogenic (in subsequent studies) potential of compounds of interest. Chemically induced transformation has been extensively studied in keratinocytes, both *in vivo* and *in vitro*. Information on these four compounds in keratinocytes varies in that there have been numerous reports on the effects of BaP and its metabolites on mammalian keratinocytes both *in vivo* and *in vitro*, whereas there a limited number of studies on the effects of DBT, CZ, and IQ singly on keratinocytes. There are, however, numerous studies that examined the dermal effects of various refined forms of crude petroleum (Chao and Nylander-French 2004; Mackerer *et al.* 2003; Monteiro-Riviere *et al.* 2004; Nesnow 1990; Weker *et al.* 2004). In our laboratory, we are interested in developing accurate risk assessment strategies for environmentally relevant chemical mixtures. To address this issue, and gather data critical for subsequent risk assessment for petroleum mixtures, NHEK was chosen as a representative model system for dermal exposure to four prominent hydrocarbon components. Although this study does not address the chemical mixture issue, it does examine the individual toxicities of four prominent hydrocarbons derivatives from petroleum. In these studies the MTT assay was used to estimate the lethal concentrations (LC) of BaP, CZ, DBT, and IQ in NHEK.

3.2. Materials and Methods

3.2.1. Chemicals and Reagents

MTT (3-[4,5-Dimethylthiazol-2-yl]-2,5-diphenyltetrazolium bromide or Thiazolyl blue), benzo[*a*]pyrene (BaP), carbazole (CZ), dibenzothiophene (DBT), isoquinoline (IQ), and dimethyl sulfoxide (DMSO) were all purchased from Sigma

Chemical Co. (St. Louis, MO). Rat liver S9 (9000 *g* supernatant) fraction, 1254 aroclor induced, in potassium chloride (KCl), was purchased from ICN Pharmaceuticals, Inc. (Aurora, OH).

3.2.2. Cell Culture Techniques

Cryopreserved normal human epidermal keratinocytes (NHEK) were purchased from the Clonetics Corp. (San Diego, CA). NHEK were grown in 5% CO_2 at 37°C in defined Keratinocyte Growth Medium (KGM) (Clonetics Corp) containing bovine pituitary extract (BPE), human epidermal growth factor (hEGF), insulin, hydrocortisone, transferrin, epinephrine, and antibiotic, GA-1000, at proprietary concentrations as determined by the manufacturer.

3.2.2.1. Subculturing NHEK

NHEK were subcultured according to the supplier's protocol. Briefly, a single 1.0 ml vial contains approximately $1x10^6$ NHEK and, upon arrival, was immediately stored in liquid nitrogen. When ready to subculture, the vial(s) containing NHEK were taken from liquid nitrogen storage and thawed by swirling the half submerged vial(s) for about 5 minutes in a water bath kept at 37°C. After thawing, cells were added to pre-warmed KGM. Ten T-25 flasks were used to seed one vial of NHEK (10,000 cells/flask). Flasks were then returned to the incubator, thus, allowing cells to anchor to the bottom of the flask surface and begin proliferating. Flask medium was replaced with fresh, pre-warmed KGM every other day. Once NHEK confluence levels reached approximately 90% (5-6 days) cells were ready to be passaged or frozen. After the removal of KGM from the flask, cells were washed with pre-warmed Clonetics HEPES Buffered Saline Solution

(HBSS) (3.0 ml/flask). Next, pre-warmed Clonetics Trypsin/EDTA (T/E) (5.0 ml/flask) was dispensed into flasks to detach cells from the bottom surface. Cells immersed in T/E were placed in a 37°C incubator until cells detached (maximum of 12.0 minutes). Once cells detached, pre-warmed Trypsin Neutralizing Solution (TNS) (3.0 ml/flask) was added to the flask. At this point, cell viability was assessed and cell counting was conducted using a hemacytometer under a light microscope (10x). Cells were then centrifuged at 1200 rpm for 5 minutes. After centrifugation, the supernatant was aspirated and the cell pellet was resuspended in pre-warmed KGM. Finally, these cells were either frozen at $1x10^6$ cells/ml in KGM containing 8% DMSO or passaged for later experimental use.

3.2.3. Cytotoxicity Experiments

Cytotoxicity studies were carried out using the MTT assay as a measure of cell viability *in vitro* (Mosmann 1983). Cells were plated in six well plates at a density of 3000 cells/well. When cells reached approximately 20% confluency (2 days), they were exposed for 24 hours to increasing concentrations of each chemical (BaP, CZ, DBT, and IQ) singly. Specific chemical concentration ranges (displayed in Results) were used in order to identify various NHEK LC_X (chemical concentration that kills X% of cells) levels from LC_{25} to LC_{75}. Using the MTT assay, once a LC_{90} was found for each chemical, compounds were serially diluted 2:1 until a LC_{10} concentration was reached; thus, providing a complete concentration spectrum to assess hydrocarbon cytotoxicity in NHEK. All hydrocarbons were dissolved in DMSO as they proved to be highly hydrophobic. NHEK exposure to DMSO (solvent control) never exceeded 0.67% in these experiments since DMSO concentrations greater than 0.75% were shown to be

significantly toxic to NHEK in our preliminary studies (data not shown). After 24 hour exposure to each hydrocarbon, KGM which contained the chemical treatment was aspirated and fresh KGM was added to each cell culture plate. Four days after chemical exposure, the MTT assay was used determine the number of viable cells at each chemical concentration according to previous protocols (Gustafson *et al.* 1996; Mosmann 1983). MTT yields a yellowish solution when dissolved in culture media. Dehydrogenase enzymes in live cells cleave the tetrazolium ring of MTT and convert it to insoluble purple formazan. Absorbance was read using a UV-spectrophotometer at 550nm after dissolving formazan crystals in DSMO.

Many cells in culture lose their metabolic capabilities towards PAH's such as BaP. To measure the ability of NHEK to bioactivate BaP, cytotoxicity experiments were conducted as described above, with the exception of adding S9 along with the BaP treatment and comparing this data to BaP treatment without S9. An S9 cocktail was added to the cell culture plates only during 24 hour BaP exposures in NHEK. S9 cocktail preparation was according to a previous study (Ames *et al.* 1975). Briefly, the cocktail consisted of 1.0M KCl, 0.25M magnesium chloride ($MgCl_2$), 0.2M sodium phosphate ($NaHPO_4$), 0.2M glucose-6-phosphate (G6P), 0.04M nicotinamide adenine dinucleotide phosphate (NADP), and hepatic microsomal S9 fraction. During cocktail preparation, all reagents were kept on ice until applied to the culture medium. S9 aliquots (stored at -80°C) were only used once to avoid experimental variation due to reduced S9 activity caused by constant thawing and freezing. The S9 concentration in the cocktail was 0.6 mg/ml and NHEK were exposed to a final S9 concentration of 0.1 mg/ml in each well of the cell culture plates. Previous studies in our lab demonstrated that there was no

significant toxicity produced by this concentration of S9 to NHEK and yet, substantial metabolic activity was present at this concentration (data not shown).

3.2.4. Statistical Analysis

Dunnett's one-way analysis of variance (ANOVA) was used to compare the difference of treated to control groups (Tamhane and Dunlop 2000). Treatment is significantly different if the P-value is 0.05 or less when compared to the appropriate control. Statistical regression models were produced for BaP, CZ, DBT, and IQ dose-dependency in NHEK by choosing a regression line, based on the correlation coefficient (r) that best fit the experimental data. These models were used to describe the relationship between increasing concentrations of BaP, CZ, DBT, or IQ and their effects on relative percent survival as an endpoint to measure chemical cytotoxicity in NHEK. From these regression models, the equation generated was used to compare the rate of change (i.e. the slope) to determine which chemicals had a more profound toxic effect on cell survival.

3.3. Results

3.3.1. The Ability of NHEK to Bioactivate Benzo[a]pyrene

To test the metabolic capability of NHEK, experiments were designed to examine whether or not S9 microsomal fraction was required to bioactivate, and thus render toxic, BaP. Previous studies have shown that primary keratinocytes express all the necessary CYPs to bioactivate BaP and other hydrocarbons (Baron *et al.* 2001; Harris *et al.* 2002; Sadek and Allen-Hoffmann 1994; Zhu *et al.* 2002). The goal of this experiment was to

confirm these findings in NHEK, as non-metabolized, parental BaP was not cytotoxic to cells such as the immortalized keratinocyte line RHEK-1 when tested in the absence of S9 during preliminary studies (data not shown). The MTT assay was used to measure cell viability after approximately four days in culture subsequent to 24 hour BaP exposure. Table 3.1 and Figure 3.1 display the data summary of six BaP cytotoxicity experiments performed; three with S9 and three without S9. BaP concentrations tested ranged from 0.1625 to 10.0 μM in experiments with and without S9. These concentrations were selected as described in section 3.2.2 in Materials and Methods.

The results of these experiments indicate that BaP in the presence of S9 was more cytotoxic to NHEK than BaP alone (Table 3.1 and Figure 3.1). BaP with S9 produced a dose-dependent response and caused significant toxicity at concentrations ≥ 0.3125 μM. Nevertheless, in these cells exogenous S9 is not absolutely required to bioactivate BaP, as is evident when examining the dose-dependent cell killing seen in Table 3.1 and Figure 3.1. Experiments in which S9 was not added to NHEK during chemical exposure demonstrate that BaP concentrations ≥ 0.625 μM caused significant cytotoxicity when compared to untreated control cells and the LC_{50} was determined to be approximately 2.0 μM under these conditions. In support of these results, a previous *in vitro* study using human epidermal keratinocytes demonstrated 2.0 μM BaP without S9 caused slightly more than 50% cell toxicity (Kuroki *et al.* 1980). In cells exposed to BaP together with S9, the LC_{50} was determined to be approximately 0.5 μM, or approximately four times more toxic than the BaP alone. These results are consistent with previous studies where it has been documented that skin cells express various CYPs, albeit at lower levels in than

the liver (Zhu *et al.* 2002). Thus, the skin has a relatively low capacity to bioactivate xenobiotics compared to the liver.

These results demonstrate that even though BaP with S9 exposure is substantially more toxic than BaP alone, NHEK is still capable of bioactivating the PAH to produce substantial toxicity at very low concentrations. Therefore, S9 was not used while testing the cytotoxicity of the remaining hydrocarbons of interest in NHEK. Moreover, the objective of this study is to assess dermal exposure of these chemicals in the most realistic environment possible; therefore, without the requirement of S9 to bioactivate these compounds this *in vitro* system is more relevant to real life situations of chemical skin exposure.

3.3.2. Cytotoxic Effects of Petroleum-Derived Hydrocarbons in NHEK

Essentially as described for BaP without the addition of S9 fraction, cytotoxicity studies for the hydrocarbons CZ, DBT, and IQ were performed as described in Materials and Methods. NHEK were exposed to CZ at concentrations of 1.25 to 80.0 μM for 24 hours. A dose-dependent decrease in cell viability was seen subsequent to CZ exposure. CZ concentrations ≥ 2.5 μM cause significant cytotoxicity when compared to control cell populations and the LC_{50} was determined to be approximately 12.0 μM (Table 3.2 and Figure 3.2).

Concentrations of DBT, which ranged from 1.5625 to 100.0 μM, were also tested to examine cell death after 24 hour chemical exposure. Again, a dose-dependent decrease in cell viability was observed following DBT exposure. DBT concentrations ≥ 12.5 μM cause significant cytotoxicity when compared to control cell populations and the LC_{50} was determined to be approximately 28.0 μM (Table 3.3 and Figure 3.3).

Finally, NHEK were exposed to IQ concentrations which ranged from 3.125 to 200.0 μM. Contrary to the other three hydrocarbons, IQ was not cytotoxic to NHEK up to 200.0 μM (Table 3.4 and Figure 3.4). Relative percent survival on NHEK was > 89% for every IQ concentration tested. Higher concentrations of IQ were not possible to assess since IQ would precipitate out in solution above 200.0 μM.

Overall, the toxicity of the different compounds varied considerably from one another. BaP proved to be the most toxic to NHEK among the four hydrocarbons tested. Cytotoxicity of the four hydrocarbons as measured by determining the LC_{50} in NHEK were as follows: BaP > CZ > DBT > IQ (Table 3.5). While IQ produced minimal toxicity in NHEK up to 200.0 μM, BaP ($LC_{50} \approx 2.0$ μM) proved to be 6-times and 14-times more toxic than CZ ($LC_{50} \approx 12.0$ μM) and DBT ($LC_{50} \approx 28.0$ μM), respectively. This trend is the same when the LC_{25} values of the compounds are compared. BaP ($LC_{25} \approx 0.5$ μM) is 8-times and 28-times more toxic than CZ ($LC_{25} \approx 4.0$ μM) and DBT ($LC_{25} \approx 14.0$ μM) respectively. However, this trend changes when comparing the LC_{75s} of both CZ and DBT, while BaP remains the most toxic. At LC_{75}, BaP (5.0 μM) is 8.8-times and 8.4 times more toxic than CZ (44.0 μM) and DBT (42.0 μM) respectively, but now DBT is slightly more toxic than CZ at these high concentrations. When examining the regression analysis for BaP and CZ, both had a similar slope and curve fit to the experimental data as chemical concentration increased (Figures 3.1 and 3.2). However, DBT's regression curve was much more sigmoidal in shape when compared to BaP and CZ. Upon closer examination, DBT produced little cell killing at concentrations ≤ 12.5 μM, however, at higher concentrations the slope of the regression curve was very steep until reaching the maximum concentration of 100.0 μM (Figure 3.3). The correlation coefficient (r) for all

regression analyses were 0.99 for BaP, CZ and DBT dose-dependent cytotoxicity plots. Regression analysis was not conducted for IQ since no cytotoxicity was observed.

The chemical concentrations tested herein are likely to be much higher when compared to those relevant to everyday human exposure. However in an industrial setting, it is possible that workers could potentially be exposed to relatively high hydrocarbon concentrations. In most cases, if humans come in contact with petroleum products, they are exposed to very small amounts of the toxic compounds within a mixture. In spite of this, exposure to a mixture of chemicals could potentially be more hazardous than being exposed to an individual compound from the mixture. This synergistic effect of mixtures has been displayed previously in several studies. Results from one particular study in mice demonstrate that the topical application of a solution containing 0.0006% BaP with toluene (solvent) did not produce skin tumors; however, a coal tar solution in toluene determined to contain 0.0006% BaP produced tumors in 51% of the mice with a latent period of 73 weeks (Warshawsky *et al.* 1993). In contrast, the opposite affect can also be observed where a mixture will inhibit the toxicity and/or carcinogenicity of a particular compound (Warshawsky *et al.* 1993). Other factors such as exposure duration, route of exposure, rates of chemical metabolism, and/or the solubility of the mixture can also have an impact on chemically-induced effects observed in humans. Although high concentrations of the four hydrocarbons were examined in this study, in order to perform a complete cytotoxicity study in NHEK a wide range of chemical concentrations are necessary to determine both extremes of chemical toxicity (i.e. examining chemical concentrations at slightly toxic to extremely toxic levels).

3.4. Discussion

Petroleum is generally considered to be a naturally occurring gaseous, liquid, or solid mixture predominately composed of hydrocarbons (Hunt 1979). Toxicity studies have been done with relatively few of these compounds because most are not commercially available in sufficient quantities for these types of studies (Kropp and Fedorak 1998). Fortunately, increasing numbers of pure condensed hydrocarbons are becoming commercially available, but most only as analytical standards (Kropp and Fedorak 1998). To gain greater insight into the toxicological effects of heavy petroleum distillates, it is in our best interest to examine prominent individual hydrocarbons which represent specific chemical classes within the chemical mixture. This was the approach taken in these studies, where four hydrocarbons were chosen (BaP, CZ, DBT, and IQ) that are major constituents in variety of petroleum mixtures.

The polycyclic aromatic hydrocarbon, BaP, is a constituent of many soots, oils, tars, tobacco smoke, overcooked foods, and air pollutants formed by incomplete pyrolysis of combustible organic material (Hanelt *et al.* 1997; Miller *et al.* 2000; Parkinson and Newbold 1980). Results generated herein demonstrate that BaP is substantially more toxic to NHEK when compared to the other three hydrocarbons. Unlike the other compounds tested in this study, the effects of BaP have been well examined in various *in vitro* and *in vivo* systems. Studies often use BaP to predict the carcinogenic potency of various complex petroleum mixtures (Warshawsky *et al.* 1993). Bioactivated BaP is a known carcinogen, acting as a mutagen and an initiating agent during transformation (Mager *et al.* 1977). There is a substantial amount of data which demonstrates toxic, mutagenic, and/or carcinogenic effects of BaP in various *in vivo* and *in vitro* keratinocyte

studies (Albert *et al.* 1991a; Albert *et al.* 1991b; Cai *et al.* 1997; Hosomi *et al.* 1982; Kuroki *et al.* 1980; Lee and O'Neill 1971; Miller *et al.* 2000; Theall *et al.* 1981; Turner *et al.* 2002). Regarding BaP-induced toxicity, the mutagenic effects of BPDE (electrophilic metabolite and ultimate carcinogen of BaP) has been shown to be accompanied by a strong cytotoxic effect, which may indicate that the DNA repair systems are overloaded (Hanelt *et al.* 1997). Thus, BaP toxicity seems to be related to its mutagenicity. Much work remains to be done, however, to clarify the relationship between BaP exposure, abnormalities in cells proliferation and differentiation, alterations in cell signaling pathways, and the development of neoplastic skin lesions.

CZ, a heterocyclic aromatic compound containing a dibenzopyrrole system, is produced during coal gasification and is present in cigarette smoke, petroleum, creosote, coal tar and clarified slurry oil (Cruzan *et al.* 1986; Riddle *et al.* 2003). Data in this study depict CZ to be the second most toxic compound in NHEK up until the LC_{75} level. After which DBT proved to be more toxic. To date there are no known studies which examine CZ toxicity in keratinocytes *in vitro* or *in vivo*. However, derivatives of CZ have been examined in various studies in this cell type. *In vitro* and *in vivo* skin penetration studies of clarified slurry oil demonstrated that CZ and its derivatives penetrate through the skin to a considerable extent (44%) (Cruzan *et al.* 1986). In another skin related study, a CZ containing compound, Godecke6976 was used as a protein kinase C (PKC) inhibitor to study the role of PKCμ in primary mouse keratinocyte differentiation and proliferation (Shapiro *et al.* 2002). Another report using cultured keratinocytes (HaCaT) demonstrate the induction of CYP1A1 by a CZ containing photoproduct, 6-formylindolo[3,2-*b*]carbazole (Wei *et al.* 1998). Numerous studies have explored dermal effects produced

by *N*-heterocyclic aromatic 7*H*-dibenzo[*c*,*g*]carbazole (DBC) and its synthetic methyl derivative *N*-methyldibenzo[*c*,*g*]carbazole (MeDBC), both of which are by-products of incomplete combustion of fossil fuels, wood, and tobacco. This work revealed that both compounds are mutagens and DBC is a potent liver and skin carcinogen. Specifically, DBC induced frequent ras^{HA} mutations in murine skin and liver tumors (Mitchell and Warshawsky 1999). MeDBC was shown to be a tissue specific sarcomagen (i.e. an agent that produces malignant tumors in connective or supportive tissue) (Gabelova *et al.* 2000; Gabelova *et al.* 2002; Mitchell and Warshawsky 1999, 2001; Taras-Valero *et al.* 2000; Warshawsky *et al.* 1994). In other cell types, *N*-methylcarbazole (NMC), a CZ derivative present in tobacco smoke, is both mutagenic and carcinogenic. Specifically, NMC has displayed these detrimental effects in lung and liver tissue (Ibe and Raj 1994; Yang *et al.* 1991). Furthermore, a report claims that the dealkylation of NMC to CZ is a possible detoxification step displayed in cultured rat hepatocytes (Yang *et al.* 1991). It is clear that much work remains to be done on the parent compound CZ. However, if derived compounds act in a similar manner to CZ, then CZ may not only be toxic, but potentially carcinogenic as well.

The heterocyclic organic sulfur compound, DBT and its derivatives comprise a major group of organic sulfur compounds in petroleum and other products from fossil fuels (Kim *et al.* 2004; Kropp and Fedorak 1998). From the data, DBT is shown to be the third most toxic compound in NHEK of the four hydrocarbons tested up until the LC_{75} level, at which point DBT becomes more cytotoxic than CZ. There are no known studies which specifically examine the effects of DBT in keratinocytes or in mammalian skin models. Numerous researchers have investigated the metabolic pathway of DBT once

bioactivated or degraded in various environmental settings by bacterium, microbial organisms, or plant species (Gallagher *et al.* 1993; Kropp and Fedorak 1998; Laborde and Gibson 1977; Monticello *et al.* 1985; Omori *et al.* 1992). There are also reports which examined DBT derivatives and other similar thiophene compounds in other model systems. DBT or its methylated derivatives did not have detectable mutagenic activity using the Ames assay (McFall *et al.* 1984; Pelroy *et al.* 1983). Other research displayed the carcinogenic potential of numerous polycyclic aromatic sulfur heterocycles and methyl-substituted derivatives in rats and mice; however, DBT was not included in this list (Jacob 1990). In another study, the *Daphnia magna* bioassay was used to measure the acute toxicity of DBT and the results indicate its oxidative metabolites were less toxic than the parent compound (Seymour *et al.* 1997; Zemanek *et al.* 1997). Overall, DBT has not been extensively studied, however, Kropp and Fedorak present a thorough review of the occurrence, toxicity, and biodegradation of condensed thiophenes with limited DBT information focusing mainly on its biodegradation in various environmental systems (Kropp and Fedorak 1998). This review concludes that several organosulfur compounds display toxic, mutagenic, and carcinogenic capabilities. However, these capabilities have yet to be extensively examined for DBT. Clearly, there is still much to be learned about DBT and its effects on mammalian model systems.

IQ is an aromatic nitrogen compound and has been identified as a component of coal tar. Results from this study show for the first time that IQ is non-cytotoxic in NHEK up to 200.0 μM. However, in previous work an IQ containing compound, 1-(5-isoquinoline-sulfonyl)-2-methyl piperazine dihydrochloride, has been identified as a PKC inhibitor in keratinocytes (Hirobe 1994; Takahashi *et al.* 1995). IQ has also been shown

to contribute to the anti-psoriatic capacities in the mouse tail model (Arnold *et al.* 1993; Foreman *et al.* 1985). Studies done in the 1990s found IQ derivatives to be endogenous neurotoxins in the etiology of Parkinson's disease (McNaught *et al.* 1998; McNaught *et al.* 1996). Another report indicated that IQ derivatives enhance neuronal survival in primary cultures of cortical neurons from mouse embryos (Ueda *et al.* 1999). An IQ alkaloid, berberine, proved to be neither genotoxic nor cytotoxic to eukaryotic microorganisms (Pasqual *et al.* 1993). Since IQ derivatives are widely distributed in the environment (plants and foodstuffs) and cause neurodegenerative changes related to Parkinson's disease, there is a popular demand to examine the effects of IQ containing compounds rather than IQ itself. Therefore, studies which have investigated the effects of IQ are rare. It is evident there is a lack of information on the effects of IQ in mammalian systems. Further investigation is required to conclude whether or not IQ itself could potentially be a toxic or carcinogenic component of coal tar.

To my knowledge, these studies are the first to systematically examine the toxic effects of BaP, CZ, DBT, and IQ in a primary keratinocyte system. Although IQ did not display any toxicity, CZ, and DBT proved to be fairly toxic, while BaP demonstrated extreme toxicity in NHEK. The cytotoxicity data gathered from these experiments was very important for selecting the appropriate concentrations to use in future studies which examined chemical effects on NHEK differentiation, proliferation, and gene expression. Initially, the goal was to examine the effects of all four hydrocarbons singly and as a mixture on these cellular processes. Two alkylated derivatives of each compound would then be studied and compared with the parental compound. However, due to the highly interesting results gathered from this study with BaP, the focus has remained on more

detailed and mechanistic analysis of this high priority PAH. As time and funding allows, future studies in the laboratory will continue the work on CZ, DBT, IQ and their alkylated derivatives. The data presented herein may be highly valuable for this future research in this area.

3.5. References

Albert, R. E., Miller, M. L., Cody, T., Andringa, A., Shukla, R., and Baxter, C. S. (1991a). Benzo[a]pyrene-induced skin damage and tumor promotion in the mouse. *Carcinogenesis* **12**, 1273-1280.

Albert, R. E., Miller, M. L., Cody, T. E., Barkley, W., and Shukla, R. (1991b). Cell kinetics and benzo[a]pyrene-DNA adducts in mouse skin tumorigenesis. *Progress in Clinical & Biological Research* **369**, 115-122.

Ames, B. N., Mccann, J., and Yamasaki, E. (1975). Methods for detecting carcinogens and mutagens with the Salmonella/mammalian-microsome mutagenicity test. *Mutat.Res.* **31**, 347-364.

Arnold, W. P., Glade, C. P., Mier, P. D., and van de Kerkhof, P. C. (1993). Effects of sphingosine, isoquinoline and tannic acid on the human tape-stripping model and the psoriatic lesion. *Skin Pharmacol.* **6**, 193-199.

Baron, J. M., Holler, D., Schiffer, R., Frankenberg, S., Neis, M., Merk, H. F., and Jugert, F. K. (2001). Expression of multiple cytochrome p450 enzymes and multidrug resistance-associated transport proteins in human skin keratinocytes. *J.Invest Dermatol.* **116**, 541-548.

Cai, Y., Baer-Dubowska, W., Ashwood-Smith, M., and DiGiovanni, J. (1997). Inhibitory effects of naturally occurring coumarins on the metabolic activation of benzo[a]pyrene and 7,12-dimethylbenz[a]anthracene in cultured mouse keratinocytes. *Carcinogenesis* **18**, 215-222.

Chao, Y. C., and Nylander-French, L. A. (2004). Determination of keratin protein in a tape-stripped skin sample from jet fuel exposed skin. *Ann.Occup.Hyg.* **48**, 65-73.

Cruzan, G., Low, L. K., Cox, G. E., Meeks, J. R., Mackerer, C. R., Craig, P. H., Singer, E. J., and Mehlman, M. A. (1986). Systemic toxicity from subchronic dermal exposure, chemical characterization, and dermal penetration of catalytically cracked clarified slurry oil. *Toxicol.Ind.Health* **2**, 429-444.

Foreman, M. I., Taylor, M., Clark, C., Devitt, H., Hanlon, G., Kelly, I., and Lukowiecki, G. (1985). Isoquinoline is a possible anti-psoriatic agent in coal tar. *Br.J.Dermatol.* **112**, 323-328.

Gabelova, A., Bacova, G., Ruzekova, L., and Farkasova, T. (2000). Role of cytochrome P4501A1 in biotransformation of a tissue specific sarcomagen N-methyldibenzo[c,g]carbazole. *Mutat.Res.* **469**, 259-269.

Gabelova, A., Farkasova, T., Bacova, G., and Robichova, S. (2002). Mutagenicity of 7H-dibenzo[c,g]carbazole and its tissue specific derivatives in genetically engineered Chinese hamster V79 cell lines stably expressing cytochrome P450. *Mutat.Res.* **517**, 135-145.

Gallagher, J. R., Olson, E. S., and Stanley, D. C. (1993). Microbial desulfurization of dibenzothiophene: a sulfur-specific pathway. *FEMS Microbiol.Lett.* **107**, 31-35.

Gershbein, L. L. (1975). Liver regeneration as influenced by the structure of aromatic and heterocyclic compounds. *Res.Commun.Chem.Pathol.Pharmacol.* **11**, 445-466.

Gustafson, D. L., Beall, H. D., Bolton, E. M., Ross, D., and Waldren, C. A. (1996). Expression of human NAD(P)H: quinone oxidoreductase (DT-diaphorase) in Chinese hamster ovary cells: effect on the toxicity of antitumor quinones. *Mol.Pharmacol.* **50**, 728-735.

Hanelt, S., Helbig, R., Hartmann, A., Lang, M., Seidel, A., and Speit, G. (1997). A comparative investigation of DNA adducts, DNA strand breaks and gene mutations induced by benzo[a]pyrene and (+/-)-*anti*-benzo[a]pyrene-7,8-diol 9,10-oxide in cultured human cells. *Mutation Research* **390**, 179-188.

Harris, I. R., Siefken, W., Beck-Oldach, K., Brandt, M., Wittern, K. P., and Pollet, D. (2002). Comparison of activities dependent on glutathione S-transferase and cytochrome P-450 IA1 in cultured keratinocytes and reconstructed epidermal models. *Skin Pharmacol.Appl.Skin Physiol* **15 Suppl 1**, 59-67.

Hartwig, A., Asmuss, M., Ehleben, I., Herzer, U., Kostelac, D., Pelzer, A., Schwerdtle, T., and Burkle, A. (2002). Interference by toxic metal ions with DNA repair processes and cell cycle control: molecular mechanisms. *Environ.Health Perspect.* **110 Suppl 5**, 797-799.

Henry, J. A. (1998). Composition and toxicity of petroleum products and their additives. *Hum.Exp.Toxicol.* **17**, 111-123.

Hirobe, T. (1994). Effects of activators (SC-9 and OAG) and inhibitors (staurosporine and H-7) of protein kinase C on the proliferation of mouse epidermal melanoblasts in serum-free culture. *J.Cell Sci.* **107 (Pt 6)**, 1679-1686.

Hosomi, J., Nemoto, N., and Kuroki, T. (1982). Metabolism of benzo[a]pyrene and other carcinogens in mouse epidermal keratinocytes in culture. *Gann* **73**, 879-886.

Hunt, J. M. (1979). *Petroleum geochemistry and geology*. W.H. Freeman & Co., New York.

Ibe, B. O., and Raj, J. U. (1994). Metabolism of N-methylcarbazole by rat lung microsomes. *Exp.Lung Res.* **20**, 207-222.

Jacob, J. (1990). *Sulfur analogues of polycyclic aromatic hydrocabons (Thiaarenes)*. Cambridge University Press, Cambridge.

Kim, Y. J., Chang, J. H., Cho, K. S., Ryu, H. W., and Chang, Y. K. (2004). A physiological study on growth and dibenzothiophene (DBT) desulfurization characteristics of *Gordonia* sp. CYKS1. *Korean J.Chem.Eng.* **21**, 436-441.

Kropp, K. G., and Fedorak, P. M. (1998). A review of the occurrence, toxicity, and biodegradation of condensed thiophenes found in petroleum. *Can.J.Microbiol.* **44**, 605-622.

Kuroki, T., Nemoto, N., and Kitano, Y. (1980). Metabolism of benzo[a]pyrene in human epidermal keratinocytes in culture. *Carcinogenesis* **1**, 559-565.

La Voie, E. J., Adams, E. A., Shigematsu, A., and Hoffmann, D. (1983). On the metabolism of quinoline and isoquinoline: possible molecular basis for differences in biological activities. *Carcinogenesis* **4**, 1169-1173.

Laborde, A. L., and Gibson, D. T. (1977). Metabolism of dibenzothiophene by a Beijerinckia species. *Appl.Environ.Microbiol.* **34**, 783-790.

Lee, P. N., and O'Neill, J. A. (1971). The effect both of time and dose applied on tumour incidence rate in benzopyrene skin painting experiments. *Br.J Cancer* **25**, 759-770.

Mackerer, C. R., Griffis, L. C., Grabowski Jr, J. S., and Reitman, F. A. (2003). Petroleum mineral oil refining and evaluation of cancer hazard. *Appl.Occup.Environ.Hyg.* **18**, 890-901.

Mager, R., Huberman, E., Yang, S. K., Gelboin, H. V., and Sachs, L. (1977). Transformation of normal hamster cells by benzo(a)pyrene diol-epoxide. *Int.J.Cancer* **19**, 814-817.

Maher, V. M., Patton, J. D., Yang, J. L., Wang, Y. Y., Yang, L. L., Aust, A. E., Bhattacharyya, N., and McCormick, J. J. (1987). Mutations and homologous recombination induced in mammalian cells by metabolites of benzo[a]pyrene and 1-nitropyrene. *Environ.Health Perspect.* **76**, 33-39.

McFall, T., Booth, G. M., Lee, M. L., Tominaga, Y., Pratap, R., Tedjamulia, M., and Castle, R. N. (1984). Mutagenic activity of methyl-substituted tri- and tetracyclic aromatic sulfur heterocycles. *Mutat.Res.* **135**, 97-103.

McNaught, K. S., Carrupt, P. A., Altomare, C., Cellamare, S., Carotti, A., Testa, B., Jenner, P., and Marsden, C. D. (1998). Isoquinoline derivatives as endogenous neurotoxins in the aetiology of Parkinson's disease. *Biochem.Pharmacol.* **56**, 921-933.

McNaught, K. S., Thull, U., Carrupt, P. A., Altomare, C., Cellamare, S., Carotti, A., Testa, B., Jenner, P., and Marsden, C. D. (1996). Toxicity to PC12 cells of isoquinoline derivatives structurally related to 1-methyl-4-phenyl-1,2,3,6-tetrahydropyridine. *Neurosci.Lett.* **206**, 37-40.

Mehlman, M. A. (1992). Dangerous and cancer-causing properties of products and chemicals in the oil refining and petrochemical industry. VIII. Health effects of motor fuels: carcinogenicity of gasoline--scientific update. *Environ.Res.* **59**, 238-249.

Miller, M. L., Vasunia, K., Talaska, G., Andringa, A., de Boer, J., and Dixon, K. (2000). The tumor promoter TPA enhances benzo[a]pyrene and benzo[a]pyrene diolepoxide mutagenesis in Big Blue mouse skin. *Environ.Mol.Mutagen.* **35**, 319-327.

Mitchell, K. R., and Warshawsky, D. (1999). Frequent Ha-ras mutations in murine skin and liver tumors induced by 7H-dibenzo[c,g]carbazole. *Mol.Carcinog.* **25**, 107-112.

Mitchell, K. R., and Warshawsky, D. (2001). Comparison of Ha-ras mutational spectra of N-methyldibenzo[c,g]carbazole and 7H-dibenzo[c,g]carbazole-induced mouse skin tumors. *Mol.Carcinog.* **32**, 55-60.

Monteiro-Riviere, N. A., Inman, A. O., and Riviere, J. E. (2004). Skin toxicity of jet fuels: ultrastructural studies and the effects of substance P. *Toxicol.Appl.Pharmacol.* **195**, 339-347.

Monticello, D. J., Bakker, D., and Finnerty, W. R. (1985). Plasmid-mediated degradation of dibenzothiophene by Pseudomonas species. *Appl.Environ.Microbiol.* **49**, 756-760.

Mosmann, T. (1983). Rapid colorimetric assay for cellular growth and survival: application to proliferation and cytotoxicity assays. *J.Immunol.Methods* **65**, 55-63.

Nesnow, S. (1990). Mouse skin tumours and human lung cancer: relationships with complex environmental emissions. *IARC Sci.Publ.*, 44-54.

Omori, T., Monna, L., Saiki, Y., and Kodama, T. (1992). Desulfurization of dibenzothiophene by Corynebacterium sp. strain SY1. *Appl.Environ.Microbiol.* **58**, 911-915.

Parkinson, E. K., and Newbold, R. F. (1980). Benzo(a)pyrene metabolism and DNA adduct formation in serially cultivated strains of human epidermal keratinocytes. *Int.J.Cancer* **26**, 289-299.

Pasqual, M. S., Lauer, C. P., Moyna, P., and Henriques, J. A. (1993). Genotoxicity of the isoquinoline alkaloid berberine in prokaryotic and eukaryotic organisms. *Mutat.Res.* **286**, 243-252.

Pelroy, R. A., Stewart, D. L., Tominaga, Y., Iwao, M., Castle, R. N., and Lee, M. L. (1983). Microbial mutagenicity of 3- and 4-ring polycyclic aromatic sulfur heterocycles. *Mutat.Res.* **117**, 31-40.

Poon, R., Davis, H., Lecavalier, P., Liteplo, R., Yagminas, A., Chu, I., and Bihun, C. (1997). Effects of benzothiophene on male rats following short-term oral exposure. *J.Toxicol.Environ.Health* **50**, 53-65.

Riddle, R. R., Gibbs, P. R., Willson, R. C., and Benedik, M. J. (2003). Recombinant carbazole-degrading strains for enhanced petroleum processing. *J.Ind.Microbiol.Biotechnol.* **30**, 6-12.

Sadek, C. M., and Allen-Hoffmann, B. L. (1994). Cytochrome P450IA1 is rapidly induced in normal human keratinocytes in the absence of xenobiotics. *J.Biol.Chem.* **269**, 16067-16074.

Seymour, D. T., Verbeek, A. G., Hrudey, S. E., and Fedorak, P. M. (1997). Acute toxicity and aqueous solubility of some condensed thiophenes and their microbial metabolites. *Environ.Toxicol.Chem.* **16**, 658-665.

Seymour, F. K., and Henry, J. A. (2001). Assessment and management of acute poisoning by petroleum products. *Hum.Exp.Toxicol.* **20**, 551-562.

Shapiro, B. A., Ray, S., Jung, E., Allred, W. T., and Bollag, W. B. (2002). Putative conventional protein kinase C inhibitor Godecke 6976 [12-(2-cyanoethyl)-6,7,12,13-tetrahydro-13-methyl-5-oxo-5H-indolo(2,3-a)py rrolo(3,4-c)-carbazole] stimulates transglutaminase activity in primary mouse epidermal keratinocytes. *J.Pharmacol.Exp.Ther.* **302**, 352-358.

Takahashi, H., Kobayashi, H., Hashimoto, Y., Matsuo, S., and Iizuka, H. (1995). Interferon-gamma-dependent stimulation of Fas antigen in SV40-transformed human keratinocytes: modulation of the apoptotic process by protein kinase C. *J.Invest Dermatol.* **105**, 810-815.

Tamhane, A. C., and Dunlop, D. D. (2000). Multiple comparisons of means. In Statistics and Data Analysis from Elementary to Intermediate, pp. 475-476. Prentice-Hall, Inc., Upper Saddle River, NJ.

Taras-Valero, D., Perin-Roussel, O., Plessis, M. J., Zajdela, F., and Perin, F. (2000). Tissue-specific activities of methylated dibenzo[c,g]carbazoles in mice: carcinogenicity, DNA adduct formation, and CYP1A induction in liver and skin. *Environ.Mol.Mutagen.* **35**, 139-149.

Theall, G., Eisinger, M., and Grunberger, D. (1981). Metabolism of benzo[a]pyrene and DNA adduct formation in cultured epidermal keratinocytes. *Carcinogenesis* **2**, 581-587.

Turner, K. J., Barlow, N. J., Struve, M. F., Wallace, D. G., Gaido, K. W., Dorman, D. C., and Foster, P. M. (2002). Effects of in utero exposure to the organophosphate insecticide

fenitrothion on androgen-dependent reproductive development in the Crl:CD(SD)BR rat. *Toxicol.Sci.* **68**, 174-183.

Ueda, Y., Nakanishi, H., and Yoshida, K. (1999). Neurotrophic effect of isoquinoline derivatives in primary cortical culture. *Life Sci.* **65**, 1477-1484.

Warshawsky, D., Barkley, W., and Bingham, E. (1993). Factors affecting carcinogenic potential of mixtures. *Fundamental & Applied Toxicology* **20**, 376-382.

Warshawsky, D., Barkley, W., Miller, M. L., LaDow, K., and Andringa, A. (1994). Carcinogenicity of 7H-dibenzo[c,g]carbazole, dibenz[a,j]acridine and benzo[a]pyrene in mouse skin and liver following topical application. *Toxicology* **93**, 135-149.

Wei, Y. D., Helleberg, H., Rannug, U., and Rannug, A. (1998). Rapid and transient induction of CYP1A1 gene expression in human cells by the tryptophan photoproduct 6-formylindolo[3,2-b]carbazole. *Chem.Biol.Interact.* **110**, 39-55.

Weker, R. A., Herrick, R. F., and Rinehart, R. D. (2004). Laboratory evaluation of a potential diesel fuel interference in the determination of polycyclic aromatic compounds on dermal samplers. *J.Occup.Environ.Hyg.* **1**, 334-342.

Wislocki, P. G., Wood, A. W., Chang, R. L., Levin, W., Yagi, H., Hernandez, O., Dansette, P. M., Herina, D. M., and Conney, A. H. (1976a). Mutagenicity and cytotoxicity of benzo(a)pyrene arene oxides, phenols, quinones, and dihydrodiols in bacterial and mammalian cells. *Cancer Res.* **36**, 3350-3357.

Wislocki, P. G., Wood, A. W., Chang, R. L., Levin, W., Yagi, H., Hernandez, O., Jerina, D. M., and Conney, A. H. (1976b). High mutagenicity and toxicity of a diol epoxide derived from benzo(a)pyrene. *Biochem.Biophys.Res.Commun.* **68**, 1006-1012.

Wood, A. W., Wislocki, P. G., Chang, R. L., Levin, W., Lu, A. Y., Yagi, J., Hernandez, O., Herina, D. M., and Conney, A. H. (1976). Mutagenicity and cytotoxicity of benzo(a)pyrene benzo-ring epoxides. *Cancer Res.* **36**, 3358-3366.

Yang, W., Jiang, T. R., Davis, P. J., and Acosta, D. (1991). In vitro metabolism and toxicity assessment of N-methylcarbazole in primary cultured rat hepatocytes. *Toxicology* **68**, 217-226.

Zemanek, M. G., Pollard, S. J., Kenefick, S. L., and Hrudey, S. E. (1997). Toxicity and mutagenicity of component classes of oils isolated from soils at petroleum- and creosote-contaminated sites. *J.Air Waste Manag.Assoc.* **47**, 1250-1258.

Zhu, Z., Hotchkiss, S. A., Boobis, A. R., and Edwards, R. J. (2002). Expression of P450 enzymes in rat whole skin and cultured epidermal keratinocytes. *Biochem.Biophys.Res.Commun.* **297**, 65-70.

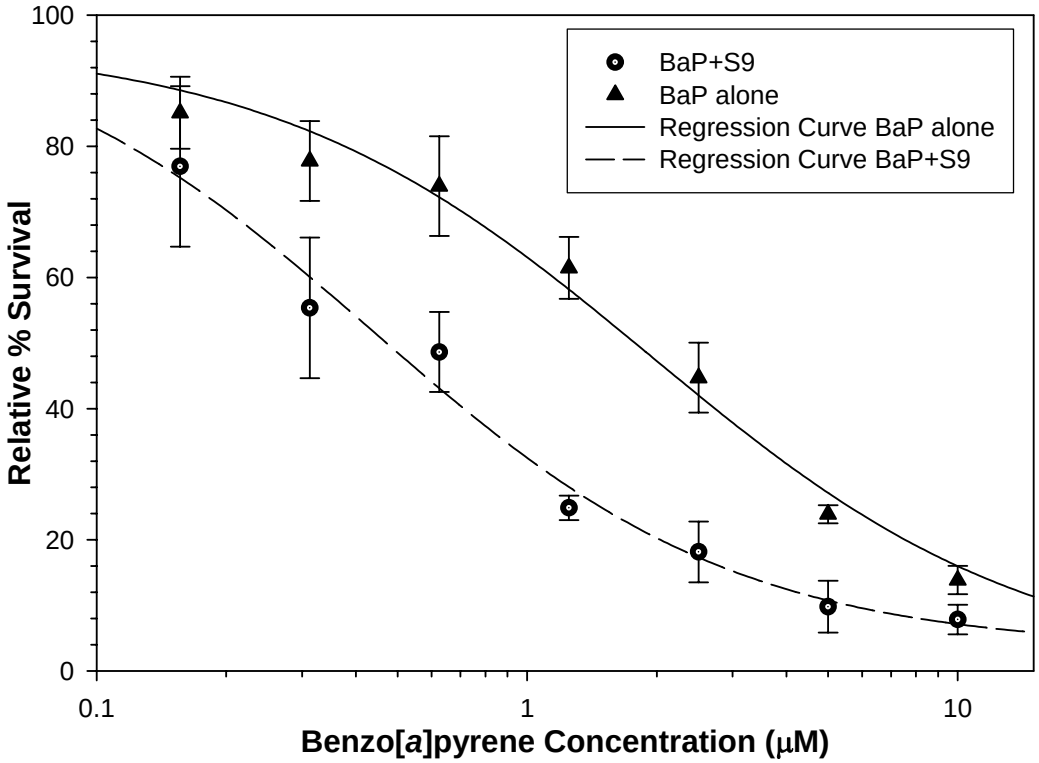

Figure 3.1. **Benzo[*a*]pyrene cytotoxicity with and without S9 in NHEK.** BaP treatment ranged from 0.1625 to 10.0 μM for 24 hr in both S9 and without S9 experiments. The MTT assay was conducted to measure cell viability as described in Materials and Methods. DMSO was utilized as the vehicle control. The percentage of cell survival for each chemical concentration is expressed as the mean of triplicates from 3 independent experiments ± SD. Statistical regression analysis was carried out to predict the best mathematical model for describing relative percent cell survival as a function of chemical concentration.

Table 3.1. Comparison of benzo[*a*]pyrene toxicity in the presence and absence of S9 in NHEK (* = significantly different when compared to controls)

Benzo[*a*]pyrene Concentration (μM)	**With S9**		**Without S9**	
	% Survival	StDev	% Survival	St.Dev
10.0	*7.85	2.25	*13.85	2.15
5.0	*9.79	3.96	*23.89	1.39
2.5	*18.15	4.63	*44.71	5.32
1.25	*24.86	1.88	*61.45	4.72
0.625	*48.62	6.10	*73.93	7.59
0.3125	*55.35	10.71	77.75	6.08
0.15625	76.93	12.23	85.10	5.49
0.0	100.08	7.07	99.94	6.67

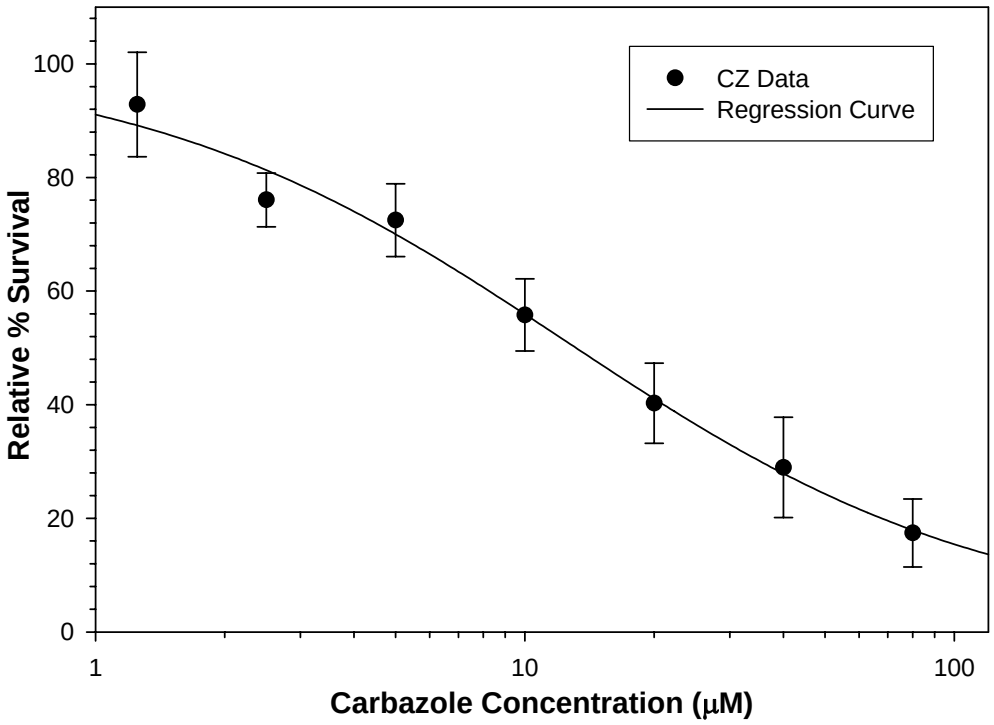

Figure 3.2. **Carbazole cytotoxicity in NHEK in the absence of S9.** CZ treatment ranged from 1.25 to 80.0 μM for 24 hr. The MTT assay was conducted to measure cell viability as described in Materials and Methods. DMSO was used as the vehicle control. The percentage of cell survival for each chemical concentration is expressed as the mean of triplicates from 3 independent experiments ± SD. Statistical regression analysis was carried out to predict the best mathematical model for describing relative percent cell survival as a function of chemical concentration.

Table 3.2. Carbazole toxicity in NHEK

Concentration (μM)	Relative % Survival	Standard Deviation
80.0	*17.42	5.98
40.0	*28.96	8.83
20.0	*40.26	7.05
10.0	*55.81	6.35
5.0	*72.48	6.41
2.5	*76.07	4.72
1.25	92.85	9.19
0.0	100.42	2.56

* Statistical significance when compared to controls

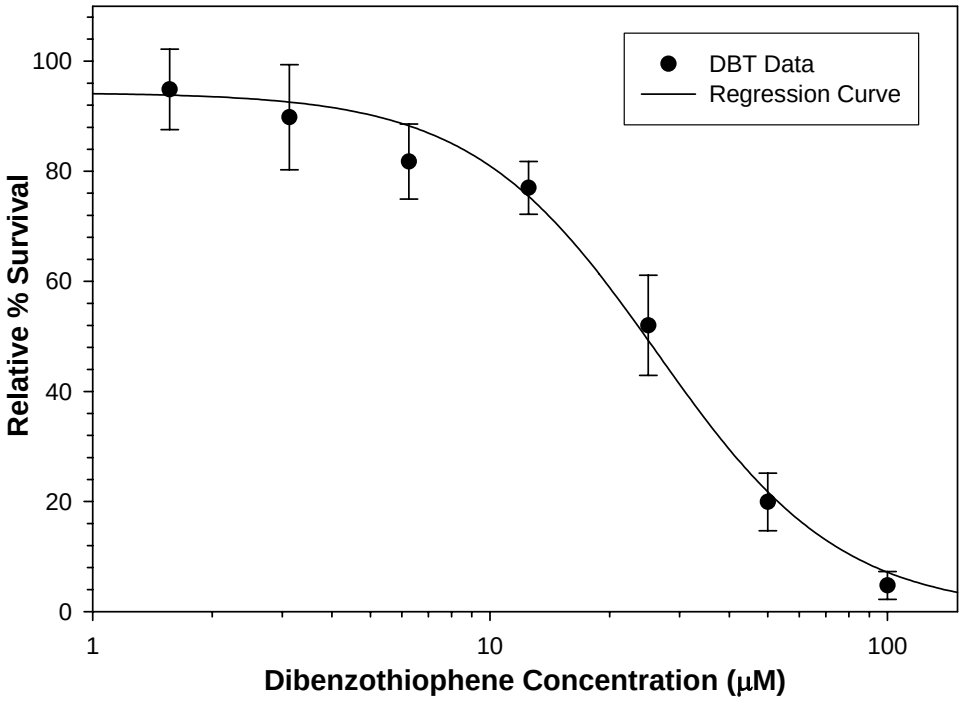

Figure 3.3. **Dibenzothiophene cytotoxicity in NHEK in the absence of S9.** DBT treatment ranged from 1.5625 to 100.0 μM for 24 hr. The MTT assay was conducted to measure cell viability as described in Materials and Methods. DMSO was used as the vehicle control. The percentage of cell survival for each chemical concentration is expressed as the mean of triplicates from 3 independent experiments ± SD. Statistical regression analysis was carried out to predict the best mathematical model for describing relative percent cell survival as a function of chemical concentration.

Table 3.3. Dibenzothiophene toxicity in NHEK

Concentration (μM)	Relative % Survival	Standard Deviation
100.0	*4.75	2.54
50.0	*19.01	5.24
25.0	*52.01	9.11
12.5	*76.99	4.81
6.25	81.76	6.83
3.125	89.81	9.55
1.5625	94.87	7.31
0.0	99.99	8.26

* statistical significance when compared to controls

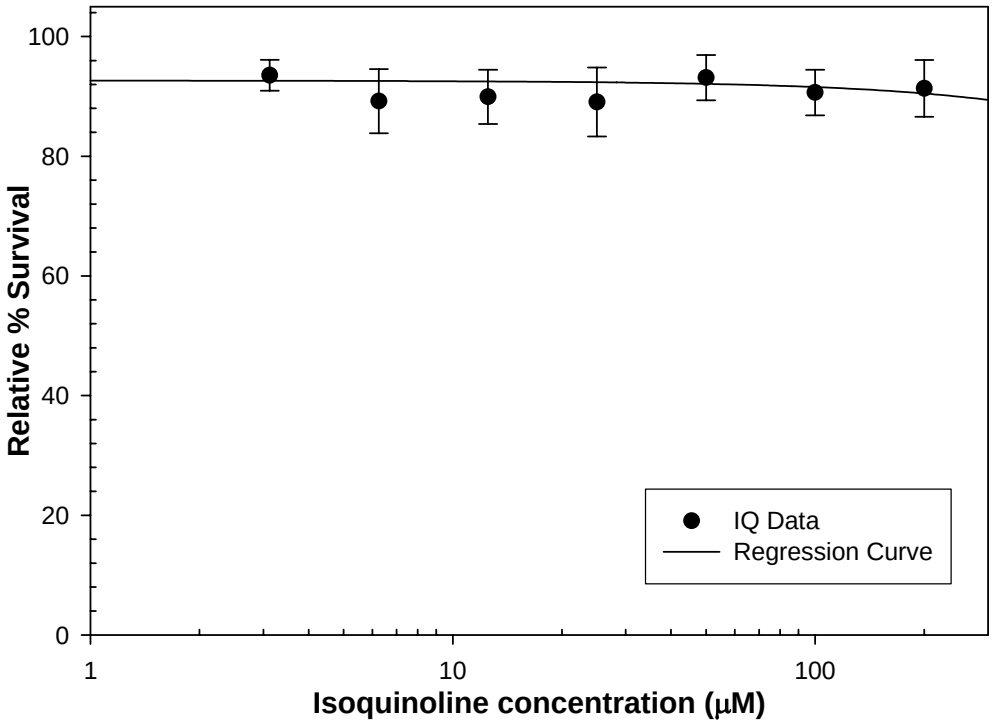

Figure 3.4. **Isoquinoline cytotoxicity in NHEK in the absence of S9.** IQ treatment ranged from 3.125 to 200.0 μM for 24 hr. The MTT assay was conducted to measure cell viability as described in Materials and Methods. DMSO was used as the vehicle control. The percentage of cell survival for each chemical concentration is expressed as the mean of triplicates from 3 independent experiments ± SD. Statistical regression analysis was carried out to predict the best mathematical model for describing relative percent cell survival as a function of chemical concentration.

Table 3.4. Isoquinoline toxicity in NHEK

Concentration (μM)	Relative % Survival	Standard Deviation
200.0	91.34	4.73
100.0	90.65	3.81
50.0	93.14	3.78
25.0	89.07	5.76
12.5	89.92	4.52
6.25	89.20	5.35
3.125	93.53	2.58
0.0	99.94	6.33

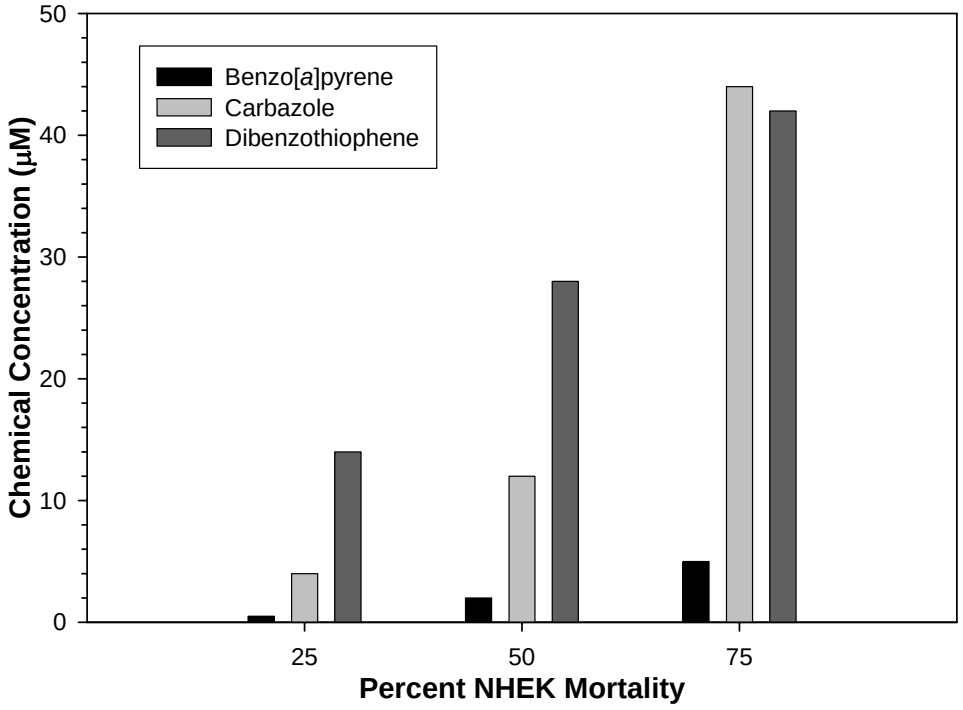

Figure 3.5. **Comparative lethal concentration analysis of benzo[*a*]pyrene, carbazole, and dibenzothiophene in NHEK.** LC_{25}, LC_{50}, and LC_{75} were compared between each cytotoxic compound. Isoquinoline was not compared since it proved to be non-cytotoxic at all concentrations tested in NHEK. Cytotoxicity of the three hydrocarbons compared at LC_{25} and LC_{50} in NHEK were as follows: BaP > CZ > DBT. However, when comparing the LC_{75} of each compound the order of cytotoxicity was: BaP > DBT > CZ.

Table 3.5. Approximate lethal concentrations for each chemical in NHEK

Chemicals	LC_{25} (μM)	LC_{50} (μM)	LC_{75} (μM)
Benzo[*a*]pyrene	0.5	2.0	5.0
Carbazole	4.0	12.0	44.0
Dibenzothiophene	14.0	28.0	42.0
Isoquinoline	-No toxicity observed-		

Chapter 4

Arsenic and Benzo[*a*]pyrene Differentially Alter the Capacity for Differentiation and Growth Properties of Primary Human Epidermal Keratinocytes

4.1. Background

The balance between proliferating and differentiating keratinocytes is essential to maintain dermal homeostasis. Once this balance is disrupted, events may occur which can potentially lead to the onset of carcinogenesis. An increase in proliferating keratinocytes with a decline in differentiating keratinocytes is one sign which may be indicative of a transformed and pre-cancerous population of cells in the skin. In this chapter, the effects of two known skin carcinogens, arsenic and benzo[*a*]pyrene (BaP), were examined on primary keratinocyte growth properties and differentiation. If chemicals alter these key cellular processes in keratinocytes, it may provide phenotypic evidence of possible roles each chemical may play to initiate cancer in the skin. Originally, the goal was to examine the effects of the four hydrocarbons presented in Chapter 3 on keratinocyte differentiation. Preliminary results from BaP-mediated effects on NHEK differentiation proved to be very interesting. Therefore, the research direction changed to concentrating on the effects produced by BaP (at various exposure concentrations) on the terminal differentiation of NHEK. Furthermore, because BaP proved to be the most toxic hydrocarbon and since there are vast quantities of information on BaP in the literature, it

gave more reason to pursue the study of this compound. There was also a unique opportunity to study this compound on cellular processes as there are very few studies that have examined the effects of BaP on epidermal differentiation. Arsenic came into the picture because it is a known inhibitor of squamous differentiation in keratinocytes; therefore, arsenic was originally used as a negative control in these experiments to compare any inhibitory effects that BaP had on NHEK differentiation. Meanwhile, since calcium is a known inducer of differentiation in keratinocytes, it was used as a positive control. From the results obtained in this chapter and other factors, the focus of this project was redirected to examine and compare the mechanistic differences between two very different skin carcinogens, arsenic and BaP. The following text has been published in the journal of *Toxicological Sciences*, Volume 76, pages 280-290 (2003). Due to reference number constraints enforced by *Toxicological Sciences*, the published version contains a limited number of citations; therefore, additional references were inserted into the originally published copy where necessary.

4.2. Abstract in the Original Publication

Normal human epidermal keratinocytes (NHEK) have been chosen as an *in vitro* model to test the hypothesis that chemicals which alter or interfere in cellular differentiation will concomitantly induce growth perturbations and are, thus, potential carcinogens. In these studies, we have focused on two known skin carcinogens, arsenic and benzo[*a*]pyrene (BaP). Our results demonstrated that BaP inhibits terminal differentiation in NHEK, as measured by cross-linked envelope (CLE) formation, by up to 5.8-fold in control and 1.7-fold in calcium (Ca^{2+})-treated cells. In comparison, arsenic decreased CLE formation by 20-fold in control cells and 5.5-fold in Ca^{2+}-treated NHEK.

To characterize the effects of these agents on the growth rate and cell cycle distribution of NHEK, flow cytometric analysis was used. BaP at 2.0 μM increased proliferation rates by 29%. Altered cell-cycle distribution in BaP-treated cells indicated a more rapid progression through the cell cycle, possibly by a shortened G2 phase. In contrast, arsenic at 5.0 μM inhibited proliferation by 25%; growth arrest (9%) was also observed in NHEK treated with 2.0 mM Ca^{2+}. Our findings suggest that, although both BaP and arsenic inhibit CLE production in NHEK, different mechanisms may be involved. Studies in progress will attempt to identify molecular markers involved in the observed chemical effects. These markers will facilitate a mechanistic understanding of how an altered balance between growth and differentiation may play a role in the transformation process in NHEK.

4.3. Introduction in the Original Publication

The epidermis is characterized by a highly regulated balance between epithelial cell growth and differentiation, with a single basal layer of proliferating keratinocytes and stratified, overlying keratinized layers. Differentiation ultimately leads to a highly specialized, “dead-end” cell that cannot divide. However, within the basal compartment, cells can be changed by carcinogenic agents such that they are blocked from achieving the normal state of differentiation and are, instead, capable of indefinite proliferation. This imbalance between two such important and opposing processes has been linked to the onset of carcinogenesis.

The skin is a useful model system for understanding the signals that drive proliferation or differentiation, particularly with respect to alterations that may lead to

cancer. Epidermal keratinocytes differentiate readily in culture and produce cross-linked envelopes (CLE), a complex protein structure that forms the protective barrier of the skin. This switch between proliferation and differentiation is regulated by phospholipase C and protein kinase C (PKC)-dependent pathways, as well as induction of tyrosine phosphorylation, among others (Denning *et al.* 1995; Filvaroff *et al.* 1990; Xie and Bikle 1999). Defects in terminal differentiation have been tied to transformation in keratinocytes, implying that targets for chemically-mediated carcinogenesis may well be pivotal signaling pathways involved in this process (Salnikow and Cohen 2002). One way to approach this issue is through comparison of the alterations induced during differentiation by multiple skin carcinogens.

Arsenic is a potent human skin carcinogen. In fact, due to arsenic-contaminated drinking water in many countries, development of neoplastic skin lesions has become a health problem of global proportions (Chen *et al.* 1992; Chowdhury *et al.* 2000; Tseng 1977). The exact mechanism involved in the transformation of keratinocytes by arsenic is unclear. Due to its clastogenic activity and inhibition of DNA repair, arsenic is presumed to act as a progressing agent during carcinogenesis (Leonard and Lauwerys 1980; Vogt and Rossman 2001). Arsenic has other effects on keratinocytes including: (1) altering expression of growth regulatory factors, (2) enhancing cell proliferation at low concentrations, and (3) inhibition of keratinization (Germolec *et al.* 1996; Kachinskas *et al.* 1994; Vega *et al.* 2001). It is likely that these effects are linked to one another and to the induction of skin cancer. Many investigators are currently attempting to address this issue through identification of important molecular switches that are negatively impacted by arsenic and which may render the skin a sensitive target to malignant transformation.

Benzo[*a*]pyrene (BaP) is among the Superfund Top 10 Priority Hazardous Substances and is a common constituent in petroleum products. BaP also represents a major class of heavy fraction hydrocarbons in mixtures such as coal tar, smoke, and automobile exhaust. There is, thus, potential for either environmental or occupational dermal exposure to BaP. The most likely source of dermal contact with toxic BaP levels would be in workers in the petroleum industry. Bioactivated BaP is a known skin carcinogen, acting as a mutagen and an initiating agent during transformation (Mager *et al.* 1977). Many of the earliest studies of BaP were carried out using the murine skin system (Lee and O'Neill 1971). When applied dermally, BaP induces cytokinetic abnormalities and inflammation, followed by skin tumors (Albert *et al.* 1996). The chemical alters differentiation in multiple cell types (Edmondson and Mossman 1991; Reiners *et al.* 1991), although primary keratinocytes themselves have not been tested. This activity is likely due to mutagenesis of proteins in crucial signal transduction paths. Clearly, much work remains to be done to clarify the relationship between BaP exposure, abnormalities in proliferation and differentiation, and development of neoplastic skin lesions.

The hypothesis around which our studies are centered is that chemicals which alter or interfere in differentiation in keratinocytes will also induce growth perturbations and are, thus, potential carcinogens. Although, all evidence points toward different primary mechanisms of action for BaP and arsenic, both induce skin cancer. It may well be that there are common pathways affected by the two chemicals, as well as, chemical-specific effects. Work described herein compares the effects of arsenic and BaP on differentiation, growth rate, and cell cycle distribution in human keratinocytes. These

studies should begin to address the issues of whether diverse chemicals with a common endpoint of skin carcinogenesis affect differentiation in a similar manner, and if so, whether cell growth characteristics are also impacted. In time, our findings should enlighten us as to exactly what is happening in cells treated with carcinogenic agents and which of these events may be involved in malignant transformation.

4.4. Materials and Methods

4.4.1. Chemicals and Reagents

Sodium meta-arsenite ($NaAsO_2$), calcium chloride ($CaCl_2$), benzo[*a*]pyrene ($C_{20}H_{12}$), dimethyl sulphoxide (DMSO), pepsin and bromodeoxyuridine (BrdU) were purchased from Sigma Chemical Co. (St. Louis, MO).

4.4.2. Cell Culture and Culture Reagents

Cryopreserved normal human epidermal keratinocytes (NHEK) were purchased from the Clonetics Corp. (San Diego, CA). NHEK were grown in 5% CO_2 at 37°C in defined Keratinocyte Growth Medium (KGM) (Clonetics Corp) containing bovine pituitary extract (BPE), human epidermal growth factor (hEGF), insulin, hydrocortisone, transferrin, epinephrine, and antibiotic, GA-1000, at proprietary concentrations as determined by the manufacturer.

4.4.3. Cytotoxicity Assay

Prior to beginning our studies on the effects of the chemical agents, BaP and arsenic, on keratinocyte differentiation and cell cycle distribution, cytotoxicity studies were carried out using the 3-[4,5-Dimethylthiazol-2-yl]-2,5-diphenyltetrazolium bromide

(MTT) assay as a measure of cell viability (Carmichael *et al.* 1987; Mosmann 1983). For these assays, NHEK were exposed to increasing concentrations of either BaP or arsenic for 24 hr. Viability, as measured by absorbance of cell lysates at 550 nm, of NHEK cells 96 hr after exposure to various concentrations of BaP or arsenic as compared to the appropriate controls (data not shown) was utilized to derive values for the lethal concentration (LC) resulting in 5, 20, and 50% death; these values were subsequently used in differentiation experiments and flow cytometric analysis. Our assumption in these studies was that the metabolic activation of BaP is necessary for its carcinogenic effects in skin and thus, is also required for inducing alterations in growth and/or differentiation. As both preliminary studies in our lab and previous work (Kuroki *et al.* 1980; Parkinson and Newbold 1980; Theall *et al.* 1981) indicated that primary keratinocytes have intact metabolic capabilities for BaP, these assays were carried out without the addition of hepatic microsomal S9 fraction. The NHEK used in these studies were from pooled lots of cells from multiple donors and were obtained commercially in this form from Clonetics. One assumption made was that by pooling cells, metabolic capabilities for a large population would, on average, be more consistent from lot to lot than cells from single individuals. Cytotoxicity studies using NHEK from this manufacturer have supported this supposition in that results on many diverse chemicals (including BaP) compared very closely between lots.

4.4.4. Differentiation Assay

Cross-linked envelope (CLE) formation as a measure of keratinocyte differentiation was quantified as described previously (Rice and Green 1979). Briefly, NHEK were plated in 60 mm petri dishes at a density of 5000 cells/plate. When cells

reached 60-70% confluency after approximately 5 days, they were treated for 24 hr with the following chemicals and concentrations: BaP [0.2-2.0 μM], arsenic [0.5-5.0 μM], Ca^{2+} [0.5-3.0 mM], arsenic [0.5-5.0 μM] + Ca^{2+}, [2.0 mM], and BaP [0.2-2.0 μM] + Ca^{2+} [2.0 mM]. Ca^{2+} was used as a positive control for induction of differentiation, thus, acting to increase CLE production in NHEK. Experiments were also conducted where cells were treated at 20% confluency (2 days after plating) with the same chemicals and concentrations mentioned above. The results showed similar trends when compared to NHEK treated at 60% confluency. However, treatment at this earlier point produced a great amount of variability in cell growth in different treatment groups, which made it difficult to synchronize CLE counting for each group. The concentrations of BaP and arsenic utilized in these experiments corresponded to the range between the LC_5 and the LC_{50} for these chemicals as determined in MTT assays for NHEK. The concentration of Ca^{2+} ranged from basal conditions (0.25 mM) that allowed proliferation of primary NHEK up to concentrations that were demonstrated, in our experiments, to induce maximum differentiation of exposed keratinocytes (2.0-3.0 mM). After the treatment period, cultures were re-fed with chemical-free medium and incubated an additional 2-3 days until they reached 90-100% confluency. At this point, NHEK cells were trypsinized, counted, and lysed with Lysis Buffer to analyze CLE formation. Lysis Buffer consisted of 1% sodium dodecyl sulfate (SDS), 1% β-mercaptoethanol, 10.0 mM Tris hydrochloride, pH 8.0, and was added (1.0 ml) to each plate. CLE were visually quantified under a light microscope using a hemacytometer. Differentiation capacity of treated and control cultures was expressed as the ratio of CLE to total cell number. Experiments to evaluate the nature of the dose-response for effects on CLE formation by

Ca^{2+}, arsenic, and BaP were also carried out. In these studies, Ca^{2+} concentrations ranged from 0.25 to 3.0 mM. Arsenic concentrations ranged from 0.125 to 5.0 μM. BaP concentrations ranged from 0.0016 to 5.0 μM. DMSO was utilized as a solvent control for BaP. The time course study was carried out by comparing CLE formation in cultures treated for 24 hr with 2.0 mM Ca^{2+} as compared to control populations (0.25 mM Ca^{2+}) at 7, 10, 13, and 15 days after plating.

4.4.5. Cell Division Rate Measurement Assay

Determination of NHEK proliferation rates was carried out via BrdU labeling and propidium iodide staining followed by flow cytometric analysis (Steel 1977; Wilson 1994). Briefly, cells were plated in 100 mm petri dishes at a density of 10,000 cells/plate. When cells reached 10-15% confluency, they were treated with BaP [0.2, 1.0, 2.0 μM] or arsenic [0.5, 2.0, 5.0 μM] for 24 hours and Ca^{2+} [2.0 mM] continuously. After the treatment period, cultures were re-fed with chemical-free medium and incubated until they reached 50-60% confluency, approximately 4-5 days. At this point, cells were pulse-labeled with 10.0 μM BrdU for 30 min. After washing to remove the BrdU, cells were cultured and fixed at 0, 2, and 4 hr time points. The fixation and staining protocol was modified from that described previously (Larsen 1994; Liao *et al.* 2001). Cells were filtered through 53.0 μm nylon mesh (Small Parts Inc., Miami Lakes, FL) prior to flow cytometric analysis.

4.4.6. Flow Cytometric Analysis

Samples were analyzed with an Epics V cell sorter (Coulter, Miami, FL) interfaced to a Cicero data acquisition and display system (Cytomation Inc., Fort Collins,

CO). Cells were illuminated by an argon ion laser at 488 nm (500 mW). FITC was measured at wavelengths between 515 to 530 nm and PI was measured at wavelengths longer than 610 nm. The PI signal was gated on peak vs. integral fluorescence to eliminate clumped cells. Thirty thousand cells were analyzed for each bivariate histogram.

The concept of potential doubling time (T_{pot}) was proposed by Steel (1977) and can be used to estimate the proliferation alterations which occur following chemical treatment (Steel 1977). The T_{pot} of individual cultures was calculated from cell labeling and flow cytometric data as described previously (Begg *et al.* 1985). T_{pot} is a cell division time that takes growth fraction, but not cell loss, into account (Steel 1977; Wilson 1994). T_{pot} was calculated with the equation: $T_{pot} = \lambda\ (T_S/LI)$, where T_S is the period of DNA synthesis, LI (labeling index) is the fraction of cells synthesizing DNA, and λ is a correction factor for the nonlinear distribution of cells through the cell cycle (Steel 1977; Wilson 1994). Estimation of T_{pot} values relies upon distinction of cells within the four different stages of the cell cycle.

4.4.7. Statistical Analysis

Dunnett's one-way analysis of variance (ANOVA) was used to compare the difference of treated to control groups (Tamhane and Dunlop 2000). Treatment is significantly different if the P-value is 0.05 or less when compared to the appropriate control. Statistical regression models were produced for BaP, arsenic, and Ca^{2+} dose-dependency in NHEK by choosing a regression line, based on the highest correlation coefficient (r), that best fit the experimental data. These models were used to describe the relationship between increasing concentrations of BaP, arsenic, or calcium and effects on

CLE formation as an endpoint of keratinocyte differentiation. From these regression models, we used the equation generated to compare the rate of change (i.e. the slope) to determine which chemicals had a more profound effect on CLE formation.

4.5 Results

4.5.1. Morphological Alterations in Chemically-treated NHEK

For analysis of differentiation, NHEK cells were treated with Ca^{2+}, arsenic, or BaP as described in Materials and Methods. Photographs were taken (at 10X magnification) to demonstrate the morphological appearance of the different cultures 3-4 days (90-100% confluent) after treatment and prior to lysis for CLE analysis. Untreated control cultures displayed typical cobblestone-like epithelial cells (Figure 4.1.A). As expected, NHEK exposed to Ca^{2+} (1.0-2.0 mM) demonstrate a substantial degree of differentiation, forming compact, stratified foci (Figure 4.1.B). Cells exposed to arsenic (1.0-2.0 μM) decreased in size and formed more compact colonies (Figure 4.1.C). In addition, there were few stratified foci visible. BaP treated cells (0.1-5.0 μM) elongated and became spindle shaped, and very few stratified foci were observed (Figure 4.1.D). These observations demonstrate all three chemicals phenotypically altered cell morphology which indicates possible chemical-mediated effects on NHEK differentiation. These observations were studied further, in subsequent sections, to examine if, in fact, chemically-treated cells exhibited perturbed capacities for differentiation and proliferation.

4.5.2. Arsenic and Benzo[a]pyrene Inhibit NHEK Differentiation in Vitro

Our primary objective in these studies was to characterize the effects of two diverse skin carcinogens, arsenic and BaP, on NHEK proliferation and terminal differentiation. From cytotoxicity analyses using the MTT assay, we chose three equitoxic concentrations of the two chemicals, which corresponded to their LC_5, LC_{20}, and LC_{50}, to use in differentiation studies. Initial experiments were carried out in the absence of Ca^{2+} to measure the impact of chemical exposure on basal (or confluency-induced) differentiation in NHEK. In our hands, both arsenic and BaP were effective inhibitors of the differentiation process in this cell type (Figure 4.2.); at all three concentrations tested, arsenic or BaP-treated cells exhibited statistically significant reductions in CLE production as compared to the untreated NHEK culture. Our findings that arsenic maximally inhibited CLE formation by approximately 20-fold at the LC_{50} or 5.0 μM, are in agreement with previous studies on the effects of the metal in differentiating keratinocytes (Jessen *et al.* 2001; Kachinskas *et al.* 1994). BaP, at equitoxic doses, was not as strong an inhibitor as arsenic, but decreased CLE formation at the LC_5, LC_{20}, and LC_{50} by 1.85, 2.25, and 5.80-fold respectively. In our treatment protocol, cells were exposed to the chemicals acutely (for only 24 hr) when they had reached approximately 60-70% confluence. It is highly likely that longer treatment or that administered when the cultures were at low density, and few cells were yet committed to differentiating, would have been even more effective at inhibiting the final formation of CLE in confluent cultures.

More detailed studies were then carried out to further explore the nature of the dose-response curves for arsenic- and BaP-mediated inhibition of CLE formation in

NHEK. As expected, arsenic significantly ($p < 0.05$) perturbed CLE formation at all concentrations greater than 0.25 μM or the LC_2 (Figure 4.3); decreases in CLE production in treated versus control NHEK averaged from 1.6-fold to the maximum of 20-fold at 5.0 μM arsenic. BaP significantly perturbed NHEK differentiation at all concentrations $\geq$ 0.04 μM; this corresponds to a non-toxic concentration in this cell type. As seen in Figure 4.4, the inhibition of CLE formation ranged from 1.1- to 5.5-fold maximum at 5.0 μM BaP. The higher concentration of BaP required to achieve 5 to 6-fold inhibition of differentiation in this series of experiments versus those described above (5.0 μM versus 2.0 μM) is likely due to the lot of keratinocytes used. As NHEK cells are pooled populations of primary cells isolated from different individuals, they are characterized by intrinsic variations in sensitivity to toxic insult (Bae *et al.* 2001). For BaP, this may well be related to differences in metabolic capability in the different lots of cells. However, in all studies, regardless of the keratinocyte population used, we observed a highly consistent and dose-dependent inhibition of CLE formation by BaP. After regression analysis, the regression model $y = b_0 - b_1 * \log(x)$ best predicted the experimental data for BaP, while the regression model $y = a^{-b*\log(x)}$ best predicted the experimental data for arsenic.

4.5.3. Effects of Calcium on NHEK Differentiation in vitro

In addition to alterations in cell-cell and cell-matrix contact, increases in extracellular Ca^{2+} may serve as the most important signal for differentiation in keratinocytes. In order to more fully understand chemically-mediated perturbations in this process, we initially examined the normal dose-response and time-course of Ca^{2+}-induced formation of CLE in NHEK. For the former series of experiments, NHEK were

exposed for 24 hr to increasing concentrations of Ca^{2+} and CLE were quantified when cells reached confluency. Our studies demonstrated that Ca^{2+} concentrations ranging from 1.0–3.0 mM acted in a dose-dependent manner to induce statistically significant increases in differentiation in NHEK (Figure 4.5). Although there was a detectable increase in CLE formation seen in cultures exposed to 0.5 mM Ca^{2+}, as compared to cells grown under basal conditions of 0.25 mM Ca^{2+}, this difference was not significant. The maximum increase in CLE formation (1.7-fold) was seen in cultures exposed to 2.0 mM Ca^{2+}. After regression analysis, the power model ($y = ax^b$) yielded the best-fit description of the experimental Ca^{2+} dose-response data.

Time course analysis of CLE formation in response to Ca^{2+} exposure was also carried out in NHEK (Figure 4.6). The purpose of this study was to determine the time of maximum CLE formation in NHEK after exposure to 2.0 mM Ca^{2+}. This series of experiments demonstrated the following: 1) CLE production was time-dependent in both control and treated cultures; 2) in control populations, CLE formation increased at each time point, reaching a maximum at 15 days of 0.53 ± 0.065 CLE per total cell number; 3) Ca^{2+} substantially increased the rate at which the NHEK populations differentiated, with the first increase over control detectable by 7 days of culture and maximum CLE formation occurring at 15 days (0.64 ± 0.076 CLE per total cell number); 4) the ratios of CLE in Ca^{2+}-treated versus control cells at days 7, 10, 13, and 15 were 1.66, 1.84, 1.34, and 1.21 respectively. By 15 days in culture, there was no longer any statistically significant difference in differentiation between control and treated cells. This is likely due to the time-dependent increase in confluency in the control populations, which is a very effective inducer of terminal differentiation.

4.5.4. Effects of Arsenic and Benzo[a]pyrene on Calcium-Induced Differentiation in NHEK

These studies were designed to explore whether BaP and/or arsenic were also inhibitory to differentiation induced by simultaneous treatment of NHEK cultures with 2.0 mM Ca^{2+}. Treatment of cells was carried out for 24 hr with Ca^{2+} and increasing concentrations of arsenic or BaP. The extent of CLE formation in the individual cultures was determined after cells reached 90-100% confluency or approximately 8 days. In general, the inhibitory effects of both BaP and arsenic on CLE formation were less striking in cells that were also exposed to high Ca^{2+}, although both chemicals still demonstrated significant inhibition of the differentiation process. Under these conditions, only the two highest concentrations of BaP (LC_{20} and LC_{50}) had a statistically significant inhibitory effect on differentiation when compared to Ca^{2+}-induced cells. The maximum inhibition achieved by BaP was 1.7-fold at a concentration of 2.0 μM (Figure 4.7). One possibility for these findings is that by induction of proliferative arrest in treated cells, Ca^{2+} decreases the impact of arsenic and BaP on cell viability and, in turn, on other closely linked processes. This issue could be explored through more detailed analysis of the time-dependent cytotoxicity of these two chemicals in the presence and absence of Ca^{2+}. Again, arsenic acted as a more effective inhibitor of differentiation in these cells, with a maximum decrease observed at 5.0 μM of 5.5-fold (Figure 4.7) and significant inhibition of CLE formation when compared to control cells at all concentrations analyzed.

4.5.5. Benzo[a]pyrene, Arsenic, and Calcium Alter Cell Cycle Distribution in NHEK

As proliferation and differentiation are opposing processes in keratinocytes, we were also interested in characterizing the cell cycle effects of BaP and arsenic, as compared to Ca^{2+} in this cell type. BrdU and propidium iodide staining and flow cytometric analysis were used to approach this issue. The resulting standard and bivariate DNA histograms allow visual observation of the dynamic changes in cell cycle distribution due to chemical exposure. Figure 4.8 shows DNA histograms of NHEK cultures treated with 2.0 mM Ca^{2+}, 5.0 µM arsenic, 2.0 µM BaP, and, for comparison, untreated control cells. It is apparent from this analysis that exposure of NHEK to arsenic under these conditions substantially altered the normal cell-cycle distribution, leading to both a G2 block and decreasing number of cells entering S-phase as compared to untreated controls; a graphical representation of the fraction of cells in treated populations versus the control in each phase of the cell cycle is shown in Figure 4.9. The effects of Ca^{2+} and BaP on cell cycle distribution were more subtle. A slight increase in the number of cells in G2/M, as well as a decrease in the number of early S-phase cells was seen in Ca^{2+}-exposed populations when compared to controls. Cells exposed to BaP increased in G1/G0, with a decrease in G2/M cells and a slight decrease in the number of cells in S-phase. These changes were statistically significant at p values of 0.01 (for the impact of BaP on G1/G0) and < 0.05 (the rest), respectively.

Bivariate histograms where obtained to explore chemical effects on the movement of cells 4 hr after being labeled in S-phase with BrdU. When BrdU incorporation and DNA content in the chemically-treated keratinocyte cultures were viewed

simultaneously, we observed the following (Figure 4.10): 1) in cultures treated with 2.0 μM BaP, BrdU-labeled cells progressed through G2 and mitosis and entered G1 during the 4 hr labeling period (Figure 4.10B); 2) this effect of BaP was dose-dependent and was not detectable in cultures treated with lower concentrations or in the DMSO-solvent controls; and 3) in these latter populations, the majority of labeled cells were found in S-phase and G2/M. These observations indicate that BaP increased the rate at which keratinocytes proceeded through the cell cycle, a hypothesis in agreement with the T_{pot} data discussed below. An increased cell cycle rate was not seen in NHEK treated with either Ca^{2+} or arsenic (Figure 4.10C & 4.10D). In fact, although difficult to discern from bivariate histograms, in these latter populations, the cell cycle rate was significantly decreased.

4.5.6. Chemical Effects Seen on NHEK Proliferation Rate

The results from flow cytometric analysis of cell cycle distributions were used to calculate the potential doubling times (T_{pot}) of cells treated with BaP, arsenic, and Ca^{2+} versus control populations (Figure 4.11). As suggested by the histograms in Figures 4.8 and 4.10, BaP, arsenic, and Ca^{2+} were all calculated to alter proliferative potential in treated NHEK. As expected from previous observations in the literature (Jensen *et al.* 1990), we observed a 3 hr (9.2%) increase in T_{pot} in NHEK cells treated with 2.0 mM Ca^{2+} when compared to control cells. Arsenic at 2.0 and 5.0 μM had a similar effect, increasing T_{pot} in treated cells by 4.3 (12.5%) and 10.3 hr (25.8%), respectively as compared to controls. Interestingly, and in contrast to the decreased proliferative rates measured in Ca^{2+}- and arsenic-treated cells, BaP at 0.2, 1.0, and 2.0 μM decreased T_{pot} by

5.4, 13.5, and 29.8% respectively. This was equivalent to decreasing the T_{pot} by an average of 2.1, 3.6, and 15.1 hr under the three treatment conditions.

4.6. Discussion

Exposure to chemical carcinogens is thought to alter cellular signals that control the switch between keratinocyte division, differentiation, or apoptosis. However, the exact molecular and biochemical mechanisms involved in this process have not been clearly elucidated to date. In order to understand the impact of chemical exposure on keratinocyte function, it was first necessary to characterize normal differentiation in this cell type *in vitro*. It has previously been demonstrated that Ca^{2+} at concentrations in excess of 1.0 mM inhibits proliferation, induces stratification, and increases the formation of CLE in keratinocyte cultures (Boyce and Ham 1983; Hennings *et al.* 1980a; Hennings *et al.* 1980b; Rice and Green 1979; Shipley and Pittelkow 1987). Approximately this same concentration of Ca^{2+} leads to induction of involucrin and transglutaminase, both of which play an intricate role in the terminal differentiation of this cell type. Our studies *in vitro* in NHEK support these findings and characterize the dose- and time-dependence of the induction of differentiation by Ca^{2+}. The T_{pot} measurements also show a decreased rate of proliferation after Ca^{2+} treatment. Potential mechanisms for involvement of Ca^{2+} in differentiation include changes in cell adhesion and cell-cell contacts (Braga *et al.* 1995), and activation of a transmembrane Ca^{2+}-dependent receptor (Denning *et al.* 2000).

Although arsenic has previously been studied in terms of its effects on expression of individual differentiation-associated markers in keratinocytes (Jessen *et al.* 2001; Kachinskas *et al.* 1994), our work is the first to demonstrate that the metalloid is a highly potent inhibitor of CLE formation as induced *in vitro* by confluence or the presence of

exogenous Ca^{2+}. One potential mechanism for the effects of arsenic on differentiation proposed by Kachinskas *et al.* (1994) involves inhibition of specific protein tyrosine phosphatases. Other mechanisms include suppression of p21 induction (Rossman *et al.* 2001; Vogt and Rossman 2001), altered receptor function and/or expression, and interference in PKC signaling (Chen *et al.* 2000).

The effect of arsenic on cell proliferation varies depending on both the cell type and concentration of the metal (Basu *et al.* 2001; Vega *et al.* 2001). Studies in keratinocytes demonstrated that low levels of arsenic or an arsenic-containing metal mixture significantly stimulated growth factor production and proliferation, while levels of arsenic associated with toxicity decreased cell division rates (Bae *et al.* 2001; Germolec *et al.* 1996). In our studies, T_{pot} increased (or proliferative rate decreased) in cultures treated with arsenic at 2.0 µM and higher, at least partly due to a G2/M phase delay, as has been seen with other cell types (Ma *et al.* 1998; States *et al.* 2002). One interesting observation from our studies was that arsenic was substantially more effective at inhibiting differentiation than proliferation. One possibility suggested by these findings is that at lower concentrations, arsenic acts to stimulate proliferation and inhibit differentiation in primary keratinocytes, both potentially carcinogenic insults. At higher concentrations, cytotoxicity may lead ultimately to cell cycle blocks and apoptosis. Recent clinical studies in therapy of acute promyleocytic leukemia and ovarian carcinoma, among others, have taken advantage of the anti-cancer activity of arsenic (Li *et al.* 2002).

We have also been able to demonstrate that BaP had substantial impacts on both cell proliferation and differentiation in human keratinocytes. As seen with arsenic, inhibition of differentiation was observed at much lower concentrations of BaP than were

alterations in proliferation. The effect of BaP on differentiation was more substantial in the absence of exogenous Ca^{2+} than in its presence. This finding is interesting given the suggestion that in the murine system, induction of differentiation by Ca^{2+} increases the metabolic capacity of keratinocytes and thus, increases activation of PAH's (Reiners *et al.* 1991). To date, there have been no published studies examining the effect of BaP on primary keratinocyte differentiation *in vitro*. However, in related work (Edmondson and Mossman 1991), treatment of hamster tracheal epithelial cells with BaP *in vitro* lead to alterations in expression of multiple differentiation-related cytokeratins. The fact that BaP is capable of altering the differentiation program of committed cells may explain, in part, why exposure of the tracheal epithelium to BaP leads to metaplasia and squamous cell carcinoma in the lung (Chopra and Joiakim 1991; Yoshimoto *et al.* 1980). Mutagenic alteration of regulatory molecules involved in growth and differentiation is the most likely mode of action for BaP in exposed cells. In previous studies, other genotoxic chemicals have been demonstrated to alter differentiation in skin (Huberman 1980; Puri *et al.* 2002). However, one must not discount the possibility that additional, epigenetic, mechanisms may also exist. In this case, metabolic activation may not be crucial, or even necessary for the observed effects of the chemical.

One potential mechanism for the effects of BaP on differentiation is the inhibitory effect it can exert on PKC activity in certain cell types (Ou and Ramos 1994). From several lines of study, it appears that different PKC isoforms are involved in steps during both early and late differentiation and that it is the ratios and locations of these different isoforms within a keratinocyte that may be important (Lee *et al.* 1997). Initiated keratinocytes derived from exposure to chemicals such as *N*-methyl-*N'*-nitro-*N*-

nitroguanidine (MNNG) and 7,12-dimethylbenz[*a*]anthracene (DMBA) display a resistance to differentiating agents due to alterations in the PKC pathway (Kulesz-Martin *et al.* 1983). Identification of other molecular targets altered in these cells, as well as the signal transduction pathways they are involved in, will greatly aid our understanding of the processes of growth, differentiation, and/or carcinogenesis in this cell type.

One thing that is clear from our studies is that cultures treated with BaP also progressed through the cell cycle more quickly, with a shorter S phase or G2/M or both. Although in our current studies, stimulatory effects on proliferation and inhibition of differentiation by BaP were generally detected within a day of each other, we did not determine the exact time course of these two events. One possibility is that by stimulating proliferative pathways in NHEK, BaP effectively opposes terminal arrest and subsequent differentiation. Alternatively, by first rendering a substantial population of keratinocytes resistant to signals that normally induce differentiation, BaP may effectively increase the number of cycling cells and thus, decrease the potential doubling time as compared to untreated cultures. It will be enlightening to carry out detailed kinetic analyses of the two events to see if such a relationship can be defined.

Although there have been no descriptions of the effects of BaP on cell cycle kinetics in primary keratinocytes in culture, previous studies examining this issue have been carried out in the murine skin system (Reiners *et al.* 1991). Albert *et al.* (1991) demonstrated that while the carcinogen was highly toxic to keratinocytes *in vivo*, it also acted to increase the labeling index in surviving cells (Albert *et al.* 1991). In these, and other, studies, proliferation correlated closely with tumor formation under the different exposure scenarios. In contrast, in other cell types *in vitro*, BaP has been shown to induce

DNA adducts, and a delayed S-phase, with or without a G2/M arrest (Jeffy *et al.* 2000; Mudzinski 1993). Among cell cycle regulatory proteins potentially involved are p53 and $p21^{WAF1}$ (Binkova *et al.* 2000). Although we are currently uncertain as to why our findings in keratinocytes contrast with these previous studies, there are many possible explanations including the use of different cell types and experimental protocols. Additionally, it is possible that the population of cells surviving BaP may be genetically altered in such a way that they proliferate more rapidly. One potential scenario is due to the mutational loss of a crucial cell cycle checkpoint function. Similar effects have been seen with caffeine or 2-aminopurine (Ford and Pardee 1999).

The long term goal of our research program is the development of accurate and efficient risk assessment strategies for environmentally relevant chemicals and chemical mixtures. One approach is through use of *in vitro* cell culture systems and biologically-based dose response models depicting toxic endpoints. The human keratinocyte cell system is useful for the study of potential carcinogens. As the cells undergo normal differentiation in culture, it is possible to explore the link between disruptions in this cellular process and malignant transformation. In studies described herein, we have demonstrated that while the known human carcinogens, arsenic and BaP, are both effective inhibitors of differentiation in primary keratinocytes *in vitro,* they exert interesting, but opposite effects on cell growth. We are currently carrying out microarray and real-time RT-PCR analysis on NHEK cultures treated with arsenic or BaP to compare the important molecular alterations that are occurring under these different exposure conditions. Interactive effects of arsenic and BaP in this system may, in the future, be a productive avenue of exploration as these two chemicals do occur together in

environmentally prevalent mixtures, such as those at hazardous waste sites. A better understanding of the balance between growth and differentiation and how it is altered by defined chemicals or chemical mixtures during carcinogenesis will aid immeasurably in the risk assessment process.

4.7. References

Albert, R. E., Miller, M. L., Cody, T. E., Barkley, W., and Shukla, R. (1991). Cell kinetics and benzo[a]pyrene-DNA adducts in mouse skin tumorigenesis. *Progress in Clinical & Biological Research* **369**, 115-122.

Albert, R. E., Miller, M. L., Cody, T. E., Talaska, G., Underwood, P., and Andringa, A. (1996). Epidermal cytokinetics, DNA adducts, and dermal inflammation in the mouse skin in response to repeated benzo[a]pyrene exposures. *Toxicology & Applied Pharmacology* **136**, 67-74.

Bae, D. S., Gennings, C., Carter, W. H., Jr., Yang, R. S., and Campain, J. A. (2001). Toxicological interactions among arsenic, cadmium, chromium, and lead in human keratinocytes. *Toxicological Sciences* **63**, 132-142.

Basu, A., Mahata, J., Gupta, S., and Giri, A. K. (2001). Genetic toxicology of a paradoxical human carcinogen, arsenic: a review. [Review] [183 refs]. *Mutation Research* **488**, 171-194.

Begg, A. C., McNally, N. J., Shrieve, D. C., and Karcher, H. (1985). A method to measure the duration of DNA synthesis and the potential doubling time from a single sample. *Cytometry* **6**, 620-626.

Binkova, B., Giguere, Y., Rossner, P., Jr., Dostal, M., and Sram, R. J. (2000). The effect of dibenzo[a,1]pyrene and benzo[a]pyrene on human diploid lung fibroblasts: the induction of DNA adducts, expression of p53 and p21(WAF1) proteins and cell cycle distribution. *Mutation Research* **471**, 57-70.

Boyce, S. T., and Ham, R. G. (1983). Calcium-regulated differentiation of normal human epidermal keratinocytes in chemically defined clonal culture and serum-free serial culture. *J.Invest Dermatol.* **81**, 33s-40s.

Braga, V. M., Hodivala, K. J., and Watt, F. M. (1995). Calcium-induced changes in distribution and solubility of cadherins, integrins and their associated cytoplasmic proteins in human keratinocytes. *Cell Adhesion & Communication* **3**, 201-215.

Carmichael, J., DeGraff, W. G., Gazdar, A. F., Minna, J. D., and Mitchell, J. B. (1987). Evaluation of a tetrazolium-based semiautomated colorimetric assay: assessment of chemosensitivity testing. *Cancer Res.* **47**, 936-942.

Chen, C. J., Chen, C. W., Wu, M. M., and Kuo, T. L. (1992). Cancer potential in liver, lung, bladder and kidney due to ingested inorganic arsenic in drinking water. *Br.J Cancer* **66**, 888-892.

Chen, N. Y., Ma, W. Y., Huang, C., Ding, M., and Dong, Z. (2000). Activation of PKC is required for arsenite-induced signal transduction. *J.Environ.Pathol.Toxicol.Oncol.* **19**, 297-305.

Chopra, D. P., and Joiakim, A. P. (1991). Alterations in sugar residues in squamous metaplasia in hamster tracheal explants induced by benzo(a)pyrene and its reversal by retinoic acid. *In Vitro Cell Dev.Biol* **27A**, 229-233.

Chowdhury, U. K., Biswas, B. K., Chowdhury, T. R., Samanta, G., Mandal, B. K., Basu, G. C., Chanda, C. R., Lodh, D., Saha, K. C., Mukherjee, S. K., Roy, S., Kabir, S., Quamruzzaman, Q., and Chakraborti, D. (2000). Groundwater arsenic contamination in Bangladesh and West Bengal, India. *Environ.Health Perspect.* **108**, 393-397.

Denning, M. F., Dlugosz, A. A., Cheng, C., Dempsey, P. J., Coffey, R. J., Jr., Threadgill, D. W., Magnuson, T., and Yuspa, S. H. (2000). Cross-talk between epidermal growth factor receptor and protein kinase C during calcium-induced differentiation of keratinocytes. *Exp.Dermatol.* **9**, 192-199.

Denning, M. F., Dlugosz, A. A., Williams, E. K., Szallasi, Z., Blumberg, P. M., and Yuspa, S. H. (1995). Specific protein kinase C isozymes mediate the induction of keratinocyte differentiation markers by calcium. *Cell Growth Differ.* **6**, 149-157.

Edmondson, S. W., and Mossman, B. T. (1991). Alterations in keratin expression in hamster tracheal epithelial cells exposed to benzo[a]pyrene. *Carcinogenesis* **12**, 679-684.

Filvaroff, E., Stern, D. F., and Dotto, G. P. (1990). Tyrosine phosphorylation is an early and specific event involved in primary keratinocyte differentiation. *Mol.Cell Biol.* **10**, 1164-1173.

Ford, H. L., and Pardee, A. B. (1999). Cancer and the cell cycle. [Review] [56 refs]. *Journal of Cellular Biochemistry* **Suppl 32-33**, 166-172.

Germolec, D. R., Yoshida, T., Gaido, K., Wilmer, J. L., Simeonova, P. P., Kayama, F., Burleson, F., Dong, W., Lange, R. W., and Luster, M. I. (1996). Arsenic induces overexpression of growth factors in human keratinocytes. *Toxicology and Applied Pharmacology* **141**, 308-318.

Hennings, H., Holbrook, K., Steinert, P., and Yuspa, S. (1980a). Growth and differentiation of mouse epidermal cells in culture: effects of extracellular calcium. *Curr.Probl.Dermatol.* **10**, 3-25.

Hennings, H., Michael, D., Cheng, C., Steinert, P., Holbrook, K., and Yuspa, S. H. (1980b). Calcium regulation of growth and differentiation of mouse epidermal cells in culture. *Cell* **19**, 245-254.

Huberman, E. (1980). The induction of mutation and differentiation in mammalian cells by chemicals which initiate or promote tumor formation. *Dev.Toxicol.Environ.Sci.* **8**, 121-132.

Jeffy, B. D., Chen, E. J., Gudas, J. M., and Romagnolo, D. F. (2000). Disruption of cell cycle kinetics by benzo[a]pyrene: inverse expression patterns of BRCA-1 and p53 in MCF-7 cells arrested in S and G2. *Neoplasia (New York)* **2**, 460-470.

Jensen, P. K., Norgard, J. O., Knudsen, C., Nielsen, V., and Bolund, L. (1990). Effects of extra- and intracellular calcium concentration on DNA replication, lateral growth, and differentiation of human epidermal cells in culture. *Virchows Arch.B Cell Pathol.Incl.Mol.Pathol.* **59**, 17-25.

Jessen, B. A., Qin, Q., Phillips, M. A., Phillips, D. L., and Rice, R. H. (2001). Keratinocyte differentiation marker suppression by arsenic: mediation by AP1 response elements and antagonism by tetradecanoylphorbol acetate. *Toxicology & Applied Pharmacology* **174**, 302-311.

Kachinskas, D. J., Phillips, M. A., Qin, Q., Strokes, J. D., and Rice, R. H. (1994). Arsenate perturbation of human keratinocyte differentiation. *Cell Growth Differ.* **5**, 12235-1241.

Kulesz-Martin, M., Kilkenny, A. E., Holbrook, K. A., Digernes, V., and Yuspa, S. H. (1983). Properties of carcinogen altered mouse epidermal cells resistant to calcium-induced terminal differentiation. *Carcinogenesis* **4**, 1367-1377.

Kuroki, T., Nemoto, N., and Kitano, Y. (1980). Metabolism of benzo[a]pyrene in human epidermal keratinocytes in culture. *Carcinogenesis* **1**, 559-565.

Larsen, J. K. (1994). Measurement of cytoplasmic and nuclear antigens. In Flow Cytometry: A Practical Approach, pp. 93-117. Oxford University Press, Oxford.

Lee, P. N., and O'Neill, J. A. (1971). The effect both of time and dose applied on tumour incidence rate in benzopyrene skin painting experiments. *Br.J Cancer* **25**, 759-770.

Lee, Y. S., Dlugosz, A. A., McKay, R., Dean, N. M., and Yuspa, S. H. (1997). Difinition by specific antisense oligonucleotides of a role for protein Cα in expression of differentiation markers in normal and neoplastic mouse epidermal keratinocytes. *Molecular Carcinogenesis* **18**, 44-53.

Leonard, A., and Lauwerys, R. R. (1980). Carcinogenicity, teratogenicity and mutagenicity of arsenic. *Mutat.Res.* **75**, 49-62.

Li, D., Du, C., Lin, Y., and Wu, M. (2002). Inhibition of growth of human nasopharyngeal cancer xenografts in SCID mice by arsenic trioxide. *Tumori* **88**, 522-526.

Liao, K. H., Gustafson, D. L., Fox, M. H., Chubb, L. S., Reardon, K. F., and Yang, R. S. (2001). A biologically based model of growth and senescence of Syrian hamster embryo (SHE) cells after exposure to arsenic. *Environ.Health Perspect.* **109**, 1207-1213.

Ma, D. C., Sun, Y. H., Chang, K. Z., Ma, X. F., Huang, S. L., Bai, Y. H., Kang, J., Liu, Y. G., and Chu, J. J. (1998). Selective induction of apoptosis of NB4 cells from G2+M phase by sodium arsenite at lower doses. *Eur.J.Haematol.* **61**, 27-35.

Mager, R., Huberman, E., Yang, S. K., Gelboin, H. V., and Sachs, L. (1977). Transformation of normal hamster cells by benzo(a)pyrene diol-epoxide. *Int.J.Cancer* **19**, 814-817.

Mosmann, T. (1983). Rapid colorimetric assay for cellular growth and survival: application to proliferation and cytotoxicity assays. *J.Immunol.Methods* **65**, 55-63.

Mudzinski, S. P. (1993). Effects of benzo[a]pyrene on concanavalin A-stimulated human peripheral blood mononuclear cells in vitro: inhibition of proliferation but no effect on parameters related to the G1 phase of the cell cycle. *Toxicology & Applied Pharmacology* **119**, 166-174.

Ou, X., and Ramos, K. S. (1994). Benzo[a]pyrene inhibits protein kinase C activity in subcultured rat aortic smooth muscle cells. *Chem.Biol.Interact.* **93**, 29-40.

Parkinson, E. K., and Newbold, R. F. (1980). Benzo(a)pyrene metabolism and DNA adduct formation in serially cultivated strains of human epidermal keratinocytes. *Int.J.Cancer* **26**, 289-299.

Puri, P. L., Bhakta, K., Wood, L. D., Costanzo, A., Zhu, J., and Wang, J. Y. (2002). A myogenic differentiation checkpoint activated by genotoxic stress. *Nat.Genet.* **32**, 585-593.

Reiners, J. J., Jr., Cantu, A. R., and Pavone, A. (1991). Distribution of constitutive and polycyclic aromatic hydrocarbon-induced cytochrome P-450 activities in murine epidermal cells that differ in their stages of differentiation. *Prog.Clin.Biol.Res.* **369**, 123-135.

Rice, R. H., and Green, H. (1979). Presence in human epidermal cells of a soluble protein precursor of the cross-linked envelope: Activation of the cross-linking by calcium ions. *Cell* **18**, 681-694.

Rossman, T. G., Uddin, A. N., Burns, F. J., and Bosland, M. C. (2001). Arsenite is a cocarcinogen with solar ultraviolet radiation for mouse skin: an animal model for arsenic carcinogenesis. *Toxicol.Appl.Pharmacol.* **176**, 64-71.

Salnikow, K., and Cohen, M. D. (2002). Backing into cancer: effects of arsenic on cell differentiation. [letter; comment.]. [Review] [31 refs]. *Toxicological Sciences* **65**, 161-163.

Shipley, G. D., and Pittelkow, M. R. (1987). Control of growth and differentiation in vitro of human keratinocytes cultured in serum-free medium. *Archives of Dermatology* **123**, 1541a-1544a.

States, J. C., Reiners, J. J., Jr., Pounds, J. G., Kaplan, D. J., Beauerle, B. D., McNeely, S. C., Mathieu, P., and McCabe, M. J., Jr. (2002). Arsenite disrupts mitosis and induces apoptosis in SV40-transformed human skin fibroblasts. *Toxicol.Appl.Pharmacol.* **180**, 83-91.

Steel, G. G. (1977). Growth kinetics of tumors: cell population kinetics in relation to the growth and treatment of cancer. In Basic theory of growing cell populations, pp. 57-85. Clarendon Press, Oxford.

Tamhane, A. C., and Dunlop, D. D. (2000). Multiple comparisons of means. In Statistics and Data Analysis from Elementary to Intermediate, pp. 475-476. Prentice-Hall, Inc., Upper Saddle River, NJ.

Theall, G., Eisinger, M., and Grunberger, D. (1981). Metabolism of benzo[a]pyrene and DNA adduct formation in cultured epidermal keratinocytes. *Carcinogenesis* **2**, 581-587.

Tseng, W. P. (1977). Effects and dose--response relationships of skin cancer and blackfoot disease with arsenic. *Environ.Health Perspect.* **19**, 109-119.

Vega, L., Styblo, M., Patterson, R., Cullen, W., Wang, C., and Germolec, D. (2001). Differential effects of trivalent and pentavalent arsenicals on cell proliferation and cytokine secretion in normal human epidermal keratinocytes. *Toxicology & Applied Pharmacology* **172**, 225-232.

Vogt, B. L., and Rossman, T. G. (2001). Effects of arsenite on p53, p21 and cyclin D expression in normal human fibroblasts -- a possible mechanism for arsenite's comutagenicity. *Mutation Research* **478**, 159-168.

Wilson, G. D. (1994). Flow Cytometry: A Practical Approach. In Analysis of DNA-measurement of cell kinetics by the bromodeoxyuridine/anti-bromodeoxyuridine method, pp. 137-156. Oxford University Press, Oxford.

Xie, Z., and Bikle, D. D. (1999). Phospholipase C-gamma1 is required for calcium-induced keratinocyte differentiation. *J.Biol.Chem.* **274**, 20421-20424.

Yoshimoto, T., Inoue, T., Iizuka, H., Nishikawa, H., Sakatani, M., Ogura, T., Hirao, F., and Yamamura, Y. (1980). Differential induction of squamous cell carcinomas and adenocarcinomas in mouse lung by intratracheal instillation of benzo(a)pyrene and charcoal powder. *Cancer Res.* **40**, 4301-4307.

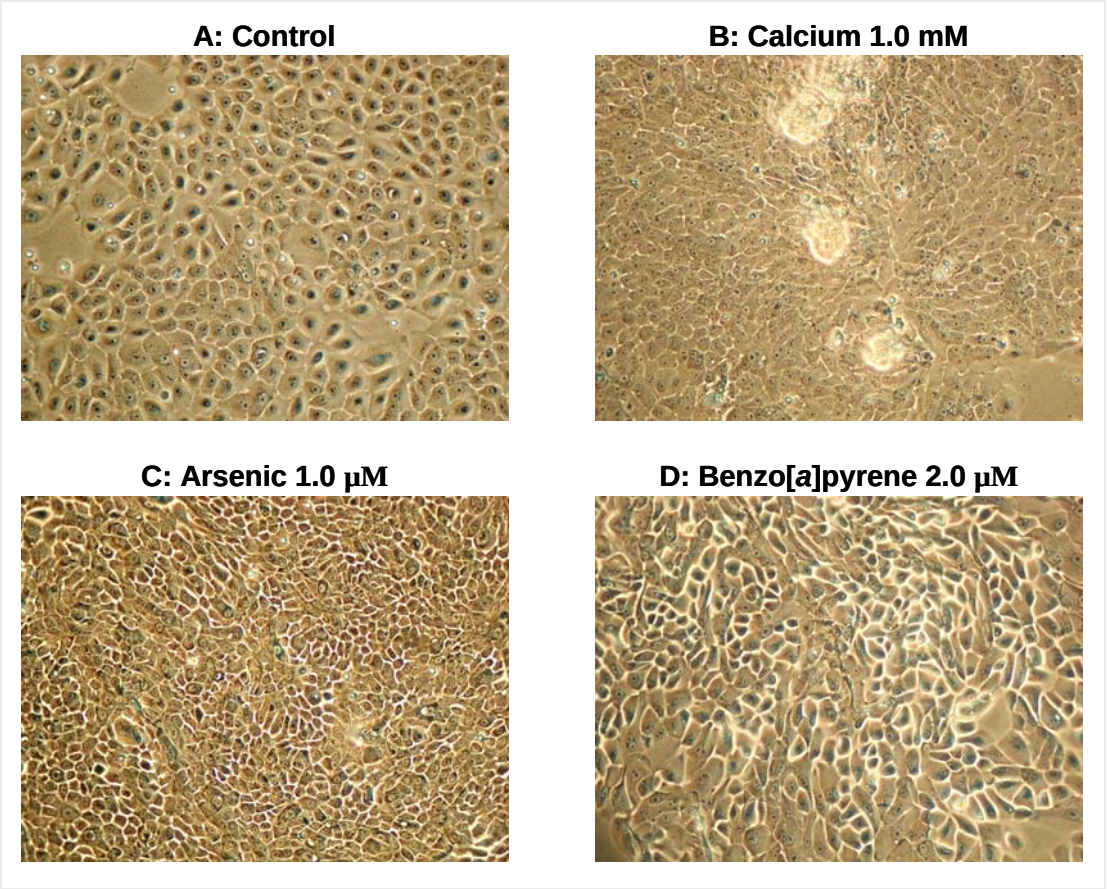

Figure 4.1. **Morphological alterations in chemically-treated NHEK.** For analysis of differentiation, NHEK cells were treated with Ca^{2+}, arsenic, or BaP as described in Materials and Methods. Photographs were taken (at 10X magnification) to demonstrate the morphological appearance of the different cultures 3-4 days (90-100% confluent) after treatment. Untreated control cultures displayed typical cobblestone-like epithelial cells (A). As expected, NHEK exposed to Ca^{2+} (1.0-2.0 mM) demonstrate a substantial degree of differentiation, forming compact, stratified foci (B). Cells exposed to arsenic (1.0-2.0 μM) decreased in size and formed more compact colonies (C). In addition, there were few stratified foci visible. BaP treated cells (0.1-5.0 μM) elongated and became spindle shaped, and very few stratified foci were observed (D).

A.

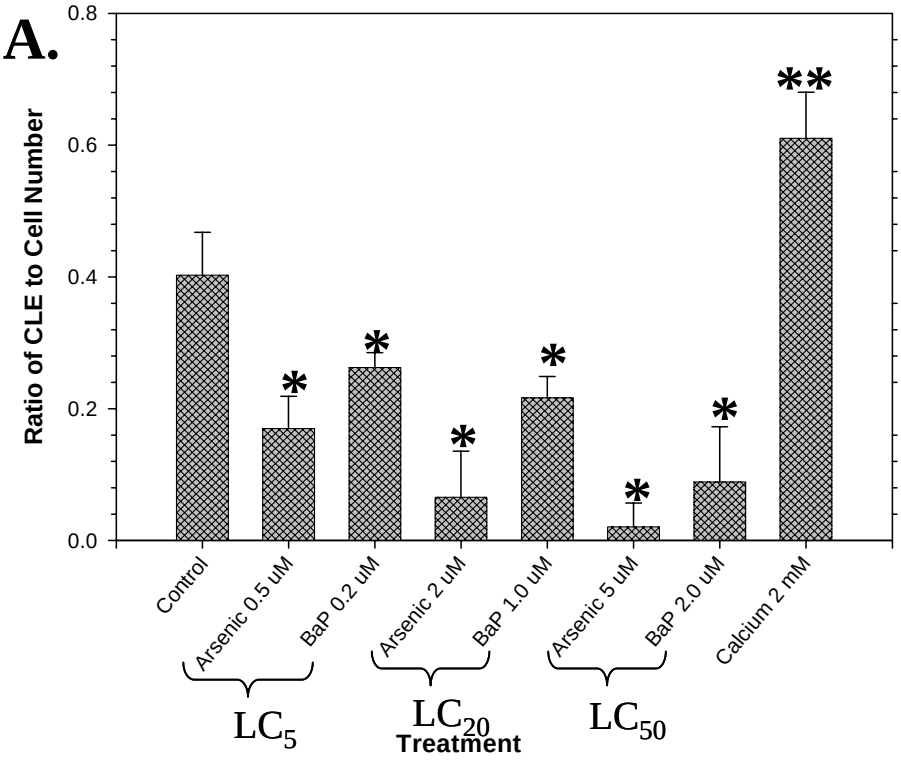

B.

Treatment	Avg. Ratio (CLE/Cell#)	Fold Difference	P-value
Control	0.4026	-	-
Arsenic 0.5 µM LC_5	0.1629	2.4715*	0.003
Arsenic 2.0 µM LC_{20}	0.0445	9.0472*	< 0.001
Arsenic 5.0 µM LC_{50}	0.0200	20.1009*	< 0.001
BaP 0.2 µM LC_5	0.2176	1.8500*	< 0.001
BaP 1.0 µM LC_{20}	0.1789	2.2500*	< 0.001
BaP 2.0 µM LC_{50}	0.0694	5.8001*	< 0.001
Calcium 2 mM	0.6710	1.6667*	0.001

Figure 4.2. **Effects of benzo[*a*]pyrene and arsenic on basal differentiation in NHEK.** Cells were treated with increasing concentrations of BaP and arsenic for 24 hr and CLE were quantified as described in Materials and Methods. Ca^{2+}, at 2.0 mM, was utilized as a positive control for induction of differentiation. Numbers of CLE for each treatment condition were standardized to cell number and are expressed as the mean of triplicates from 3 independent experiments ± SD. *Significantly different from the control using one way ANOVA followed by Dunnett's test, $p<0.05$. **Signifies Ca^{2+} exposed cells being significantly different from control cells. A is graphical representations of the data in Table B.

A.

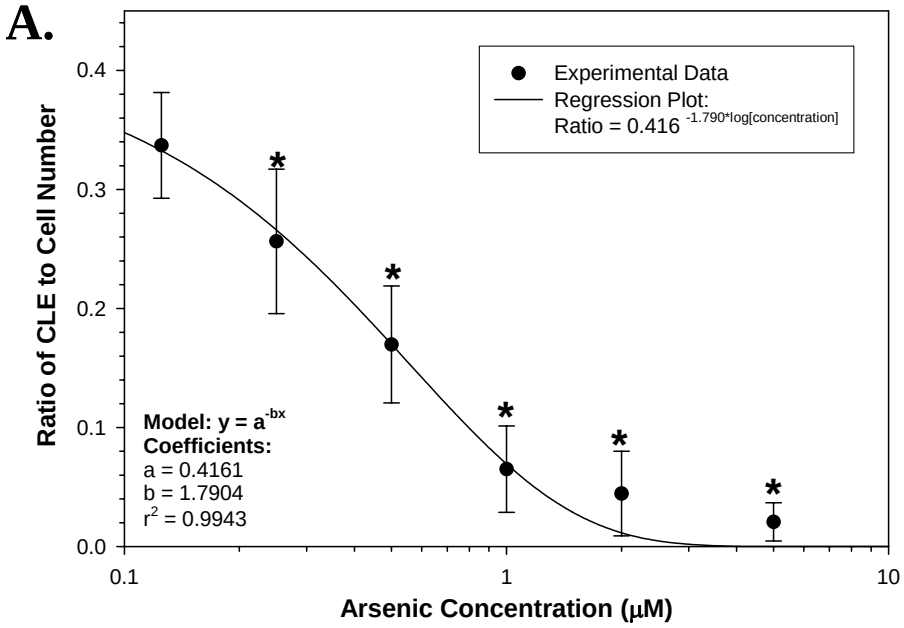

B.

Treatment	Avg. Ratio (CLE/Cell#)	Fold Difference	P-value
Control	0.4186	-	-
Arsenic 0.125 μM	0.3370	-1.2420	0.087
Arsenic 0.25 μM	0.2564	-1.6327*	0.020
Arsenic 0.5 μM	0.1698	-2.4652*	0.003
Arsenic 1.0 μM	0.0651	-6.4298*	< 0.001
Arsenic 2.0 μM	0.0445	-9.4064*	< 0.001
Arsenic 5.0 μM	0.0208	-20.0921*	< 0.001

Figure 4.3. **Dose-dependent inhibition of CLE formation in NHEK by arsenic.** NHEK were treated with increasing concentrations of arsenic for 24 hr as indicated in the figure, and CLE were quantified as described in Materials and Methods. Control was untreated NHEK cultured in an identical manner. Numbers of CLE were standardized to cell number and are presented as the mean of triplicates from 8 independent experiments ±SD. *Significantly different from the control using one way ANOVA followed by Dunnett's test, $p<0.05$. Statistical regression analysis was carried out to predict the best mathematical model for describing CLE formation as a function of chemical concentration. A is a graphical representations of the data in Table B.

A.

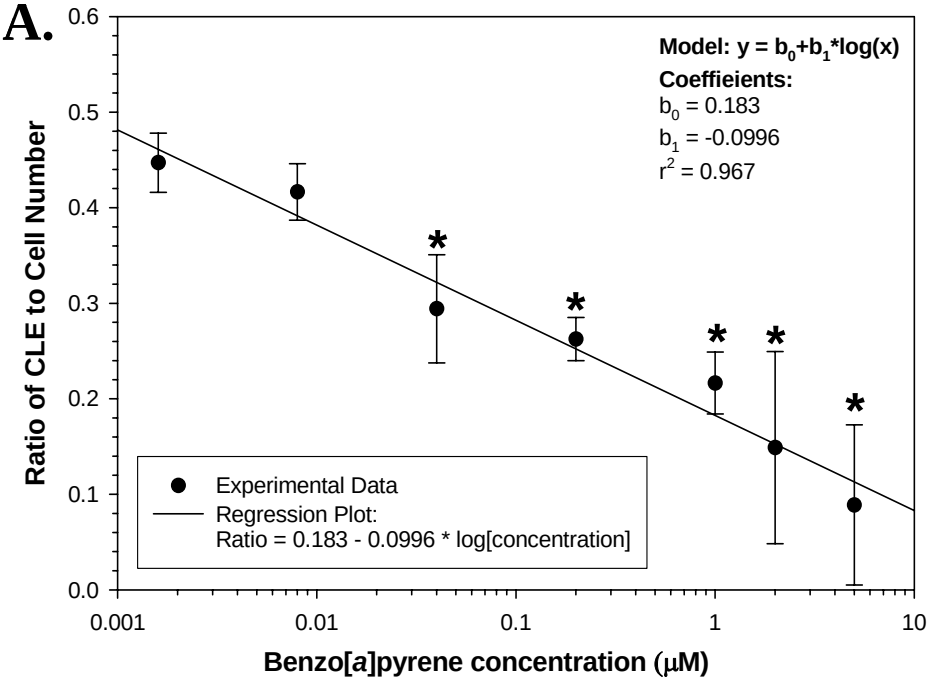

B.

Treatment	Avg. Ratio (CLE/Cell#)	Fold Difference	P-value
Control	0.4861	-	-
DMSO	0.4758	-1.0215	-
BaP 0.0016 μM	0.4471	-1.0873	0.497
BaP 0.008 μM	0.4166	-1.1669	0.170
BaP 0.04 μM	0.2942	-1.6524*	0.002
BaP 0.2 μM	0.2625	-1.8520*	< 0.001
BaP 1.0 μM	0.2165	-2.2452*	< 0.001
BaP 2.0 μM	0.1489	-3.2644*	< 0.001
BaP 5.0 μM	0.0889	-5.4683*	< 0.001

Figure 4.4. **Dose-dependent inhibition of CLE formation in NHEK by benzo[*a*]pyrene.** NHEK were treated with increasing concentrations of BaP for 24 hr as indicated in the figure, and CLE were quantified as described in Materials and Methods. Controls were untreated NHEK and those treated with the DMSO solvent. Numbers of CLE were standardized to cell number and are expressed as the mean of triplicates ±SD from 16 independent experiments. *Significantly different from the control using one way ANOVA followed by Dunnett's test, $p<0.05$. Statistical regression analysis was carried out to predict the best mathematical model for describing CLE formation as a function of chemical concentration. A is graphical representations of the data in Table B.

A.

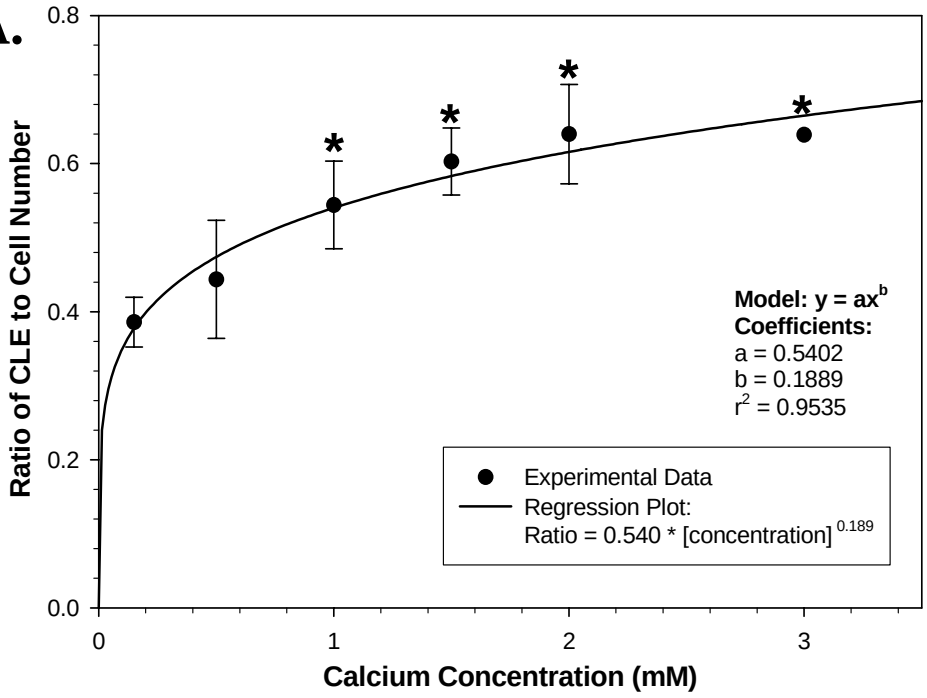

B.

Treatment	Avg. Ratio (CLE/Cell#)	Fold Difference	P-value
Control	0.3859	-	-
Calcium 0.5 mM	0.4436	1.1495	0.072
Calcium 1.0 mM	0.5441	1.4099*	0.013
Calcium 1.5 mM	0.6029	1.5623*	0.002
Calcium 2.0 mM	0.6398	1.6579*	0.001
Calcium 3.0 mM	0.6390	1.6558*	0.001

Figure 4.5. **Dose-dependent induction of differentiation in NHEK by calcium.** NHEK cells were treated with Ca^{2+} and CLE quantified as described in Materials and Methods. Numbers of CLE as a function of Ca^{2+} concentration were standardized to cell number and expressed as a mean of triplicates from 6 independent experiments ± SD. Note the first data point shows basal levels of Ca^{2+} at normal culture conditions, which is a concentration of 0.25 mM. *Significantly different from the control using one way ANOVA followed by Dunnett's test, $p<0.05$. Statistical regression analysis was carried out to predict the best mathematical model for describing CLE formation as a function of chemical concentration. A is a graphical representation of the data in Table B.

A.

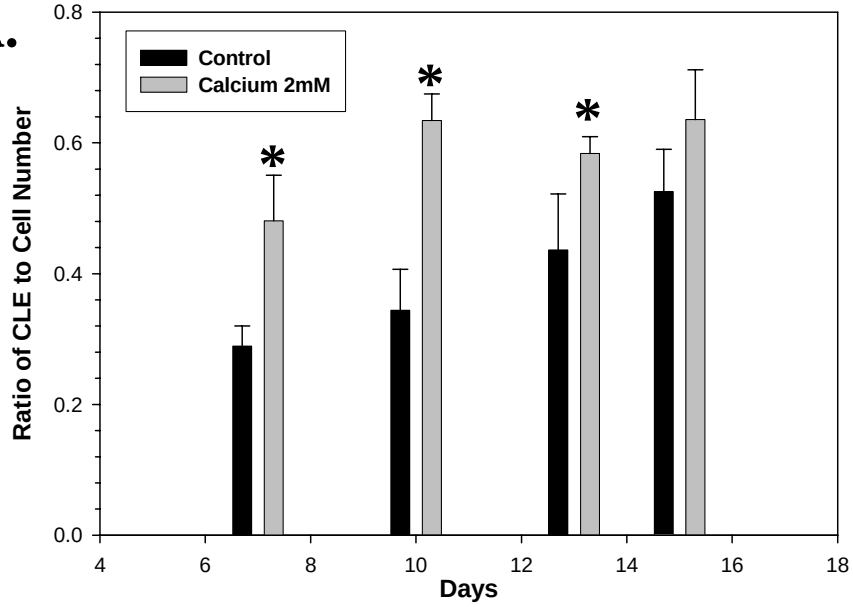

B.

Day in Culture	Percent (%) Confluence	Control	Calcium
		Avg. Ratio (CLE/Cell#)	Avg. Ratio (CLE/Cell#)
7	60	0.2893±0.0306	0.4808±0.0698*
10	80	0.3439±0.0629	0.6341±0.0408*
13	90-95	0.4362±0.0857	0.5838±0.0256*
15	100	0.5256±0.0648	0.6357±0.0762

Figure 4.6. **Time-dependent effects of calcium on differentiation in NHEK.** Cells were treated with 2.0 mM Ca^{2+} for increasing times and CLE production was determined as described in Materials and Methods. Numbers of CLE were standardized to cell number and are shown as the mean of triplicates ± SD from 3 experiments. *Significantly different from the control using one way ANOVA followed by Dunnett's test, $p<0.05$. A is a graphical representation of the data in Table B.

A.

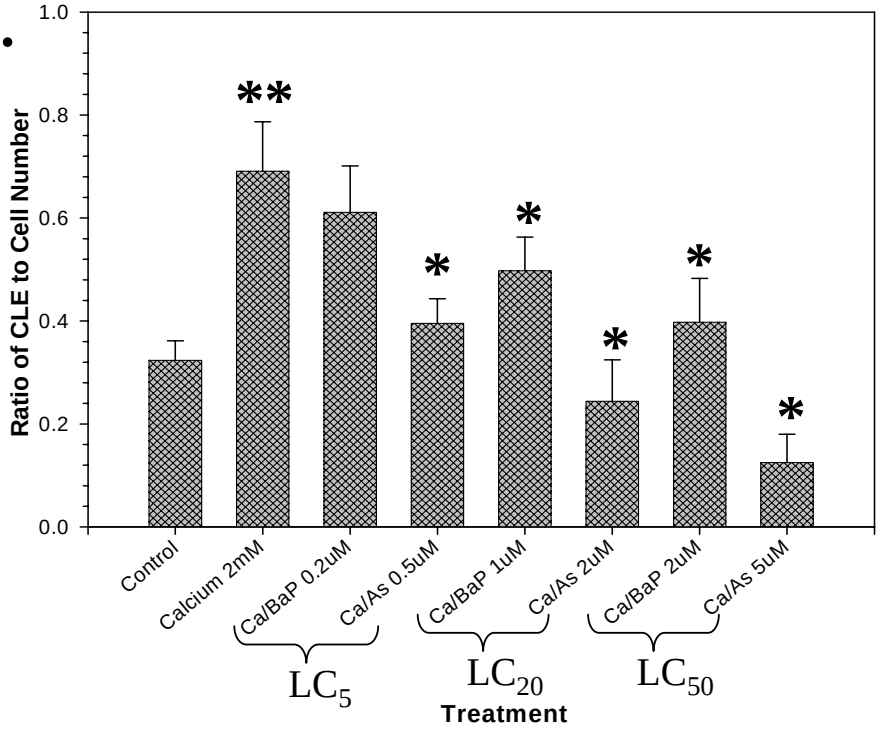

B.

Treatment	Avg. Ratio (CLE/Cell#)	Fold Difference	P-value
Control	0.3236	-	-
Calcium 2.0 mM	0.6911	+2.1353*	< 0.001
Ca^{2+}/BaP 0.2 µM	0.6110	-1.1310	0.108
Ca^{2+}/BaP 1.0 µM	0.4975	-1.3890*	< 0.001
Ca^{2+}/BaP 2.0 µM	0.3975	-1.7387*	< 0.001
Ca^{2+}/Arsenic 0.5 µM	0.3953	-1.7482*	< 0.001
Ca^{2+}/Arsenic 2.0 µM	0.2440	-2.8324*	< 0.001
Ca^{2+}/Arsenic 5.0 µM	0.1248	-5.5368*	< 0.001

Figure 4.7. **Effects of benzo[*a*]pyrene and arsenic on calcium-induced differentiation in NHEK.** Keratinocytes were induced to differentiate by treatment with 2.0 mM Ca^{2+} in the presence of increasing concentrations of BaP or arsenic as indicated in the figure. Controls were untreated cells (control) and cells exposed only to Ca^{2+}. CLE were quantified as described in Materials and Methods. Numbers of CLE were standardized to cell number and are expressed as the mean of triplicates from 3 experiments ±SD. *Significantly different from the Ca^{2+}-treated control using one way ANOVA followed by Dunnett's test, $p<0.05$. **Signifies Ca^{2+} exposed cells being significantly different from control cells. A is graphical representations of the data in Table B.

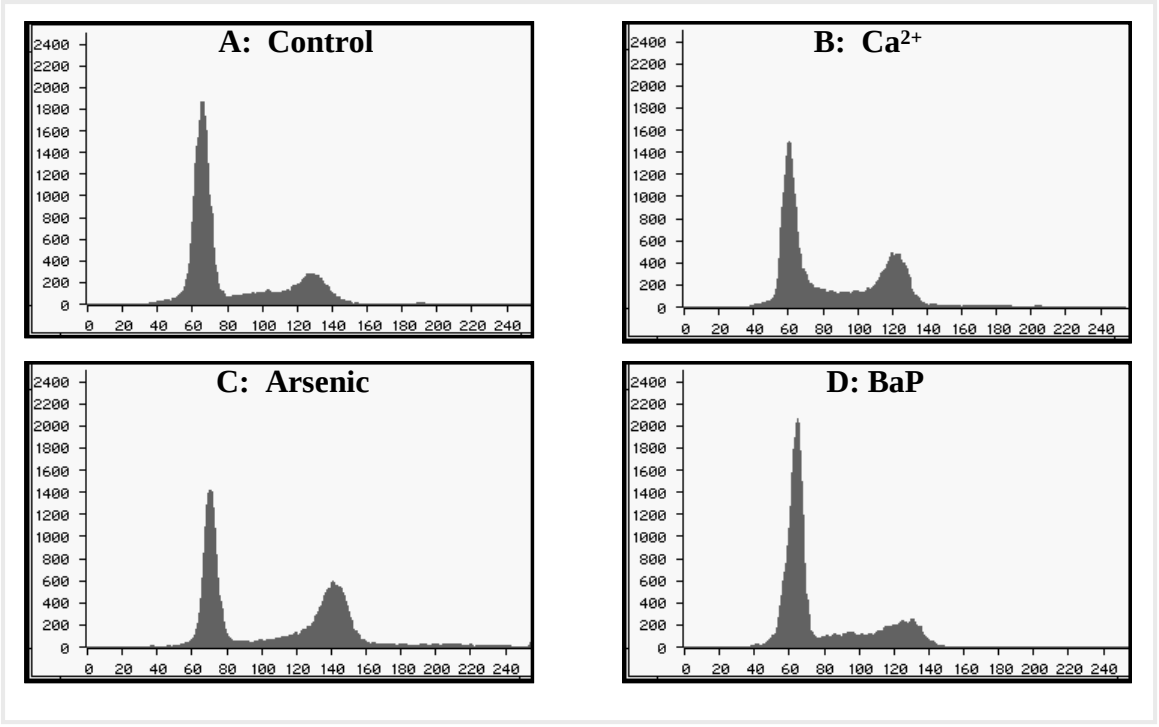

Figure 4.8. **DNA histograms of NHEK exposed to benzo[*a*]pyrene, arsenic, and calcium.** NHEK were treated with chemical effectors for 24 hr, stained with propidium iodide, and analyzed by flow cytometry as described in Materials and Methods. DNA histograms demonstrate cell number versus DNA content of viable cells in treated and control populations as indicated in the figure and are representative of multiple (n=8) experiments. Actual percentages in each phase were determined by computer analysis using Multicycle®. The concentrations of chemical effectors utilized were (B) 2.0 mM Ca^{2+}, (C) 5.0 µM arsenic, and (D) 2.0 µM BaP.

A.

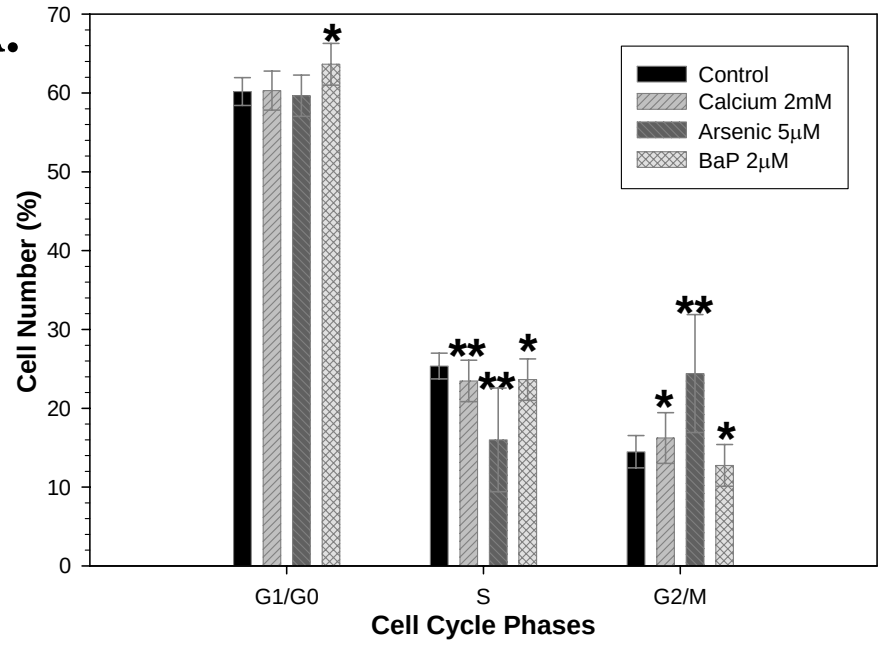

B.

Treatment	Average Percentage (%) of Cells in each Cell Cycle Phase					
	G1/G0	P-value	S	P-value	G2/M	P-value
Control	60.18	-	25.35	-	14.48	-
Calcium	60.30	0.853	23.46**	0.008	16.23*	0.041
Arsenic	59.66	0.455	16.00**	< 0.001	24.4**	< 0.001
BaP	63.65*	< 0.021	23.63*	0.016	12.74*	0.024

Figure 4.9. **Alterations in cell cycle distribution in NHEK populations treated with benzo[*a*]pyrene, arsenic, and calcium.** NHEK were treated with chemical effectors for 24 hr, stained with propidium iodide, and analyzed by flow cytometry as described in Materials and Methods. Cell percentages are expressed as the mean of triplicates ±SD from 7 experiments. Significant differences in the proportion of each population in the three (G1/G0, S, or G2/M) phases of the cell cycle were determined by one way ANOVA followed by Dunnett's test, **p<0.01; *p<0.05. A is graphical representations of the data in Table B.

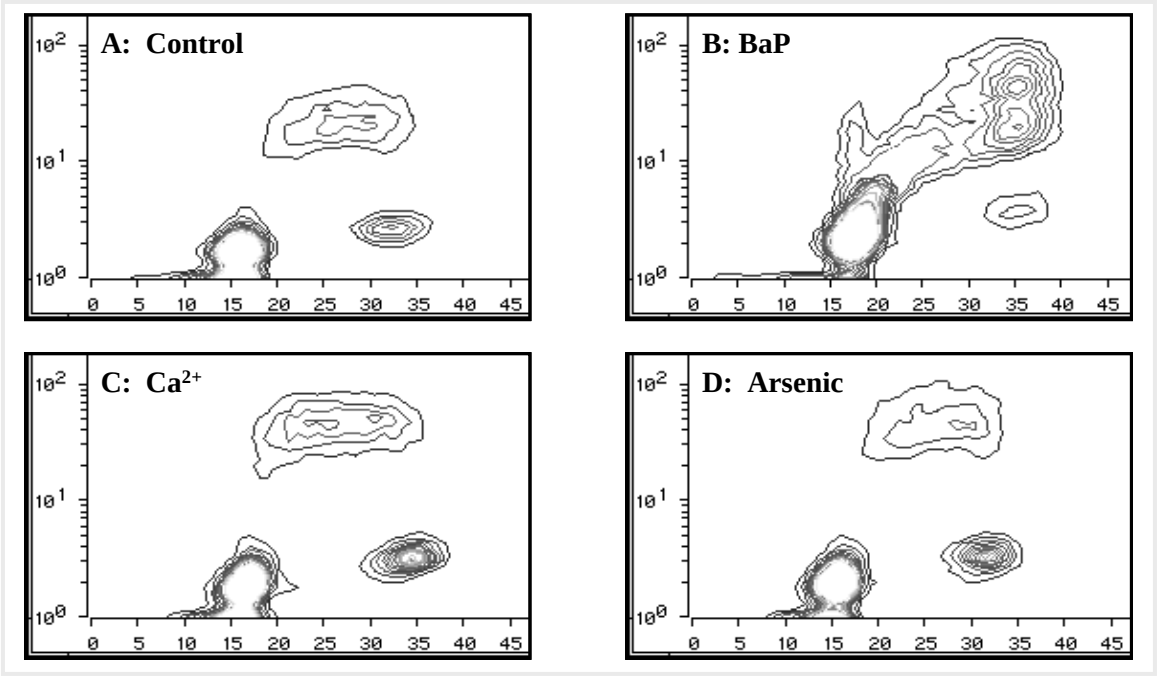

Figure 4.10. **Bivariate histograms of control and chemically-treated NHEK.** Cells were left untreated (A) or were exposed to 2.0 µM BaP (B), 2.0 mM Ca^{2+} (C), and 5.0 µM arsenic (D) as described in Materials and Methods. Staining with BrdU and propidium iodide, and analysis by flow cytometry was carried out as described in Materials and Methods. Representative histograms of chemically-treated and control populations demonstrate BrdU incorporation versus DNA content of viable cells from one of several experiments.

A.

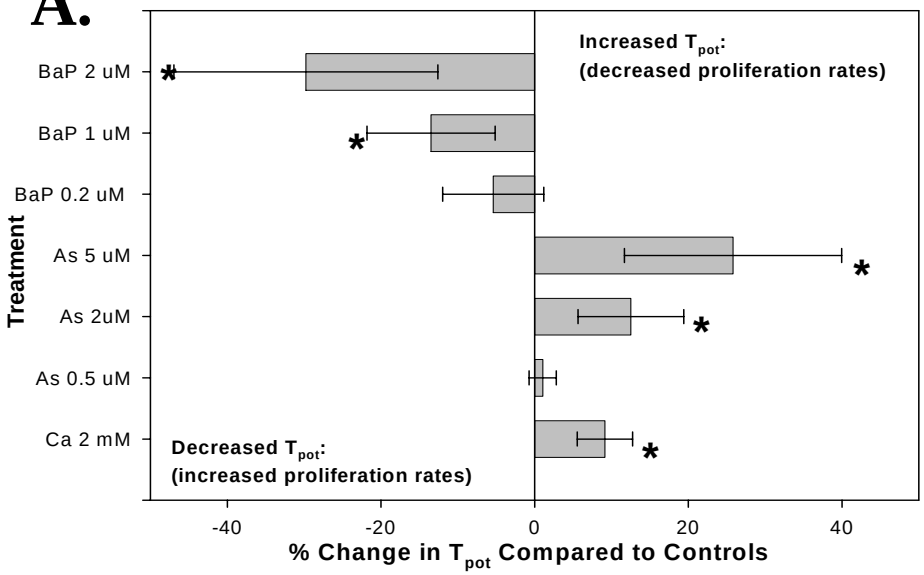

B.

Treatment	Change from Control (hrs)	Percent Change from Control (%)	P-value
Calcium 2.0 mM	3.0696	+9.1564±3.5988*	0.001
Arsenic 0.5 µM	0.2882	+1.0615±1.7624	0.212
Arsenic 2.0 µM	4.3059	+12.5311±6.8802*	0.002
Arsenic 5.0 µM	10.3231	+25.8307±14.1493*	< 0.001
BaP 0.2 µM	-2.0667	-5.3925±6.5726	0.160
BaP 1.0 µM	-3.6471	-13.4753±8.3403*	0.003
BaP 2.0 µM	-15.0500	-29.7637±17.1677*	< 0.001

Figure 4.11. **Effects of benzo[*a*]pyrene, arsenic, and calcium on T_{pot} in NHEK.** NHEK cells were treated with increasing concentrations of BaP or arsenic or with 2.0 mM Ca^{2+} for 24 hr, stained with BrdU and propidium iodide, and analyzed by flow cytometry as described in Materials and Methods. T_{pot} for each culture was calculated as described by Steel (1977) and Wilson (1994) and is shown relative to that in untreated control cultures in terms of both change in hours and percent change. Both arsenic (2.0 µM and 5.0 µM) and Ca^{2+} (2.0 mM) decreased proliferations rates while BaP (1.0 µM and 2.0 µM) stimulated cell proliferation as compared to control NHEK. Twelve independent experiments were run. *Significant differences in T_{pot} were determined by one way ANOVA followed by Dunnett's test, $p<0.05$. A is graphical representations of the data in Table B.

Chapter 5

Gene Expression Changes Associated with Altered Growth and Differentiation in Benzo[*a*]pyrene or Arsenic Exposed Normal Human Epidermal Keratinocytes

5.1. Abstract

Both arsenic and benzo[*a*]pyrene (BaP) inhibit terminal differentiation and alter growth potential in normal human epidermal keratinocytes (NHEK) *in vitro*. To identify molecular alterations that may be involved, microarray analysis was carried out on NHEK treated with BaP or arsenic. Results using the BD Bioscience Human 3.8 II array are as follows: 1) in total, 86 genes were induced and 17 genes were suppressed ≥2-fold by 2.0 μM BaP. 2) Arsenic at an equitoxic dose (5.0 μM) induced 107 and suppressed 15 genes. Highly quantitative real-time PCR was subsequently used to confirm microarray findings on selected genes involved in keratinocyte growth and differentiation pathways. These studies confirmed induction in NHEK by BaP of α-integrin binding protein 63 (α-integrin-bp) (2.48-fold), retinoic acid- and interferon-inducible protein (RA-IFN) (2.74-fold), interleukin-1α (IL-1α) (2.64-fold), interleukin-1β (IL-1β) (2.84-fold) and Ras guanyl releasing protein 1 (Ras-GRP) (3.14-fold). Real-time PCR confirmed that arsenic induced the following genes: retinoblastoma 1 (Rb-1) (5.4-fold), retinoblastoma-binding protein 1 (Rb-bp1) (6.8-fold), transforming growth factor β-stimulated protein (TSC-22) (6.84-fold), MAX binding protein (MNT) (2.44-fold), and RAD50 (4.24-fold).

Mechanistic studies with a subset of genes may provide an opportunity to correlate alterations in these molecular markers with chemical-specific blocks to differentiation in NHEK.

*Note: Please refer to Table 5.7 for gene information and abbreviated names used throughout this chapter.

5.2. Introduction

The skin is an important exposure route for a variety of xenobiotics. This lab is specifically interested in chemically induced alterations in human skin that may lead to development of neoplastic epidermal tumors. In particular, I am interested in the regulation of keratinocyte differentiation and proliferation and how an imbalance in these opposing processes is linked to the onset of carcinogenesis in this cell type. Chemically-mediated skin carcinogenesis has been directly linked to defects in the normal pathway of squamous differentiation (Kulesz-Martin *et al.* 1980; Yuspa and Morgan 1981). One approach to studying the cellular and molecular effects of carcinogenic chemicals on human skin is to utilize a realistic *in vitro* system such as normal human epidermal keratinocytes (NHEK). As these cells undergo squamous differentiation in culture, one may study the process under controlled conditions and in the presence of a variety of chemical or physical agents that may influence its efficiency. Characterization in this system, of multiple chemical agents with diverse cellular activities and targets, yet with the common endpoint of induction of cancer in this cell type, will allow a clearer mechanistic understanding of the link between proliferation, differentiation, and transformation. Identification of common and unique pathways affected by different carcinogens may also aid in predictive hazard identification studies.

BaP and arsenic, two chemicals selected for the studies herein, are of important toxicological concern to humans from both environmental and occupational standpoints. BaP is a ubiquitous environmental pollutant and is among the Superfund Top 10 Priority Hazardous Substances (ATSDR 1999b, 2003b). The polycyclic aromatic hydrocarbon (PAH) is a potent mutagen and carcinogen in both humans and animals, and has been classified as an initiating agent. BaP, which is a common constituent in petroleum products, also represents a major class of heavy fraction hydrocarbons in mixtures such as coal tar, smoke, and automobile exhaust. Likewise, inorganic arsenic species have been ranked highest in priority on the list of Top 20 Hazardous Substances by the ATSDR and USEPA (ATSDR 1999a, 2003a). Although arsenic is a known human carcinogen, it is only slightly mutagenic at high concentrations. Thus, arsenic has been characterized as a promoting, progressing, and/or co-mutagenic agent. Exposure to arsenic occurs through arsenic-rich geological soil, nonferrous smelters, pesticide manufacturing and use, microelectronics, burning of fossil fuels, or from consumption of contaminated drinking water.

The most likely source of dermal contact with toxic BaP levels would be in workers in the petroleum industry. Bioactivated BaP is a potent skin carcinogen (Mager *et al.* 1977). When applied dermally, BaP induces cytokinetic abnormalities and inflammation, followed by skin tumors (Albert *et al.* 1996). Many of the earliest studies of BaP were carried out using the murine skin system (Lee and O'Neill 1971). BaP also alters differentiation in multiple cell types (Edmondson and Mossman 1991; Perez *et al.* 2003; Reiners *et al.* 1991). The myriad of activities of BaP are likely due to mutagenesis of proteins in crucial signal transduction paths. However, with a few exceptions, such as

the *ras* and *p53* gene, few cellular distinct targets for BaP mutagenesis have been identified. Clearly, much work remains to be done to clarify the relationship between BaP exposure, abnormalities in expression of genes involved in proliferation and differentiation, and development of neoplastic skin lesions.

Ingestion, inhalation, and dermal contact are all significant in exposure of humans to arsenic. Due to arsenic-contaminated water supplies in many countries, development of neoplastic skin lesions has become a health problem of global proportions (Tseng 1977). Arsenic has been shown to be a potent differentiation inhibitor in keratinocytes by decreasing cornified envelope formation or by altering differentiation-associated markers (Jessen *et al.* 2001; Kachinskas *et al.* 1994; Perez *et al.* 2003). In addition, arsenic has been shown to have dose-dependent effects on cell proliferation and to affect expression of a variety of growth regulatory factors in this cell type (Germolec *et al.* 1996; Vega *et al.* 2001). Although arsenic is a potent human skin carcinogen, the exact mechanism whereby it induces cellular transformation is currently being investigated. It is likely the above effects are linked to one another and to the induction of skin cancer in keratinocytes.

My previous research characterized the chemical specific effects of arsenic and BaP on the opposing processes of proliferation and squamous differentiation in NHEK (Perez *et al.* 2003). Results of these studies suggested that although both skin carcinogens act to inhibit expression of a differentiated phenotype *in vitro*, BaP and arsenic elicit opposite effects on cell proliferation and may, therefore, be mechanistically distinct. The purpose of the work described herein is to address this issue through characterization of gene expression profiles in NHEK treated with BaP and arsenic, both of which

effectively inhibit differentiation, as compared to untreated controls. The hypothesis is that the gene expression alterations induced by the two carcinogenic chemicals will provide mechanistic clues as to their mode of operation during the differentiation process and may allow identification of crucial signal transduction pathways which, when expressed inappropriately, will favor transformation under conditions of exposure.

5.3. Materials and Methods

5.3.1. Chemicals and Reagents

Sodium meta-arsenite ($NaAsO_2$), calcium chloride ($CaCl_2$), benzo[*a*]pyrene (BaP) ($C_{20}H_{12}$), and dimethyl sulphoxide (DMSO) were purchased from Sigma Chemical Co. (St. Louis, MO).

5.3.2. Cell Culture

Cryopreserved normal human epidermal keratinocytes (NHEK) were purchased from the Clonetics Corp. (San Diego, CA). NHEK were grown in 5% CO_2 at 37°C in defined Keratinocyte Growth Medium (KGM) (Clonetics Corp) containing bovine pituitary extract (BPE), human epidermal growth factor (hEGF), insulin, hydrocortisone, transferrin, epinephrine, and antibiotic, GA-1000, at proprietary concentrations as determined by the manufacturer.

5.3.3. Treatment Regime and RNA Isolation

NHEK were plated in T-150 flasks and treated at 70-75% confluency (6-7 days) with 2.0 μM BaP (the LC_{50} as determined for this cell type in cytotoxicity assays) or 5.0 μM sodium meta arsenite (LC_{50}) for 24 hours. The concentrations of chemicals were

chosen based on the fact that in previous published studies they acted to maximally inhibit squamous differentiation and alter cell growth properties in treated NHEK (Perez *et al.* 2003); a summary of the cellular effects of these two chemicals at the chosen concentrations is provided in Table 5.1. As a separate control to maximally induce differentiation, NHEK were continuously treated with calcium chloride (2.0 mM) (Hennings *et al.* 1980; Rice and Green 1979; Shipley and Pittelkow 1987). Chemical containing medium was replaced after 24 hour exposure with fresh medium free of chemicals. Cells were cultured an additional 5 days in culture prior to RNA isolation. RNA was isolated from treated cultures using an RNA isolation kit (RNAqueous) from Ambion Inc. (Austin, TX) and following the manufacturer's directions. RNA purity and concentration was measured spectrophotometrically, and only those samples with a 260:280 nm ratio of >1.6 were used in subsequent experiments.

5.3.4. Microarray

The BD Atlas PowerScript Fluorescent Labeling Kit (BD Biosciences Clontech Inc., Palo Alto, CA) was used to prepare probes for hybridization of microarrays. The kit is based on an indirect, two-step procedure for probe labeling and the procedure was carried out according to the Atlas PowerScript Fluorescent Labeling Kit User Manuel. First strand cDNA was synthesized from isolated total RNA (2.0 μg per sample) using BD PowerScript Reverse Transcriptase. During cDNA synthesis, primary aliphatic amino groups were incorporated using an optimized deoxyribonucleoside triphosphate (dNTP) mix, which includes the deoxythymidine triphosphate (dTTP) analog, aminoallyl-deoxyuridine triphosphate (dUTP). Monofunctional, N-hydroxysuccinimide-activated fluorescent dyes, cyanine 3 (Cy3) and cyanine 5 (Cy5) (Amersham Biosciences,

Piscataway, NJ) were subsequently coupled to the cDNA by reaction with the amino functional groups. QIAquick PCR Purification Kit (Qiagen, Valencia, CA) was used to purify single stranded cDNA probes. Probe quality was assessed via UV/Visible spectrophotometry according to the manufacturer's protocol. Labeled cDNA probe was hybridized to Atlas Glass Human 3.8 II Microarrays (BD Biosciences) according to the User Manual. This array includes 3,757 single-stranded oligos and nine housekeeping genes, as well as positive and negative controls, immobilized on a glass slide. Hybridized slides were scanned with the Packard BioChip Imager Scanner 3000 (Packard, Meriden, CT), which generates Tiff images of both the Cy3 and Cy5 channels. Laser and photomultiplier tube voltages were adjusted manually to maximize the signal to noise ratio. Cy 3 and Cy5 signal intensities were standardized relative to one another by comparing the total signal intensities of all spots in each chemical. Tiff images were quantified and analyzed using ScanAlyze (software developed by M. Eisen, University of California at Berkeley). Gene expression changes ≥ 2-fold in each of the triplicate experiments were considered significantly different when compared to the control array. To assure biological consistency, the entire experiment, including cell culture, treatment, and RNA analysis was repeated three times for each chemical exposure.

5.3.5. Real-Time Reverse Transcription-Polymerase Chain Reaction (Real-Time RT-PCR)

Two micrograms of total RNA was reverse transcribed to produce single-stranded cDNA using Superscript (GibcoBRL, Rockville, MD) for PCR. PCR was carried out using the Eppendorf Mastercycler (Hamburg, Germany). To eliminate one potential

source of variability between the microarray and real-time PCR, the same RNA samples were used for both types of analysis.

Primer sets for a specific gene of interest were developed using OLIGO, version 6.5.1.0. software (Molecular Biology Insights, Inc., Cascade, CO). Primers were then purchased from Bio-Synthesis Inc. (Lewisville, TX). Primer sequence information is listed in Table 5.2.

The real-time PCR protocol used for these studies was an adaptation of previously published protocols (Bae *et al.* 2003; Solum and Handa 2002). Quantitative measurement of cDNA in chemically-treated and control NHEK was measured using the LightCycler system (Roche Molecular Biochemicals, Indianapolis, IN) and the LightCycler DNA Master SYBR Green I (Roche Molecular Biochemicals, Indianapolis, IN) reaction mix for PCR. Fluorescence at 530 nm was recorded at the end of the elongation phase, and increasing amounts of PCR product were monitored from cycle to cycle.

Briefly, a standard curve for each primer pair was generated using five to seven serially diluted known amounts of cDNA product. From this standard curve, the absolute concentration of cDNA for the known gene was determined (Figure 5.1A and B). Melting curve analysis and length verification by gel electrophoresis were carried out to confirm the specificity of PCR products (Figure 5.2A and B). In all experiments, samples containing no cDNA template (cDNA replaced with PCR-grade water) were included to serve as negative controls.

After real-time PCR, the absolute concentration of cDNA in each sample was determined by analysis with LightCycler data software. This software plots the standard curve of the crossing line intercepts of the standards versus the known concentrations of

these standards. The crossing line intercept is parallel to the *x*-axis on a graph of fluorescence intensity versus cycle number and occurs at the point where template amplification enters the logarithmic phase of the curve. Samples with a higher concentration of starting material enter the logarithmic phase earlier than samples with a lower concentration of starting material and therefore have a smaller crossing point value. The crossing line intercept of an unknown sample is subsequently compared with the standard curve to generate a quantitative amount of starting material. In each case, the point at which the crossing line intercepts the log-linear region of each curve is used to generate the concentration of that sample.

5.3.6. Statistical Analysis

Dunnett's one-way analysis of variance (ANOVA) was used to compare the difference of treated to control samples (Tamhane and Dunlop 2000). Treatment is significantly different if the p-value ≤ 0.05 when compared to control samples.

5.4. Results

5.4.1. Characterization of Gene Expression Changes Associated with Exposure to Benzo[a]pyrene and Arsenic in NHEK using Microarray Technology

To analyze the effects of BaP and arsenic on gene expression, cDNA microarray technology was first used to identify candidate mRNA species that are over- or under-expressed in NHEK treated versus control cells for 24 hours with arsenic of BaP. Approximately 3800 genes were present on the BD Bioscience Human 3.8 II array used

for this analysis. This array included functional groups of genes which are involved in regulation of cell adhesion and integrity, cell growth, apoptosis, cell cycle, mitosis, necrosis, differentiation, numerous kinases, GTPases, various transcription factors, DNA repair genes, genes involved in chromatin structure, genes that are differentially expressed in cancerous tissue, metabolic enzymes, immune response, and receptor signaling.

5.4.1.1. Benzo[*a*]pyrene Altered Genes from Microarray Analysis

After a dissecting analysis of almost 3800 genes in three separate experiments, BaP was shown to significantly (2-fold or greater as described in the Materials and Methods) alter the expression levels of a total of 103 genes (inducing 86 genes, while suppressing 17). A complete list of these altered genes is displayed in Table 5.3 and 5.4. As hypothesized, many genes which have been demonstrated in other studies to play a role in differentiation and cell division were significantly altered by BaP exposure. Among the genes induced by BaP were those involved in: (1) growth regulation [insulin-like growth factor 1(IGF-1), interleukin 1 alpha (IL-1α), interleukin 1 beta (IL-1β), RAS guanyl releasing protein 1 (Ras-GRP), Ras-related associated with diabetes**,** RAS-related on chromosome 22, activating transcription factor 2 (ATF-2), ataxia telangiectasia mutated (ATM), and TRAF-interacting protein]; (2) differentiation [retinoic acid- and interferon-inducible protein (RA-IFN), YY1-associated factor 2 (Yaf2), upregulated by 1,25-dihydroxyvitamin D-3]; (3) RNA synthesis and/or processing [exportin, tRNA, RNA cyclase homolog, TATA box binding protein (TBP)-associated factor RNA polymerase I A 48kD (RNA polymerase I–A), TATA box binding protein (TBP)-associated factor RNA polymerase I C 110kD (RNA polymerase I-C), U2 small nuclear

ribonucleoprotein auxiliary factor (U2 snRNP aux. factor), U5 snRNP-specific protein U5 (snRNP), and chromatin-specific transcription elongation factor]; and (4) cell structure and adhesion [enhancer of filamentation 1 (cas-like docking protein), α-integrin binding protein 63 (α-integrin-bp), and PAK-interacting exchange factor beta (RAC1-GEF)]. Compared to the number of induced genes (Table 5.3), BaP suppressed only the small number of genes which are listed in Table 5.4. Among these repressed genes were Cbp/p300-interacting transactivator (obstructs transcription), cyclin A1 (cell cycle regulator), cytochrome P450, subfamily 21A2 (metabolizing enzyme), and CCR4-NOT transcription complex (transcription regulator). As can be seen from Tables 5.3 and 5.4, the maximum level of gene induction detected by microarray was approximately 31.9-fold (ISL1 transcription factor), while the gene for the G-protein coupled receptor 64 was maximally suppressed at 5.5-fold.

5.4.1.2. Arsenic Altered Genes from Microarray Analysis

Microarray data from arsenic-treated cells demonstrated that the metal significantly altered the expression levels of 122 genes (inducing 107, while suppressing 15). Arsenic also altered the expression levels of many genes which were previously shown to be involved in differentiation and proliferation in keratinocytes or other cell types. The functional families of genes demonstrating increased expression after arsenic treatment (Table 5.5) included: (1) cell cycle regulators [cyclins A2 and H, cyclin-dependent kinase 5 (Cdk-5)], (2) regulators of growth and differentiation [cell cycle progression protein 8, mitogen-activated protein kinase kinase 6 (MAPKK6), retinoblastoma 1 (Rb-1), retinoblastoma-binding protein 1 (Rb-bp1), protein kinase C-zeta (PKC-ζ), transforming growth factor beta-stimulated protein TSC-22 (TSC-22), toll-

like receptor, MAX binding protein (MNT)], (3) apoptosis [programmed cell death 10, CASP8-associated protein 2], (4) cell structure and adhesion [active BCR-related gene (RAC GTPase), cadherin 5, type 2, VE-cadherin (Cad-5), RNB6], and (5) chromatin structure and function [REV1, origin recognition complex, subunit 3 (ORC subunit 3), RAD50, Sir2-like1]. As seen in Table 5.6, Chromobox homologs 2 and 5 (interact with chromatin), nuclear factor I/C (transcription factor), and CK4 antigen-p55 (involved in immune response) were among the genes suppressed by arsenic. Tables 5.5 and 5.6 summarize gene expression changes detected by microarray, which ranged from 9.1-fold induction (protease, serine, 7) to 2.8-fold suppression (putative transmembrane protein).

5.4.1.3. Common or Similar Genes Altered by both BaP and Arsenic in NHEK

The microarray data indicate only four commonly affected genes from BaP and arsenic treatments. The four commonly induced genes are activating transcription factor 2 (M31630), hypothetical protein (NM_015916), suppressor of S. *cerevisiae* gcr2 (NM_007265), and zinc-finger protein 186-Kruppel type (NM_012480). These results also show exposure to these chemicals commonly alter genes which are not identical, but are very similar in nature (CGI-proteins, guanylate cyclase 1, myosin, phosphotidylinositol transfer protein, replication factor C, RNA polymerases, ubiquitin specific proteases, and various zinc-finger proteins). Thus, since there are very few commonly affected genes, it seems likely these chemicals target different mechanisms involved in NHEK differentiation, growth regulation, and other cellular processes.

5.4.1.4. Additional Information with regards to Microarray Experimentation

At times in this study, despite efforts to minimize experimental inconsistencies, variations in the expression level of the same gene among the triplicate arrays were quite large. This type of variation has been observed in previous microarray studies in this laboratory (Bae *et al.* 2003). One contributing factor could be inconsistency in cDNA spotting among the commercial arrays. Whatever the factors may be, I was stringent when compiling the lists presented in Tables 5.3, 5.4, 5.5, and 5.6. First, gene spots which had very high background levels were eliminated from analysis. Second, genes with substantial variations in spot intensity between treated and control arrays were discarded. For each gene to be included in the final list it had to be induced or suppressed ≥ 2-fold consistently in each of the triplicate experiments (three samples per treatment group).

5.4.2. Quantitative Analysis of Selected Chemically-Altered Genes by Real-Time RT-PCR

From microarray analysis, genes that were consistently altered by BaP or arsenic treatment, and that were known to be involved in the regulation of keratinocyte growth and differentiation, were selected for more detailed analysis using highly quantitative real-time RT-PCR.

5.4.2.1. Benzo[*a*]pyrene Altered Genes Detected by Real-Time PCR

Genes examined by real-time PCR included RA-IFN, Yaf2, α-integrin-bp, IL-1α, IL-1β, and Ras-GRP. In general, real time RT-PCR confirmed the majority of the gene expression alterations seen in the microarray studies. However, the magnitude of difference in expression levels between BaP treated and control samples was

substantially lower when analyzed by real-time RT-PCR, a common finding in this and other laboratories when the two technologies are compared (Bae *et al.* 2003). Table 5.8 compares PCR and microarray results for the six selected genes. Sensitive quantitation with real-time PCR demonstrated that BaP induced the expression of IL-1α (2.64±0.31-fold), IL-1β (2.84±0.19-fold), and Ras-GRP (3.14±0.29-fold), genes that are all involved in cell proliferation, Additionally, the PAH increased mRNA levels for two proteins involved in regulation of differentiation RA-IFN (2.74±0.68) and α–integrin-bp (2.48±0.22-fold). Contrary to microarray results, when measured by real-time PCR, Yaf2 mRNA levels were slightly suppressed (-1.33-fold) in BaP-treated cells as compared to control. To gain an understanding of the differential effects the arsenic and BaP in NHEK, these same six genes were analyzed in arsenic-exposed cells. The results of this analysis are also shown in Table 5.8. With the exception of Ras-GRP, which was induced slightly (1.76-fold), there was little alteration in expression of these same genes following arsenic exposure, which supports the data observed in the microarray studies.

5.4.2.2. Arsenic Altered Genes Detected by Real-Time PCR

Six genes, Rb-1, Rb-bp1, RAD50, TSC-22, MNT, and Cad-5, which were identified by microarray analysis as being modified under conditions of arsenic exposure were further studied by real-time PCR. The PCR data demonstrated that arsenic induced the expression of Rb-1 (5.4±0.51-fold), Rb-bp1 (6.8±1.46-fold), TSC-22 (6.84±0.51-fold), MNT (2.44±0.02-fold) and RAD50 (4.24±2.59-fold) as shown in Table 5.9. Induction of the Cad-5 gene as measured by real-time PCR was lower than the ≥2-fold cut off and, therefore, was not considered significant in these studies. Table 5.9 also displays the microarray data from these same samples for comparison purposes. Real-

time PCR confirmed most arsenic induced gene alterations seen in the microarray studies (Table 5.9). However, the expression levels between arsenic treated and control samples was higher in most genes (except Cad-5) analyzed by real-time RT-PCR when compared to microarray results. The effect of BaP on these same genes were also investigated (Table 5.9). There was little change in the expression of these same genes following BaP exposure, which supports results from the microarray studies.

5.4.3. Comparing Real-Time PCR Data to Microarray Results

From a quantitative standpoint, both types of analysis gave comparable results for the majority of specific genes analyzed. That is, genes were consistently induced or suppressed under the different treatment regimens when measured by either technique. The absolute level of change in expression measured by microarray verses real-time PCR varied by a maximum of approximately 3-fold, with the values of induction being larger in BaP studies and smaller in arsenic studies by microarray analysis for most genes examined. This contrast between the two studies may be due to variation in microarray scanning and/or analysis since the BaP and arsenic experiments were conducted weeks apart from each other. The low expression levels displayed in the arsenic microarray experiments may be due to low spot intensities observed on the arsenic treated arrays. Since the signal intensities were low in the treated arrays, the signal that was detected may be an underestimation of the actual signal. This may be a reason why the expression levels of arsenic microarray data are lower when compared to the higher expression levels seen in the real-time PCR data. When comparing the control spot of the Cy3 (control) to Cy5 (arsenic treated), their signals matched up very well; however, it is possible that certain regions of the array did not hybridize efficiently with the

fluorescently labeled cDNA. The quality of each cDNA probe was evaluated by taking absorbance reading for both Cy3 and Cy5 prior to hybridization and all analyses proved to be satisfactory. However, it is possible that there was either variation between the arrays themselves, or the hybridization step was somehow insufficient. In addition, one of the three arsenic treated arrays displayed consistently lower signals than the other two arsenic arrays. In order for a gene to be significantly altered, it was required that all genes be induced 2-fold in each of the three experiments. Hence, this lone experiment may have caused the under estimated expression of numerous genes which were near this 2-fold level of significance. Thus, this lone microarray experiment could be responsible for the lower average expression level of many genes when compared to the expression levels of the same genes analyzed by real-time PCR. Overall, real-time PCR results tended to be more consistent (observed by the small standard deviation values) as compared to microarray data which exhibited substantial variability across samples. Thus, this data suggests that real-time PCR may be a more accurate and quantitative technique for examining changes in gene expression when compared to microarray analysis.

5.5. Discussion

Previous research demonstrated that two high priority skin carcinogens, arsenic and BaP, differentially altered the capacity for differentiation and growth properties of normal human epidermal keratinocytes (Perez *et al.* 2003). Both chemicals were potent inhibitors of differentiation in NHEK. Arsenic also decreased proliferation in these cells in a manner suggestive of a G2 block. In contrast, BaP increased proliferation rates and induced rapid progression through the cell cycle. The studies presented here utilized microarray analysis and real-time RT-PCR to characterize molecular alterations in NHEK

that may correlate with the selective effects of these two skin carcinogens. These results demonstrate that exposure to each chemical induces highly specific gene expression patterns in NHEK, altering mRNA levels for several proteins previously implicated in crucial cellular processes such as proliferation and differentiation. These findings suggest that diverse skin carcinogens may act by selectively targeting different steps in cellular signal transduction pathways.

Microarray studies such as these aid in identification of large numbers of genes that are altered in their expression in response to defined cellular exposures. It is, however, the analysis and meaningful interpretation of the data that become difficult. The initial goal using this technology was to identify candidate genes whose expression appeared to be consistently altered in NHEK by exposure to the two carcinogenic chemicals, BaP and arsenic. The resulting data were subsequently used for two purposes: 1) to compare the "global" gene expression patterns induced by BaP and arsenic and to determine whether the two chemicals acted on entirely different genes or whether there was overlap in genes affected which may indicate mechanistic similarities; and 2) to select a small subset of genes which, through previous characterization, had been implicated in the switch between proliferation or differentiation in keratinocytes, and to characterize in a more quantitative manner, their expression in response to chemical administration.

The microarray selected for this study contained, among its 3800 genes, those belonging to families with diverse functions in the cell including regulation of the cell cycle, apoptosis, differentiation, and DNA repair. As detected by this analysis, a total of 103 and 122 genes were altered (showing either increased or decreased expression) by

BaP and arsenic, respectively; many (or all) of these genes could potentially be involved in the multiple cellular effects of the individual chemicals. Several previous investigators have carried out this type of analysis on arsenic-treated cells, although few researchers used a keratinocyte model system. One study performed microarray analysis on arsenic treated NHEK; however, this group exposed cells to non-cytotoxic levels of arsenite (Hamadeh *et al.* 2002). Even though this study used cytotoxic concentrations of arsenic, results presented by Hamadeh *et al.* show arsenite altering similar genes and/or gene families to those observed in this study. Some of these commonly altered genes include: REV, TGF-β, PKC, MAP kinase, zinc finger transcription factors, MAX binding protein. In support of this work other laboratories also show arsenic-mediated changes in the expression of the following genes or gene families: PKC, MAPK6, cyclins, interleukins, transcription factor A, colony stimulating factor-1 receptor, hypothetical proteins, retinoblastoma, TGF-β, RNA polymerase, programmed cell death, activating transcription factor 2, CASP8, prefolden, and replication factor C to name a few (Chen *et al.* 2001; Rea *et al.* 2003; Wu *et al.* 2003; Yih *et al.* 2002; Zheng *et al.* 2003). To date, there are very few studies which used microarrays to screen the effects of BaP on gene expression levels and none of these studies used an epidermal model system.

The six genes selected from BaP microarrays for quantitative analysis using real-time PCR were RA-IFN, Yaf2, α-integrin-bp, IL-1α, IL-1β, and Ras-GRP. These genes all demonstrated increased expression in microarrays from BaP-treated as compared to control cells. Cytokines IL-1α and IL-1β were of interest as, in general, these family members behave as potent growth factors in keratinocytes and tend to show decreased expression in cells undergoing squamous differentiation (Gniadecki 1997; Hammerberg

et al. 1998). Moreover, both cytokines have also been shown to suppress 1,25-dihydroxyvitamin D_3 stimulated differentiation in keratinocytes (Gniadecki 1997). Resulting PCR data confirmed that under conditions of exposure to BaP where keratinocytes exhibit poor potential for differentiation and are proliferating more rapidly, both IL-1α and IL-1β are overexpressed. From a mechanistic standpoint, increased expression of these cytokines may block the process of differentiation through inducing the expression of keratins K6 and K16 which are typically expressed during high proliferative activity (Gniadecki 1997; Jiang *et al.* 1993). Ras-GRP was also induced by BaP in exposed NHEK. The Ras-GRP gene is a guanine nucleotide exchange factor and is involved in regulation of growth and differentiation through activation of Ras (and Ras-related) GTPases (Rong *et al.* 2002). In keratinocytes specifically, expression of Ras has been demonstrated to promote proliferation while inhibiting squamous differentiation (Rambaratsingh *et al.* 2003). RasGRP1 itself has been shown to inhibit calcium-induced expression of differentiation markers keratin 1 and keratin 10 in this cell type (Rambaratsingh *et al.* 2003) Induction of Ras activity by BaP, directly or indirectly through mutation, may be one mechanism whereby the chemical induces rapid traverse through the cell cycle, potentially favoring cellular transformation (Perez *et al.* 2003).

BaP exposure was also found to induce the expression of RA-IFN in both microarray and real-time PCR analysis in NHEK. This gene, which is highly inducible in keratinocytes in response to retinoids and interferons, was of particular interest as these molecules are both important endogenous regulators of keratinocyte differentiation. In keratinocytes, retinoids are potent suppressors of differentiation *in vitro*; however, *in vivo* and *in vitro* responses are dose-dependent and sometimes differ (Agarwal and Eckert

1990; Agarwal *et al.* 1993; Agarwal *et al.* 1991; Eckert *et al.* 1997; Gilfix and Eckert 1985). Alternatively, interferon γ suppresses keratinocyte proliferation and increases expression of differentiation markers (Eckert *et al.* 1997; Saunders and Jetten 1994). It is clear that many mechanistic questions still exist regarding the regulation of keratinocyte growth and differentiation in the skin via retenoids and the interferons, and the exact role of the RA-IFN protein in these processes. However, significant chemically-induced alterations in the expression of the latter could potentially signal aberrations in the normal signal transduction pathways at work in these cells.

The expression of α-integrin-bp was induced by BaP in both microarray and real-time PCR analysis. Integrin structures are thought to function as important signaling centers controlling the switch among keratinocyte growth, differentiation, and apoptosis (Dotto 1999; Frisch and Ruoslahti 1997; Giancotti 1997). Specifically, α-integrin-bp is thought to interact with the cytoplasmic domain of integrin α_3 and is involved in regulating the general functions of integrins (Wixler *et al.* 1999). In particular, the expression of $\alpha_4\beta_5$ integrin has been observed in proliferating keratinocytes through the stimulation Ras-Erk and Rac-Jnk mitogen-activated protein kinase (MAP kinase) signaling pathways (Mainiero *et al.* 1997). Moreover, studies have reported the down-modulation of integrin expression levels in differentiating keratinocytes (Tennenbaum *et al.* 1996). This evidence correlates well with previous finding that BaP simultaneously inhibits cross-linked envelope formation and induces expression of this proliferation-associated cellular protein (Perez *et al.* 2003).

Six arsenic-induced genes were examined more closely using real-time PCR. This research first focused on two genes in the retinoblastoma pathway, Rb-1 and Rb-bp1. In

general, Rb acts as a potent cellular tumor suppressor. Specifically, Rb (when hypo-phosphorylated) binds to and inhibits E2F-mediated trans-activation, the latter of which is necessary for cells to enter into S-phase of the cell cycle (King and Cidlowski 1998). The expression and hypophosphorylation, therefore, of Rb at or before the G1/S transverse will block cells in G1. Rb also recruits and targets histone methyltransferase Suv39h leading to epigenetic transcriptional repression (Ait-Si-Ali *et al.* 2004). Rb-bp1, a known pRB pocket-binding protein, possess transcriptional activity and associates with p130-E2F and pRB-E2F complexes specifically during growth arrest (Lai *et al.* 1999). The overexpression of Rb-bp1 has shown to inhibit E2F-dependent gene expression and suppress cell growth (Lai *et al.* 1999). In previous flow cytometry studies (Chapter 4), the results demonstrate that arsenic decreased division rates in treated cells; DNA histograms indicated that the primary effect of the metalloid was piling of cells in G1, in turn decreasing the fraction entering into S-phase and increasing the length of the cell cycle (Perez *et al.* 2003). It is possible that these cell cycle perturbations induced by arsenic are mediated, at least in part, through inappropriate expression of proteins in the Rb pathway.

Increased mRNA for RAD50 in NHEK in response to arsenic exposure was also confirmed by real-time PCR in these experiments. The ATM gene recognizes DNA strand breaks and initiates a cascade of pathways which involve the induction of DNA repair proteins such as RAD50 and the arrest of cells in G2/M (Christmann *et al.* 2003; Yih and Lee 2000). RAD50 is involved in DNA recombinational repair complexing with MRE11 and NBS1, and plays a key role in both non-homologous end joining (NHEJ) and homologous recombination during repair of double stranded DNA breaks (Christmann *et al.* 2003). Many studies have investigated the ability of arsenic to cause DNA strand

breaks and the subsequent repair of the damaged DNA (Hamadeh *et al.* 2002; Hartmann and Speit 1996; Mei *et al.* 2003; Yih and Lee 2000). Reports have also shown arsenite to activate ATM pathways and cause G2/M arrest in dividing cells (Mei *et al.* 2003; Yih and Lee 2000). The decreased division rates and cell cycle blocks seen in arsenic treated cells could potentially reflect the additional time required to repair DNA damage produced by the metal and, in part, the up-regulation of RAD50 and other genes involved in the DNA repair pathways.

Arsenic also induced the expression of MNT in both gene expression assays. Constitutive myc expression stimulates cell cycle progression, and blocks differentiation of various cell types (Smith *et al.* 2004). MNT is a modulator of myc function and interacts with Max to mask Myc-Max recognition sites. Abrogation of Myc-Max binding and the resulting MNT/Myc interaction acts to repress activation of genes such as cyclin G1 cyclin-dependent kinase, cyclin D1 and D2, Cdk4, Cdc25A, and E2F (Sears and Nevins 2002). Therefore, the MNT/Myc complex acts as a transcriptional repressor specifically through an E. box driver reporter gene repression system through interaction between the N-terminus and SIN3 co-repressor, potentially involved in proliferation and differentiation (Meroni *et al.* 1997; Smith *et al.* 2004). It is plausible that the arsenic-mediated induction of MNT could be involved in the reduced proliferation rates seen in previous flow cytometry studies (Chapter 4), since MNT has proven to antagonize the proliferative effects of myc activity.

TSC-22 mRNA levels were also induced by arsenic exposure when measured using both gene expression technologies. TSC-22 is stimulated by exposure of cells to TGF-β1 and is considered a transcriptional repressor (Uchida *et al.* 2003). One study

demonstrated the ability of various stimuli, including anti-cancer drugs and growth inhibitors such as vesnarinone, ATRA, and dB-cAMP, to up-regulate TSC-22 gene expression (Uchida *et al.* 2003). Therefore, arsenic-mediated TSC-22 induction may be involved in the reduction of NHEK division rates as seen in previous flow cytometry experimentation (Chapter 4).

In summary, microarray and real-time PCR analyses have been used to identify changes in gene expression in NHEK in response to arsenic and BaP exposure, two diverse skin carcinogens that have substantial effects on the growth potential and ability to differentiate of this cell type (Perez *et al.* 2003). Microarray studies demonstrated that a wide assortment of genes, with various cell functions, were affected by BaP and arsenic exposure in these important target cells. Real-time PCR was used to confirm altered expression of 12 select genes by the two chemicals; these genes have previously been implicated in regulation of cell growth and differentiation in keratinocytes and other cell types. Molecular analysis of cells treated individually with the two chemicals should, in time, allow for the identification of candidate genes that may be mechanistically involved in their cell cycle effects. In turn, further studies should provide a link between chemically-induced perturbations in cell growth and differentiation and toxicological effects, especially with regard to induction of cellular transformation.

5.6. References

Agarwal, C., and Eckert, R. L. (1990). Immortalization of human keratinocytes by simian virus 40 large T-antigen alters keratin gene response to retinoids. *Cancer Res.* **50**, 5947-5953.

Agarwal, C., Rorke, E. A., Boyce, M., Howard, J., Crish, J., Hufeisen, S., and Eckert, R. L. (1993). Retinoid-dependent transcriptional suppression of cytokeratin gene expression in human epidermal squamous cell carcinoma cells. *Differentiation* **52**, 185-191.

Agarwal, C., Rorke, E. A., Irwin, J. C., and Eckert, R. L. (1991). Immortalization by human papillomavirus type 16 alters retinoid regulation of human ectocervical epithelial cell differentiation. *Cancer Res.* **51**, 3982-3989.

Ait-Si-Ali, S., Guasconi, V., Fritsch, L., Yahi, H., Sekhri, R., Naguibneva, I., Robin, P., Cabon, F., Polesskaya, A., and Harel-Bellan, A. (2004). A Suv39h-dependent mechanism for silencing S-phase genes in differentiating but not in cycling cells. *EMBO J.* **23**, 605-615.

Albert, R. E., Miller, M. L., Cody, T. E., Talaska, G., Underwood, P., and Andringa, A. (1996). Epidermal cytokinetics, DNA adducts, and dermal inflammation in the mouse skin in response to repeated benzo[a]pyrene exposures. *Toxicology & Applied Pharmacology* **136**, 67-74.

ATSDR (1999a). Toxicological profile for arsenic. *Agency for Toxic Substance and Disease Registry* **Atlanta**.

ATSDR (1999b). Toxicological profile for polycyclic aromatic hydrocarbons (PAHs). *Agency for Toxic Substance and Disease Registry* **Atlanta**.

ATSDR (2003a). Toxicological profile for arsenic. *Agency for Toxic Substance and Disease Registry* **Atlanta**.

ATSDR (2003b). Toxicological profile for polycyclic aromatic hydrocarbons (PAHs). *Agency for Toxic Substance and Disease Registry* **Atlanta**.

Bae, D. S., Handa, R. J., Yang, R. S., and Campain, J. A. (2003). Gene expression patterns as potential molecular biomarkers for malignant transformation in human keratinocytes treated with MNNG, arsenic, or a metal mixture. *Toxicol.Sci.* **74**, 32-42.

Chen, H., Liu, J., Merrick, B. A., and Waalkes, M. P. (2001). Genetic events associated with arsenic-induced malignant transformation: applications of cDNA microarray technology. *Mol.Carcinog.* **30**, 79-87.

Christmann, M., Tomicic, M. T., Roos, W. P., and Kaina, B. (2003). Mechanisms of human DNA repair: an update. *Toxicology* **193**, 3-34.

Dotto, G. P. (1999). Signal transduction pathways controlling the switch between keratinocyte growth and differentiation. *Crit Rev Oral Biol Med* **10**, 442-457.

Eckert, R. L., Crish, J. F., and Saunders, N. A. (1997). The epidermal keratinocyte as a model for the study of gene regulation and cell differentiation. *Physiological Reviews* **77**, 397-424.

Edmondson, S. W., and Mossman, B. T. (1991). Alterations in keratin expression in hamster tracheal epithelial cells exposed to benzo[a]pyrene. *Carcinogenesis* **12**, 679-684.

Frisch, S. M., and Ruoslahti, E. (1997). Integrins and anoikis. *Curr.Opin.Cell Biol.* **9**, 701-706.

Germolec, D. R., Yoshida, T., Gaido, K., Wilmer, J. L., Simeonova, P. P., Kayama, F., Burleson, F., Dong, W., Lange, R. W., and Luster, M. I. (1996). Arsenic induces overexpression of growth factors in human keratinocytes. *Toxicology and Applied Pharmacology* **141**, 308-318.

Giancotti, F. G. (1997). Integrin signaling: specificity and control of cell survival and cell cycle progression. *Curr.Opin.Cell Biol.* **9**, 691-700.

Gilfix, B. M., and Eckert, R. L. (1985). Coordinate control by vitamin A of keratin gene expression in human keratinocytes. *J.Biol.Chem.* **260**, 14026-14029.

Gniadecki, R. (1997). Effects of 1,25-dihydroxyvitamin D3 and its 20-epi analogues (MC 1288, MC 1301, KH 1060), on clonal keratinocyte growth: evidence for differentiation of keratinocyte stem cells and analysis of the modulatory effects of cytokines. *Br.J.Pharmacol.* **120**, 1119-1127.

Hamadeh, H. K., Trouba, K. J., Amin, R. P., Afshari, C. A., and Germolec, D. (2002). Coordination of altered DNA repair and damage pathways in arsenite-exposed keratinocytes. *Toxicol.Sci.* **69**, 306-316.

Hammerberg, C., Bata-Csorgo, Z., Voorhees, J. J., and Cooper, K. D. (1998). IL-1 and IL-1 receptor antagonist regulation during keratinocyte cell cycle and differentiation in normal and psoriatic epidermis. *Archives of Dermatological Research* **290**, 367-374.

Hartmann, A., and Speit, G. (1996). Effect of arsenic and cadmium on the persistence of mutagen-induced DNA lesions in human cells. *Environ.Mol.Mutagen.* **27**, 98-104.

Hennings, H., Michael, D., Cheng, C., Steinert, P., Holbrook, K., and Yuspa, S. H. (1980). Calcium regulation of growth and differentiation of mouse epidermal cells in culture. *Cell* **19**, 245-254.

Jessen, B. A., Qin, Q., Phillips, M. A., Phillips, D. L., and Rice, R. H. (2001). Keratinocyte differentiation marker suppression by arsenic: mediation by AP1 response elements and antagonism by tetradecanoylphorbol acetate. *Toxicology & Applied Pharmacology* **174**, 302-311.

Jiang, C. K., Magnaldo, T., Ohtsuki, M., Freedberg, I. M., Bernerd, F., and Blumenberg, M. (1993). Epidermal growth factor and transforming growth factor alpha specifically induce the activation- and hyperproliferation-associated keratins 6 and 16. *Proc.Natl.Acad.Sci.U.S.A* **90**, 6786-6790.

Kachinskas, D. J., Phillips, M. A., Qin, Q., Strokes, J. D., and Rice, R. H. (1994). Arsenate perturbation of human keratinocyte differentiation. *Cell Growth Differ.* **5**, 12235-1241.

King, K. L., and Cidlowski, J. A. (1998). Cell cycle regulation and apoptosis. [Review] [89 refs]. *Annual Review of Physiology* **60**, 601-617.

Kulesz-Martin, M. F., Koehler, B., Hennings, H., and Yuspa, S. H. (1980). Quantitative assay for carcinogen altered differentiation in mouse epidermal cells. *Carcinogenesis* **1**, 995-1006.

Lai, A., Marcellus, R. C., Corbeil, H. B., and Branton, P. E. (1999). RBP1 induces growth arrest by repression of E2F-dependent transcription. *Oncogene* **18**, 2091-2100.

Lee, P. N., and O'Neill, J. A. (1971). The effect both of time and dose applied on tumour incidence rate in benzopyrene skin painting experiments. *Br.J Cancer* **25**, 759-770.

Mager, R., Huberman, E., Yang, S. K., Gelboin, H. V., and Sachs, L. (1977). Transformation of normal hamster cells by benzo(a)pyrene diol-epoxide. *Int.J.Cancer* **19**, 814-817.

Mainiero, F., Murgia, C., Wary, K. K., Curatola, A. M., Pepe, A., Blumemberg, M., Westwick, J. K., Der, C. J., and Giancotti, F. G. (1997). The coupling of alpha6beta4 integrin to Ras-MAP kinase pathways mediated by Shc controls keratinocyte proliferation. *EMBO J.* **16**, 2365-2375.

Mei, N., Lee, J., Sun, X., Xing, J. Z., Hanson, J., Le, X. C., and Weinfeld, M. (2003). Genetic predisposition to the cytotoxicity of arsenic: the role of DNA damage and ATM. *FASEB J.* **17**, 2310-2312.

Meroni, G., Reymond, A., Alcalay, M., Borsani, G., Tanigami, A., Tonlorenzi, R., Nigro, C. L., Messali, S., Zollo, M., Ledbetter, D. H., Brent, R., Ballabio, A., and Carrozzo, R. (1997). Rox, a novel bHLHZip protein expressed in quiescent cells that heterodimerizes with Max, binds a non-canonical E box and acts as a transcriptional repressor. *EMBO J.* **16**, 2892-2906.

Perez, D. S., Armstrong-Lea, L., Fox, M. H., Yang, R. S., and Campain, J. A. (2003). Arsenic and benzo[a]pyrene differentially alter the capacity for differentiation and growth properties of primary human epidermal keratinocytes. *Toxicol.Sci.* **76**, 280-290.

Rambaratsingh, R. A., Stone, J. C., Blumberg, P. M., and Lorenzo, P. S. (2003). RasGRP1 represents a novel non-protein kinase C phorbol ester signaling pathway in mouse epidermal keratinocytes. *J.Biol.Chem.* **278**, 52792-52801.

Rea, M. A., Gregg, J. P., Qin, Q., Phillips, M. A., and Rice, R. H. (2003). Global alteration of gene expression in human keratinocytes by inorganic arsenic. *Carcinogenesis* **24**, 747-756.

Reiners, J. J., Jr., Cantu, A. R., and Pavone, A. (1991). Distribution of constitutive and polycyclic aromatic hydrocarbon-induced cytochrome P-450 activities in murine epidermal cells that differ in their stages of differentiation. *Prog.Clin.Biol.Res.* **369**, 123-135.

Rice, R. H., and Green, H. (1979). Presence in human epidermal cells of a soluble protein precursor of the cross-linked envelope: Activation of the cross-linking by calcium ions. *Cell* **18**, 681-694.

Rong, S. B., Enyedy, I. J., Qiao, L., Zhao, L., Ma, D., Pearce, L. L., Lorenzo, P. S., Stone, J. C., Blumberg, P. M., Wang, S., and Kozikowski, A. P. (2002). Structural basis of RasGRP binding to high-affinity PKC ligands. *J.Med.Chem.* **45**, 853-860.

Saunders, N. A., and Jetten, A. M. (1994). Control of growth regulatory and differentiation-specific genes in human epidermal keratinocytes by interferon gamma. Antagonism by retinoic acid and transforming growth factor beta 1. *J.Biol.Chem.* **269**, 2016-2022.

Sears, R. C., and Nevins, J. R. (2002). Signaling networks that link cell proliferation and cell fate. *J Biol Chem* **277**, 11617-11620.

Shipley, G. D., and Pittelkow, M. R. (1987). Control of growth and differentiation in vitro of human keratinocytes cultured in serum-free medium. *Archives of Dermatology* **123**, 1541a-1544a.

Smith, A. G., Popov, N., Imreh, M., Axelson, H., and Henriksson, M. (2004). Expression and DNA-binding activity of MYCN/Max and Mnt/Max during induced differentiation of human neuroblastoma cells. *J.Cell Biochem.* **92**, 1282-1295.

Solum, D. T., and Handa, R. J. (2002). Estrogen regulates the development of brain-derived neurotrophic factor mRNA and protein in the rat hippocampus. *J.Neurosci.* **22**, 2650-2659.

Tamhane, A. C., and Dunlop, D. D. (2000). Multiple comparisons of means. In Statistics and Data Analysis from Elementary to Intermediate, pp. 475-476. Prentice-Hall, Inc., Upper Saddle River, NJ.

Tennenbaum, T., Li, L., Belanger, A. J., De Luca, L. M., and Yuspa, S. H. (1996). Selective changes in laminin adhesion and alpha 6 beta 4 integrin regulation are associated with the initial steps in keratinocyte maturation. *Cell Growth Differ.* **7**, 615-628.

Tseng, W. P. (1977). Effects and dose--response relationships of skin cancer and blackfoot disease with arsenic. *Environ.Health Perspect.* **19**, 109-119.

Uchida, D., Omotehara, F., Nakashiro, K., Tateishi, Y., Hino, S., Begum, N. M., Fujimori, T., and Kawamata, H. (2003). Posttranscriptional regulation of TSC-22 (TGF-beta-stimulated clone-22) gene by TGF-beta 1. *Biochem.Biophys.Res.Commun.* **305**, 846-854.

Vega, L., Styblo, M., Patterson, R., Cullen, W., Wang, C., and Germolec, D. (2001). Differential effects of trivalent and pentavalent arsenicals on cell proliferation and

cytokine secretion in normal human epidermal keratinocytes. *Toxicology & Applied Pharmacology* **172**, 225-232.

Wixler, V., Laplantine, E., Geerts, D., Sonnenberg, A., Petersohn, D., Eckes, B., Paulsson, M., and Aumailley, M. (1999). Identification of novel interaction partners for the conserved membrane proximal region of alpha-integrin cytoplasmic domains. *FEBS Lett.* **445**, 351-355.

Wu, M. M., Chiou, H. Y., Ho, I. C., Chen, C. J., and Lee, T. C. (2003). Gene expression of inflammatory molecules in circulating lymphocytes from arsenic-exposed human subjects. *Environ.Health Perspect.* **111**, 1429-1438.

Yih, L. H., and Lee, T. C. (2000). Arsenite induces p53 accumulation through an ATM-dependent pathway in human fibroblasts. *Cancer Res.* **60**, 6346-6352.

Yih, L. H., Peck, K., and Lee, T. C. (2002). Changes in gene expression profiles of human fibroblasts in response to sodium arsenite treatment. *Carcinogenesis* **23**, 867-876.

Yuspa, S. H., and Morgan, D. L. (1981). Mouse skin cells resistant to terminal differentiation associated with initiation of carcinogenesis. *Nature* **293**, 72-74.

Zheng, X. H., Watts, G. S., Vaught, S., and Gandolfi, A. J. (2003). Low-level arsenite induced gene expression in HEK293 cells. *Toxicology* **187**, 39-48.

Table 5.1. Previously published results on the phenotypic effects of arsenic and BaP on NHEK differentiation and proliferation (Perez *et al.* 2003).

Treatment	**Chemical Effects on NHEK:**	
	Differentiation	**Proliferation**
Arsenic 5.0 μM (LC_{50})	20.1-fold inhibition	25.8% decrease
Benzo[*a*]pyrene 2.0 μM (LC_{50})	5.8-fold inhibition	29.8% increase

(See Chapter 4 for more details)

Table 5.2. Selected primers for genes examined in real-time RT-PCR experiments

mRNA	Product Length (base pairs)	Primer	Sequence (5'→ 3')
α-integrin-bp	136	Forward	CGTTCGGCATTCCATTACCA
		Reverse	ACTTTCAGATCAGGGCTCGTGT
Cad-5	283	Forward	CCTTGGGATAGCAAACTCCA
		Reverse	CTTTGCCTCCAGGCAGATAG
IL-1α	118	Forward	TAGTAGCAACCAACGGGAAG
		Reverse	CTCTGAGTCATTGGCGATG
IL-1β	97	Forward	CAGGATATGGAGCAACAAGT
		Reverse	ATCTTTCAACACGCAGGA
MNT	209	Forward	GGAGCAGGAAGAGCA
		Reverse	GTAGAGGCTGAGGGGAGTTGGT
RA-IFN	215	Forward	CGGCTGGATGATTCTGATAGAG
		Reverse	TTGGCTGCATAACGAAGGAC
RAD50	125	Forward	AGAACCCGTGACTGTTACTT
		Reverse	CGTGATTACATTTAGGACCC
Ras-GRP	126	Forward	AAGGAGACAAGTTCGCATGT
		Reverse	GCCGGTAATTGTCGTAGTTT
Rb-1	207	Forward	TTGTTTGGGTGAGTCCTAAG
		Reverse	AAAGAAGGCAAAGTAGTCAGAC
Rb-bp1	242	Forward	ACTGAAATTGATGACGGAGA
		Reverse	ATGTTTGATGAGAGGGTTGA
TSC-22	167	Forward	ATACAGGTGATATGCAGAAACC
		Reverse	GGCACAGTTACTCACTTTGTG
Yaf2	166	Forward	CGGCTCTAGCTCTGATAACA
		Reverse	TGTGGTACCTCTTGGCATAAT

(See Figure 5.7 for complete gene information)

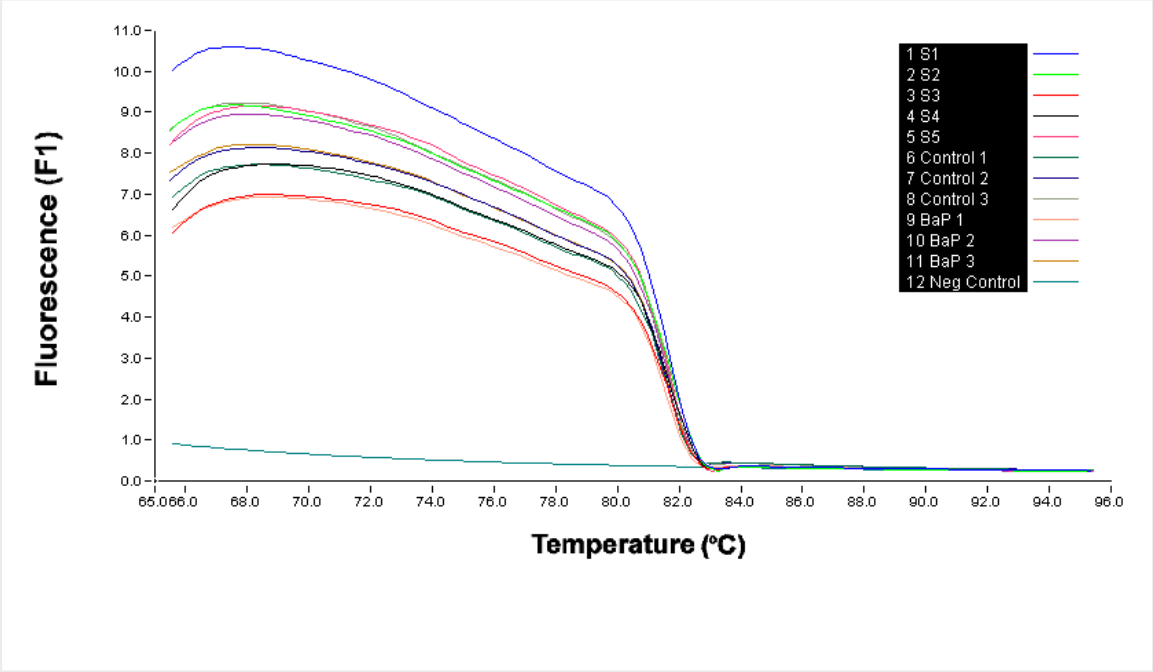

Figure 5.1A. **Melting curve analysis for determining the specificity of amplified PCR product.** After the final amplification step, samples were gradually heated to reach the maximum temperature of 95°C. The degree of denaturation was measured automatically by LightCycler. This graph displays the fluorescence data showing the typical decrease in fluorescence with temperature increase. The legend in the upper right displays all the samples that were analyzed during this experimental run. Samples S1-S5 are the DNA standards of known amounts of DNA product, and Ctrl 1-3 (control-untreated NHEK)) and BaP 1-3 (BaP-treated NHEK) are the samples in which the amount of DNA product is to be investigated. Representing a negative control for the experiment, water instead of DNA was added to the last sample (Neg Ctrl).

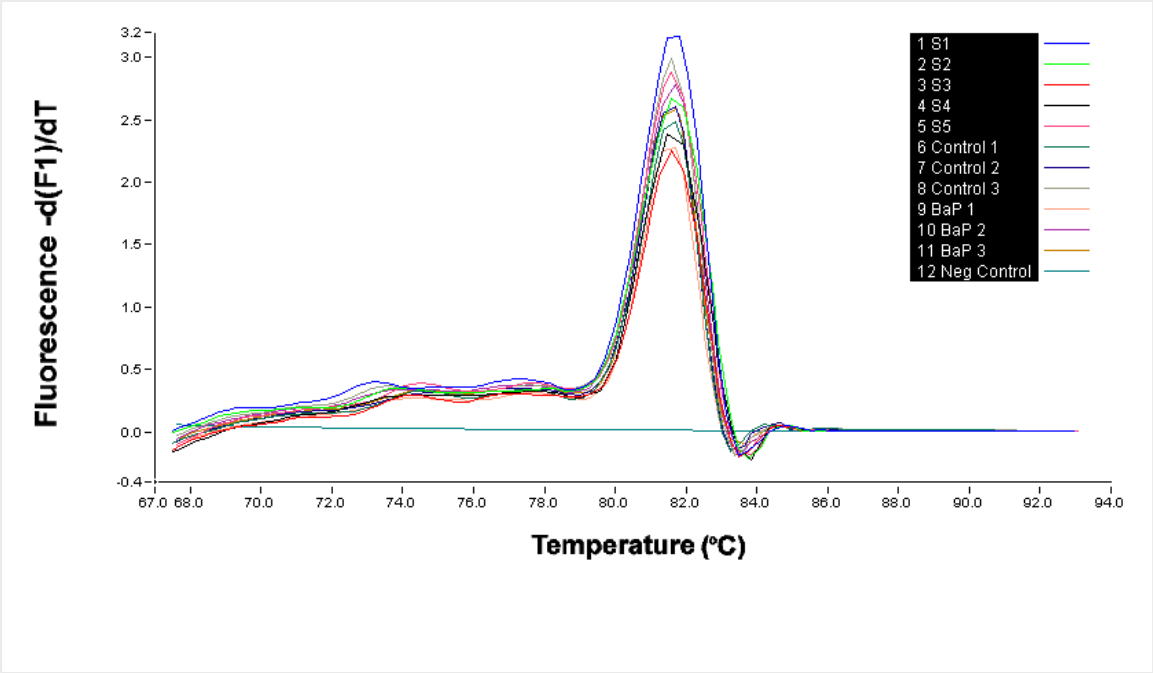

Figure 5.1B. **Melting curve analysis for determining the specificity of amplified PCR product.** This graph provides the data converted from Figure 5.1A to a display where the first negative derivative (-dF/dT) is displayed versus the temperature, showing the melting peaks. Melting curve analysis allows differentiation between primer dimers and specific amplified product. The specific Yaf2 product melted at 82.2°C, whereas primer dimers (not shown here) melt at a lower temperature. The legend in the upper right displays all the samples that were analyzed during this experimental run. Samples S1-S5 are the DNA standards of known amounts of DNA product, and Ctrl 1-3 (control-untreated NHEK) and BaP 1-3 (BaP-treated NHEK) are the samples in which the amount of DNA product is to be investigated. Representing a negative control for the experiment, water instead of DNA was added to the last sample (Neg Ctrl).

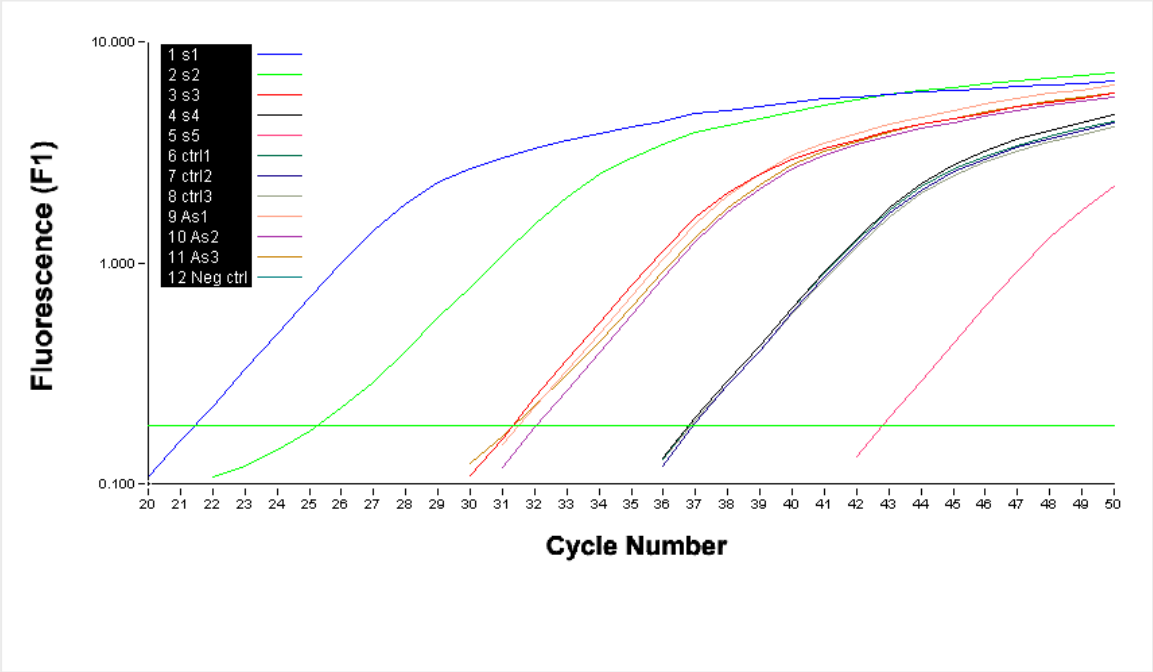

Figure 5.2A. **Demonstration of using the standard curve for product quantification.** This graph displays the increase in fluorescence (i.e., increase in cDNA) as cycle number increases. Five known cDNA concentrations (S1-S5), diluted 10-fold, were run with unknown samples (Ctrl 1-3, untreated NHEK and As 1-3, arsenic-treated NHEK). The quantity of cDNA of interest in target cells accumulates according to the function $T_n=T_0*E^n$, where T_n is the amount of target sequence at cycle n, T_0 is the initial amount of target, and E is the efficiency of amplification. From the standard curve (Figure 5.2B), parameters E and K (the number of copies of PCR product) were obtained. The equation for the standard curve is $C_p = -(1/\log E)*\log T_0+(\log K/\log E)$, where C_p is the crossing point. These results were then utilized to calculate T_0 in conjunction with the experimentally determined C_p for the unknown samples. Arithmetic background subtraction was used and the fluorescent channel was set to F1 (specifically to detect SYBRGreen I). Representing a negative control for the experiment, water instead of DNA was added to the last sample (Neg Ctrl).

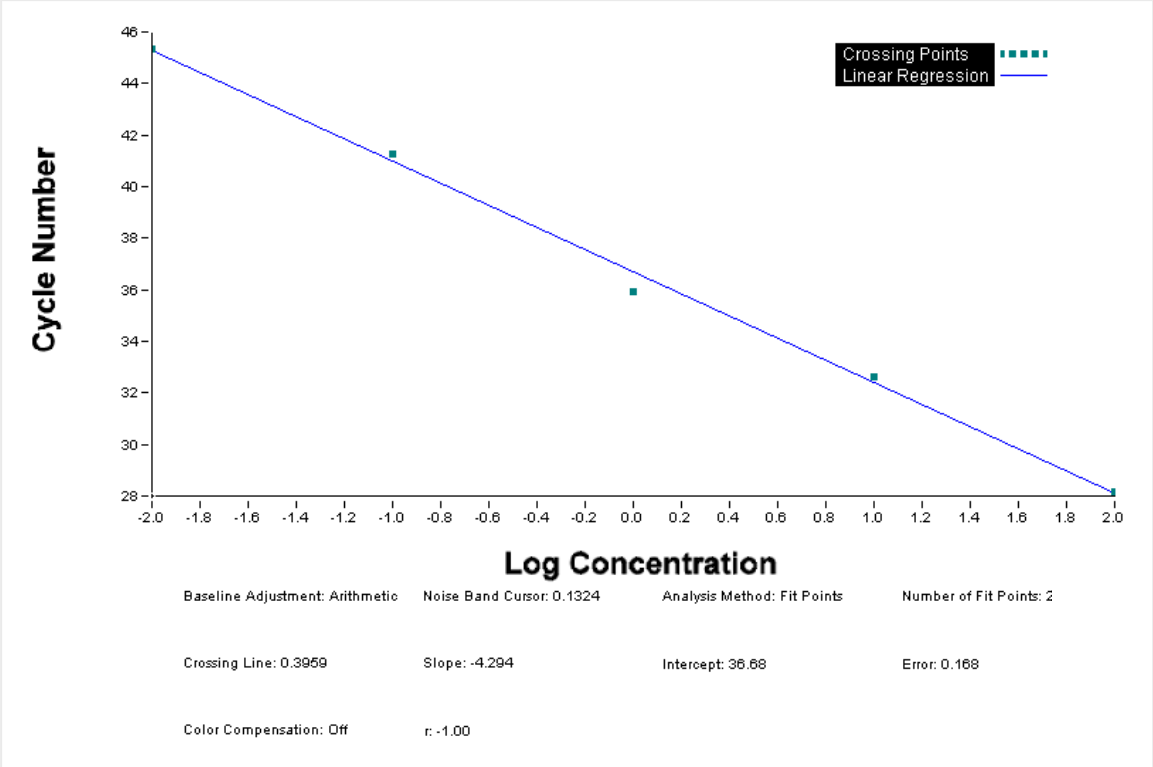

Figure 5.2B. **Demonstration of using the standard curve for product quantification.** Displayed in this graph are the 10-fold dilutions of known cDNA concentrations used in calculating unknown cDNA concentrations. The software automatically performs all calculation steps which are necessary to generate a standard curve. The Crossing Points (C_P) of unknown samples are determined and the corresponding concentrations are automatically calculated.

Table 5.3. Benzo[*a*]pyrene induced genes detected by microarray analysis. Gene expression changes ≥ 2-fold in each of the triplicate experiments (n=3) were considered significantly different when compared to the control array.

GenBank accession #	Gene Name	Function	Fold
M31630	activating transcription factor 2	cAMP response element binding protein; Activated by E1A and binds the camp response element (cre); Binds DNA as a dimmer; Interacts with SMAD3 and SMAD4	3.0
NM_007216	alpha integrin binding protein 63	Integrin-mediated signaling pathway; Regulates integrin function; Encodes a protein that may play a role in organelle biogenesis associated with melanosomes, platelet dense granules, and lysosomes; This protein interacts with Hermansky-Pudlak syndrome 6 protein and may interact with the cytoplasmic domain of integrin, alpha-3; Mutations in this gene are associated with Hermansky-Pudlak syndrome type 5; Multiple transcript variants encoding two distinct isoforms have been identified for this gene	15.7
NM_015928	androgen-induced prostate proliferative shutoff associated protein	Androgen-induced inhibition of proliferation of cell proliferation (step2, proliferative shutoff in the regulation of prostate gland cell members, in the BRCA2, RB1 region); Maybe a new suppressor gene in relation with prostate cancer	10.0
U33841	ataxia telangiectasia mutated (includes complementation groups A, C and D)	Involved in signal transduction, cell cycle control and DNA repair; May function as a tumor suppressor; Necessary for activation of ABL1 and SAPK. Phosphorylates p53, NFKBIA, BRCA1, CTIP, NIBRIN (NBS1), TERF1, and RAD9; May play a role in vesicle and/or protein transport; Inhibited by wortmaninn; Could play a role in T-cell development, gonad and neurological function	10.0
NM_004725	BUB3 (budding uninhibited by benzimidazoles 3, yeast) homolog	Spindle checkpoint gene; Required for kinetochore localization of BUB1; Modulating the timing of anaphase initiation in mitotic cells with improperly aligned chromosomes	3.9
NM_006688	C1q-related factor	Involved in motor functions in nervous system	7.0
NM_001236	carbonyl reductase 3	Convert carbonyl compounds into alcohols; NADPH-dependent oxidoreductase	2.6
NM_015858	cellular growth-regulating protein	Essential for cell cycle transversal and encodes growth-regulation gene product	3.0
NM_016053	CGI-116 protein	Unknown	3.4
NM_006430	chaperonin containing TCP1, subunit 4 (delta)	Molecular chaperone; Assist the folding of proteins upon ATP hydrolysis: known to play a role, *in vitro*, in the folding of actin and tubulin; Required for the maturation of cyclin E	3.9
NM_004921	chloride channel, calcium activated, family member 3	Membrane channel; Outwardly rectifying, widely expressed, not acting as a channel but unknown function	8.9
NM_007192	chromatin-specific transcription elongation factor, 140 kDa subunit	Required for transcription of chromatin templates *in vitro*; Facilitates activator-dependent transcription initiation on chromatin templates	17.6

AF119497	chromosome 11 open reading frame 5	New member of FAUNA gene cluster; Neighbor of FAU, in the MEN1 region	3.7
NM_004898	clock (mouse) homolog	Circadian regulator that acts as a transcription factor; Clock-BMAL1 heterodimers bind to an E-Box element (3'-CACGTG-5'), thereby activating transcription of PER1, and possibly of other circadian clock proteins; Mutant clock and BMAL1 form hetereodimer that bind DNA, but fail to activate transcription	6.0
AF067972	DNA (cytosine-5-)-methyltransferase 3 alpha	Required for genome wide de novo methylation and is essential for development; Abundantly expressed in ES cells but at very low levels in differentiated embryoid bodies or adult tissues, essential for de novo DNA methylation and development (at least in mouse)	3.3
M76180	dopa decarboxylase (aromatic L-amino acid decarboxylase)	Catalyzes the decarboxylation of L-3,4- dihydroxyphenylalanine (DOPA) to dopamine, L-5-hydroxytryptophan to serotonin and L-tryptophan to tryptamine; Defects in DDC lead to severe hypotonia and developmental delay	2.9
NM_005711	EGF-like repeats and discoidin I-like domains 3	Homolog to mouse Del1, initially expressed in the endothelial progenitor and in embryonic mesenchymal cells, promoting the adhesion of endothelial cells through interaction with the AVB3 integrin receptor, putative regulator of vascular morphogenesis or remodeling in embryonic development; Promoting the adhesion of endothelial cells through interaction with the AVB3 integrin receptor, putative regulator of vascular morphogenesis or remodeling in embryonic development	5.3
NM_006403	enhancer of filamentation 1 (cas-like docking; Crk-associated substrate related)	SH3-domain-containing protein; Linking element between extracellular signaling and regulation of the cytoskeleton	4.1
NM_016357	epithelial protein lost in neoplasm beta	Suppress cell proliferation when overexpressed; This cytoskeletal protein co-localizes with actin stress fibers and focal adhesion plaques; Down-regulated in some cancer cell lines; Eplin-alpha is induced by serum; Eplin-beta is constitutively expressed	6.2
NM_007235	exportin, tRNA (nuclear export receptor for tRNAs)	Mediates nuclear export of all tRNAs; Binds to GTP-bound form of Ran; RanGTP-binding, importin beta-related factor with predominantly nuclear localization, specific mediator of tRNA export, shuttling between nucleus and cytoplasm and interacting with nuclear pore complexes (NPC)	5.1
M64082	flavin containing monooxygenase 1	This protein is involved in the oxidative metabolism; Form I catalyzes the N-oxygenation of secondary and tertiary amines	8.0
NM_003878	gamma-glutamyl hydrolase (conjugase, folylpolygammaglutamyl hydrolase)	Hydrolyses the polyglutamate sidechains of pteroylpolyglutamates; Progressively removes gamma-glutamyl residues from pteroylpoly-gamma-glutamate to yield pteroyl-alpha-glutamate (folic acid) and free glutamate; May play an important role in the bioavailability of dietary pteroylpolyglutamates and in the metabolism of pteroylpolyglutamates and antifolates; Involved in the metabolism of folic acid	4.2
NM_002091	gastrin-releasing peptide	GRP stimulates gastrin release as well as other gastrointestinal hormones	4.0
NM_004837	geranylgeranyl diphosphate synthase 1	Catalyzes the trans-addition of the three molecules of IPP onto DMAPP to formgeranylgeranyl pyrophosphate, an important precursor of carotenoids and geranylatedgeranylated proteins; Isoprenoid biosynthetic pathway	5.4

NM_012413	glutaminyl-peptide cyclotransferase (glutaminyl cyclase)	Responsible for the biosynthesis of pyroglutamyl peptides; Has a bias against acidic and tryptophan residues adjacent to the N-terminal glutaminyl residue and a lack of importance of chain length after the second residue	4.9
X63282	guanylate cyclase 1, soluble, alpha 2	Has guanylyl cyclase on binding to the beta-1 subunit; The alternative spliced isoform, alpha-2-I, acts as a negative regulator of guanylyl cylase activity as it forms non-functional heterodimers with the beta subunits; Activated by nitric oxide in the presence of magnesium or manganese ions; Heterodimerizing with GUCY1B1	3.8
NM_016650	HDCME31P protein	May be involved in signal transduction as a component of a multimeric receptor complex	3.6
NM_015980	HMP19 protein	Type II membrane protein (Probable); Mainly Golgi stack, but also found in small vacuolar organelles and multivesicular bodies	2.3
NM_015916	hypothetical protein	Unknown	20.2
M27544	insulin-like growth factor 1 (somatomedin C)	The insulin-like growth factors, isolated from plasma, are structurally and functionally related to insulin but have a much higher growth-promoting activity; Regulator of somatic growth and cellular proliferation, inducer of the phosphatidylinositol 3-kinase survival pathway through activation of AKT1, AKT2, inhibited by TNF in its neuroprotective role, also inducer of calcineurin mediated signaling and activation of GATA2, associated with intrauterine growth retardation and severe short stature in a patient carrying a homozygous deletion of IGF1	3.6
X02851	interleukin 1, alpha	Produced by activated macrophages, IL-1 stimulates thymocyte proliferation by inducing IL-2 release, B-cell maturation and proliferation, and fibroblast growth factor activity; IL-1 proteins are involved in the inflammatory response, being identified as endogenous pyrogens, and are reported to stimulate the release of prostaglandin and collagenase from synovial cells	3.9
K02770	interleukin 1, beta	Produced by activated macrophages; IL-1 stimulates thymocyte proliferation by inducing IL-2 release, B-cell maturation and proliferation, and fibroblast growth factor activity; IL-1 proteins are involved in the inflammatory response, being identified as endogenous pyrogens, and are reported to stimulate the release of prostaglandin and collagenase from synovial cells; Mainly expressed by macrophages osteoblastic cells and putatively stimulating osteoclastogenesis, inducing the association of TRAF6 with IRAK1, involved in the inflammatory response, susceptibility factor for inflammatory bowel diseases	4.4
NM_002202	ISL1 transcription factor, LIM/homeodomain, (islet-1)	Binds to one of the cis-acting domain of the insulin gene enhancer; Binding to the enhancer region of the insulin gene, LIM-homeo domain family	31.9
NM_013269	lectin-like NK cell receptor	Mediates activation signals	5.0
NM_012064	major intrinsic protein of lens fiber	Water channel; May be responsible for regulating the osmolarity of the lens	8.9
NM_003980	microtubule-associated protein 7	Microtubule-stabilizing protein that may play an important role during reorganization of microtubules during polarization and differentiation of epithelial cells	2.4

NM_006471	myosin, light polypeptide, regulatory, non-sarcomeric (20kD)	Plays an important role in regulation of both smooth muscle and non-muscle cell contractile activity	2.7
NM_005003	NADH dehydrogenase (ubiquinone) 1, alpha/beta subcomplex, 1 (8kD, SDAP)	Transport of electrons from NADH to ubiquinone, which is accompanied by translocation of protons from the mitochondrial matrix to the intermembrane space; Hydrophobic fraction of the complex I multi-subunit enzyme of the oxidative phosphorylation (OXPHOS), inner mitochondrial membrane	14.6
NM_003899	PAK-interacting exchange factor beta	Acts as a RAC1 guanine nucleotide exchange factor (GEF) and can induce membrane ruffling; Interacts with PAK kinases through the SH3 domain	2.7
NM_004855	phosphatidylinositol glycan, class B	Transfers the third mannose; Anchor synthesis	2.9
NM_004910	phosphatidylinositol transfer protein, membrane-associated	Has functional domains of Ca^{2+}-ATPase; May have a role as an intracellular messenger in vertebrate phototransduction; Membrane-associated, ortholog of the Drosophila retinal degeneration B, expressed (in mammals) at high level in the neural retina and the central nervous system	2.6
U40370	phosphodiesterase 1A, calmodulin-dependent	Has a higher affinity for cGMP than for cAMP; Type I PDE are activated by the binding of calmodulin in the presence of Ca^{2+}	2.6
U38545	phospholipase D1, phophatidylcholine-specific	Implicated as a critical step in numerous cellular pathways, including signal transduction, membrane trafficking, and the regulation of mitosis; May be involved in the regulation of perinuclear intravesicular membrane traffic; Phosphatidylcholine specific, membrane associated, activated by ADP-ribosylation factor 1 by protein kinase C alpha, and Rho A; Involved in inflammation, metabolic regulation, oncogenesis, neural, and cardiac stimulation	2.4
NM_016566	pparl	On chromosome 4; Unknown function	4.3
NM_005742	protein disulfide isomerase-related protein	Has oxidoreductase activity of disulfide bonds against polypeptides and that it acts as a catalyst of protein folding in the lumen of the ER	2.6
NM_007223	putative G protein coupled receptor	Member of the 7 transmembrane domain receptor family	7.5
NM_003967	putative neurotransmitter receptor	7 transmembrane domain protein receptor	3.6
NM_005739	RAS guanyl releasing protein 1 (calcium and DAG-regulated)	Regulator of growth, differentiation, and malignant transformation; Guanine nucleotide releasing (exchange) protein 1, RAS activator, calcium- and DAG-regulated, expressed in the nervous system	8.1
L24564	Ras-related associated with diabetes	Overexpressed in muscle of type II diabetics; Small monomeric GTPase activity; Ras-GTPase activating protein family member, with high homology to GEM, overexpressed in non-insulin dependent diabetes mellitus (increasing insulin resistant)	3.2
NM_006477	RAS-related on chromosome 22	Regulator of growth, differentiation, and malignant transformation; Small monomeric GTPase activity; Involved in oncogenesis; Also known as RADD or RAD	7.0
NM_006394	regulated in glioma	Serves as a molecular marker for or may play a role in malignant progression of glioblastoma;	10.3

		Predominantly expressed in normal brain, also expressed in heart and lung, down-regulated in glioblastoma	
M87339	replication factor C (activator 1) 4 (37kD)	The elongation of primed DNA templates by DNA polymerase delta and epsilon requires the action of the accessory proteins proliferating cell nuclear antigen (PCNA) and activator 1; The 37 kDa subunit may be involved in the elongation of the multiprimed DNA template; Component of complex A-1, DNA polymerase accessory protein "clamp loader", ATP dependent, required to assemble PCNA and polymerase delta on the DNA template	2.4
NM_012420	retinoic acid- and interferon-inducible protein (58kD)	Regulate differentiation; Induced by interferons	4.2
NM_005772	RNA cyclase homolog	Does not have cyclase activity; Role in 40S- ribosomal-subunit biogenesis in the early pre-RNA processing steps at sites A0, A1 and A2 that are required for proper maturation of the 18S RNA	2.3
AF059617	serum-inducible kinase	Role in the division of at least some cell types, such as fibroblasts, and could function in embryogenesis, wound healing or neoplasia	6.5
NM_004858	solute carrier family 4, sodium bicarbonate cotransporter, member 8	Membrane transporter regulating intracellular pH in neurons, glia, and other cells	7.3
NM_012443	sperm associated antigen 6	Role in sperm flagellar motility and maintenance of structural integrity; Highly expressed in testis located to the tails of permeabilized human sperm but mediating protein-protein interacting	6.2
NM_012444	SPO11, meiotic protein covalently bound to DSB (S. cerevisiae)-like	Required for meiotic recombination; Mediates DNA cleavage that forms the double-strand breaks that initiate meiotic recombination; Required for double strand break formation required for initiation of recombination in S cerevisiae, expressed in prostate, testis, and other tissues with an alternatively spliced isoform	11.9
U04735	stress 70 protein chaperone, microsome-associated, 60kD	Has peptide-independent ATPase activity; Involved in the processing of cytosolic and secretory proteins	3.3
NM_012447	stromal antigen 3	Involved in chromosome pairing and maintenance of synaptonemal complex structure during the pachytene phase of meiosis in a cohesion-like manner	2.9
NM_007265	suppressor of S. cerevisiae gcr2	Transcriptional regulator	14.2
NM_005681	TATA box binding protein (TBP)-associated factor, RNA polymerase I, A, 48kD	Universal transcription factor; Involved in the initiation of rRNA synthesis by RNA polymerase I	4.1
NM_005679	TATA box binding protein (TBP)-associated factor, RNA polymerase	Universal transcription factor	8.8

	I, C, 110kD		
NM_012472	testis specific leucine rich repeat protein	Leucine rich repeat containing 6	12.3
NM_012466	tetraspanin TM4-B	Integral membrane protein (Probable)	4.6
NM_004202	thymosin, beta 4, Y chromosome	Plays an important role in the organization of the cytoskeleton; Binds to and sequesters actin monomers (G actin) and therefore inhibits actin polymerization; Identical to the interferon inducible gene 6-26 (4/26), potential actin sequestering protein, ubiquitous in a AZF deleted region	4.3
NM_004817	tight junction protein 2 (zona occludens 2)	Plays a role in tight junctions and adherens junctions; Homolog to yeast guanylate kinase and Drosophila lethal discs large tumor suppressor protein (Dlg), interacting with occludin, TJP1, the F actin skeleton and alpha catenin	3.4
NM_006528	tissue factor pathway inhibitor 2	Seems to inhibit trypsin, factor VII(A)/tissue factor, weakly factor XA; Has no effect on thrombin; Serine proteinase inhibitor (see TSG7B)	3.4
NM_005879	TRAF interacting protein	Inhibits tumor necrosis factor-2 mediated NF-kappaB activation	12.5
NM_007344	transcription termination factor, RNA polymerase I	Direct termination of ribosomal gene transcripts	2.7
NM_004621	transient receptor potential channel 6	Thought to form a receptor-activated non-selective calcium permeant cation channel; Probably is operated by a phosphatidylinositol second messenger system activated by receptor tyrosine kinases or G-protein coupled receptors; Activated by diacylglycerol (DAG) in a membrane-delimited fashion, independently of PKC; Seems not to be activated by intracellular calcium store depletion; Involved in Ca^{2+} entry stimulated by a G protein coupled receptor from extracellular space by a process called calcium capacitative entry (CCE)	11.8
X78627	translin	DNA-binding protein that specifically recognizes consensus sequences at the breakpoint junctions in chromosomal translocations, mostly involving immunoglobulin (Ig)/T-cell receptor gene segments; Seems to recognize single-stranded DNA ends generated by staggered breaks occurring at recombination hot spots; Dimerizing DNA binding protein at the breakpoint junctions in chromosomal translocations, involved in DNA damage repair and in mRNA transport	2.6
NM_007279	U2 small nuclear ribonucleoprotein auxiliary factor (65kD)	Mediator of enhancer-dependent splicing; Required for presliceosome formation	3.2
NM_004247	U5 snRNP-specific protein, 116 kD	Role in the pre-mRNA splicing process	11.5
NM_005154	ubiquitin specific protease 8	Oncogenic fusion product of PI-3 kinase p85 subunit and HUMORF8; Regulate many proteins that control cell growth and proliferation; Similar to the tre oncogene, with homology to ubiquitin carboxy-terminal hydrolase, deubiquitin enzyme family	5.2
NM_007125	ubiquitously transcribed tetratricopeptide repeat gene, Y chromosome	At least 2 isoforms; A long form and a short form are produced by alternative splicing; Ubiquitous in a AZF deleted region	3.2

NM_013244	UDP-N-acetylglucosamine	Carbohydrate metabolism; Transferase activity	25.2
NM_004277	uncoupling protein 4	UCP are mitochondrial transporter proteins that create proton leaks across the inner mitochondrial membrane, thus uncoupling oxidative phosphorylation from ATP synthesis; As a result, energy is dissipated in the form of heat; May play a role in thermoregulatory heat production and metabolism in brain	4.2
NM_006472	upregulated by 1,25-dihydroxyvitamin D-3	Vitamin D(3) upregulated protein 1 upregulated by TGF-beta1 and 1,25-dihydorxyvitamin D3 inhibits tumor cell growth by blocking cell-cycle progression	3.9
NM_005703	upstream regulatory element binding protein 1	Ubiquitin-protein ligase activity	6.8
NM_004906	Wilms` tumour 1-associating protein	Transcriptional and post-transcriptional regulation; Splicing regulation	3.0
NM_005748	YY1-associated factor 2	Multifunctional transcription factor; Yaf2 enhances MycN-mediated transactivation from a E-box promoter; Transcription co-repressor	9.6
NM_007145	zinc finger protein 146	Krueppel family of C2H2-type zinc-finger proteins; Amplified or overexpressed in pancreatic carcinoma and contributing to the progression of tumor	2.7
NM_012480	zinc finger protein 186 (Kruppel type)	May be involved in transcriptional regulation; Krueppel family of C2H2-type zinc-finger proteins	3.3
NM_006007	zinc finger protein 216	Cochlear-expressed, unlikely to be responsive for hearing loss in DFNB7	4.7

Table 5.4. Benzo[*a*]pyrene suppressed genes detected by microarray analysis. Gene expression changes ≥ 2-fold in each of the triplicate experiments (n=3) were considered significantly different when compared to the control array.

GenBank Accession #	Gene Name	Function	Fold
M11233	cathepsin D (lysosomal aspartyl protease)	Acid protease active in intracellular protein breakdown; Involved in the pathogenesis of several diseases such as breast cancer and possibly Alzheimer's disease; Major retinal pigment epithelial aspartic proteinase, lysosomal, cleaving procaspase 3, ubiquitously expressed; Involved in epidermal differentiation and major factor in the proteolysis of opsin; Potentially recruited during apoptosis; Bound to ceramide for proteolytic activity, at most a mild risk factor for sporadic Alzheimer's disease, not decreased in age related maculopathy	-2.0
NM_006079	Cbp/p300-interacting transactivator, with Glu/Asp-rich carboxy-terminal domain, 2	Interferes with the binding of transcription factors HIF-1a and STAT2 to p300/CBP; CBP/p300 interactive transactivator with ED rich tail 2,with two isoforms p35srj; Ubiquitously expressed; Involved in the recruitment of p300/CBP by hypoxia-inducible factor HIF1A and mrg1 (MSG1-related gene), cytokine inducible transcription factor with transformation activity	-2.0
NM_013316	CCR4-NOT transcription complex, subunit 4	RNA polymerase II transcription regulator; CNOT4 - CCR4-NOT complex is implicated in repression of RNA polymerase II transcription	-2.3
U66838	cyclin A1	May be involved in the control of the cell cycle at the G1/S (start) and G2/M (mitosis) transitions; May primarily function in the control of the germline meiotic cell cycle and additionally in the control of mitotic cell cycle in some somatic cells; Interacts with the cdk2 and the cdc2 protein kinases to form a serine/threonine kinase holoenzyme complex; The cyclin subunit imparts substrate specificity to the complex; Does not bind cdk4 and cdk5 (*in vitro*); The cyclin A1-cdk2 complex interacts with transcription factor E2F-1 and RB proteins	-2.1
M17252	cytochrome P450, subfamily XXIA (steroid 21-hydroxylase, congenital adrenal hyperplasia), polypeptide 2	Heme-thiolate monooxygenases; Oxidize a variety of structurally unrelated compounds, including steroids, fatty acids, and xenobiotics; Disease: congenital adrenal hyperplasia (CAH) is a common recessive disease caused mostly by p450-c21 deficiency, resulting in the inability to synthesize cortisol with over production of cortisol precursors; The disease is characterized by androgen excess including ambiguous genitalia in affected females, rapid somatic growth during childhood in both sexes with premature closure of the epiphyses and short adult stature; Four clinical types	-2.2
M57730	ephrin-A1	Eph-related receptor tyrosine kinase, class A, ligand, high affinity; Involved in short-range contact-mediated axonal guidance; Induction by TNF-alpha and interleukin-1 beta	-4.3
NM_012183	forkhead box D3	Transcription factor-like; Restrictively expressed in hematopoietic cells, with a Drosophila homeo fork head DNA binding domain, mouse hepatocyte nuclear factor 3 homolog; Regulates morphogenesis in Drosophila	-2.0
NM_005756	G protein-coupled receptor 64	Tissue-specific seven-transmembrane receptor of the human epididymis	-5.5
NM_006042	heparan sulfate (glucosamine)	Anticoagulant; Putative regulator of heparan sulfate proteoglycan properties	-2.4

	3-O-sulfotransferase 3A1		
NM_006805	heterogeneous nuclear ribonucleoprotein A0	Protein which binds pre-messenger RNA; Component of ribonucleosomes	-2.0
M10051	insulin receptor	Receptor binds insulin and has a tyrosine-protein kinase activity; Autophosphorylation activates the kinase activity	-2.0
NM_007244	lacrimal proline rich protein	Mediated protective functions in the eye such as modulation of the microflora	-2.1
NM_012134	leiomodin 1 (smooth muscle)	Component of the smooth muscle actin cytoskeleton	-2.0
NM_005565	lymphocyte cytosolic protein 2 (SH2 domain-containing leukocyte protein of 76kD)	Involved in T cell antigen receptor mediated signaling; Interacts with the adapter proteins GRB2 and FYB; Phosphorylated after T-cell receptor activation by ZAP-70	-2.3
X75308	matrix metalloproteinase 13 (collagenase 3)	Degrades collagen type I; Does not act on gelatin or casein; Could have a role in tumoral process; Requires calcium and zinc for activity	-2.2
NM_012429	SEC14 (S. cerevisiae)-like 2	Carrier protein; Binds to some hydrophobic molecules and promotes their transfer between the different cellular sites; Binds with high affinity to alpha-tocopherol; Also binds with a weaker affinity to other tocopherols and to tocotrienols; May have a transcriptional activatory activity via its association with alpha-tocopherol; Probably recognizes and binds some squalene structure, suggesting that it may regulate cholesterol biosynthesis by increasing the transfer of squalene to a metabolic active pool in the cell	-2.8
NM_006664	small inducible cytokine subfamily A (Cys-Cys), member 27	Chemotactic factor that attracts skin-associated memory T-lymphocytes; Role in mediating homing of lymphocytes to cutaneous sites; Binds to CCR10	-2.1

Table 5.5. Arsenic induced genes detected by microarray analysis. Gene expression changes ≥ 2-fold in each of the triplicate experiments (n=3) were considered significantly different when compared to the control array.

GenBank accession #	Gene Name	Function	Fold
NM_007238	24 kDa intrinsic membrane protein	Peroxisomal membrane protein	3.1
M31630	activating transcription factor 2	Binds the camp response element (cre) (consensus: 5'GTGACGT(A/C)(A/G)-3'), a sequence present in many viral and cellular promoters; Subunit binds DNA as a dimmer; Interacts with SMAD3 and SMAD4; Phosphorylation of THR-51 and THR-53 by MAPK14 causes increased transcriptional activity; Also phosphorylated and activated by JNK	2.4
U01147	active BCR-related gene	GTPase-activating protein for RAC and CDC42; Promotes the exchange of RAC or CDC42-bound GDP by GTP, thereby activating them	2.9
NM_006803	adaptor-related protein complex 3, mu 2 subunit	Part of the AP-3 complex, an adaptor-related complex which is not clathrin associated; The complex is associated with the Golgi region as well as more peripheral structures; It facilitates the budding of vesicles from the Golgi membrane and may be directly involved in trafficking to lysosomes	2.5
L05500	adenylate cyclase 1 (brain)	Calmodulin-sensitive adenylyl cyclase; May be involved in regulatory processes in the central nervous system; It may play a role in memory acquisition and learning	6.1
S44195	agrin	Component of the synaptic basal lamina; Shown to induce clustering of Ach receptors on muscle fiber surfaces; May play a role in development and regeneration	2.3
X58794	azurocidin 1 (cationic antimicrobial protein 37)	This is a neutrophil granule-derived antibacterial and monocyte- and fibroblast-specific chemotactic glycoprotein; Binds heparin; The cytotoxic action is limited to many species of gram-negative bacteria, this specificity may be explained by a strong affinity of the very basic N-terminal half for the negatively charged lipopolysaccharides that are unique to the gram-negative bacterial outer envelope; It may play a role in mediating recruitment of monocytes in the second wave of inflammation	2.1
NM_012104	beta-site APP-cleaving enzyme	Responsible for the proteolytic processing of the amyloid precursor protein (APP); Cleaves at the amino terminus of the a-beta peptide sequence, between residues 671 and 672 of APP, leads to the generation and extracellular release of beta-cleaved soluble APP, and a corresponding cell-associated carboxy-terminal fragment which is later release by gamma-secretase	2.5
NM_013450	bromodomain adjacent to zinc finger domain, 2B	May play a role in transcriptional regulation interacting with ISWI; Bromodomain is a structural motif characteristic of proteins involved in chromatin-dependent regulation of transcription and are integral components of chromatin remodeling complexes and frequently possess histone acetyltransferase activity	5.5
NM_006995	butyrophilin, subfamily 2,	B box family of proteins; Involved in cell proliferation and development; Possibly influences	2.5

	member A2	T-cell activation	
X79981	cadherin 5, type 2, VE-cadherin (vascular epithelium)	Mediates homophilic, Ca^{2+}-dependent aggregation, and cell-to-cell adhesion; Cadherins are calcium dependent cell adhesion proteins; They preferentially interact with themselves in a homophilic manner in connecting cells; Cadherins may thus contribute to the sorting of heterogeneous cell types; This cadherin may play a important role in endothelial cell biology through control of the cohesion and organization of the intercellular junctions; It associates with alpha-catenin forming a link to the cytoskeleton	2.8
NM_012115	CASP8 associated protein 2	Interacts with FLASH which is a component of the death-inducing signaling complex in receptor-mediated apoptosis; FLASH coordinates downstream NF-kappaB activity via a TRAF2-dependent pathway in the TNF-alpha signaling; FLASH is necessary for the activation of caspase-8 in Fas-mediated apoptosis	2.6
AF011794	cell cycle progression 8 protein	Cell cycle regulator (G1); When overexpressed is capable to specifically overcoming G1 arrest signals from the cell cycle branch of the mating pheromone pathway	2.1
NM_016063	CGI-130 protein	Chromosome 6 open reading frame 74; Evolutionarily conserved in Caenorhabditis elegans	3.9
NM_015960	CGI-32 protein	CutC copper transporter homolog; Evolutionarily conserved in Caenorhabditis elegans	4.6
NM_016001	CGI-48 protein	WD40 domain, found in a number of eukaryotic proteins that cover a wide variety of functions including adaptor/regulatory modules in signal transduction, pre-mRNA processing and cytoskeleton assembly; Evolutionarily conserved in Caenorhabditis elegans	2.9
NM_013286	chromosome 3p21.1 gene sequence	RNA recognition motif	4.3
NM_006438	collectin sub-family member 10 (C-type lectin)	Involved in different biological pathways; Contain collagen-like region and are involved in first-line host defense; Can bind to carbohydrate antigens of microorganisms and inhibit their infection	2.8
X03663	colony stimulating factor 1 receptor, formerly McDonough feline sarcoma viral (v-fms) oncogene homolog	This protein is the receptor for CSF-1, it is a protein tyrosine-kinase transmembrane receptor	2.3
NM_016129	COP9 complex subunit 4	COP9 complex is an important cellular regulator modulating multiple signaling pathways; Subunits of the COP9 complex include regulators of the Jun N-terminal kinase (JNK) and c-Jun, a nuclear hormone receptor binding protein and a cell-cycle regulator	2.8
X51688	cyclin A2	Control of the cell cycle at the G1/S and the G2/M transitions; Complexing with CDC2, regulating late S and G2 phase of the cell cycle, putative up-regulated c-Myc target gene; Interacts with the CDK2 and CDC2 protein kinases to form a serine/threonine kinase holoenzyme complex; Accumulate steadily during G2 and is abruptly destroyed at mitosis	2.7
U11791	cyclin H	Regulates CDK7, the catalytic subunit of the CDK- activating kinase (CAK) enzymatic complex; CAK activates the cyclin-associated kinases CDC2/CDK1, CDK2, CDK4 and CDK6	2.6

		by threonine phosphorylation; CAK complexed to the core-TFIIH basal transcription factor activates RNA polymerase II by serine phosphorylation of the repetitive carboxyl-terminus domain (CTD) of its large subunit (POLR2A), allowing its escape from the promoter and elongation of the transcripts; Involved in cell cycle control and in RNA transcription by RNA polymerase II; Its expression and activity are constant throughout the cell cycle; Component of CDK activating kinase (CAK1), forming a ternary complex with CDK7 and MNAT1, associating in the multisubunit complex TFIIH (GTF2H), putatively involved in cell cycle control, transcription, and DNA repair	
X66364	cyclin-dependent kinase 5	Probably involved in the control of the cell cycle; Interacts with D1 and D3-type G1 cyclins; Can phosphorylate histone H1, TAU, MAP2 and NF-H and NF-M; Also interacts with p35 which activates the kinase; Specifically expressed in post-mitotic neurons and in muscle cells, associating for activation with its regulatory subunit p35 (CDK5R1) to form one of the two main tau-kinases, complexing with cyclin D (D1,D2,D3), involved in cell-cycle regulation of G1 to S transition, phosphorylating DARRP2 dopamine and cAMP regulated and modulating dopamine signaling, associating with p25, a truncated form of p35 with a resultant increase in CDK5 kinase activity, hyperphosphorylation of tau which reduces tau's ability to associate microtubules	8.3
NM_012137	dimethylarginine dimethylaminohydrolase 1	Hydrolyzes N(G),N(G)-dimethyl-L-arginine (ADMA) and N(G)-monomethyl-L arginine (MMA) which act as inhibitors of NOS; Has therefore a role in nitric oxide generation	2.3
U20552	dynein, cytoplasmic, heavy polypeptide 2	Participate in regeneration of external cilia on the embryo; Encode axonemal dyneins	2.5
NM_001406	ephrin-B3	May play a pivotal role in forebrain function; Binds to, and induce the collapse of, commissural axons/growth cones *in vitro*; May play a role in constraining the orientation of longitudinally projecting axons; Eph-related receptor tyrosine kinase, class B ligand; Involved in short-range contact-mediated axonal guidance; Expressed in fetal brain, and in adult forebrain	2.8
U02687	fms-related tyrosine kinase 3	Receptor for the FL cytokine; Has a tyrosine-protein kinase activity; Expressed on endothelial cell, duplicated in childhood acute myeloid leukemia with poor prognosis and acute lymphoblastic leukemia but not in myelodysplastic syndrome	2.4
NM_012192	fracture callus 1 (rat) homolog	Possible role in cell differentiation during fracture healing	3.0
NM_000144	Friedreich ataxia	Probably involved in iron homeostasis; Associated with mitochondrial membrane; Playing a role in regulating mitochondrial iron transport and in the stability of DNA structure	2.5
NM_000143	fumarate hydratase	Mitochondrial; Catalyzing the seventh step of citric acid cycle; Also acts as a tumor suppressor; Fumarase deficiency can result in several disease states	3.6
NM_013345	G protein-coupled receptor	Member of the 7 transmembrane domain receptor family; G2A, a G protein-coupled receptor for which lysophosphatidylcholine (LPC) is a high affinity ligand; Transcriptionally up-regulated by stress-inducing and cell-damaging agents, and ectopic expression of G2A leads to	2.4

		growth inhibition	
NM_005287	G protein-coupled receptor 10	Member of the 7 transmembrane domain receptor family; Encodes G protein-coupled receptors; Encodes a receptor that shares highest identity with neuropeptide Y receptor	3.1
X15376	gamma-aminobutyric acid (GABA) A receptor, gamma 2	The major inhibitory neurotransmitter in the vertebrate brain, mediates neuronal inhibition by binding to the GABA/benzodiazepine receptor and opening an integral chloride channel; Component of a pentameric receptor mediating inhibitory neurotransmission, complexing with DRD5 and promoting mutually inhibitory functional interactions between these receptor systems, putatively involved in the physiological dependence on alcohol, and in the maintenance of psychomotor disease states	2.5
NM_006529	glycine receptor, alpha 3	Neurotransmitter-gated ion channel; Binding of glycine to its receptor increases the chloride conductance and produces hyperpolarization (inhibition of neuronal firing)	2.3
AF038499	guanylate cyclase 1, soluble, beta 2	Activated by nitric oxide (NO) in the presence of magnesium or manganese ions; Inhibiting the NO stimulated activity of the alpha 1/beta 1 form of guanylate cyclase; Maybe involved in the regulation of blood pressure	2.5
NM_006041	heparan sulfate (glucosamine) 3-O-sulfotransferase 3B1	Widely expressed with multiple transcripts active according to the saccharide structures around the GLN residue, putative regulator of heparan sulfate proteoglycan properties; Anticoagulant	3.0
NM_007067	histone acetyltransferase	Binds to ORC1; ORC mediates acetylation of chromatin in control of both DNA replication and gene expression; Regulates androgen receptor-dependent genes in normal and prostate cancer	2.2
NM_012269	hyaluronoglucosaminidase 4	Differentially expressed in placenta and skeletal muscle; Involved in glycosaminoglycan catabolism, clustered with HYAL1P1 and SPAM1	2.4
NM_015916	hypothetical protein	Unknown	3.3
NM_016626	hypothetical protein	Unknown	2.3
U12897	imprinted in Prader-Willi syndrome	Role in imprinting process; Paternally expressed gene, imprinted in Prader-Willi region, may be the same as Par-1 or 7 (see PWCR)	2.9
L15344	interleukin 14	Induce B-cell proliferation, inhibit immunoglobulin secretion and selectively expand certain B-cell populations; Produced by T cells and some malignant B cells	2.1
NM_016156	KIAA1073 protein	Function not known; Could be a tyrosine phosphatase; Defects in MTMR2 are a cause of charcot-marie-tooth disease type 4B (CMT4B), an autosomal recessive demyelinating neuropathy with myelin outfoldings	2.8
NM_013344	leucine zipper-like protein	N-acetyltransferase activity; transcriptional activator activity	2.3
NM_006552	lipophilin A (uteroglobin family member)	May bind androgens and other steroids, may also bind estramustine, a chemotherapeutic agent used for prostate cancer; May be under transcriptional regulation of steroid hormones	5.0
NM_013317	lung type-I cell membrane-associated glycoprotein	Involved in fluid transport	2.3
NM_012214	mannosyl (alpha-1,3-)-	Transferase activity, transferring hexosyl groups; Alpha-1,3-mannosylglycoprotein 4 beta-N-	3.4

	glycoprotein beta-1,4-N-acetylglucosaminyltransferase, isoenzyme A	acetylglucosaminyltransferases activity	
X96401	MAX binding protein	(Interacting with Max to bind Myc-Max recognition sites), MYC family acting as a transcriptional repressor in an E. box driver reporter gene repression system through interaction between the N-terminus and SIN3 co-repressor, potentially involved in proliferation and differentiation, not involved in lung cancer; Binds DNA as a heterodimer with MAX and represses transcription; Binds to the canonical E box sequence 5'-CACGTG-3' and, with higher affinity, to 5'-CACGCG-3'	2.1
U39657	mitogen-activated protein kinase kinase 6	Catalyzes the concomitant phosphorylation of a threonine and a tyrosine residue in map kinase p38 exclusively; Activated by TNFA, involved in TNFA mediated endothelial SCYA2 (MCP1) expression, activating PRKMK8 and p38 kinase (MAPK) and required for ABL1 induced apoptosis	4.5
M62397	mutated in colorectal cancers	Candidate for the putative colorectal tumor suppressor gene located at 5q21; Probably involved in early stages of colorectal neoplasia in both sporadic and familial tumors	2.4
X13988	myosin, heavy polypeptide 3, skeletal muscle, embryonic	Functions during muscle contraction; Motor contractile protein moving towards the "plus" end of actin track	2.8
M73980	Notch (Drosophila) homolog 1 (translocation-associated)	Functions as a receptor for membrane-bound ligands Jagged1, Jagged2 and Delta1 to regulate cell-fate determination; Upon ligand activation through the released notch intracellular domain (NICD) it forms a transcriptional activator complex with RBP-J kappa and activates genes of the enhancer of split locus; Affects the implementation of differentiation, proliferation and apoptotic programs; May be important for normal lymphocyte function; In altered form, may contribute to transformation or progression in some T-cell neoplasms; Involved in the maturation of both CD4+ and CD8+ cells in the thymus; Mediating cell-cell interactions that specify cell fate during development, undergoing a first proteolytic cleavage by furin (PACE1) in the Golgi during trafficking of Notch to the cell surface, undergoing further cleavage by gamma secretase (see PSEN1) releasing an intracellular domain (NICD) which translocates to the nucleus and modulates transcription of target genes, involved in acute lymphocytic leukemia with translocation t(7;9)(q34;q34.3), expressed in CD34+ hematopoietic cells (see TAN1) and in the developing cochlear duct, inducing delay of hematopoietic differentiation and alteration of cell cycle kinetics	3.9
NM_012250	oncogene TC21	Plasma membrane-associated GTP-binding protein with GTPase activity; TC21 might transduce growth inhibitory signals across the cell membrane, exerting its effect through an effector shared with the RAS proteins but in an antagonistic fashion	2.4
NM_015853	ORF	Domain present in ubiquitin-regulatory proteins; Present in FAF1 and Shp1p	2.4
NM_012381	origin recognition complex, subunit 3 (yeast homolog)-like	Component of the origin recognition complex (ORC) that binds origins of replication; It has a role in both chromosomal replication and mating type transcriptional silencing; Binds to the	3.3

		ARS consensus sequence (ACS) of origins of replication in an ATP-dependent manner	
AF112465	osteoglycin (osteoinductive factor, mimecan)	Induces bone formation in conjunction with TGF-beta-1 or TGF-beta-2	2.8
NM_012399	phosphotidylinositol transfer protein, beta	Catalyzes the transfer of PTDins and phosphatidylcholine between membranes	2.6
Y15065	potassium voltage-gated channel, KQT-like subfamily, member 2	Probably important in the regulation of neuronal excitability; Associates with KCNQ3 to form a potassium channel with essentially identical properties to the channel underlying the native M-current, a slowly activating and deactivating potassium conductance which plays a critical role in determining the subthreshold electrical excitability of neurons as well as the responsiveness to synaptic inputs. KCNQ2/KCNQ3 current is blocked by linopirdine and XE991, and activated by the anticonvulsant retigabine; Muscarinic agonist oxotremorine-M strongly suppress KCNQ2/KCNQ3 current in cells in which cloned KCNQ2/KCNQ3 channels were co-expressed with M1 muscarinic receptors.	2.8
NM_002624	prefoldin 5	Binds specifically to cytosolic chaperonin (C-CPN) and transfers target proteins to it; Binds to nascent polypeptide chain and promotes folding in an environment in which there are many competing pathways for nonnative proteins	2.3
NM_012409	prion gene complex, downstream	Function not known; Causes neurodegeneration	2.1
NM_007217	programmed cell death 10	Encodes a protein, originally identified in a premyeloid cell line, with similarity to proteins that participate in apoptosis	3.2
NM_002772	protease, serine, 7 (enterokinase)	Responsible for initiating activation of pancreatic proteolytic proenzymes (trypsin, chymotrypsin and carboxypeptidase A); It catalyzes the conversion of trypsinogen to trypsin which in turn activates other proenzymes including chymotrypsinogen, procarboxypeptidases, and proelastases	9.1
NM_007229	protein kinase C and casein kinase substrate in neurons 2	May play a role in vesicle formation and transport; Regulates the metalloprotease/disintegrin ADAM13 by influencing its subcellular localization or its catalytic activity; May participate in the organization of the actin cytoskeleton	3.0
J03075	protein kinase C substrate 80K-H	Substrate for PKC in fibroblasts and epidermal carcinoma; May be dependent on Ca^{2+} binding; Regulates N-glycosylation of proteins and signal transduction via fibroblast growth-factor receptor	2.4
NM_002744	protein kinase C, zeta	PKC is activated by diacylglycerol which phosphorylates a range of cellular proteins; Receptor for phorbol esters, a class of tumor promoters	2.5
NM_012411	protein tyrosine phosphatase, non-receptor type 22 (lymphoid)	Lymphoid-specific; Involved in regulation of the function of protooncogene CBL; Seems to act on CBL; May play a role in regulating the function of CBL and its associated protein kinases	2.3
NM_012197	rab6 GTPase activating protein (GAP and centrosome-	Coordinates microtubule and Golgi dynamics during the cell cycle	2.2

	associated)		
U63139	RAD50 (S. cerevisiae) homolog	Involved in DNA recombinational repair and meiosis specific double strand break formation, complexing with MR11 and NBS1	2.3
NM_016374	RBP1-like protein	Encodes an antigenic epitope abundantly expressed in human carcinoma and normal testes; Encodes tumor-associated antigen epitopes relevant to immune response in cancer patients	3.6
NM_006394	regulated in glioma	Role in malignant progression of human glioblastoma; Predominantly expressed in normal brain, also expressed in heart and lung; Down-regulated in glioblastoma	2.2
M87338	replication factor C (activator 1) 2 (40kD)	Component of complex A-1, DNA polymerase accessory protein "clamp loader", ATP dependent, required to assemble proliferating cell nuclear antigen (PCNA) and polymerase delta on the DNA template; Elongation of primed DNA templates by DNA polymerase delta and epsilon requires the action of the accessory proteins PCNA and activator 1; The 40 kDa subunit binds ATP	2.5
NM_013435	retinal homeobox protein	Plays a critical role in eye formation by regulating the initial specification of retinal cells and/or their subsequent proliferation; Binds to the photoreceptor conserved element-I (PCE-1/Ret 1) in the photoreceptor cell-specific arrestin promoter	2.5
M15400	retinoblastoma 1 (including osteosarcoma)	Probably acts as a regulator of other genes; Forms a complex with adenovirus E1A and with SV40 large T antigen; Acts as a tumor suppressor; May bind and modulate functionally certain cellular proteins with which T and E1A compete for pocket binding; Potent inhibitor of E2F-mediated trans-activation; Phosphorylated from S to M phase of the cell cycle and is dephosphorylated in G1; T, but not E1A, binds only to the unphosphorylated form; Cell-cycle dependent (regulator of cell growth), interacting with E2F-like transcription factor, also interacting with histone deacetylase (HDAC1) to repress transcription CDC2 substrate and with BOG (B5T overexpressed gene) to suppress growth inhibitory effect of TGFB1, overexpressed in bladder cancer with poor prognosis and in parathyroid hyperplasia, deleted in pituitary tumors (somatotrophinomas)	2.5
S57153	retinoblastoma-binding protein 1	Interacts with the viral protein-binding domain of the retinoblastoma protein; Undergoes alternative splicing; Interacts with pRB; Large, nuclear phosphoprotein with structural motifs that suggest a role in transcriptional regulation	2.1
NM_016316	REV1 (yeast homolog)- like	REV1 transferase may play a critical role during mutagenic translesion DNA synthesis bypassing a template AP site; Codes for a DNA template-dependent dCMP transferase	2.7
NM_002929	rhodopsin kinase	Phosphorylates rhodopsin thereby initiating its deactivation; G protein coupled receptor kinase, expressed in cones and rods, with two alternatively spliced isoforms, GRK1a and GRK1b, exported to the cytosol, involved in quenching of light-induced signal transduction in phosphoreceptor (dark state recovery after phosphoactivation), inhibited by recoverin (RCV1)	3.5
NM_016337	RNB6	Critically involved in the development of CNS probably through the control of neural cell motility and/or including neuronal fiber extension	3.3
NM_006558	Sam68-like phosphotyrosine	Nuclear RNA-binding protein	2.5

	protein, T-STAR		
NM_012431	sema domain, immunoglobulin domain (Ig), short basic domain, secreted, (semaphorin) 3E	Correlates positively with tumor progression; Involved in embryonic development and has expression in developing lungs, developing skeletal elements, and ventral horns of developing neural tubes	2.5
NM_006089	sex comb on midleg (Drosophila)-like 2	Involved in transcriptional repression of HOX genes, clustered with SCML1; Candidate gene for Xp22-linked developmental disorders	2.2
NM_005794	short-chain alcohol dehydrogenase family member	May inhibit cell replication either by catalyzing the oxidation of estrogens and androgens or by converting cortisone in cortisol	3.7
NM_012238	sir2-like 1	Regulates epigenetic gene silencing and as a antiaging effect it suppresses recombination of rDNA; May function via mono-ADP-ribosylation of proteins	2.6
NM_006419	small inducible cytokine B subfamily (Cys-X-Cys motif), member 13 (B-cell chemoattractant)	Chemotactive for B lymphocytes but not for T lymphocytes, monocytes and neutrophils; Does not induce Ca2+ release in B lymphocytes; Binds to BLR1/CXCR5	3.3
NM_006049	small nuclear RNA activating complex, polypeptide 5, 19kD	Complex required for the transcription of both RNA polymerase II and III small nuclear RNA genes; Binds to the proximal sequence element (PSE), a non TATA-box basal promoter element common to these 2 types of genes	2.1
S78203	solute carrier family 15 (H+/peptide transporter), member 2	Proton-coupled intake of oligopeptides of 2 to 4 amino acids with a preference for dipeptides; Family member of H(+)-coupled transport systems in the mammalian plasma membrane	3.8
L31801	solute carrier family 16 (monocarboxylic acid transporters), member 1	Proton-linked monocarboxylate transporter; Catalyzes the rapid transport across the plasma membrane of many monocarboxylates such as lactate, pyruvate, branched chain oxo acids derived from leucine, valine and isoleucine, and the ketone bodies acetoacetate, beta-hydroxybutyrate and acetate	3.0
NM_006074	stimulated trans-acting factor (50 kDa)	Mechanistic role in the transactivation of the interferon antiviral action	2.3
NM_007265	suppressor of S. cerevisiae gcr2	Transcriptional activator; Encodes regulatory factor of glycolytic gene expression	2.7
NM_016349	susceptibility protein NSG-x	Chromosome 9 open reading frame 53	2.3
NM_003185	TATA box binding protein (TBP)-associated factor, RNA polymerase II, C1, 130kD	Makes part of TFIID is a multimeric protein complex that plays a central role in mediating promoter responses to various activators and repressors; Potentiates transcriptional activation by the AF-2S of the retinoic acid, vitamin D3 and thyroid hormone	3.4
NM_003187	TATA box binding protein (TBP)-associated factor, RNA polymerase II, G, 32kD	TAFS are components of the transcription factor IID (TFIID) complex that are essential for mediating regulation of RNA polymerase transcription; TAFII31 is a co-activator for the p53 protein; Also interacts with the acidic transactivator viral protein 16 (VP16) as well as with the general transcription factor TFIIB	2.5

NM_012461	TERF1 (TRF1)-interacting nuclear factor 2	Involved in the regulation of telomere length; Prevents excessive telomere elongation; Binds to TRF1	2.1
NM_012472	testis specific leucine rich repeat protein	Leucine rich repeat containing 6	3.6
NM_003265	toll-like receptor 3	Participates in the innate immune response to microbial agents; May be involved in the recognition of ds-RNA; Acts via MyD88 and TRAF6, leading to NF-kappa-B activation, cytokine secretion and the inflammatory response; Involved in immune defense	2.7
NM_016610	Toll-like receptor 8	Participates in the innate immune response to microbial agents; Acts via MyD88 and TRAF6, leading to NF-kappa-B activation, cytokine secretion and the inflammatory response	6.7
NM_003223	transcription factor AP-4 (activating enhancer-binding protein 4)	Transcription factor that activates both viral and cellular genes by binding to the symmetrical DNA sequence 5'-CAGCTG-3'; Involved in signal-mediated trafficking of integral membrane proteins	2.8
NM_006022	transforming growth factor beta-stimulated protein TSC-22	Transcriptional repressor; Acts on the C-type natriuretic peptide (CNP) promoter	5.0
NM_012253	transketolase-like 1	Belongs to the transketolase family	2.5
NM_012456	translocase of inner mitochondrial membrane 10 (yeast) homolog	Essential for escorting a class of multimembrane-spanning proteins; Encodes deafness/dystonia peptide (DDP)	2.2
NM_004205	ubiquitin specific protease 2	Role in recycling ubiquitin by hydrolysis; May be produced by alternative splicing	2.9
X66087	v-myb avian myeloblastosis viral oncogene homolog-like 1	Strong transcriptional activator; Could have a role in the proliferation and/or differentiation of neurogenic, spermatogenic and B-lymphoid cells	2.1
NM_006784	WD repeat domain 3	Involved in cell cycle progression, signal transduction, apoptosis, and gene regulation	2.4
NM_012480	zinc finger protein 186 (Kruppel type)	May be involved in transcriptional regulation	2.4
NM_013250	zinc finger protein 215	May function as a transcription factor	2.3
NM_005096	zinc finger protein 261	Ubiquitously expressed predominantly in brain, subject to X-inactivation, strongly homolog to ZNF198	2.3
NM_007222	zinc-fingers and homeoboxes 1	With two alternatived spliced isoforms, ubiquitously expressed, interacting with the nuclear transcription factor NF-Y	2.3

Table 5.6. Arsenic suppressed genes detected by microarray analysis. Gene expression changes ≥ 2-fold in each of the triplicate experiments (n=3) were considered significantly different when compared to the control array.

GenBank Accession #	Gene Name	Function	Fold
M12807	CD4 antigen (p55)	Cell differentiation antigen CD4 (p55), 59kDa, HIV and MHC class II receptor, accessory protein for MHC class-II antigen/T-cell receptor interaction; May regulate T-cell activation; Identified by monoclonal antibodies T4, Leu-3a, 91D6, transmembrane glycoprotein (see LAG3), containing a tissue-specific promoter made of an initiator-like sequence, an ETS and an ATF consensus site, and a locus control region like, see LCR-CD4	-2.0
X77824	chromobox homolog 2 (Drosophila Pc class)	Involved in maintaining the transcriptionally repressive state of genes; Modifies chromatin, rendering it heritably changed in its expressibility; Involved in the compaction of chromatin	-2.2
L07515	chromobox homolog 5 (Drosophila HP1 alpha)	Component of heterochromatin; May interact with lamin B receptor (LBR); This interaction can contribute to the association of the heterochromatin with the inner nuclear membrane; Phosphorylation of HP1 and LBR may be responsible for some of the alterations in chromatin organization and nuclear structure which occur at various times during the cell cycle; Binds directly to CHAF1A	-2.5
NM_015921	divalent cation tolerant protein CUTA	CutA1 divalent ion tolerance protein	-2.0
U01839	Duffy blood group	Non-specific receptor for many chemokines such as IL-8, GRO, rantes, MCP-1 and TARC; It is also the receptor for the human malaria parasites plasmodium vivax and plasmodium knowlesi; Individuals that do not produce the duffy antigen (FY(A- B-)) are more resistant to vivax malaria; This allele is found predominantly in population of African origin	-2.0
NM_003922	hect (homologous to the E6-AP (UBE3A) carboxyl terminus) domain and RCC1 (CHC1)-like domain (RLD) 1	Located in the cytosol in the Golgi apparatus, stimulating guanine nucleotide, forming a cytosolic ternary complex with clathrin and Hsp70, involved in protein trafficking; Guanine nucleotide exchange factor for ARFand Rab family proteins	-2.3
D49783	histamine receptor H2	The H2 subclass of histamine receptors mediates gastric acid secretion, also appears to regulate gastrointestinal motility and intestinal secretion; Possible role in regulating cell growth and differentiation; The activity of this receptor is mediated by G proteins which activate adenylyl cyclase and, through a separate G protein-dependent mechanism, the Phosphoinositide/protein kinase (PKC) signaling pathway	-2.0
M62831	immediate early protein	Human transcription factor ETR101 mRNA	-2.0
X12492	nuclear factor I/C (CCAAT-binding transcription factor)	Recognizes and binds the palindromic sequence 5'- TTGGCNNNNNGCCAA-3' present in viral and cellular promoters and in the origin of replication of adenovirus type 2; These proteins are individually capable of activating transcription and replication; DNA binding protein; Binds DNA as an homodimer	-2.0

NM_013439	paired immunoglobulin-like receptor alpha	Immunoreceptor tyrosine-based inhibitory motif-bearing protein, recruits SHP-1 upon tyrosine phosphorylation	-2.0
NM_016109	PPAR(gamma) angiopoietin related protein	Role for PGAR in the regulation of systemic lipid metabolism or glucose homeostasis; Associated with adipose differentiation, systemic lipid metabolism, energy homeostasis, and possibly angiogenesis; Prevents endothelial-cell apoptosis	-2.0
NM_012342	putative transmembrane protein	Integral membrane protein; Expression in poorly metastatic human melanoma cell lines; No expression in highly metastatic human melanoma cell lines	-2.8
M15465	pyruvate kinase, liver and RBC	Requires magnesium and potassium; Defects in PKLR are the most common cause of chronic hereditary non-spherocytic hemolytic anemia (CNSHA or HNSHA) among glycolytic enzymes; Transcribed from a distinct promoter, glycolysis, energy pathway, generating ATP from ADP	-2.0
NM_005854	receptor (calcitonin) activity modifying protein 2	Transports calcitonin-receptor-like receptor (CRLR) to the plasma membrane where it acts as an adrenomedullin receptor.	-2.0
U16752	stromal cell-derived factor 1	Small cytokines belonging to the intercrine CXC subfamily; Chemoattractant active on T-lymphocytes, monocytes, but not neutrophils	-2.5

Table 5.7. Identification of specific genes examined in real-time PCR experiments

GenBank Accession #	Complete Gene Name	Abbreviated Name
NM_007216	α-integrin binding protein 63	α-integrin-bp
X79981	cadherin 5, type 2, VE-cadherin	Cad-5
X02851	interleukin 1, α	IL-1α
K02770	interleukin 1, β	IL-1β
X96401	MAX binding protein	MNT
U63139	RAD50 (S. cerevisiae) homolog	RAD50
NM_005739	Ras guanyl releasing protein 1 (Ca^{2+} and DAG regulated)	Ras-GRP
M15400	retinoblastoma 1 (including osteosarcoma)	Rb-1
S57153	retinoblastoma-binding protein 1	Rb-bp1
NM_005750	retinoic acid- and interferon-inducible protein	RA-IFN
NM_006022	transforming growth factor β-stimulated protein TSC-22	TSC-22
NM_005748	YY1-associated factor 2	Yaf2

Table 5.8. Comparison of gene expression changes measured by microarray and real-time RT-PCR using six benzo[*a*]pyrene-induced genes from microarray analysis

BaP Induced Genes Identified from Microarray	**Benzo[*a*]pyrene**		**Arsenic**	
	Array	**RT PCR**	**Array**	**RT PCR**
α-integrin-bp	15.74±13.5	2.48±0.22	2.23±0.48	-1.10±0.01
IL-1α	3.91±2.60	2.64±0.31	3.89±4.06	-1.05±0.07
IL-1β	4.4±2.25	2.84±0.19	1.56±0.08	-1.23±0.08
RA-IFN	4.16±1.60	2.74±0.68	1.37±0.22	-1.08±0.13
Ras-GRP	8.1±1.69	3.14±0.29	2.14±0.67	1.76±0.15
Yaf2	9.61±1.30	-1.33±0.09	2.12±0.53	-1.18±0.08

(Real-time PCR experiments: n = 9 and gene expression levels were required to meet the same standards as in microarray experiments, i.e. ≥ 2-fold difference when compared to control samples)

Table 5.9. Comparison of gene expression changes measured by microarray and real-time RT-PCR using six arsenic-induced genes from microarray analysis

Arsenic Induced Genes Identified from Microarray	**Arsenic**		**Benzo[*a*]pyrene**	
	Array	**RT PCR**	**Array**	**RT PCR**
Cad-5	2.77±0.81	1.26±0.28	2.19±1.03	1.61±0.69
MNT	2.13±0.11	2.44±0.02	1.36±0.33	1.61±0.25
RAD50	2.31±0.31	4.24±2.59	1.24±0.65	2.23±0.08
Rb-1	2.47±0.22	5.40±0.51	1.86±0.25	-1.08±0.28
Rb-bp1	2.13±0.8	6.80±1.46	3.76±2.99	1.41±0.08
TSC-22	5.0±3.7	6.84±0.51	1.32±3.11	1.34±0.18

(Real-time PCR experiments: n = 9 and gene expression levels were required to meet the same standards as in microarray experiments, i.e. ≥ 2-fold difference when compared to control samples)

Chapter 6

Computational Model of the Step-Wise Processes of Terminal Growth Arrest and Squamous Differentiation in Keratinocytes

6.1. Introduction

The importance and utility of computational modeling as a vital component of biomedical research programs has previously been addressed by Hartwell, Hopfield, Leibler, and Murray (Hartwell *et al.* 1999). According to these investigators: "The best test of our understanding of cells will be to make quantitative predictions about their behavior and test them". This will require detailed simulations of the biochemical processes taking place within cells, which then direct various modifications of cell conditions and phenotypic behavior. In addition, there is a necessity to develop simplifying, higher level models and find general principles that will allow us to grasp and manipulate the functions of biochemical networks. In an extension of this thought, Tyson, Csikasz-Nagy, and Novak state: "We must cast our hypotheses in precise mathematical terms, compute accurate solutions of the equations, and compare the solutions in quantitative detail with a wide variety of experimental observations" (Tyson *et al.* 2002). Computational modeling can help researchers achieve a higher understanding of biological problems through several mechanisms. Initial development of a model defines working hypotheses, organizes preexisting data, and identifies obvious

data gaps around which laboratory experimentation can be designed. Through an iterative process of laboratory studies and continual model refinement based on the resulting data, hypotheses can be tested and reformulated as seems appropriate to bring them into accord with the basic biological facts. Quantitative models can be modified to incorporate new experimental data as it becomes available and thus can, in effect, grow with our knowledge of the system under study.

Several models of keratinocyte differentiation have been developed for *in vivo* systems. These models looked at both mouse (Aarnaes *et al.* 1993; Aarnaes *et al.* 1990; Clausen *et al.* 1984; Potten *et al.* 1982; Thorud *et al.* 1988) and human epidermis (Loeffler *et al.* 1987; Savill 2003), with multiple different approaches and have highlighted the following issues: the hierarchical and heterogeneous make-up of the cell populations in the germinative (basal) compartment of the skin, the importance of the fraction of basal cells that are cycling, symmetrical versus asymmetrical division of transient-amplifying (TA) cells, the importance of apoptosis in normal epidermis, and the lateral and vertical movement of differentiating cells within the skin. Although the lack of appropriate and complete data sets addressing these issues has hindered the process, these modeling exercises are useful in that they have defined areas of high research/experimental priority.

The *in vitro* keratinocyte system was chosen for this work based on the fact that these cells can be readily induced to differentiate in culture and are, therefore, highly amenable to quantitative cellular and molecular studies of this process. The *in vitro* system is also more rapid, less expensive, and preserves animal life in studies of multiple experiments, in which cells are examined under various conditions. There has to date,

however, been only one, biologically-based model of keratinocyte differentiation developed for *in vitro* systems (Kimmel *et al.* 1986). These investigators utilized stathmokinetic techniques (which rely on cell cycle blockade via treatment of cells with exogenous agents) to examine the cell cycle kinetics of human epidermal cells in culture. Flow cytometric data generated by staining of cellular DNA and RNA was coupled with mathematical modeling to describe quantitatively the movement of basal epidermal cells through stages of altered proliferation and increasing differentiation. The resulting model was then used to predict the growth kinetics of cultured keratinocyte populations over time. Other models have described *in vitro* differentiation in non-keratinocyte cell types, including those developed for oligodendrocyte type-2 astrocyte progenitor cells (Boucher *et al.* 2001; Yakovlev *et al.* 1998). These latter models examined a variety of hypotheses/parameters for their importance in accurately predicting the number of terminally differentiated oligodendrocytes with time in culture. Among the issues addressed were: the concept of competence in determining the number of mitotic cycles required before a cell arrests and terminally differentiates and the influence of environmental factors on the probability of differentiation.

In this research, modeling efforts extended and expanded studies conducted throughout the 1980's and early 1990's to incorporate currently available information using a "Systems Biology" approach. There are many advantages, both for this study and for this research area in general, in further development of a biologically-based model capable of accurately describing keratinocyte differentiation *in vitro.* Among the areas that could potentially benefit from this approach are the following: (1) biological/mechanistic studies into the balance between proliferation and differentiation

under a variety of culture conditions, or in the presence of endogenous inducers/inhibitors of the differentiation process; (2) studies to define defects in differentiation in cells from individuals with a variety of hereditary skin disorders such as ichthyosis (several types) and epidermolytic hyperkeratosis; (3) toxicological studies on chemicals to link perturbations in specific model parameters with defined toxic endpoints such as hyperkeratosis or carcinogenesis; (4) predictive studies on new and novel chemical agents; and (5) linkage to more complex cell cycle/signal transduction models taking advantage of RNA and protein expression technologies to generate and validate molecular changes that accompany any of the above biological phenomena. Before tackling any of the areas mentioned above, the initial goal is to develop a computational model of the step-wise process of terminal growth arrest and squamous differentiation in this cell type under normal conditions. Once a working mathematical model is developed researchers can then apply this model to aid in mechanistic studies and in developing predictive abilities in identification of hazardous chemicals and chemical mixtures, especially those that target the skin.

The hypothesis of this research is that integrating cell and molecular biology information with computational modeling will improve our understanding of keratinocyte growth and differentiation, and help predict chemically-induced cell kinetic changes due to carcinogen exposure. Developing a quantitative biologically-based computer model for the differentiation of human keratinocytes will provide an *in silico* experimental platform which will incorporate data from previous experimentation. More specifically, the goal of this study was to utilize various parameters that were calculated from flow cytometry experimentation (Chapter 4) and incorporate these data into the mathematical model;

thus, creating computer simulations describing the movement and behavior of keratinocytes within the skin. The effects of chemical exposures may then be simulated as perturbations of critical biological processes in an otherwise normal state. In all, two mathematical models were constructed to illustrate and understand keratinocyte behavior in terms of cell cycle kinetics and differentiation abilities within the epidermis.

6.2. Materials and Methods

6.2.1. Cell culture

Cryopreserved normal human epidermal keratinocytes (NHEK) were purchased from the Clonetics Corp. (San Diego, CA). NHEK were grown in 5% CO_2 at 37°C in defined Keratinocyte Growth Medium (KGM) (Clonetics Corp) containing bovine pituitary extract (BPE), human epidermal growth factor (hEGF), insulin, hydrocortisone, transferrin, epinephrine, and antibiotic, GA-1000, at proprietary concentrations as determined by the manufacturer.

6.2.3. Cell Division Rate Measurement Assay

Determination of NHEK proliferation rates was carried out via BrdU labeling and propidium iodide staining followed by flow cytometric analysis (Steel 1977; Wilson 1994b)**.** Briefly, cells were plated in 100 mm petri dishes at a density of 10,000 cells/plate. When cells reached 10-15% confluency, they were treated with either BaP [2.0 μM] and arsenic [5.0 μM] for 24 hours or continuously with Ca^{2+} [2.0 mM]. After the treatment period, cultures were re-fed with chemical-free medium and incubated until they reached 50-60% confluency, approximately 4-5 days. At this point, cells were pulse-

labeled with 10.0 μM BrdU for 30 min. After washing to remove the BrdU, cells were cultured and fixed at 0, 2, and 4 hr time points. The fixation and staining protocol was modified from that described previously (Larsen 1994; Liao *et al.* 2001). Cells were filtered through 53.0 μm nylon mesh (Small Parts Inc., Miami Lakes, FL) prior to flow cytometric analysis.

6.2.3. Flow Cytometric Analysis

Flow cytometric analysis was performed to gather information on various NHEK growth properties such as cell cycle distribution and potential doubling time. Samples were analyzed with an Epics V cell sorter (Coulter, Miami, FL) interfaced to a Cicero data acquisition and display system (Cytomation Inc., Fort Collins, CO). Cells were illuminated by an argon ion laser at 488 nm (500 mW). FITC was measured at wavelengths between 515 to 530 nm and PI was measured at wavelengths longer than 610 nm. The PI signal was gated on peak vs. integral fluorescence to eliminate clumped cells. Thirty thousand cells were analyzed for each bivariate histogram.

6.2.4. Examination of Cell Cycle Kinetics

The concept of potential doubling time (T_{pot}) was proposed by Steel, G. G. (1977) and can be used to estimate the proliferation alterations which occur following chemical treatment (Steel 1977). The T_{pot} of individual cultures was calculated from cell labeling and flow cytometric data as described previously (Begg *et al.* 1985). T_{pot} is a cell division time that takes growth fraction, but not cell loss, into account (Steel 1977; Wilson 1994b). T_{pot} was calculated with the following equation:

$$T_{pot} = \lambda \times \frac{T_S}{LI} \qquad (6\text{-}1)$$

where T_S is the period of DNA synthesis, LI (labeling index) is the fraction of cells synthesizing DNA, and λ is a correction factor for the nonlinear distribution of cells through the cell cycle (Steel 1977; Wilson 1994b). Estimation of T_{pot} values relies upon distinction of cells within the four different stages of the cell cycle.

In order to accurately derive cell kinetic parameters the following equation was used to calculate cell cycle time (T_C):

$$T_C = \frac{\ln \alpha}{\ln 2} T_{pot} \qquad (6\text{-}2)$$

T_C is the interval within which one group of cells complete a mitotic cycle, i.e. from birth at mitosis to eventual splitting to form two progeny at the next mitosis (Wilson 1994a). The term α is the average number of proliferating daughter cells produced at each division and this value realistically lies between 1 and 2 (Steel 1977). An estimated value for the NHEK growth fraction (GF) was used to calculate α from Steel's equation:

$$GF = \alpha - 1 \qquad (6\text{-}3)$$

The term GF is used to describe the proportion of proliferative cells in a given tissue or population. GF parameter values were utilized from a study that specifically investigated the growth fraction in normal epidermal cells (Heenen and Galand 1997). Once T_C and α are obtained, one can determine phase times given the fraction of cells in each phase with the following equation provided by Steel (1977):

$$T_i = -\frac{T_C}{\ln \alpha} \ln \left\{ e^{-\left(\frac{T_{i-1}}{T_C}\right) \ln \alpha} - \frac{\alpha - 1}{\alpha} P_i \right\} \qquad (6\text{-}4)$$

where T_i is the cumulative time including the phase of interest (i.e., $T_1 = T_{G1}$, $T_2 = T_{G1}+T_S$, and $T_3 = T_{G1}+T_S+T_{G2/M} = T_C$). P_i is the fraction of cells in phase i. Once the average time in each cell cycle phase is computed, the rate of conversion (k) from one cell cycle phase to the next can be calculated from the following equation as previously described (Basse *et al.* 2003; Takahashi 1968):

$$T_i = \frac{1}{k_i + \beta_i} \qquad (6\text{-}5)$$

where β_i is the death rate parameter of a particular cell cycle phase. Since there are no reports of death rate in keratinocytes, cell death rate estimates were taken from SHE cells in studies performed by Liao *et al.* (2001).

6.2.5. Mathematical Models

6.2.5.1. Two Stage Keratinocyte Differentiation Model: Model A

To mathematically describe the process of differentiation in NHEK, Model A (Figure 6.1) was constructed and is represented by four compartments; three cell cycle phases and a post-mitotic phase. Both stem and transit-amplifying (TA) cells are lumped (STA) into one compartment (Stage 1). A fraction of cells within the STA compartment cycle or remain quiescent (G0), while the remaining fraction differentiate into non-cycling post-mitotic cells (Stage 2 of Figure 6.1). The dividing STA cells progress through the cell cycle which, in this model consists of three compartments (G1+G0, S, and G2+M). The cell cycle phase where cells reside is distinguished by the amount of DNA content. Cell distribution data, obtained using flow cytometry, displays the fraction of cells in each phase of the cell cycle based on the following DNA content:

$$\text{G1+G0 cells} = n \qquad (6\text{-}6)$$

$$\text{G2+M cells} = 2n \tag{6-7}$$

$$n < \text{S-phase cells} < 2n \tag{6-8}$$

where n is the DNA content in a normal diploid cell.

The movement between the four compartments is represented by the schematic diagram in Figure 6.1 which expresses the accumulation of cells in each compartment and the movement between compartments. The modeling equations for Model A are:

$$\frac{dSTA_{G1+G0}}{dt} = 2(k_{G2M})STA_{G2M} - (k_{G1})STA_{G1+G0} - (\beta_{G1+G0})STA_{G1+G0} - (\delta)STA_{G1+G0} \tag{6-9}$$

$$\frac{dSTA_{S}}{dt} = (k_{G1})STA_{G1+G0} - (k_{S})STA_{S} - (\beta_{S})STA_{S} \tag{6-10}$$

$$\frac{dSTA_{G2M}}{dt} = (k_{S})STA_{S} - (k_{G2M})STA_{G2M} - (\beta_{G2M})STA_{G2M} \tag{6-11}$$

$$\frac{dPM}{dt} = (\delta)STA_{G1+G0} - (\delta_{T})PM \tag{6-12}$$

where STA represents the fractions of stem cells and TA depicts transit-amplifying cell fractions in a particular cycle phase. PM denotes post-mitotic cells and δ is the rate of conversion from cycling STA cells to PM cells. The term δ_T represents the rate at which cornified cells of the PM compartment desquamate from the outer skin surface. In reality, cell death can occur during each phase of the cell cycle; therefore, death rates (β) are included for each cell cycle compartment. The parameter k represents the rate of conversion of cells from one cell cycle phase to the next. Note that the cell cycle phases are subscripted after the appropriate parameter. G2M represents cells in both G2 and M (cells undergoing mitosis) phases while G1+G0 corresponds to cells in both G1 and G0 (quiescent cells). In regards to the rate of conversion (k) of keratinocytes from compartment G1+G0 to compartment S, the subscript G1 is used (instead of G0+G1)

since G0 cells are not cycling. A complete list of parameters for Model A and Equations 6-9 to 6-12 are listed and described in Table 6.1.

6.2.5.2. Three Stage Keratinocyte Differentiation Model: Model B

The creation of a complex, and more realistic three-stage mathematical model (Model B) was developed to more accurately describe the cell cycle kinetics and differentiation process in NHEK. In regards to the modeling dynamics and structure, Model B (Figure 6.2) is quite similar to Model A. However, the main difference between the two models is that stem cells and TA cells are separated into two cell populations, in which each cell population demonstrates its own cell kinetic parameters. In Model B, stem cells (Stage 1) can either cycle or differentiate into TA cells (Stage 2). TA cells which continue to cycle will eventually differentiate further into non-cycling PM cells (Stage 3 of Figure 6.2).

The movement between the four compartments is characterized by the schematic diagram in Figure 6.2 which expresses the accumulation of cells in each compartment and the movement between compartments. The differential equations for Model B are:

$$\frac{dS_{G1+G0}}{dt} = 2(k_{S[G2M]})S_{[G2M]}(1-c) - (k_{S[G1]})S_{[G1+G0]} - (\beta_{S[G1+G0]})S_{[G1+G0]} \quad (6\text{-}13)$$

$$\frac{dS_S}{dt} = (k_{S[G1]})S_{[G1+G0]} - (k_{S[S]})S_{[S]} - (\beta_{S[S]})S_{[S]} \quad (6\text{-}14)$$

$$\frac{dS_{G2M}}{dt} = (k_{S[S]})S_{[S]} - (k_{S[G2M]})S_{[G2M]} - (\beta_{S[G2M]})S_{[G2M]} \quad (6\text{-}15)$$

$$\frac{dTA_{G1+G0}}{dt} = 2(k_{TA[G2M]})TA_{[G2M]} + 2c(k_{S[G2M)})S_{[G2M]} - (k_{TA[G1]})TA_{[G1+G0]} - (\beta_{TA[G1+G0]})TA_{[G1+G0]} \quad (6\text{-}16)$$

$$\frac{dTA_S}{dt} = (1-d)(k_{TA[G1]})TA_{[G1+G0]} - (k_{TA[S]})TA_{[S]} - (\beta_{TA[S]})TA_{[S]} \quad (6\text{-}17)$$

$$\frac{dTA_{G2M}}{dt} = (k_{TA[S]})TA_{[S]} - (k_{TA[G2M]})TA_{[G2M]} - (\beta_{TA[G2M]})TA_{[G2M]} \quad (6\text{-}18)$$

$$\frac{dPM}{dt} = d(k_{TA[G1]})TA_{[G1+G0]} - (\delta_T)PM \quad (6\text{-}19)$$

where S represents the stem cell fraction and TA denotes the transit-amplifying cell fraction in a particular cell cycle phase. Terms within the equations are accompanied with a subscript describing the cell population type (S or TA), and the cell cycle phase in which cell population resides and are depicted in subscripted brackets ([G1], [S], [G2M]) after the denoted population type. After stem cell division, a fraction c of daughter cells differentiate and enter G1+G0 phase of the TA compartment. The remaining cells (fraction 1 – c) re-enter the cycle within the same stem cell compartment. Fraction d of TA cells within G1+G0 differentiate further entering the post-mitotic (PM) compartment, while the remainder of the fraction (1 – d) continues to cycle within the TA cell population. Death rates (β) are included for each cell cycle compartment. The parameter k represents the rate of conversion of cells from one cell cycle phase to the next. In regards to the rate of conversion (k) of keratinocytes from compartment G1+G0 to compartment S, the subscript G1 is used (instead of G0+G1) since G0 cells are not cycling. Finally, the term δ_T represents the rate at which terminally differentiated cornified cells of the PM compartment desquamate from the outer skin surface. A complete set of parameters for Model B and Equations 6-13 to 6-19 are listed and described in Table 6.2.

6.2.6. General Modeling Assumptions and Parameter Estimates

In order to derive analytical equations and parameters to complete our models, I made the following assumptions: (1) The GF parameter was estimated based on previous literature (Heenen and Galand 1997; van Erp *et al.* 1994; van Ruissen *et al.* 1994) and its estimation will be discussed in ensuing sections. (2) Death rate parameters were taken from *in vitro* SHE cell data from Liao *et al.* (2001), and these death rates are assumed to be similar to that in cultured keratinocytes. (3) Death rates are assumed to be the same for cells in each phase of the cell cycle. (4) In Model A, the normal epidermis is in equilibrium, that is, the amount of cells in each stage will eventually reach a state of homeostasis. (5) In Model A, stem and TA cells are lumped into one proliferative stage, therefore, the cell kinetics of all proliferating cells are the average of both TA and stem cells. (6) In Model A, the differentiation rate from TA to PM cells (δ) is assumed to be the same as the desquamation rate (δ_T) during homeostatic conditions. (7) In Model B, the differentiating faction of TA cells, d, enters the PM stage at the same rate in which cells enter S-phase from G1+G0 ($k_{TA[S]}$) within the TA cell population. (8) In Model B, the differentiating fraction of stem cells, c, enters G1+G0 phase of TA cells at the same rate at which G2+M cells enter G1+G0 ($k_{S[G2M]}$) within the stem cell population. (9) In Model B, the fractions of differentiating cells (c and d) were obtained from Kimmel *et al.* (1986) and modified slightly to better simulate the experimental data.

6.2.6.1. Growth Fraction and Differentiation Rate Estimates in NHEK for Model A

Before completing Model A, crucial parameter estimates were required for both δ and GF in order to re-create a realistic modeling system. Fractions of differentiated cells (i.e. post-mitotic keratinocytes) have been measured both *in vivo* and *in vitro* (Clausen *et al.* 1984; Dover and Watt 1987; Kimmel *et al.* 1986; Thorud *et al.* 1988). From these reports, differentiation rates were calculated and are displayed in Table 6.3, 6.4, and 6.5. In general, δ from the literature varied from 0.017-0.09 hr^{-1} and the values used for Model A are comparable to these differentiation rates. GFs are notably much higher *in vitro* when compared to *in vivo* studies, mostly due to the fact that cells in the epidermis have already reached steady state of growth, while cultured keratinocytes grow rapidly and divide freely (without surrounding cell-cell and cell-substratum constraints) before reaching high confluence levels (Heenen and Galand 1997; Loeffler *et al.* 1987; Savill 2003; van Erp *et al.* 1994; van Ruissen *et al.* 1994). In particular, two *in vitro* studies report GF estimates for normal keratinocytes to be 80-95% in subconfluent cultures and 10-30% in cells at or near total confluence (van Erp *et al.* 1994; van Ruissen *et al.* 1994). Since there were a wide range of GF values in the literature, my model simulations applied three different GF parameters (0.4, 0.6, and 0.8). It is important to note, by changing the GF, α will also change; thus, consequently perturbing T_C via Equation 6-2. In reality, T_C should remain constant unless something alters the time to progress through the cell cycle, such as DNA damage that might cause cell cycle blocks or delays. I anticipate one of the estimated GF values will be a relatively accurate estimate for describing NHEK growth properties and cell cycle kinetics. Furthermore, in control cells,

for each GF parameter examined the differentiation rate was optimized to ensure there was a balance of keratinocyte growth and differentiation. If the number of cells in each cell cycle phase stabilizes and remains constant over time, then the model was considered to be in a homeostatic state. Therefore, in the computational simulations, as GF increased, δ must also increase for the cell population to remain at homeostasis.

6.2.6.2. Estimating Parameters used in Model B

To construct Model B, information from the literature was examined to collect all necessary parameters required to best describe NHEK cell cycle kinetics and differentiation. Specifically, experimental data of cultured primary keratinocytes presented previously in the literature was chosen for the model (Staiano-Coico *et al.* 1986). The core interest here was to utilize this data to model both stem and TA cell populations during different growth phases: initial, peak, and plateau. The initial phase represents the first few days after cell seeding at low density and occurs during days 1, 2, 4, and 5 after cell plating. Peak growth describes cells in culture which are growing at exponential rates during days 7, 8, and 9. The plateau growth phase represents cultured cells near total confluence and occurs from days 12-14 to 19-21. For each proliferative population and during each of the three growth phases, T_{pot} (estimated during initial growth only) and GF were adjusted accordingly to most accurately describe normal keratinocyte conditions in culture. In general, it is assumed that as GF fluctuates, so will T_{pot}. For example, T_{pot} is lower when the GF is high since during these conditions there are more cells cycling which decrease the amount of time necessary to double the cell population.

In order to determine accurate NHEK GF parameters of both stem and TA cells I relied on cell cycle distribution and doubling time data from previous studies. Data from Staiano-Coico *et al.* (1986) provides T_{pot} information on both proliferative cell populations during peak and plateau growth phases. Unfortunately, this report does not supply any growth fraction data nor did it provide T_{pot} data during cell initial growth; hence, I was forced to estimate these values. Multiple reports have measured GF to be 80-95% in cultured keratinocytes during exponential or peak growth (Savill 2003; van Erp *et al.* 1994; van Ruissen *et al.* 1994). Therefore, in regards to the TA population, Equation 6-2 was used to calculate T_C from both my assumed GF of 90% and Staiano-Coico's T_{pot} measurements during the peak growth phase. Now that an estimated T_C and a measured T_{pot} value are known, one can solve for α by rearranging Equation 6-2.

$$\alpha = e^{\frac{(Tc)\ln(2)}{Tpot}} \tag{6-20}$$

Once α is calculated, it is possible to calculate the GF of TA cell during the initial and plateau growth phases via Equation 6-3. It is important that once T_C is determined, it remain stable for each cell type and during each growth phase since T_C should not change unless a delay or block in the cell cycle is produced.

It begins to get complicated when addressing the GF of the stem cell population because these cells tend to cycle slower than TA cells. In order to deal with this issue, the assumption was made that T_C is twice as long for stem cells when compared to TA populations. This difference in T_C between the two cell types has been measured in many previous kinetic studies (Dover and Potten 1983; Potten and Bullock 1983; Savill 2003). Therefore, the T_C of stem cells was estimated to be twice that of TA cells, and for each growth phase stem cell GF was determined by calculating α as described above. After all

modeling parameters were in place, transit times (T) and rates of conversion (k) were calculated from the data originating from Staiano-Coico *et al.* (1986) and values for these parameters are displayed in Tables 6.8 and 6.9.

6.2.7. Modeling Software

For modeling purposes in this study, a series of simultaneous differential equations describing the movement of stem cells through compartments of increasing commitment to differentiation and altered proliferative capacity were incorporated into a computer program utilizing the simulation-modeling package Advanced Continuous Simulation Language (ACSL, AEgis Technologies, Huntsville, AL). MatLab (The MathWorks, Natick, MA) was also used in calculating cell kinetic parameters necessary to confirm solutions produced in ACSL. ACSL code for each model is presented in the Appendix.

6.3. Results

6.3.1. Model A Simulations

A simple, two-stage mathematical model was developed to describe cell cycle kinetics and differentiation in NHEK. The purpose of this study was to utilize flow cytometry data to simulate normal dividing and differentiating cells within the epidermis. Once a homeostatic model was developed for control NHEK, data gathered from NHEK treated with arsenic, benzo[*a*]pyrene (BaP) and calcium (Ca^{2+}) were then substituted into the model to examine any alteration of parameters and/or simulations produced by chemical exposure. Previously, my research demonstrated that arsenic and Ca^{2+} increased

T_{pot} (decreasing cell proliferation) in NHEK by 25% and 9% respectively, while BaP decreased T_{pot} (stimulating proliferation) when compared to control cell populations (Perez *et al.* 2003). Thus, it was hypothesized that the data from chemically-treated cells would produce changes in NHEK cell cycle kinetics and squamous differentiation as measured by the quantitation of cornified envelope formation as discussed in Chapter 4. Modeling simulations were carried out for all data at following GF parameter values: 0.4, 0.6, and 0.8. A higher GF value indicates that there are more proliferative or cycling cells within the entire population. All kinetic simulations for Model A were carried out to 50 hours since the data used to derive essential parameters were measured and analyzed using flow cytometry at 0, 2 and 4 hours as described in Materials and Methods and Chapter 4.

6.3.1.1. Chemically-Mediated Effects on the Cell Kinetics of NHEK

In control NHEK, flow cytometric analysis calculated an average T_{pot} of 36.38 hours and the average cell distribution was 60.81%, 25.35%, and 14.48% for G1+G0, S, and G2+M respectively. These data, calculated transit times (T), and rates of conversion (k) for control NHEK at different GF values are displayed in Tables 6.3, 6.4, and 6.5. Figures 6.3A, B, and C display model simulations of cell numbers in each compartment of the model as a function of time. Within all compartments cell totals reach a point of homeostasis. The point of homeostasis (balance between proliferation and differentiation) was determined when the numbers of cells in each phase of the cell cycle remains constant as time increases. The homeostatic levels of each cell cycle compartment were similar but varied at different GF values (Figure 6.3A, B, and C). This is expected since

altered GF will impact T_{pot} and thus changing T_C, consequently, impacting both transit times and rates of conversion throughout the cell cycle.

Flow cytometric results in BaP exposed NHEK display an average T_{pot} of 24.59 hours and an average cell distribution of 63.65%, 23.63%, and 12.74% for G1+G0, S, and G2+M respectively. BaP data were inserted into the model and simulated as depicted in Figure 6.4A, B, and C. The simulations convey a time-dependent increase in cell numbers in every phase of the cell cycle for each GF value examined. As GF increased from 0.4 to 0.8, cell amounts in G1+G0 increased while cell numbers in both S and G2+M decreased. These trends in BaP exposed NHEK could be indicative of a slight build up of cells in G1+G0 displayed in DNA histograms from previous published work (Chapter 4) (Perez *et al.* 2003). In addition, all transit times in BaP exposed cells (T_{G1+G0}, T_S, and T_{G2+M}) were substantially shorter when compared to controls for each GF value tested. BaP-mediated decrease in cell transit times signify increased proliferation rates which may lead to a state of hyperplasia. Also, BaP has demonstrated to inhibit keratinocyte differentiation as presented in Chapter 4, thus, further contributing to the state of hyperplasia. However, time course data of BaP-mediated cornified envelope formation is not available. Therefore, BaP-induced change of the squamous differentiation rate was not incorporated into Model A. All BaP data at varying GF values, including calculated transit times (T) and rates of conversion (k) are shown in Tables 6.3, 6.4, and 6.5.

In arsenic exposed NHEK, flow cytometric results show an average T_{pot} of 58.82 hours and an average cell distribution of 59.66%, 16.0%, and 24.4% for G1+G0, S, and G2+M respectively. When arsenic data was inserted into the model, simulations display a

time-dependent decrease in cell numbers in each cell cycle compartment for every GF parameter tested (Figures 6.5A, B, and C). When comparing transit times from Table 6.3 (GF = 0.8), arsenic treated NHEK T_C, T_{G1+G0}, and T_{G2M} are substantially longer (approximately 1.6-, 1.6-, and 3-fold respectively) than in control cells, while T_S is almost equal in both arsenic exposed and control NHEK. The increase in T_{G1+G0} and T_{G2+M} observed in arsenic treated cells indicates possible cell cycle blocks occurring at G1+G0 and G2+M. As discussed in Chapter 2 and 5, arsenic is known to produce significant DNA damage causing cells to arrest in G1+G0 and G2+M. Also supporting these results, DNA histograms from previous research (Chapter 4) demonstrate arsenic mediated alterations to cell numbers in S and G2+M phase, which may indicate chemically-induced cell cycle arrest (Perez *et al.* 2003). All arsenic data at varying GF values, including calculated transit times (T) and rates of conversion (k) are shown in Tables 6.3, 6.4, and 6.5.

Flow cytometric results in Ca^{2+} exposed NHEK display an average T_{pot} of 39.38 hours and an average cell distribution of 60.3%, 23.46%, and 16.23% for G1+G0, S, and G2+M respectively. After the insertions of Ca^{2+}data into Model A, simulations displayed a slight time-dependent decrease of cell amounts in each cell cycle compartment for every GF parameter examined (Figures 6.6A, B, and C). It is interesting to note in the NHEK model displaying a GF of 0.4, cell amounts in both S and G2+M phase decreased very rapidly after 8 hours into the simulation. This simulated decline in S and G2+M cell numbers is not observed to this extent in Ca^{2+} exposed NHEK with a GF value of 0.6 or 0.8. Ca^{2+} exposed NHEK data, calculated transit times (T), and rates of conversion (k) at different GF parameters are displayed in Tables 6.3, 6.4, and 6.5.

6.3.1.2. Simulating Differentiation in Chemically-Exposed NHEK

It is evident that both BaP and arsenic inhibit NHEK to differentiate (Chapter 4) (Perez *et al.* 2003). However, time course differentiation data (cornified envelope quantification) for either of these chemicals does not exist. Thus, it is uncertain to know the time-dependent impact that BaP and arsenic have in perturbing differentiation rates in NHEK. Therefore, the differentiation conditions (i.e. parameters δ and δ_T) were not changed for any of the chemical treatments during these simulations. In spite of this, all simulations indicate that the amount of PM cells varied due to chemical exposure. For example, simulations demonstrate a time-dependent decrease in PM cells in the arsenic model (Figures 6.5A, B, and C) and a time-dependent increase of PM in the BaP model (Figures 6.4A, B, and C). Nevertheless, only cell cycle kinetic alterations produced these changes since the model did not consider any other factor for which differentiation could be altered. It is possible the chemically-induced changes in cell cycle kinetics could ultimately play a role in differentiation perturbation; however, it is highly probable more factors (i.e. gene expression changes that favor differentiation over proliferation and vice versa) are involved in altering NHEK differentiation which was not considered in this computational model.

6.3.2. Model B Simulations

Model B represents the normal dividing and differentiating NHEK population without considering the effects potentially produced due to chemical exposure. The creation of a complex, and more realistic three-stage mathematical model was developed to more accurately describe the cell cycle kinetics and differentiation process in NHEK. What makes this model more complex is that Model B incorporates two separate

keratinocyte populations (stem and TA cells), two separate differentiating events (represented by parameters c and d), and cell cycle kinetic changes that occur during different cell growth phases (initial, peak, and plateau growth phases). The purpose of this study was to attempt to fit simulated models to the data presented by Staiano-Coico *et al.* (1986) (Tables 6.6 and 6.7). Specifically, this model will attempt to simulate cell movement or kinetics (i.e. track the movement and amount of cells in each cell cycle phase over time) over a 25 day period. After all modeling parameters were in place for Model B (see section 6.2.6.2 for details), transit times (T) and rates of conversion (k) were calculated from the data originating from Staiano-Coico *et al.* (1986) and displayed in (Tables 6.8 and 6.9).

Overall, computer simulation efforts could not accurately validate the experimental data as a whole; however, the model did display certain trends that imitate portions of the data. The experimental cell number data for the G1+G0 stem cell compartment was simulated very well with this mathematical model (Figure 6.7). Unfortunately, simulations for the two subsequent stem cell compartments (S and G2+M) did not match up well with the data; however, the computer simulation does mimic portions of the data (Figures 6.8 and 6.9). After closer examination the of computer simulations, it seems stem cells are entering into both S and G2+M at a much faster rate than the experimental data depicts. However, the transit times and rates of conversion within the stem cells compartment were calculated from this data so it is unusual to observe such a discrepancy. The observed divergence between experimental data and computer simulations could be due to inaccurate parameters estimations as discussed later in this section. Figure 6.10 depicts an overestimated simulation for the number of

cells in G1+G0 within the TA cell population. However, this overestimation is necessary in order to validate the cell number data in subsequent TA cells compartments S and G2+M (Figures 6.11 and 6.12). This inconsistency between simulations and the data observed in the G1+G0 compartment of TA cells could be related to an inaccurate differentiation fraction value (c or d) or due to more inaccurate parameter values used in this or previous compartments. As discussed previously, parameters such as GF, T_C, β, d, and c (among others) were all estimated and/or taken from other literature sources. In addition, some calculated parameters used in Model B were derived from these estimated parameters. Therefore, these issues could explain why the computer simulation efforts did not accurately validate the experimental data as a whole.

It is interesting to note that TA cell cycle compartment simulations (Figures 6.10, 6.11, and 6.12) fit better to the data than did simulations of cell cycle compartments within stem cells (Figures 6.7, 6.8, and 6.9). This could be due to the fact that the majority of dividing cells are TA cells, thus, possibly concealing the cell kinetic effects produced by stem cells. Also, kinetic parameter changes that occur as cells enter each growth phase is evident from erratic and sometimes jagged simulation curves. For the most part, adjusting rate of conversion (k) parameters can greatly influence the simulation alterations observed during different growth phases. The buildup of PM cells is displayed in Figure 6.13 and is dependent on the differentiating fraction (d) of TA cells and the rate of d exiting this compartment.

After estimating GF and T_C values to the best of my ability, differentiating cell fraction parameters (c and d) were adjusted in attempt to simulate the data. Kimmel *et al.* (1986) measured d which ranged from 0.28 to 0.56 (averaged 0.45) while assuming c to

be between 0.1 and 0.5. The most important aspect to consider while changing parameters is to retain a semblance of reality, i.e. avoid selecting improbable parameter values. For Model B, the assumption was made that the differentiating fractions (c and d) change during each growth phase for both stem and TA cells (Tables 6.6 and 6.7). Altering both differentiation parameters at each growth phase was necessary in order to produce the computer simulations that validate the data in three of the six cell cycle compartments. After all modifications were complete, differentiation fraction parameters displayed in Tables 6.6 and 6.7 produced the best model simulations while maintaining realistic values. Through trial and error parameter estimation, it is evident that slight changes to either c or d greatly influent the dynamics of the model as a whole, especially those compartments which are directly connected by these parameters.

Unfortunately, simulations do not provide a complete reproduction of the experimental data for each compartment. The assumptions made concerning GF and T_C of stem cells, if imprecise, could influence all consequential parameters, thus rendering model validation almost impossible. Also, combining data from several different studies is not an ideal situation; however, this was the only option since no study exists that conducted experimentation to gather all the data necessary to accurately describe this system. Therefore, it seems the coupling of 15 to 25 year old literature data from various sources and parameter estimation is likely the cause for the observed simulation imprecision. Nevertheless, I firmly believe the model structure itself (with a few minor modifications) is very capable of describing NHEK cell kinetics and differentiation. Although, attempting to validate this model to the experimental data was a difficult task as there are many uncertain parameters, the creation of a model such as this will be

extremely valuable in highlighting data requirements for researchers who intend to mathematically model keratinocyte systems in the future.

6.4. Discussion

Initial modeling efforts of the process of squamous differentiation in keratinocytes *in vitro* are fairly simple descriptions of stem and TA cell movements through compartments of increasing commitment to differentiation and altered proliferative capacity. Two model versions were conceptualized, A and B; both models were developed, parameterized, and can be used to better understand and predict the rate of growth and extent of differentiation as a function of time in control keratinocyte cultures and those treated with BaP, arsenic and Ca^{2+}. In regards to Model A, key biological processes for which data was available in our laboratory were individually described, while non-essential components (or those for which we do not yet have sufficient data to support a more detailed description) was collapsed together into a single appropriate compartment (Stage 1 of Model A) (Figure 6.1). There are several advantages to Model A, the first being that it follows the Law of Parsimony, i.e., simple is better unless proven otherwise. Secondly, Model A facilitates early incorporation of extensive data that was generated in the laboratory for growth and differentiation of NHEK populations in the absence and presence of BaP, arsenic and Ca^{2+} (Chapter4). However, as discussed by Savill (2003), assuming a homogeneous cycling population in the epidermis and assigning average cell cycle times is not the most biologically plausible approach to this problem. As a population of cells goes through the differentiation process, at each different time step, the various fractions of cells in this population will change. Thus, to more accurately describe the complex biology behind the process of squamous

differentiation and to dissect more closely where the chemically-mediated perturbations are occurring, one can subsequently focus on the more complex model that was developed, Model B. Model B is an integration of various differentiation models described previously for keratinocytes or other cell types in culture (Boucher *et al.* 2001; Kimmel *et al.* 1986; Liao *et al.* 2001; Yakovlev *et al.* 1998). Model B provides a more complete picture of the events that occur as keratinocytes grow and differentiate. Unfortunately, vital parameters and other details to describe this modeling system are incomplete, thus, requiring further experimentation to fill in these critical data gaps.

Currently there are numerous groups who have utilized mathematical modeling to describe cell cycle kinetics in many cell types. However, very few complete models have been developed for keratinocytes either *in vivo* or *in vitro*. Describing the skin mathematically becomes complicated in that the model must encompass several different cell types and the conversion of one cell type to another through differentiation. The most complex model (Model B) only describes three of the five potential cell types of keratinocytes within the epidermis, namely stem, TA, and PM cells. Stem and TA cells represent keratinocytes which reside in the basal layer of the epidermis while PM cells represents 3 to 4 differentiated cell types that lie within the stratum spinosum, stratum granulosum, stratum lucidum, and the stratum corneum. Since these cells are non-cycling they have little impact on cell cycle kinetics and cell growth. As a result, skin modelers commonly lump all PM cells into one compartment as I have done in both models. It is likely unnecessary to divide the different PM cell types into different compartments due to the fact that all PM cells behave in a similar manner from a modeling standpoint. In actuality, keratinocyte terminal differentiation is a type of prolonged cell death. The only

issue to address for PM cells is the fact that eventually cell death and desquamation occur when cells from the stratum granulosum become cornified and ultimately slough off the outer most layer of the skin. In contrast to non-cycling keratinocytes, it may be necessary to separate both proliferating stem and TA cell populations into their own compartment. Additionally, TA cells go through multiple divisions within this compartment prior to arresting, and it is not clear that these cells are a homogeneous population themselves. Although, there are few skin models which disconnect stems cells from TA cell, it may be necessary since each cell population encompasses very different cell kinetic parameters when compared with each other (Kimmel *et al.* 1986; Staiano-Coico *et al.* 1989; Staiano-Coico *et al.* 1986). If one divides these two proliferative populations, consequently the model becomes twice as complex. There are now twice as many factors to link together which could influence the end results of the modeling simulations. Consequently, if one parameter is not optimum in the beginning of the model, results in subsequent compartments could be drastically altered, thus, depicting a model which is far from the truth.

Another reason the skin is a difficult system to model is because the modeler must incorporate the differentiation process and its regulators and link it with each proliferative compartment. Keratinocyte differentiation itself is a complex process in which the mechanistic details cannot be described using relatively simple models. According to literature, differentiation can initiate at any phase of the cell cycle (Jensen *et al.* 1999); however, evidence indicates that basal cells differentiate from G1+G0 phase only (Kirkhus and Clausen 1990; Thorud *et al.* 1988). There are several biological phenomena that likely contribute to the degree of differentiation in keratinocyte cultures, but for

which data is currently unavailable or is technically difficult to acquire. An awareness of these issues are important in that the most realistic and useful models of the differentiation process will eventually require their consideration. For example, it is assumed in skin that only a small fraction of the stem cells are actively cycling, i.e. the remainder are in G0. The fraction of cycling stem cells is thought to be highly important in models describing *in vivo* growth and differentiation of keratinocytes, such as that developed by Savill (2003). However, there is currently no estimate for the proliferative stem cell fraction *in vivo*. *In vitro*, differentiating between G0 (non-cycling) and G1 (cycling) cells in the low RNA (stem cell) population would require simultaneous analysis for RNA content and expression of a marker for proliferation such as Ki-67 (Staiano-Coico *et al.* 1989; van Erp *et al.* 1994). Although not impossible, these experiments would likely require extensive optimization. Additionally, it is likely that keratinocytes undergo apoptosis in all phases of the cell cycle and that these "phase-specific" death rates are not uniform. Even total death rates are notoriously low and difficult to measure accurately in many cells populations (Bertuzzi *et al.* 1997; Liao *et al.* 2001; Norrby and Mellgren 1971). Until reports are able to demonstrate that these individual death rates are more important for accurately describing keratinocyte growth and differentiation in culture, modelers will continue to work with the more simplistic assumption that death rates in stem and TA cells are negligible and uniform and that the majority of death in untreated populations will be due to terminal differentiation of granular cells and eventual desquamation.

The computational mathematical models presented herein were created to describe the cell cycle kinetics and differentiation process in NHEK. Cell cycle kinetic

parameters were modeled over time in control cultures, and those exposed to BaP, arsenic, Ca^{2+}, to allow description of the relationship between the opposing processes of proliferation and differentiation in each case. Model A, used data from both flow cytometric data (Chapter 4) and parameters from the literature, while Model B was created exclusively from data presented by Staiano-Coico *et al.* (1986) and other parameters gathered from the literature as discussed above. Although, these models were constructed using incomplete data, future research could find these models extremely useful when conceptualizing necessary experiments in order to gather all essential data to accurately simulate the system that is being modeled. Eventually, the body of knowledge that accumulates on how quantitative changes in the normal rates of differentiation and proliferation induced by a variety of agents are related to one another, to specific gene expression changes, and to transformation will facilitate characterization/analysis of other unknown agents that exhibit the same behavior. In future studies, it will be extremely important to validate these mathematical models with experiments that generate all the necessary data to precisely describe the growth, cell cycle kinetics, and differentiation processes in NHEK.

6.5. References

Aarnaes, E., Clausen, O. P., Kirkhus, B., and De Angelis, P. (1993). Heterogeneity in the mouse epidermal cell cycle analysed by computer simulations. *Cell Prolif.* **26**, 205-219.

Aarnaes, E., Kirkhus, B., and Clausen, O. P. (1990). Mathematical model analysis of mouse epidermal cell kinetics measured by bivariate DNA/anti-bromodeoxyuridine flow cytometry and continuous [3H]-thymidine labelling. *Cell Tissue Kinet.* **23**, 409-424.

Basse, B., Baguley, B. C., Marshall, E. S., Joseph, W. R., Van Brunt, B., Wake, G., and Wall, D. J. (2003). A mathematical model for analysis of the cell cycle in cell lines derived from human tumors. *J.Math.Biol.* **47**, 295-312.

Begg, A. C., McNally, N. J., Shrieve, D. C., and Karcher, H. (1985). A method to measure the duration of DNA synthesis and the potential doubling time from a single sample. *Cytometry* **6**, 620-626.

Bertuzzi, A., Gandolfi, A., Sinisgalli, C., Starace, G., and Ubezio, P. (1997). Cell loss and the concept of potential doubling time. *Cytometry* **29**, 34-40.

Boucher, K., Zorin, A., Yakovlev, A. Y., Mayer-Proschel, M., and Noble, M. (2001). An alternative stochastic model of generation of oligodendrocytes in cell culture. *J.Math.Biol.* **43**, 22-36.

Clausen, O. P., Aarnaes, E., Kirkhus, B., Pedersen, S., Thorud, E., and Bolund, L. (1984). Subpopulations of slowly cycling cells in S and G2 phase in mouse epidermis. *Cell Tissue Kinet.* **17**, 351-365.

Dover, R., and Potten, C. S. (1983). Cell cycle kinetics of cultured human epidermal keratinocytes. *J.Invest Dermatol.* **80**, 423-429.

Dover, R., and Watt, F. M. (1987). Measurement of the rate of epidermal terminal differentiation: expression of involucrin by S-phase keratinocytes in culture and in psoriatic plaques. *J.Invest Dermatol.* **89**, 349-352.

Hartwell, L. H., Hopfield, J. J., Leibler, S., and Murray, A. W. (1999). From molecular to modular cell biology. *Nature* **402**, C47-C52.

Heenen, M., and Galand, P. (1997). The growth fraction of normal human epidermis. *Dermatology* **194**, 313-317.

Jensen, U. B., Lowell, S., and Watt, F. M. (1999). The spatial relationship between stem cells and their progeny in the basal layer of human epidermis: a new view based on whole-mount labelling and lineage analysis. *Development* **126**, 2409-2418.

Kimmel, M., Darzynkiewicz, Z., and Staiano-Coico, L. (1986). Stathmokinetic analysis of human epidermal cells *in vitro*. *Cell Tissues Kinet.* **19**, 289-304.

Kirkhus, B., and Clausen, O. P. (1990). Cell kinetics in mouse epidermis studied by bivariate DNA/bromodeoxyuridine and DNA/keratin flow cytometry. *Cytometry* **11**, 253-260.

Larsen, J. K. (1994). Measurement of cytoplasmic and nuclear antigens. In Flow Cytometry: A Practical Approach, pp. 93-117. Oxford University Press, Oxford.

Liao, K. H., Gustafson, D. L., Fox, M. H., Chubb, L. S., Reardon, K. F., and Yang, R. S. (2001). A biologically based model of growth and senescence of Syrian hamster embryo (SHE) cells after exposure to arsenic. *Environ.Health Perspect.* **109**, 1207-1213.

Loeffler, M., Potten, C. S., and Wichmann, H. E. (1987). Epidermal Cell Proliferation: A Comprehensive Mathematical Model of Cell Proliferation and Migration in the Basal

Layer predicts some Unusual Properties of Epidermal Stem Cells. *Virchows Arch B* **53**, 286-300.

Norrby, K., and Mellgren, J. (1971). Birth, death and net growth of normal, transforming, neoplastic and malignant cell lines. Decrease of death rate in neoplastic alteration. *Pathol.Eur.* **6**, 56-74.

Perez, D. S., Armstrong-Lea, L., Fox, M. H., Yang, R. S., and Campain, J. A. (2003). Arsenic and benzo[a]pyrene differentially alter the capacity for differentiation and growth properties of primary human epidermal keratinocytes. *Toxicol.Sci.* **76**, 280-290.

Potten, C. S., and Bullock, J. C. (1983). Cell kinetic studies in the epidermis of the mouse. I. Changes in labeling index with time after tritiated thymidine administration. *Experientia* **39**, 1125-1129.

Potten, C. S., Wichmann, H. E., Loeffler, M., Dobek, K., and Major, D. (1982). Evidence for discrete cell kinetic subpopulations in mouse epidermis based on mathematical analysis. *Cell Tissue Kinet.* **15**, 305-329.

Savill, N. J. (2003). Mathematical models of hierarchically structured cell populations under equilibrium with application to the epidermis. *Cell Prolif.* **36**, 1-26.

Staiano-Coico, L., Darzynkiewicz, Z., and McMahon, C. K. (1989). Cultured human keratinocytes: discrimination of different cell cycle compartments based upon measurement of nuclear RNA or total cellular RNA content. *Cell Tissue Kinet.* **22**, 235-243.

Staiano-Coico, L., Higgins, P. J., Darzynkiewicz, Z., Kimmel, M., Gottlieb, A. B., Pagan-Charry, I., Madden, M. R., Finkelstein, J. L., and Hefton, J. M. (1986). Human keratinocyte culture. Identification and staging of epidermal cell subpopulations. *J.Clin.Invest* **77**, 396-404.

Steel, G. G. (1977). Growth kinetics of tumors: cell population kinetics in relation to the growth and treatment of cancer. In Basic theory of growing cell populations, pp. 57-85. Clarendon Press, Oxford.

Takahashi, M. (1968). Theoretical basis for cell cycle analysis: II. Further studies on labelled mitosis wave method. *J.Theor.Biol.* **18**, 195-209.

Thorud, E., Clausen, O. P., and Aarnaes, E. (1988). Turnover and maturation kinetics in the hairless mouse epidermis. Continuous [3H]TdR labelling and mathematical model analyses. *Cell Tissue Kinet.* **21**, 301-314.

Tyson, J. J., Csikasz-Nagy, A., and Novak, B. (2002). The dynamics of cell cycle regulation. *BioEssays* **24**, 1095-1109.

van Erp, P. E., de Jongh, G. J., Boezeman, J. B., and Schalkwijk, J. (1994). The growth and differentiation of human keratinocytes in vitro: a combined immunohistochemical and flow cytometric study. *Arch.Dermatol.Res.* **286**, 115-122.

van Ruissen, F., van Erp, P. E., de Jongh, G. J., Boezeman, J. B., van de Kerkhof, P. C., and Schalkwijk, J. (1994). Cell kinetic characterization of growth arrest in cultured human keratinocytes. *J Cell Sci.* **107 (Pt 8)**, 2219-2228.

Wilson, G. D. (1994a). Analysis of DNA - measurement of cell kinetics by the bromodeoxyuridine/anti-bromodeoxyuridine method. In Flow cytometry: a practical approach (M.G.Ormerod, ed., pp. 137-156. Oxford University Press, New York.

Wilson, G. D. (1994b). Flow Cytometry: A Practical Approach. In Analysis of DNA-measurement of cell kinetics by the bromodeoxyuridine/anti-bromodeoxyuridine method, pp. 137-156. Oxford University Press, Oxford.

Yakovlev, A. Y., Boucher, K., Mayer-Proschel, M., and Noble, M. (1998). Quantitative insight into proliferation and differentiation of oligodendrocyte type 2 astrocyte progenitor cells in vitro. *Proc.Natl.Acad.Sci.U.S.A* **95**, 14164-14167.

6.6. Appendix A: ACSL Code for Model A - NHEK Cell Cycle Kinetics and Differentiation

```
!This program was written in ACSL to simulate a simple, two stage cell cycle kinetic and differentiation
!model of NHEK (Figure 6.1). Stem and transit-amplifying cells are lumped into one compartment and the
!cell numbers in each compartment were simulated over time. Differentiation rate (TD and delta), growth
!fraction (GF), and death rate (beta) parameters were estimated as discussed in Chapter 6. Control Tpot and
!cell distribution data gathered from flow cytometry analysis was averaged and inserted into Model A.
!From this data, cell phase transit times (T) and rates of conversion (k) were calculated in this model as
!described in Chapter 6.
!*Note this is the exact same model used in simulating BaP, arsenic, and calcium exposed NHEK, except
!values for Tpot and cell distribution data from each chemical treatment were inserted. As there are no cell
!cycling, the GF increases. To vary NHEK GF this Constant was simply changed from 0.4 to 0.6 and to 0.8.
!ACSL file CC2.csl

PROGRAM

INITIAL
  !Data
      N=30000.0              !Total number of cells analyzed by flow cytometry

   !Average percent of cells in each cell cycle phase from flow cytometry data
      CONSTANT G=60.18       !G=G1+G0 cells
      CONSTANT S=25.35       !S=S phase cells
      CONSTANT M=14.48       !M=G2+M cells

      CONSTANT Tpot=36.38    !Average potential doubling time (Tpot)
      CONSTANT GF=0.4        !GF=growth fraction (GF) *Estimated

  !Estimated parameters from literature
      CONSTANT beta=0.0000983    !death rate (1/h) divided by 3 for each cycle phase
      CONSTANT delta=0.1007      !Estimated differentiation rate from Kimmel et al. 1986...
                                 !...and from Dover et al. 1987
      TD=delta                   !TD=Desquamation rate

  !Calculations

      a=GF+1                     !"a" is number of cycling daughter cells for each division...
                                 !...from a mother cell
      Tc=(log(a)/log(2.0))*Tpot !Calculating Tc (cell cycle time) using Steel's equation

   !Calculating the fraction of cells (F) in each cell cycle phase
      FG=N*(G/100.0)
      FS=N*(S/100.0)
      FM=N*(M/100.0)

   !Calculating average cell transit times (T) through each cell cycle phase

      TG=-(Tc/log(a))*(log((1.0-((a-1.0)/a)*(G/100.0))))
      TS=-(Tc/log(a))*(log((exp(-TG/Tc*log(a))-((a-1.0)/a)*(S/100.0))))-TG
```

```
        TM=Tc-TG-TS

    !Calculating rate of conversion (1/hr)
        KG=1.0/(TG+beta)
        KS=1.0/(TS+beta)
        KM=1.0/(TM+beta)


        TSTOP=50.0              !Experiment length (hrs)
        POINTS = 100.0          !Communication intervals
        CINT=TSTOP/POINTS       !Length of communication intervals

END     !End of Initial segment

DYNAMIC                 !Beginning of execution section


  DERIVATIVE
    !amount "A" of cells in G1 (G)
        RAG = 2*KM*AM-KG*AG-beta*AG-delta*AG
        AG = INTEG(RAG,FG)          !FG=fraction of cells in G at 0hr

    !amount "A" of cells in S (S)
        RAS = KG*AG-KS*AS-beta*AS
        AS = INTEG(RAS,FS)          !FS=fraction of cells in S at 0hr

    !amount "A" of cells in G2+M (M)
        RAM = KS*AS-KM*AM-beta*AM
        AM = INTEG(RAM,FM)          !FM=fraction of cells in M at 0hr

    !amount "A" of differentiated post-mitotic cells (P)
        RAP = delta*AG-beta*AP-TD*AP
        AP = INTEG(RAP,0.0)

        TERMT (T.GE.TSTOP)          !Condition for terminating simulation

  END  !End Derivative block

END     !End of Dynamic section

END     !End of Program
```

```
!ACSL command file for control data – Model A
!File CC2.cmd

output T AG AS AM AP

Prepare T, AG, AM, AP, AS
Data expl &
(T, AG)
0.0 16470.0
2.0 19110.0
4.0 19620.0
End
```

```
Data exp2 &
(T, AS)
0.0 8340.0
2.0 7590.0
4.0 7500.0
END

Data exp3 &
(T, AM)
0.0 5190.0
2.0 3300.0
4.0 2880.0
END

START
proc P1
        plot/data=expl/Character=2 AG      !Plot amount of cells in G
END
proc P2
        plot/data=exp2/Character=2 AS      !Plot amount of cells in S
END
proc P3
        plot/data=exp3/Character=2 AM      !Plot amount of cells in M
END
proc P4
        plot/data=exp4/character=2 AP      !Plot amount of differentiated cells-P
END
proc p5
        plot/data=exp5/character=2 AG AS AM AP  !Combine all plots
END

END
```

6.7. Appendix B: ACSL Code for Model B – NHEK Cell Cycle Kinetics and Differentiation

```
!This program was written in ACSL to simulate a complex, three stage cell cycle kinetic and differentiation
!model of NHEK (Figure 6.2). In contrast to Model A, stem and transit-amplifying cells are divided into
!separate compartments, in which cell numbers in each compartment were simulated over time. The
!following parameters were estimated as discussed in Chapter 6: Differentiation rate (TD), growth fractions
!(isGF, sGF, psGF, itGF, tGF, and ptGF), potential doubling time (isTpot and itTpot), and death rate (beta).
!Data used to create this model was taken from Staiano-Coico et al. (1986). Primarily, Tpot and cell
!distribution data from both stem and TA cells and from each of the three growth phases were modeled.
!From this data, cell phase transit times (T) and rates of conversion (k) were calculated in this model as
!described in Chapter 6.
!ACSL file CC2.csl

PROGRAM
        !Initial growth phase - Days 1, 2, 4, & 5
        !Peak growth phase - Days 7, 8, & 9
        !Plateau growth phase - Days 12-14 & 19-21 and are denoted as 13 & 20 respectively

INITIAL
 !Data from Staiano-Coico et al. (1986)

        CONSTANT N=10000.0   !N = total number of cells at time zero

  !Cell distribution of stem cell populations (%) and cell fractions (F)
    !Percent of stem cells (s) in each cell cycle phase
     !Day 1
        CONSTANT sG1=97.1     !G = G1 phase (%)
        CONSTANT sS1=1.1      !S = S phase (%)
        CONSTANT sM1=1.8      !M = G2+M phases (%)
        CONSTANT st1=95.2     !stem cell (st) total (%)
        Fst1=N*(st1/100.0)          !Fraction of stem cells within the entire population
        FsG1=Fst1*(sG1/100.0)  !Fraction of stem cells in G1 phase
        FsS1=Fst1*(sS1/100.0)  !Fraction of stem cells in S phase
        FsM1=Fst1*(sM1/100.0)  !Fraction of stem cells in G2M phases

     !Day 2
        CONSTANT sG2=95.8
        CONSTANT sS2=1.9
        CONSTANT sM2=2.3
        CONSTANT st2=86.0
        Fst2=N*(st2/100.0)
        FsG2=Fst2*(sG2/100.0)
        FsS2=Fst2*(sS2/100.0)
        FsM2=Fst2*(sM2/100.0)

     !Day 4
        CONSTANT sG4=91.5
        CONSTANT sS4=5.7
        CONSTANT sM4=2.9
```

```
        CONSTANT st4=63.7
        Fst4=N*(st4/100.0)
        FsG4=Fst4*(sG4/100.0)
        FsS4=Fst4*(sS4/100.0)
        FsM4=Fst4*(sM4/100.0)

!Day 5
        CONSTANT sG5=78.5
        CONSTANT sS5=17.0
        CONSTANT sM5=4.6
        CONSTANT st5=50.5
        Fst5=N*(st5/100.0)
        FsG5=Fst5*(sG5/100.0)
        FsS5=Fst5*(sS5/100.0)
        FsM5=Fst5*(sM5/100.0)

!Day 7
        CONSTANT sG7=68.0
        CONSTANT sS7=24.0
        CONSTANT sM7=8.0
        CONSTANT st7=26.8
        Fst7=N*(st7/100.0)
        FsG7=Fst7*(sG7/100.0)
        FsS7=Fst7*(sS7/100.0)
        FsM7=Fst7*(sM7/100.0)

!Day 8
        CONSTANT sG8=74.6
        CONSTANT sS8=18.0
        CONSTANT sM8=7.4
        CONSTANT st8=17.5
        Fst8=N*(st8/100.0)
        FsG8=Fst8*(sG8/100.0)
        FsS8=Fst8*(sS8/100.0)
        FsM8=Fst8*(sM8/100.0)

!Day 9
        CONSTANT sG9=69.1
        CONSTANT sS9=23.2
        CONSTANT sM9=7.7
        CONSTANT st9=28.5
        Fst9=N*(st9/100.0)
        FsG9=Fst9*(sG9/100.0)
        FsS9=Fst9*(sS9/100.0)
        FsM9=Fst9*(sM9/100.0)

!Day 12-14 (referred to as day 13)
        CONSTANT sG13=76.8
        CONSTANT sS13=13.1
        CONSTANT sM13=10.2
        CONSTANT st13=51.4
        Fst13=N*(st13/100.0)
        FsG13=Fst13*(sG13/100.0)
        FsS13=Fst13*(sS13/100.0)
        FsM13=Fst13*(sM13/100.0)
```

```
  !Day 19-21 (referred to as days 20)
        CONSTANT sG20=78.8
        CONSTANT sS20=12.7
        CONSTANT sM20=8.5
        CONSTANT st20=56.8
        Fst20=N*(st20/100.0)
        FsG20=Fst20*(sG20/100.0)
        FsS20=Fst20*(sS20/100.0)
        FsM20=Fst20*(sM20/100.0)

!Cell distribution of transit-amplifying (TA) cells
  !Percent of TA cells (t) in each cell cycle phase
  !Day 1
        CONSTANT tG1=100.0   !G = G1 phase (%)
        CONSTANT tS1=0.0     !S = S phase (%)
        CONSTANT tM1=0.0     !M = G2+M phases (%)
        CONSTANT t1=4.8      !TA cell total (%)
        Ft1=N*(t1/100.0)     !Fraction of TA cells within the entire population
        FtG1=Ft1*(tG1/100.0) !Fraction of TA cells in G1 phase
        FtS1=Ft1*(tS1/100.0) !Fraction of TA cells in s phase
        FtM1=Ft1*(tM1/100.0) !Fraction of TA cells in G2M phases

  !Day 2
        CONSTANT tG2=94.7
        CONSTANT tS2=1.7
        CONSTANT tM2=3.6
        CONSTANT t2=14.0
        Ft2=N*(t2/100.0)
        FtG2=Ft2*(tG2/100.0)
        FtS2=Ft2*(tS2/100.0)
        FtM2=Ft2*(tM2/100.0)

  !Day 4
        CONSTANT tG4=80.7
        CONSTANT tS4=9.0
        CONSTANT tM4=10.3
        CONSTANT t4=37.3
        Ft4=N*(t4/100.0)
        FtG4=Ft4*(tG4/100.0)
        FtS4=Ft4*(tS4/100.0)
        FtM4=Ft4*(tM4/100.0)

  !Day 5
        CONSTANT tG5=71.1
        CONSTANT tS5=14.9
        CONSTANT tM5=14.9
        CONSTANT t5=49.5
        Ft5=N*(t5/100.0)
        FtG5=Ft5*(tG5/100.0)
        FtS5=Ft5*(tS5/100.0)
        FtM5=Ft5*(tM5/100.0)

  !Day 7
        CONSTANT tG7=58.3
        CONSTANT tS7=22.3
        CONSTANT tM7=19.4
```

```
        CONSTANT t7=65.1
        Ft7=N*(t7/100.0)
        FtG7=Ft7*(tG7/100.0)
        FtS7=Ft7*(tS7/100.0)
        FtM7=Ft7*(tM7/100.0)

    !Day 8
        CONSTANT tG8=64.2
        CONSTANT tS8=22.1
        CONSTANT tM8=13.7
        CONSTANT t8=73.2
        Ft8=N*(t8/100.0)
        FtG8=Ft8*(tG8/100.0)
        FtS8=Ft8*(tS8/100.0)
        FtM8=Ft8*(tM8/100.0)

    !Day 9
        CONSTANT tG9=59.3
        CONSTANT tS9=23.0
        CONSTANT tM9=18.7
        CONSTANT t9=64.8
        Ft9=N*(t9/100.0)
        FtG9=Ft9*(tG9/100.0)
        FtS9=Ft9*(tS9/100.0)
        FtM9=Ft9*(tM9/100.0)

    !Day 12-14 (13)
        CONSTANT tG13=52.8
        CONSTANT tS13=32.1
        CONSTANT tM13=15.1
        CONSTANT t13=42.2
        Ft13=N*(t13/100.0)
        FtG13=Ft13*(tG13/100.0)
        FtS13=Ft13*(tS13/100.0)
        FtM13=Ft13*(tM13/100.0)

    !Day 19-21 (20)
        CONSTANT tG20=66.8
        CONSTANT tS20=17.7
        CONSTANT tM20=15.5
        CONSTANT t20=38.1
        Ft20=N*(t20/100.0)
        FtG20=Ft20*(tG20/100.0)
        FtS20=Ft20*(tS20/100.0)
        FtM20=Ft20*(tM20/100.0)


!Potential doubling time (Tpot) [days]
 !Stem cells (s)
        CONSTANT isTpot=6.25        !150hr;Tpot of stem cells in initial growth (i) *Estimated
        CONSTANT sTpot=4.1667       !100hr;Tpot of stem cells in peak growth
        CONSTANT psTpot=10.4167     !250hr;Tpot of stem cells in plateau growth (p)
 !TA cells (t)
        CONSTANT itTpot=1.458       !35hr;Tpot of TA cells in initial growth (i) *Estimated
        CONSTANT tTpot=1.25         !30hr;Tpot of TA cells in peak growth
        CONSTANT ptTpot=1.667       !40hr;Tpot of TA cells in plateau growth (p)
```

```
!Growth fraction (GF) *Estimated
 !Stem cells (s)
      CONSTANT isGF=0.2925          !GF of stem cells in initial growth (i)
      CONSTANT sGF=0.4695           !GF of stem cells in peak growth
      CONSTANT psGF=0.16646         !GF of stem cells in the plateau growth (p)
 !TA cells (t)
      CONSTANT itGF=0.733  !GF of TA cells in initial growth (i)
      CONSTANT tGF=0.9     !GF of TA cells in peak growth
      CONSTANT ptGF=0.617 !GF of TA cells in plateau growth (p)

!"a" is number of cycling daughter cells for
 !Stem cells (s) cell division
      isa=isGF+1.0      !During initial (i) growth of stem cells
      sa=sGF+1.0        !During peak growth of stem cells
      psa=psGF+1.0      !During plateau (p) growth phase of stem cells
 !TA cells (t) cell division
      ita=itGF+1.0      !During initial (i) growth of TA cells
      ta=tGF+1.0        !During peak growth of TA cells
      pta=ptGF+1.0      !During plateau (p) growth phase of TA cells

 !Calculating cell cycle time (Tc)
 !Stem cells (s)
      isTc=(log(isa)/log(2.0))*isTpot              !Initial growth
      sTc=(log(sa)/log(2.0))*sTpot                 !Peak growth
      psTc=(log(psa)/log(2.0))*psTpot              !Plateau growth
 !TA cells (t)
      itTc=(log(ita)/log(2.0))*itTpot              !Initial growth
      tTc=(log(ta)/log(2.0))*tTpot                 !Peak growth
      ptTc=(log(pta)/log(2.0))*ptTpot              !Plateau growth

      CONSTANT beta=0.00101136      !Death rate converted into days (1/day)..
                                    !..and divided by 7 for each compartment
 !Differentiating fraction from Kimmel et al. (1986)
      CONSTANT c=0.55       !Fraction of stem cells that differentiate into TA cells
      CONSTANT d=0.55       !Fraction of TA cells that differentiate into post-mitotic cells
      !TD=0.                !Rate desquamation (TD)


!Calculating STEM CELL (s) transit times (T)

 !Substitute "y", "z", & "o" to shorten equation length (80 character limit per line)
      y=(isTc/log(isa))          !"y" is used during initial growth
      z=(sTc/log(sa))            !"z" is used during peak growth
      o=(psTc/log(psa))          !"o" is used during plateau growth phase

 !Day 1
      sTG1=-y*(log((1.0-((isa-1.0)/isa)*(sG1/100.0))))
      sTS1=-y*(log((exp(-sTG1/isTc*log(isa))-((isa-1.0)/isa)*(sS1/100.0))))-sTG1
      sTM1=isTc-sTG1-sTS1

 !Day 2
      sTG2=-y*(log((1.0-((isa-1.0)/isa)*(sG2/100.0))))
      sTS2=-y*(log((exp(-sTG2/isTc*log(isa))-((isa-1.0)/isa)*(sS2/100.0))))-sTG2
      sTM2=isTc-sTG2-sTS2
```

```
!Day 4
      sTG4=-y*(log((1.0-((isa-1.0)/isa)*(sG4/100.0))))
      sTS4=-y*(log((exp(-sTG4/isTc*log(isa))-((isa-1.0)/isa)*(sS4/100.0))))-sTG4
      sTM4=isTc-sTG4-sTS4

!Day 5
      sTG5=-y*(log((1.0-((isa-1.0)/isa)*(sG5/100.0))))
      sTS5=-y*(log((exp(-sTG5/isTc*log(isa))-((isa-1.0)/isa)*(sS5/100.0))))-sTG5
      sTM5=isTc-sTG5-sTS5

!Day 7
      sTG7=-z*(log((1.0-((sa-1.0)/sa)*(sG7/100.0))))
      sTS7=-z*(log((exp(-sTG7/sTc*log(sa))-((sa-1.0)/sa)*(sS7/100.0))))-sTG7
      sTM7=sTc-sTG7-sTS7

!Day 8
      sTG8=-z*(log((1.0-((sa-1.0)/sa)*(sG8/100.0))))
      sTS8=-z*(log((exp(-sTG8/sTc*log(sa))-((sa-1.0)/sa)*(sS8/100.0))))-sTG8
      sTM8=sTc-sTG8-sTS8

!Day 9
      sTG9=-z*(log((1.0-((sa-1.0)/sa)*(sG9/100.0))))
      sTS9=-z*(log((exp(-sTG9/sTc*log(sa))-((sa-1.0)/sa)*(sS9/100.0))))-sTG9
      sTM9=sTc-sTG9-sTS9

!Day 12-14 (13)
      sTG13=-o*(log((1.0-((psa-1.0)/psa)*(sG13/100.0))))
      sTS13=-o*(log((exp(-sTG13/psTc*log(psa))-((psa-1.0)/psa)*(sS13/100.0))))-sTG13
      sTM13=psTc-sTG13-sTS13

!Day 19-21 (20)
      sTG20=-o*(log((1.0-((psa-1.0)/psa)*(sG20/100.0))))
      sTS20=-o*(log((exp(-sTG20/psTc*log(psa))-((psa-1.0)/psa)*(sS20/100.0))))-sTG20
      sTM20=psTc-sTG20-sTS20


!Calculating TA cells (t) transit times (T) through each cell cycle phase for each day

  !Substitute "u", "v", & "w" to shorten equation length (80 character limit per line)
      u=(itTC/log(ita))          !"u" used during initial growth
      v=(tTc/log(ta))            !"v" used during peak growth
      w=(ptTc/log(pta))          !"w" used during plateau growth phase

  !Day 1
      tTG1=-u*(log((1.0-((ita-1.0)/ita)*(tG1/100.0))))
      tTS1=-u*(log((exp(-tTG1/itTc*log(ita))-((ita-1.0)/ita)*(tS1/100.0))))-tTG1
      tTM1=itTc-tTG1-tTS1

  !Day 2
      tTG2=-u*(log((1.0-((ita-1.0)/ita)*(tG2/100.0))))
      tTS2=-u*(log((exp(-tTG2/itTc*log(ita))-((ita-1.0)/ita)*(tS2/100.0))))-tTG2
      tTM2=itTc-tTG2-tTS2

  !Day 4
      tTG4=-u*(log((1.0-((ita-1.0)/ita)*(tG4/100.0))))
      tTS4=-u*(log((exp(-tTG4/itTc*log(ita))-((ita-1.0)/ita)*(tS4/100.0))))-tTG4
```

```
        tTM4=itTc-tTG4-tTS4

 !Day 5
        tTG5=-u*(log((1.0-((ita-1.0)/ita)*(tG5/100.0))))
        tTS5=-u*(log((exp(-tTG5/itTc*log(ita))-((ita-1.0)/ita)*(tS5/100.0))))-tTG5
        tTM5=itTc-tTG5-tTS5

 !Day 7
        tTG7=-v*(log((1.0-((ta-1.0)/ta)*(tG7/100.0))))
        tTS7=-v*(log((exp(-tTG7/tTc*log(ta))-((ta-1.0)/ta)*(tS7/100.0))))-tTG7
        tTM7=tTc-tTG7-tTS7

 !Day 8
        tTG8=-v*(log((1.0-((ta-1.0)/ta)*(tG8/100.0))))
        tTS8=-v*(log((exp(-tTG8/tTc*log(ta))-((ta-1.0)/ta)*(tS8/100.0))))-tTG8
        tTM8=tTc-tTG8-tTS8

 !Day 9
        tTG9=-v*(log((1.0-((ta-1.0)/ta)*(tG9/100.0))))
        tTS9=-v*(log((exp(-tTG9/tTc*log(ta))-((ta-1.0)/ta)*(tS9/100.0))))-tTG9
        tTM9=tTc-tTG9-tTS9

 !Day 12-14 (13)
        tTG13=-w*(log((1.0-((pta-1.0)/pta)*(tG13/100.0))))
        tTS13=-w*(log((exp(-tTG13/ptTc*log(pta))-((pta-1.0)/pta)*(tS13/100.0))))-tTG13
        tTM13=ptTc-tTG13-tTS13

 !Day 19-21 (20)
        tTG20=-w*(log((1.0-((pta-1.0)/pta)*(tG20/100.0))))
        tTS20=-w*(log((exp(-tTG20/ptTc*log(pta))-((pta-1.0)/pta)*(tS20/100.0))))-tTG20
        tTM20=ptTc-tTG20-tTS20

!Averaging transit times (T) in each growth phase for stem (s) and TA cells (t)
 !Initial Growth (i)
        isTG=(sTG1+sTG2+sTG4+sTG5)/4
        isTS=(sTS1+sTS2+sTS4+sTS5)/4
        isTM=(sTM1+sTM2+sTM4+sTM5)/4
        itTG=(tTG1+tTG2+tTG4+tTG5)/4
        itTS=(tTS1+tTS2+tTS4+tTS5)/4
        itTM=(tTM1+tTM2+tTM4+tTM5)/4

 !Peak Growth
        sTG=(sTG7+sTG8+sTG9)/3
        sTS=(sTS7+sTS8+sTS9)/3
        sTM=(sTM7+sTM8+sTM9)/3
        tTG=(tTG7+tTG8+tTG9)/3
        tTS=(tTS7+tTS8+tTS9)/3
        tTM=(tTM7+tTM8+tTM9)/3

!Plateau Growth (p)
        psTG=(sTG13+sTG20)/2
        psTS=(sTS13+sTS20)/2
        psTM=(sTM13+sTM20)/2
        ptTG=(tTG13+tTG20)/2
        ptTS=(tTS13+tTS20)/2
        ptTM=(tTM13+tTM20)/2
```

```
  !Calculating rates of conversion (k) (1/day) from transit times
    !Initial Growth (i)

          isKG=1.0/(isTG+beta)
          isKS=1.0/(isTS+beta)
          isKM=1.0/(isTM+beta)
          itKG=1.0/(itTG+beta)
          itKS=1.0/(itTS+beta)
          itKM=1.0/(itTM+beta)

    !Peak Growth (a)
          asKG=1.0/(sTG+beta)
          asKS=1.0/(sTS+beta)
          asKM=1.0/(sTM+beta)
          atKG=1.0/(tTG+beta)
          atKS=1.0/(tTS+beta)
          atKM=1.0/(tTM+beta)

    !Plateau Growth (p)
          psKG=1.0/(psTG+beta)
          psKS=1.0/(psTS+beta)
          psKM=1.0/(psTM+beta)
          ptKG=1.0/(ptTG+beta)
          ptKS=1.0/(ptTS+beta)
          ptKM=1.0/(ptTM+beta)


          TSTOP=25.0              !Experiment length (Days)
          POINTS = 100.0          !Communication intervals
          CINT=TSTOP/POINTS       !Length of communication intervals

END     !End of Initial segment

DYNAMIC       !Beginning of execution section

   DERIVATIVE

    PROCEDURAL

!Change rates of conversion (K) for appropriate growth phase
    !From days 0-5-initial growth
          If (T .LT. 6.0) then
          sKG=isKG
          sKS=isKS
          sKM=isKM
          tKG=itKG
          tKS=itKS
          tKM=itKM

    !From days 5-11-peak growth
          Else if (T. GE. 6.and.T .LE. 11) then
          sKG=asKG
          sKS=asKS
          sKM=asKM
          tKG=atKG
```

```
            tKS=atKS
            tKM=atKM

        !From 11days to end of experiment (TSTOP)-plateau growth
            Else If (T .GT. 11.0) then
            sKG=psKG
            sKS=psKS
            sKM=psKM
            tKG=ptKG
            tKS=ptKS
            tKM=ptKM
            End if

        END ! End Procedural


!amount "A" of stem cells (s) in G1+G0 (AsG)
            RAsG = 2.0*sKM*AsM*(1.0-c)-(sKG)*AsG-beta*AsG
            AsG = INTEG(RAsG,Fst1)

        !amount "A" of stem cells (s) in S (AsS)
            RAsS = sKG*AsG-sKS*AsS-beta*AsS
            AsS = INTEG(RAsS,0.0)

        !amount "A" of stem cells (s) in G2+M (AsM)
            RAsM = sKS*AsS-sKM*AsM-beta*AsM
            AsM = INTEG(RAsM,0.0)

        !amount "A" of TA cells (t) in G1+G0 (AtG)
            RAtG = 2.0*(tKM)*AtM+2.0*c*(sKM)*AsM-(tKG)*AtG-beta*AtG
            AtG = INTEG(RAtG,Ft1)

        !amount "A" of TA cells (t) in S (AtS)
            RAtS = (1.0-d)*(tKG)*AtG-(tKS)*AtS-beta*AtS
            AtS = INTEG(RAtS,0.0)

        !amount "A" of TA cells (t) in G2+M (AtM)
            RAtM = (tKS)*AtS-(tKM)*AtM-beta*AtM
            AtM = INTEG(RAtM,0.0)

        !amount "A" of post mitotic cells (p)
            RAp = d*(tKG)*AtG-beta*Ap
            Ap = INTEG(RAp,0.0)

            TERMT (T.GE.TSTOP)    !Condition for terminating simulation

       END  !End Derivative block

END     !End of Dynamic section

END     !End of Program
```

```
!ACSL command file for Model B
!File CC2.cmd
```

```
output t skg sks skm tkg tks tkm

Prepare T, AsG, AsM, AsS, AtG, AtM, AtS, Ap
Data expl &
(T, AsG)
1.0 9243.92
2.0 8238.8
4.0 5828.55
5.0 3964.25
7.0 1822.4
8.0 1305.5
9.0 1969.35
13.0 3947.52
20.0 4475.84
End

Data exp2 &
(T, AsS)
1.0 104.72
2.0 163.4
4.0 363.09
5.0 858.5
7.0 643.2
8.0 315.0
9.0 661.2
13.0 673.34
20.0 721.36
End

Data exp3 &
(T, AsM)
1.0 171.36
2.0 197.8
4.0 184.73
5.0 30.3
7.0 214.4
8.0 129.5
9.0 219.45
13.0 524.28
20.0 482.8
END

Data exp4 &
(T, AtG)
1.0 480.0
2.0 1325.8
4.0 3010.11
5.0 3519.45
7.0 3795.33
8.0 4699.44
9.0 3842.64
13.0 2228.16
20.0 2545.08
End
```

```
Data exp5 &
(T, AtS)
1.0 0.0
2.0 23.8
4.0 335.7
5.0 737.55
7.0 1451.73
8.0 1617.72
9.0 1490.4
13.0 1354.62
20.0 674.37
END

Data exp6 &
(T, AtM)
1.0 0.0
2.0 50.4
4.0 384.19
5.0 697.95
7.0 1262.94
8.0 1002.84
9.0 1211.76
13.0 637.22
20.0 590.55

END   !End of data to be plotted

START
proc P1
        plot/data=expl/Character=2 AsG
END

proc P2
        plot/data=exp2/Character=2 AsS
END

proc P3
        plot/data=exp3/Character=2 AsM
END

proc P4
        plot/data=exp4/character=2 AtG
END

proc P5
        plot/data=exp5/character=2 AtS
END

proc P6
        plot/data=exp6/character=2 AtM
END

proc P7
        plot/data=exp7/character=2 Ap
END
proc Ps
```

```
        plot/data=exp1/character=2 AsG AsS AsM
END
proc Pt
        plot/data=exp4/character=2 AtG AtS AtM Ap


END !End of section
```

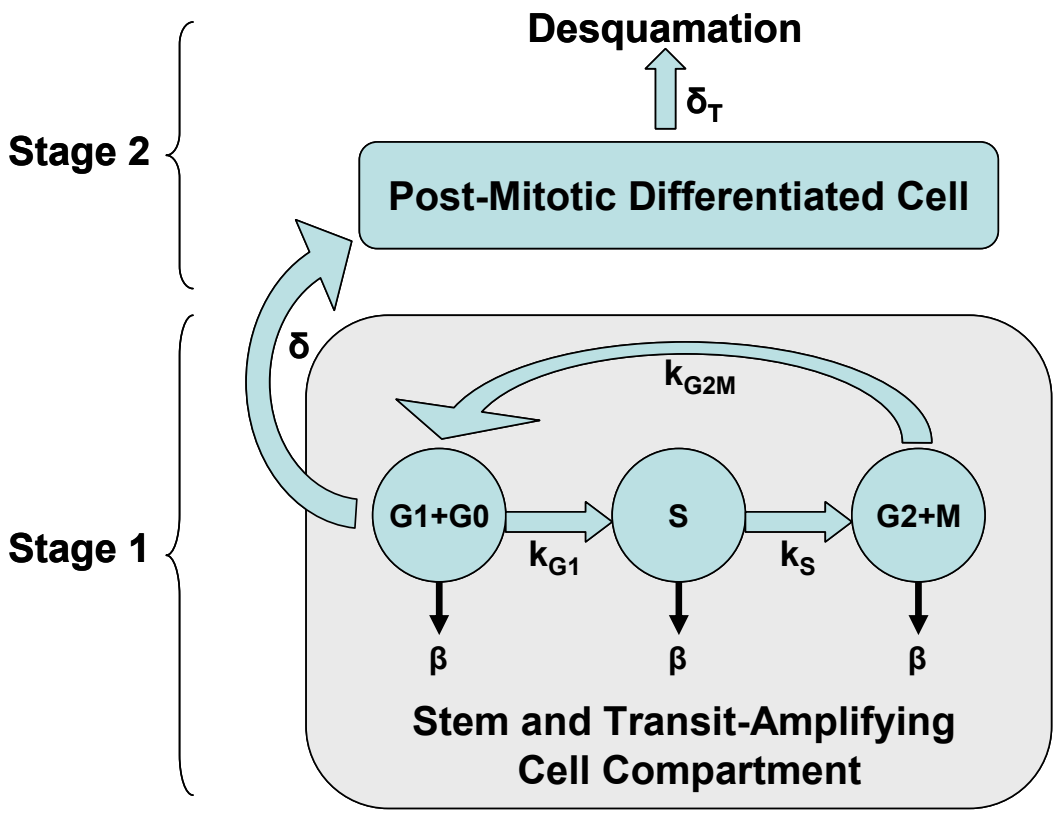

Figure 6.1. **Model A - A simple conceptual model for the process of differentiation in normal human epidermal keratinocytes.** This version of the model describes one lumped proliferative population comprised of both stem and transit-amplifying (STA) cells (Stage 1). The model includes three cell cycle compartments (G1+G0, S, and G2+M), and post-mitotic differentiated cells (Stage 2). STA cells leave the proliferating compartment and enter the post-mitotic compartment according to the differentiation rate δ. Terminally differentiated post-mitotic cells eventually cornify and desquamate off the outer most skin layer at the rate δ_T. Cell death (β) occurs at each compartment. Rates of conversions (k) from one cell phase to the next are also included in the model.

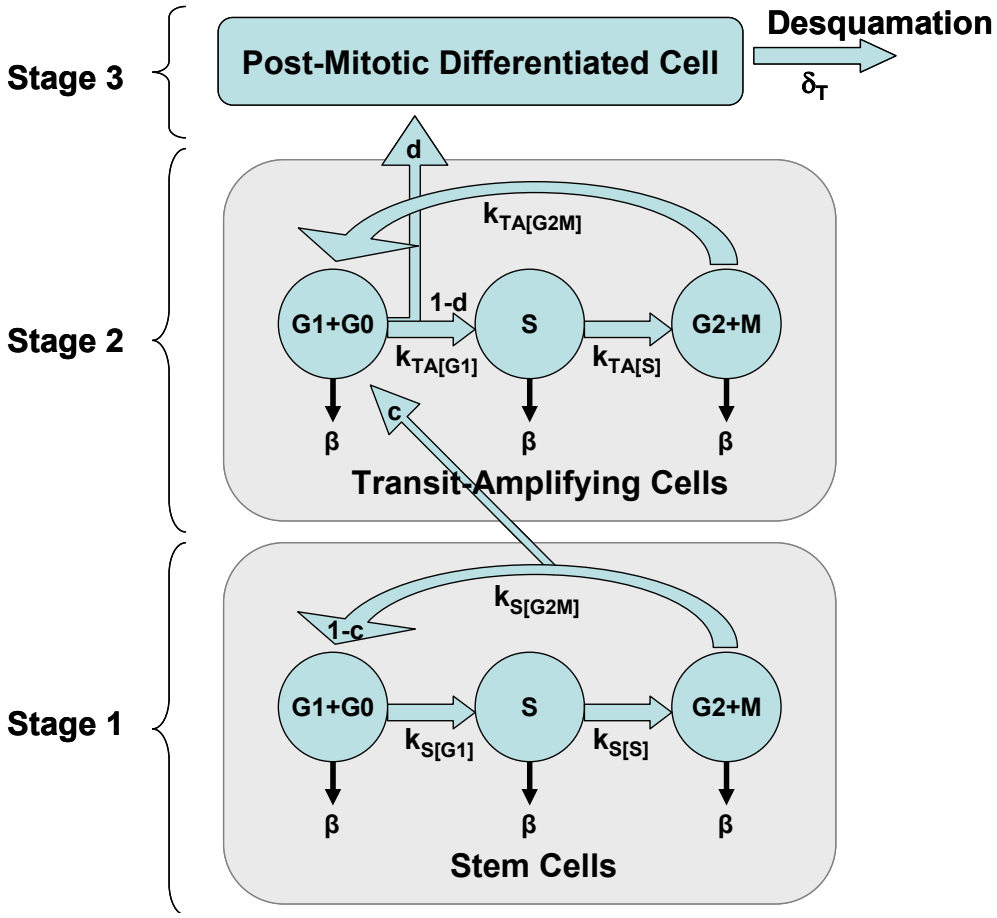

Figure 6.2. **Model B - A complex conceptual model for the process of differentiation in normal human epidermal keratinocytes**. Three cell populations are present in this model: stem (S), transit-amplifying (TA), and post-mitotic cells. The overall progression that will be modeled is as follows: Stem cells (Stage 1) can convert to TA cells (Stage 2), which then further undergo multiple cycles of division before converting into post-mitotic (Stage 3) (i.e., granular and cornified) cells which expressing the differentiated phenotype. Of these three populations, only stem and TA cells are capable of cycling. The model includes three cell cycle compartments (G1+G0, S, and G2+M), for both stem and TA cells, and a post-mitotic differentiated cell compartment. After stem cell division, a fraction c of daughter cells differentiate and enter G1+G0 phase of the TA compartment. The remaining cells (fraction 1 – c) re-enter the cycle within the same stem cell compartment. Fraction d of TA cells within G1+G0 differentiate further, entering the post-mitotic compartment, while the remainder of the fraction (1 – d) continues to cycle within the TA cell population. Terminally differentiated post-mitotic cells eventually cornify and desquamate off the outer most skin layer at the rate δ_T. Cell death (β) occurs at each compartment. Rates of conversions (k) from one cell phase to the next are also included in the model.

Table 6.1. Parameters Required for Model A

Parameter	Description	Source/Reference
STA_{G1+G0}	# of STA cells in G1+G0 phase	Flow cytometry data from Perez *et al.* 2003
STA_S	# of STA cells in S	Flow cytometry data from Perez *et al.* 2003
STA_{G2M}	# of STA cells in G2+M	Flow cytometry data from Perez *et al.* 2003
PM	# of post-mitotic cells	Stathmokinetic analysis from Kimmel *et a*l, 1986.
$FSTA_{G1+G0}$	Fraction of STA cells in G1+G0	Flow cytometry data from Perez *et al.* 2003
$FSTA_S$	Fraction of STA cells in S	Flow cytometry data from Perez *et al.* 2003
$FSTA_{G2M}$	Fraction of STA cells in G2+M	Flow cytometry data from Perez *et al.* 2003
δ	Rate of differentiation from Stage 1 to Stage 2	Estimated from Kimmel *et al.* 1986 & Dover *et al.* 1987; $\delta = 0.1007\ hr^{-1}$
δ_T	Desquamation rate of terminal differentiation	Estimated; $\delta_T = 0.1007\ hr^{-1}$
T_{G1+G0}	Transit time of cells in G1	Flow cytometry data; Calculated from fraction of cells in G1+G0 (Equation 6-4)
T_S	Transit time of cells in S	Flow cytometry data; Calculated from fraction of cells in S (Equation 6-4)
T_{G2M}	Transit time of cells in G2+M	Flow cytometry data; Calculated from fraction of cells in G2+M (Equation 6-4)
k_{G1}	Rate of conversion of cells from G1 to S	Calculated from corresponding transit time (Equation 6-5)
k_S	Rate of conversion of cells from S to G2+M	Calculated from corresponding transit time (Equation 6-5)
k_{G2M}	Rate of conversion of cells from G2+M back to G1+G0	Calculated from corresponding transit time (Equation 6-5)
β_i	Death rate in compartment i	Liao *et al.* 2001

Table 6.2. Parameters Required for Model B.

Parameter	Description	Source/Reference
S	Total # of stem cells	Kimmel *et al.* 1986 & Staiano-Coico *et al.* 1986
S_{G1+G0}	# stem cells in G0+G1	Kimmel *et al.* 1986 & Staiano-Coico *et al.* 1986; Measured as an initial value at t=0
S_S	# stem cells in S	Kimmel *et al.* 1986 & Staiano-Coico *et al.* 1986; Measured as an initial value at t=0
S_{G2M}	# stem cells in G2+M	Kimmel *et al.* 1986 & Staiano-Coico *et al.* 1986; Measured over 1-8 hr
TA	Total # of transit amplifying cells	Kimmel *et al.* 1986 & Staiano-Coico *et al.* 1986; Measured as an initial value at t=0
TA_{G1+G0}	# TA cells in G0+G1	Kimmel *et al.* 1986 & Staiano-Coico *et al.* 1986; Measured over 1-8 hr
TA_S	# TA cells in S	Kimmel *et al.* 1986 & Staiano-Coico *et al.* 1986
TA_{G2M}	# TA cells in G2+M	Kimmel *et al.* 1986 & Staiano-Coico *et al.* 1986
PM	# post-mitotic cells	Kimmel *et al.* 1986 & Staiano-Coico *et al.* 1986
FS_{G1+G0}	Fraction of stem cells in G0+G1	Kimmel *et al.* 1986 & Staiano-Coico *et al.* 1986
FS_S	Fraction of stem cells in S	Kimmel *et al.* 1986 & Staiano-Coico *et al.* 1986
FS_{G2M}	Fraction of stem cells in G2+M	Kimmel *et al.* 1986 & Staiano-Coico *et al.* 1986
FTA_{G1+G0}	Fraction of TA cells in G0+G1	Kimmel *et al.* 1986 & Staiano-Coico *et al.* 1986
FTA_S	Fraction of TA cells in S	Kimmel *et al.* 1986 & Staiano-Coico *et al.* 1986
FTA_{G2M}	Fraction of TA cells in G2+M	Kimmel *et al.* 1986 & Staiano-Coico *et al.* 1986
c	Fraction of stem cells that convert to TA cells	Kimmel *et al.* 1986 assumed c to be between 0.1 and 0.5 *in vitro*; See Table 6.6
1-c	Fraction of stem cells that remain as stem cells	Calculated from value of c
d	Fraction of TA cells that become post-mitotic	Estimated to be 0.5 by Kimmel *et al.* 1986; See Table 6.7
1-d	Fraction of TA cells that continue to cycle	Calculated from the value of d
δ_T	Desquamation rate of terminal differentiation	Estimated
$T_{S[G1+G0]}$	Transit time of stem cells in G1	Flow cytometry data; Calculated from fraction of stem cells in G1+G0 (Equation 6-4)
$T_{S[S]}$	Transit time of stem cells in S	Flow cytometry data; Calculated from fraction of stem cells in S (Equation 6-4)

$T_{S[G2M]}$	Transit time of stem cells in G+/M	Flow cytometry data; Calculated from fraction of stem cells in G2+M (Equation 6-4)
$T_{TA[G1+G0]}$	Transit time of TA cells in G1	Flow cytometry data; Calculated from fraction of TA cells in G1+G0 (Equation 6-4)
$T_{TA[S]}$	Transit time of TA cells in S	Flow cytometry data; Calculated from fraction of TA cells in S (Equation 6-4)
$T_{TA[G2M]}$	Transit time of TA cells in G2+M	Flow cytometry data; Calculated from fraction of TA cells in G2+M (Equation 6-4)
$k_{S[G1]}$	Rate of movement of a G1 stem cell to S phase	Calculated from corresponding transit time (Equation 6-5)
$k_{S[S]}$	Rate of movement of an S phase stem cell to G2+M	Calculated from corresponding transit time (Equation 6-5)
$k_{S[G2M]}$	Rate of movement of a stem cell out of G2+M	Calculated from corresponding transit time (Equation 6-5)
$k_{TA[G1]}$	Rate of movement of a G1 phase TA cell into S	Calculated from corresponding transit time (Equation 6-5)
$k_{TA[S]}$	Rate of movement of an S phase TA cell into G2+M	Calculated from corresponding transit time (Equation 6-5)
$k_{TA[G2M]}$	Rate of movement of a G2+M phase cell back into G1+G0	Calculated from corresponding transit time (Equation 6-5)
β_i	Death rate in compartment i	Liao *et al.* 2001

Table 6.3. Model A: Cell kinetic parameter data when NHEK GF is estimated to be 0.8

Parameter	Control	BaP (2.0 µM)	As^{3+} (5.0 µM)	Ca^{2+} (2.0 mM)
T_{pot}	36.38	24.59	58.82	39.38
% G1+G0	60.18	63.65	59.66	60.3
% S	25.35	23.63	16.0	23.46
% G2+M	14.48	12.74	24.4	16.23
T_C	30.85	20.85	49.88	33.33
T_{G1+G0}	16.34	11.79	26.14	17.69
T_S	8.77	5.62	8.64	8.71
T_{G2+M}	5.75	3.44	15.09	6.93
k_{G1}	0.0612	0.0848	0.0382	0.0565
k_S	0.114	0.178	0.116	0.115
k_{G2+M}	0.174	0.291	0.0662	0.144
β	0.0000983			
δ	0.061			

T_{pot} and % of cells distributed in G1+G0, S, and G2+M are all original data from flow cytometric analysis used to create Model A. T is transit time expressed in hours, and rate constants (k, β, δ) are expressed in reciprocal hours (hr^{-1}).

Table 6.4. Model A: Cell kinetic parameter data when NHEK GF is estimated to be 0.6

Parameter	Control	BaP (2.0 µM)	As^{3+} (5.0 µM)	Ca^{2+} (2.0 mM)
T_{pot}	36.38	24.59	58.82	39.38
% G1+G0	60.18	63.65	59.66	60.3
% S	25.35	23.63	16.0	23.46
% G2+M	14.48	12.74	24.4	16.23
T_C	24.67	16.67	39.88	26.65
T_{G1+G0}	13.42	9.67	21.49	14.54
T_S	6.87	4.39	6.82	6.84
T_{G2+M}	4.37	2.61	11.57	5.27
k_{G1}	0.0745	0.103	0.0465	0.0688
k_S	0.145	0.228	0.146	0.146
k_{G2+M}	0.229	0.383	0.0864	0.189
β	0.0000983			
δ	0.0742			

T_{pot} and % of cells distributed in G1+G0, S, and G2+M are all original data from flow cytometric analysis used to create Model A. T is transit time expressed in hours, and rate constants (k, β, δ) are expressed in reciprocal hours (hr^{-1}).

Table 6.5. Model A: Cell kinetic parameter data when NHEK GF is estimated to be 0.4

Parameter	**Control**	**BaP (2.0 µM)**	**As^{3+} (5.0 µM)**	**Ca^{2+} (2.0 mM)**
T_{pot}	36.38	24.59	58.82	39.38
% G1+G0	60.18	63.65	59.66	60.3
% S	25.35	23.63	16.0	23.46
% G2+M	14.48	12.74	24.4	16.23
T_C	17.66	11.94	28.55	19.08
T_{G1+G0}	9.90	7.12	15.86	10.72
T_S	4.80	3.05	4.81	4.79
T_{G2+M}	2.95	1.76	7.88	3.57
k_{G1}	0.101	0.140	0.0631	0.0932
k_S	0.208	0.327	0.208	0.209
k_{G2+M}	0.339	0.568	0.127	0.280
β	0.0000983			
δ	0.1007			

T_{pot} and % of cells distributed in G1+G0, S, and G2+M are all original data from flow cytometric analysis used to create Model A. T is transit time expressed in hours, and rate constants (k, β, δ) are expressed in reciprocal hours (hr^{-1}).

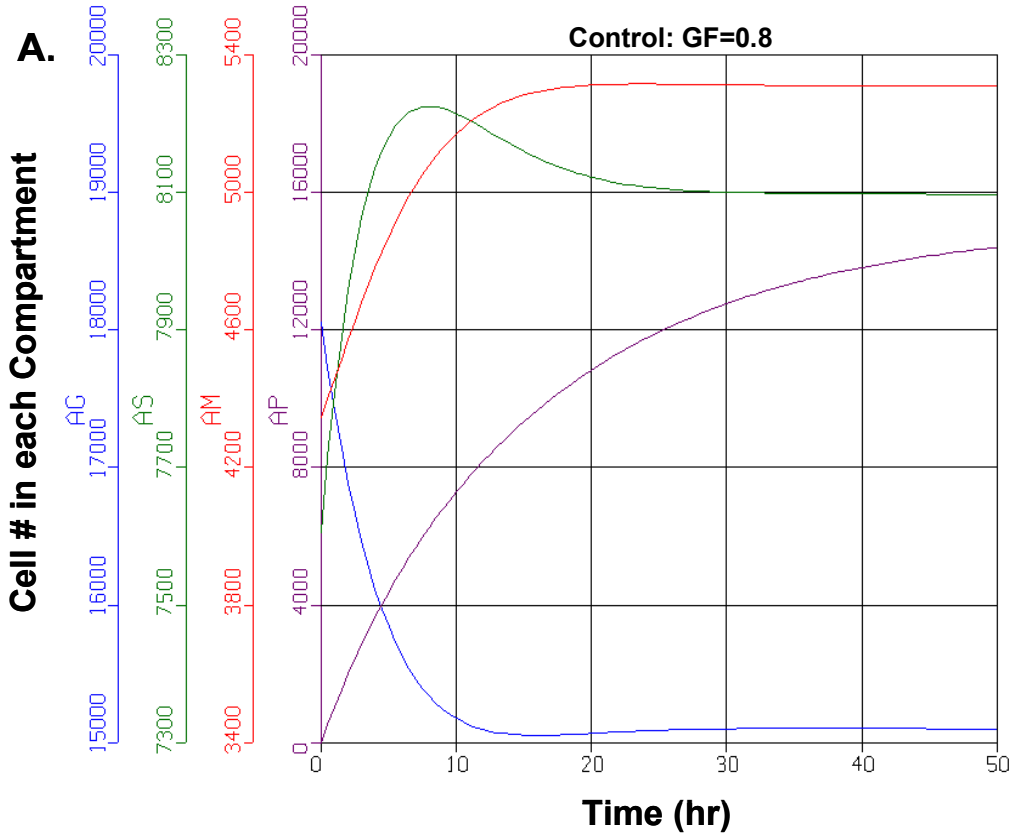

Figure 6.3A. **Model A:** This modeling simulation represents the cell cycle kinetics of control NHEK that have a GF of 0.8. Data generated by flow cytometric analysis and adjusted parameters were inserted into the model to create a homeostatic model system. AG = amount of cells in G1+G0; AS = amount of cells in S-phase; AM = amount of cells in G2+M; AP = amount of post-mitotic cells. Please note the y-axis scale can vary substantially between cell cycle compartments.

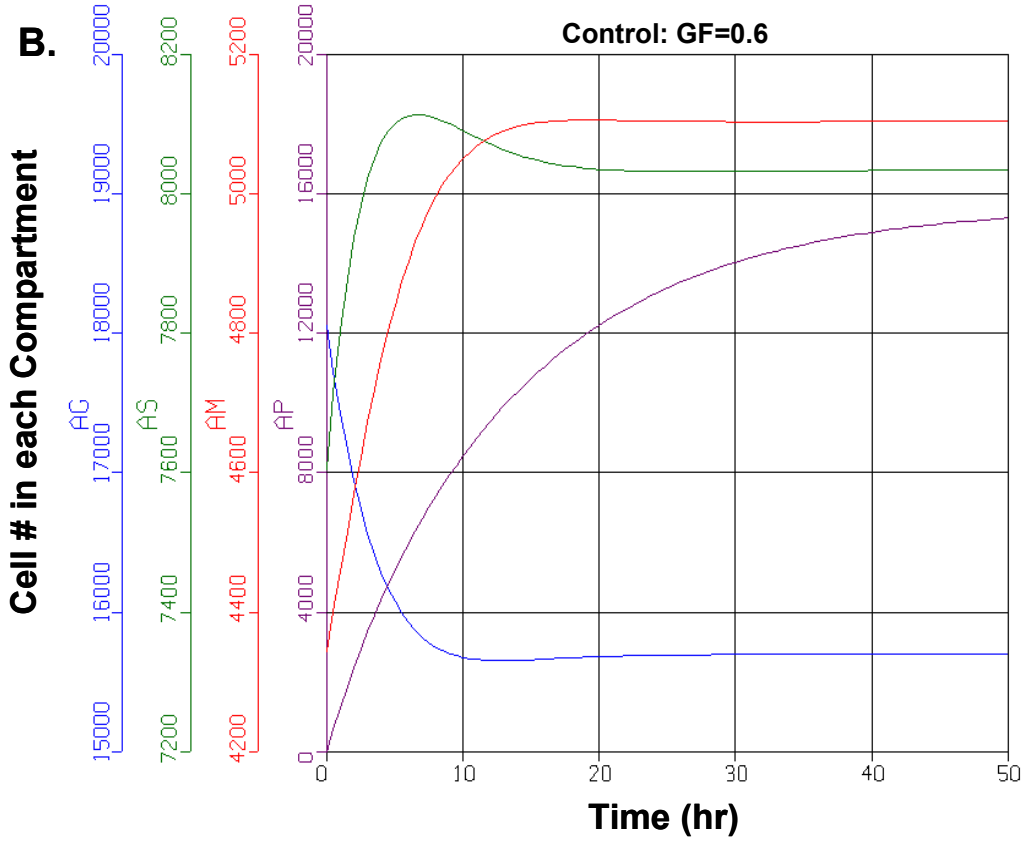

Figure 6.3B. **Model A:** This modeling simulation represents the cell cycle kinetics of control NHEK that have a GF of 0.6. Data generated by flow cytometric analysis and adjusted parameters were inserted into the model to create a homeostatic model system. AG = amount of cells in G1+G0; AS = amount of cells in S-phase; AM = amount of cells in G2+M; AP = amount of post-mitotic cells. Please note the y-axis scale can vary substantially between cell cycle compartments.

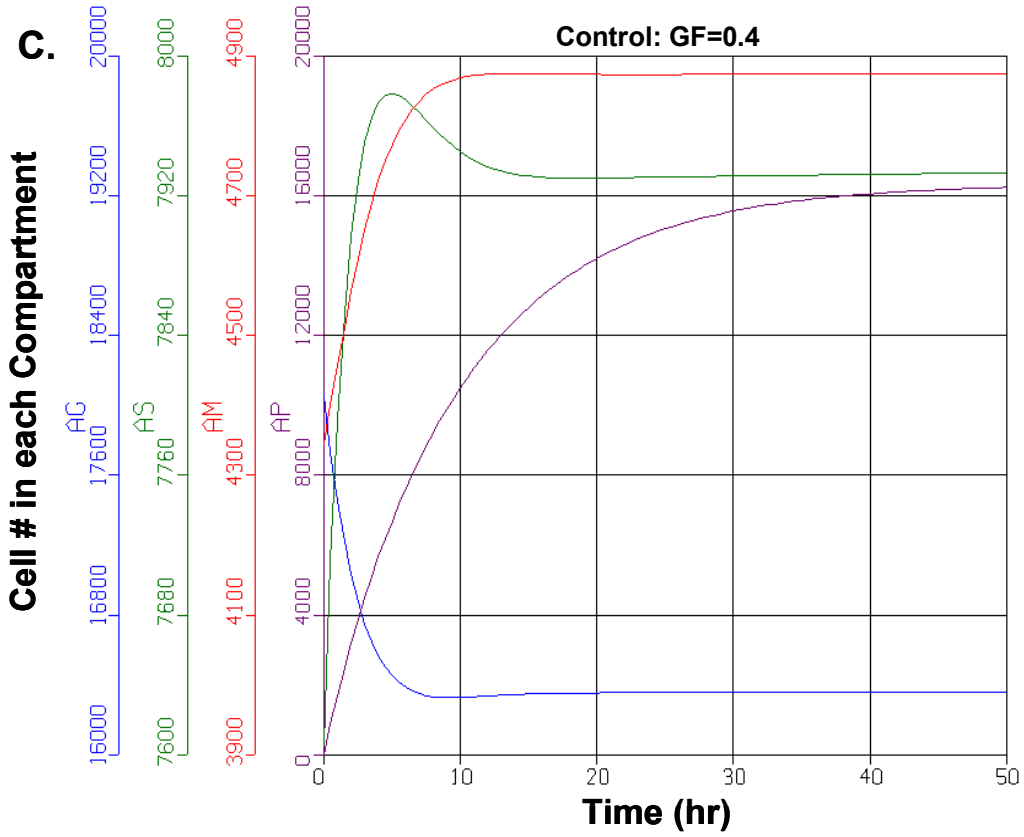

Figure 6.3C. **Model A:** This modeling simulation represents the cell cycle kinetics of control NHEK that have a GF of 0.4. Data generated by flow cytometric analysis and adjusted parameters were inserted into the model to create a homeostatic model system. AG = amount of cells in G1+G0; AS = amount of cells in S-phase; AM = amount of cells in G2+M; AP = amount of post-mitotic cells. Please note the y-axis scale can vary substantially between cell cycle compartments.

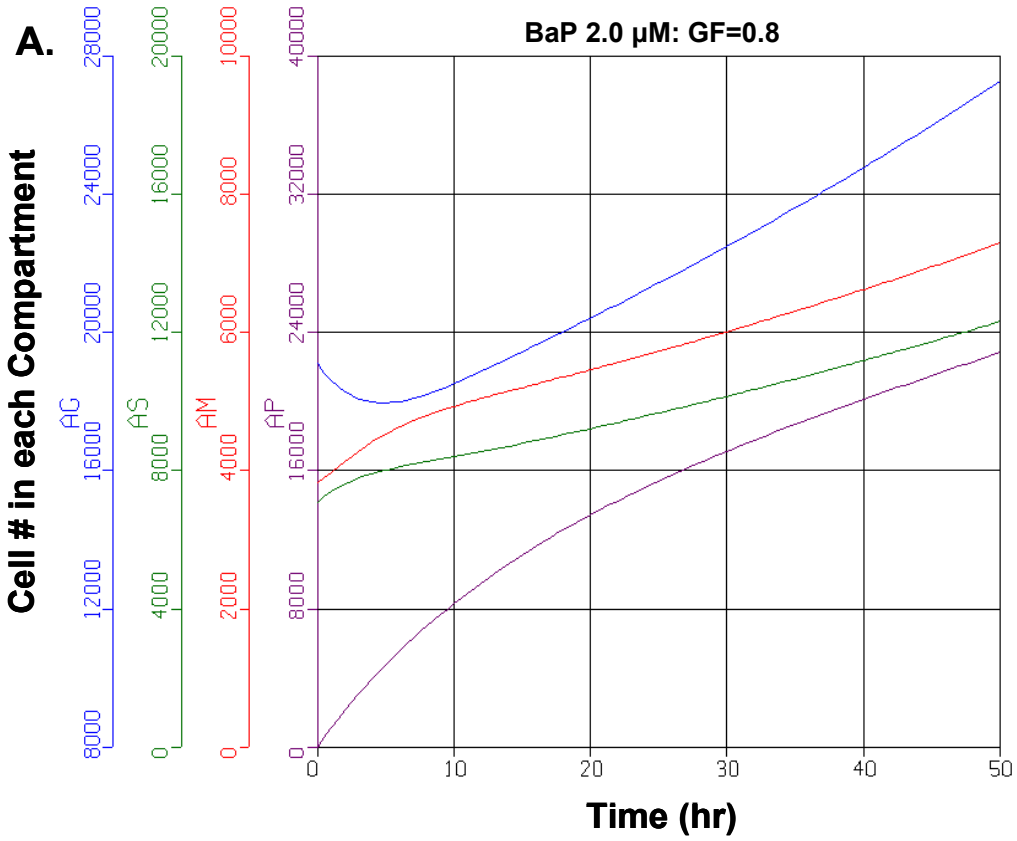

Figure 6.4A. **Model A:** This modeling simulation represents the cell cycle kinetics of BaP (2.0 µM) treated cells that have a GF of 0.8. Flow cytometry data from the analysis of BaP exposed NHEK were inserted into the homeostatic model (Figure 6.3A) to examine any chemical-induced kinetic perturbations. AG = amount of cells in G1+G0; AS = amount of cells in S-phase; AM = amount of cells in G2+M; AP = amount of post-mitotic cells. Please note the y-axis scale can vary substantially between cell cycle compartments.

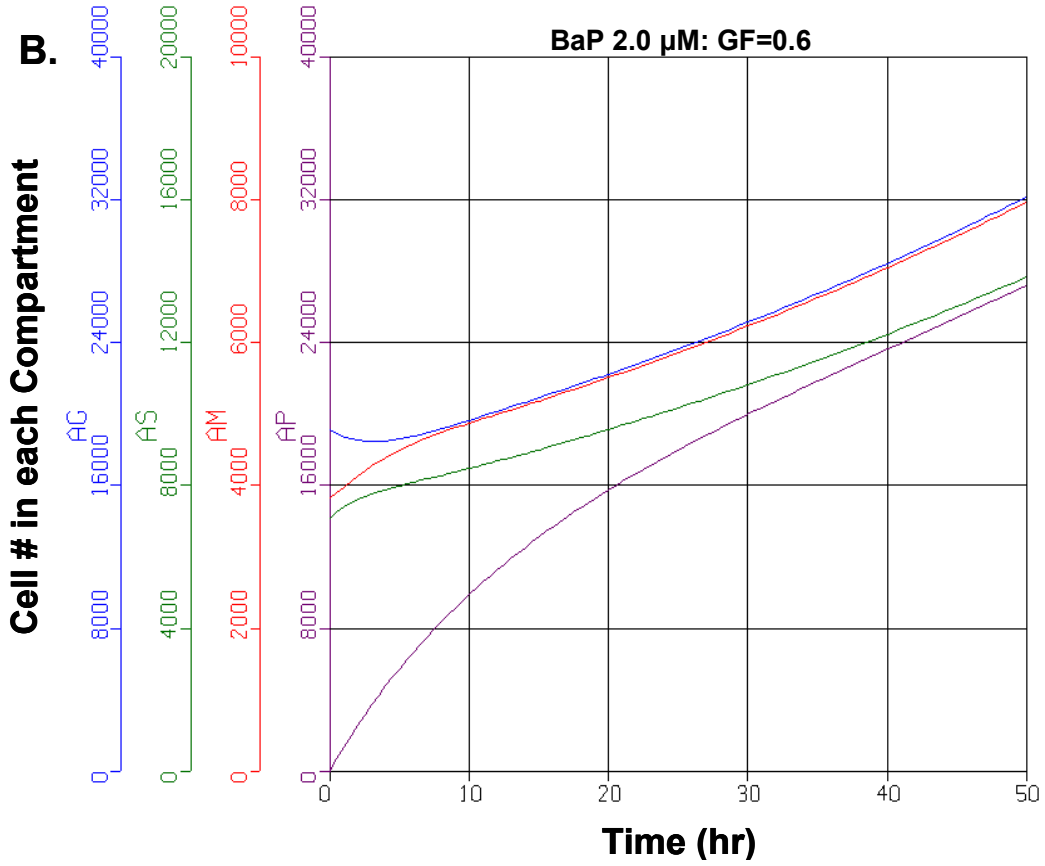

Figure 6.4B. **Model A:** This modeling simulation represents the cell cycle kinetics of BaP (2.0 µM) treated cells that have a GF of 0.6. Flow cytometry data from the analysis of BaP exposed NHEK were inserted into the homeostatic model (Figure 6.3B) to examine any chemical-induced kinetic perturbations. AG = amount of cells in G1+G0; AS = amount of cells in S-phase; AM = amount of cells in G2+M; AP = amount of post-mitotic cells. Please note the y-axis scale can vary substantially between cell cycle compartments.

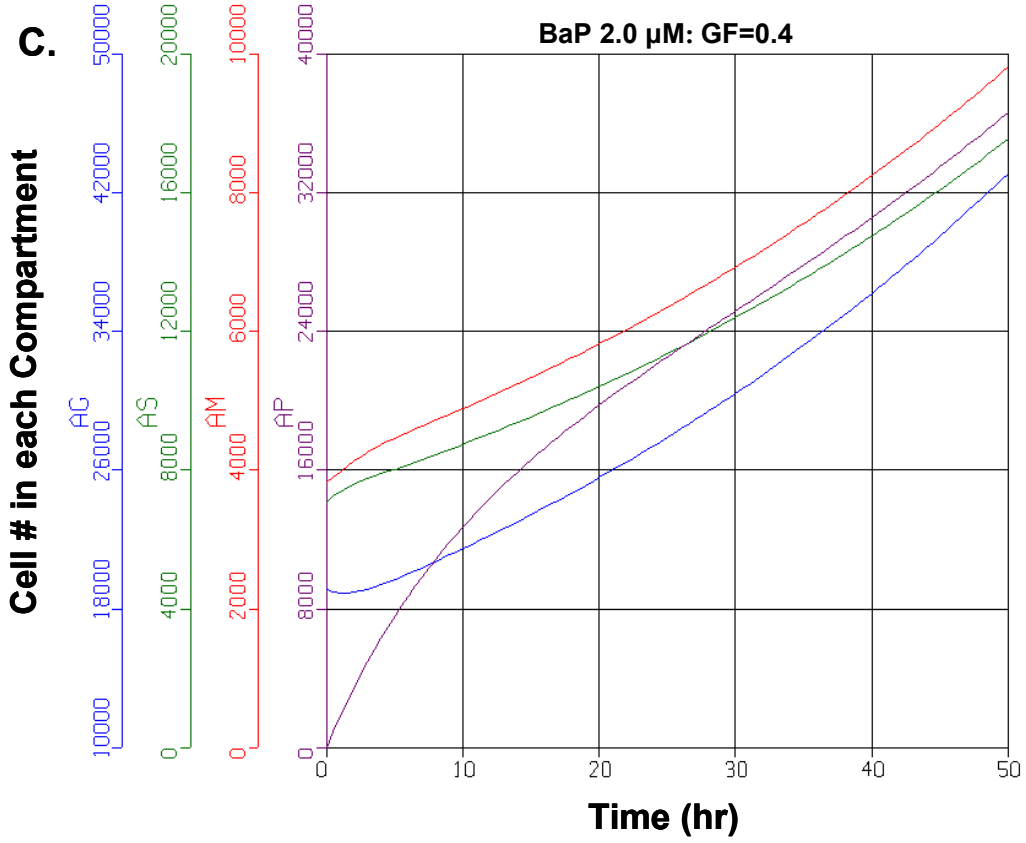

Figure 6.4C. **Model A:** This modeling simulation represents the cell cycle kinetics of BaP (2.0 µM) treated cells that have a GF of 0.4. Flow cytometry data from the analysis of BaP exposed NHEK were inserted into the homeostatic model (Figure 6.3C) to examine any chemical-induced kinetic perturbations. AG = amount of cells in G1+G0; AS = amount of cells in S-phase; AM = amount of cells in G2+M; AP = amount of post-mitotic cells. Please note the y-axis scale can vary substantially between cell cycle compartments.

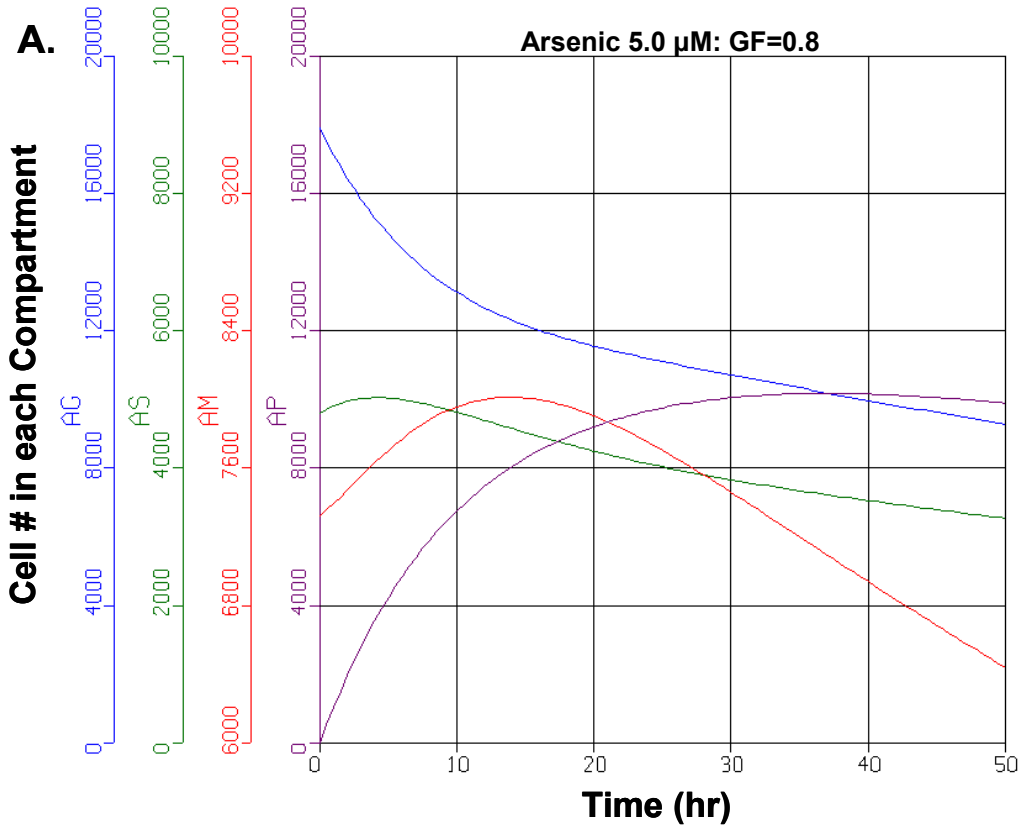

Figure 6.5A. **Model A:** This modeling simulation represents the cell cycle kinetics of arsenic (5.0 µM) treated cells that have a GF of 0.8. Flow cytometry data from the analysis of arsenic exposed NHEK were inserted into the homeostatic model (Figure 6.3A) to examine any chemical-induced kinetic perturbations. AG = amount of cells in G1+G0; AS = amount of cells in S-phase; AM = amount of cells in G2+M; AP = amount of post-mitotic cells. Please note the y-axis scale can vary substantially between cell cycle compartments.

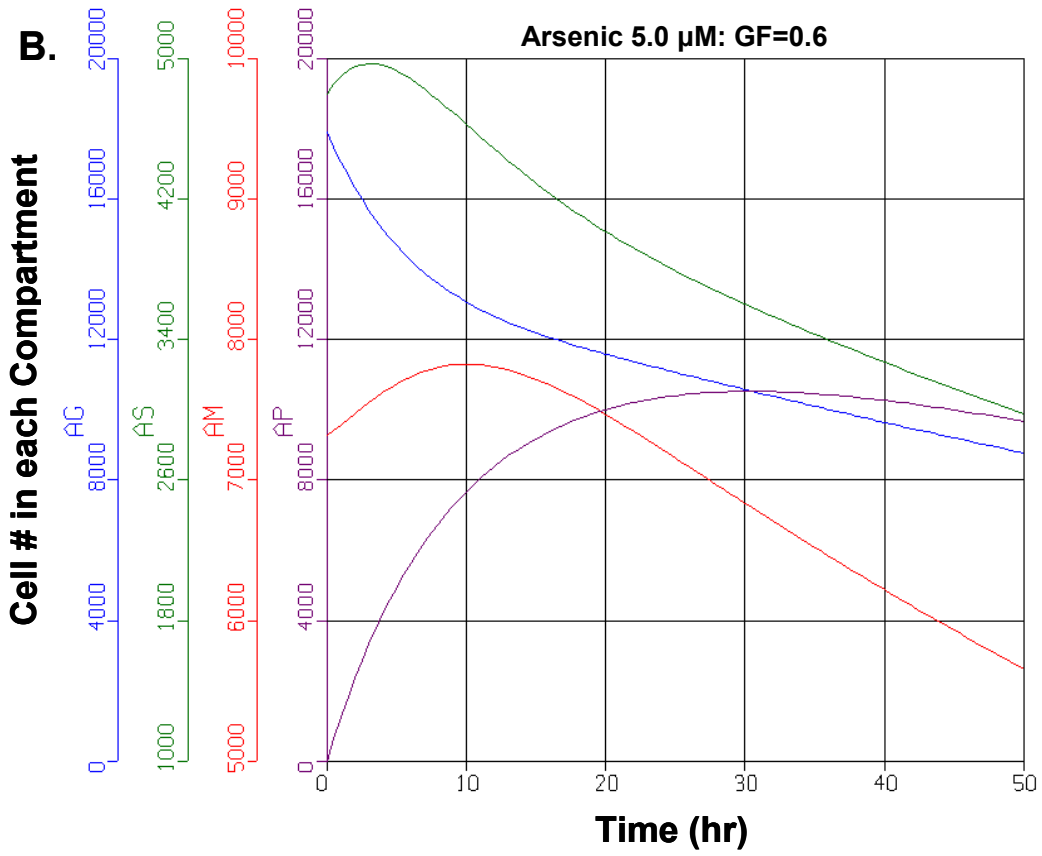

Figure 6.5B. **Model A:** This modeling simulation represents the cell cycle kinetics of arsenic (5.0 µM) treated cells that have a GF of 0.6. Flow cytometry data from the analysis of arsenic exposed NHEK were inserted into the homeostatic model (Figure 6.3B) to examine any chemical-induced kinetic perturbations. AG = amount of cells in G1+G0; AS = amount of cells in S-phase; AM = amount of cells in G2+M; AP = amount of post-mitotic cells. Please note the y-axis scale can vary substantially between cell cycle compartments.

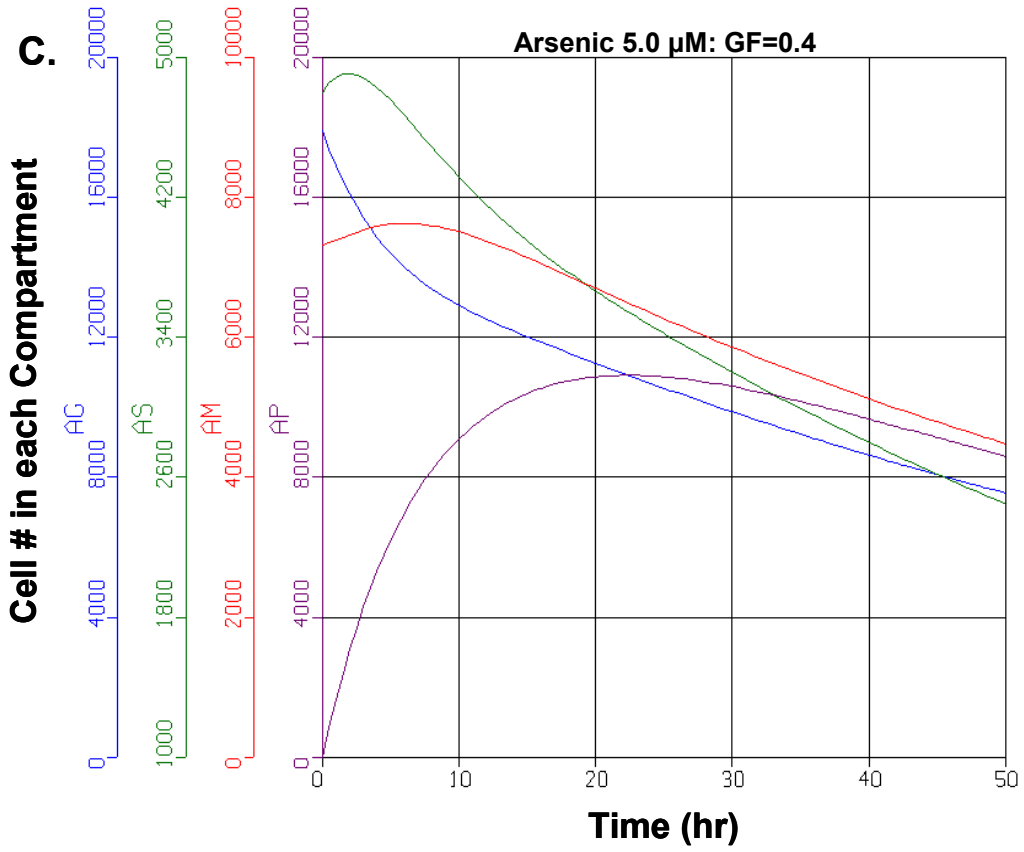

Figure 6.5C. **Model A:** This modeling simulation represents the cell cycle kinetics of arsenic (5.0 µM) treated cells that have a GF of 0.4. Flow cytometry data from the analysis of arsenic exposed NHEK were inserted into the homeostatic model (Figure 6.3C) to examine any chemical-induced kinetic perturbations. AG = amount of cells in G1+G0; AS = amount of cells in S-phase; AM = amount of cells in G2+M; AP = amount of post-mitotic cells. Please note the y-axis scale can vary substantially between cell cycle compartments.

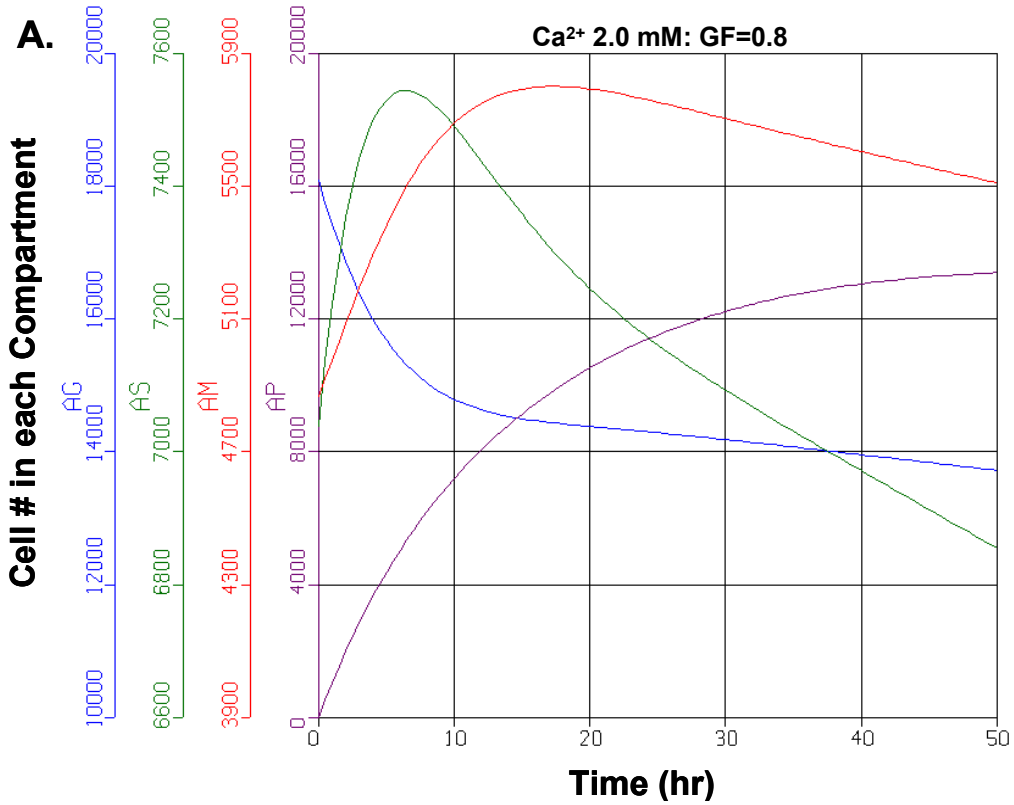

Figure 6.6A. **Model A:** This modeling simulation represents the cell cycle kinetics of Ca^{2+} (2.0 mM) treated cells that have a GF of 0.8. Flow cytometry data from the analysis of Ca^{2+} exposed NHEK were inserted into the homeostatic model (Figure 6.3A) to examine any chemical-induced kinetic perturbations. AG = amount of cells in G1+G0; AS = amount of cells in S-phase; AM = amount of cells in G2+M; AP = amount of post-mitotic cells. Please note the y-axis scale can vary substantially between cell cycle compartments.

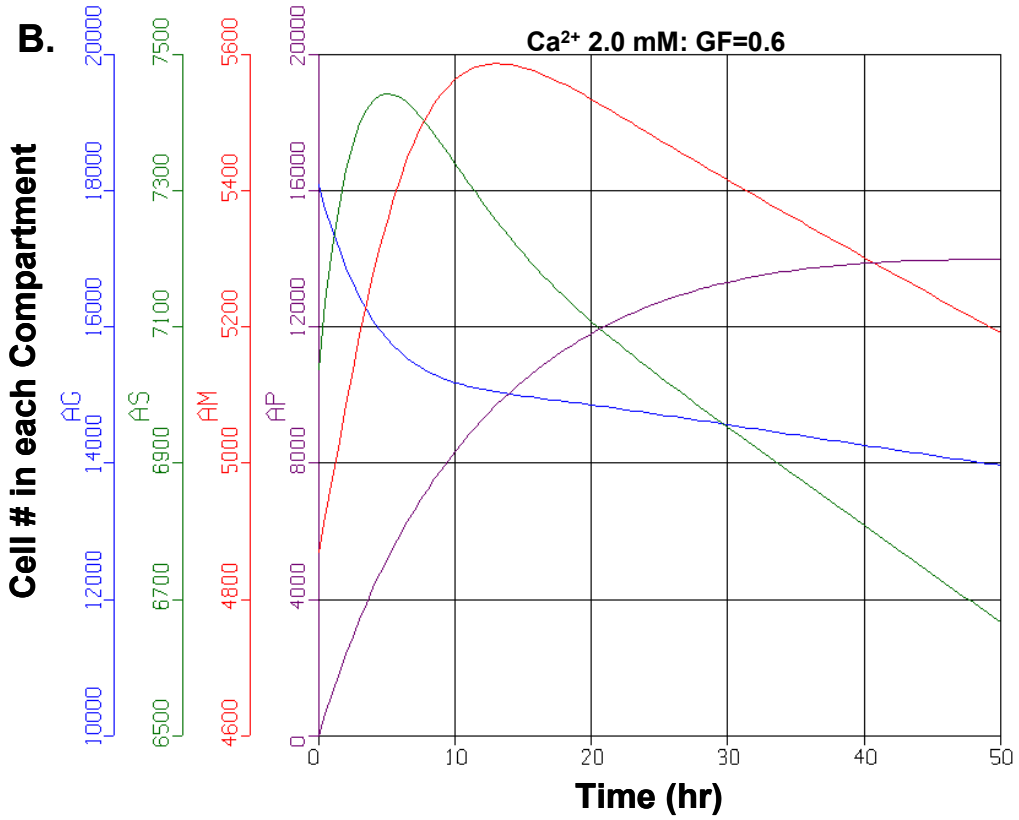

Figure 6.6B. **Model A:** This modeling simulation represents the cell cycle kinetics of Ca^{2+} (2.0 mM) treated cells that have a GF of 0.6. Flow cytometry data from the analysis of Ca^{2+} exposed NHEK were inserted into the homeostatic model (Figure 6.3B) to examine any chemical-induced kinetic perturbations. AG = amount of cells in G1+G0; AS = amount of cells in S-phase; AM = amount of cells in G2+M; AP = amount of post-mitotic cells. Please note the y-axis scale can vary substantially between cell cycle compartments.

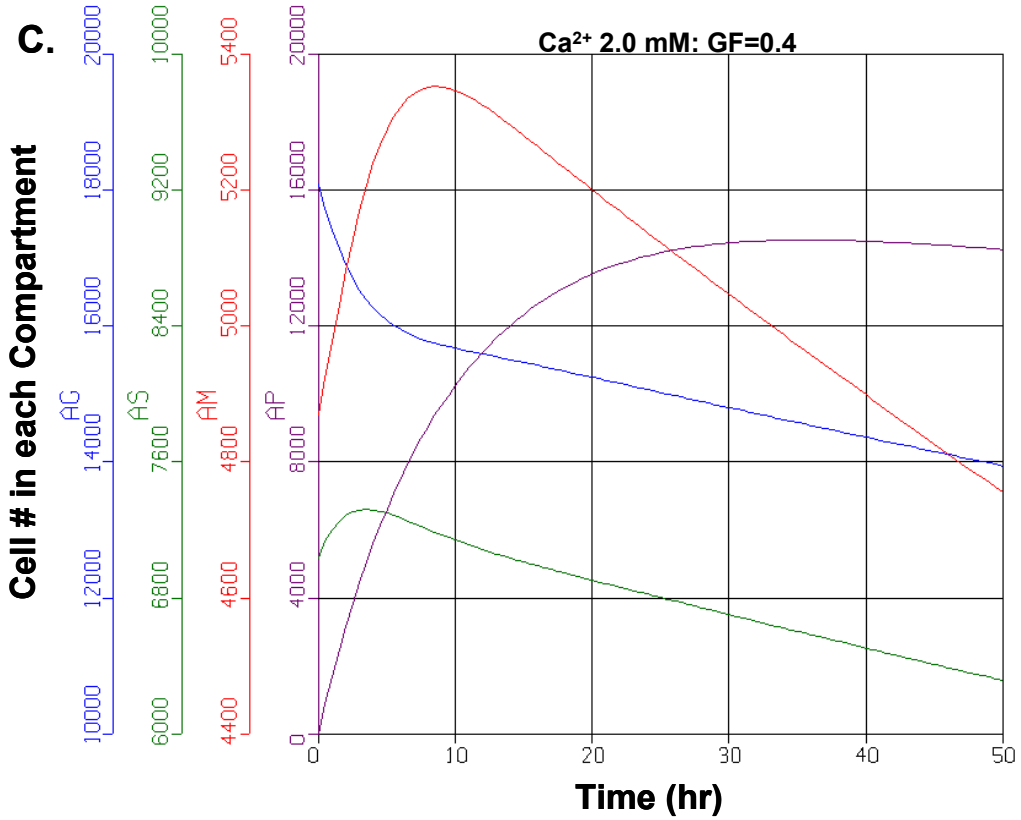

Figure 6.6C. **Model A:** This modeling simulation represents the cell cycle kinetics of Ca^{2+} (2.0 mM) treated cells that have a GF of 0.4. Flow cytometry data from the analysis of Ca^{2+} exposed NHEK were inserted into the homeostatic model (Figure 6.3C) to examine any chemical-induced kinetic perturbations. AG = amount of cells in G1+G0; AS = amount of cells in S-phase; AM = amount of cells in G2+M; AP = amount of post-mitotic cells. Please note the y-axis scale can vary substantially between cell cycle compartments.

Table 6.6. Experimental data from Staiano-Coico *et al.* (1986) used to create Model B for the stem cell population in NHEK

Stem Cells							
Days in culture	% of total cells	Cell distribution (%)			c	T_{pot} (days)	GF (Estimated)
		G1	S	G2M			
1	95.2	97.1	1.1	1.8	0.7	6.25 (150 hr)	0.2925
2	86.0	95.8	1.9	2.3			
4	63.7	91.5	5.7	2.9			
5	50.5	78.5	17.0	4.6			
7	26.8	68.0	24.0	8.0	0.32	4.167 (100 hr)	0.4695
8	17.5	74.6	18.0	7.4			
9	28.5	69.1	23.2	7.7			
12-14	51.4	76.8	13.1	10.2	0.5	10.417 (250 hr)	0.1664
19-21	56.8	78.8	12.7	8.5			

Initial growth phase: Days 1, 2, 4, and 5
Peak growth phase: Days 7, 8, and 9
Plateau growth phase: Days 12-14 and 19-21
c = the fraction of stem cells differentiating into TA cells
T_{pot} = potential doubling time
GF = estimated growth fraction

Table 6.7. Experimental data from Staiano-Coico *et al.* (1986) used to create Model B for the transit-amplifying cell population in NHEK

Transit-Amplifying Cells							
Days in culture	% of total cells	Cell distribution (%)			d	T_{pot} (days)	GF (Estimated)
		G1	S	G2M			
1	4.8	100.0	0	0	0.5	1.458 (35 hr)	0.733
2	14.0	94.7	1.7	3.6			
4	37.3	80.7	9.0	10.3			
5	49.5	71.1	14.9	14.1			
7	65.1	58.3	22.3	19.4	0.55	1.25 (30 hr)	0.9
8	73.2	64.2	22.1	13.7			
9	64.8	59.3	23.0	18.7			
12-14	42.2	52.8	32.1	15.1	0.6	1.667 (40 hr)	0.617
19-21	38.1	66.8	17.7	15.5			

Initial growth phase: Days 1, 2, 4, and 5
Peak growth phase: Days 7, 8, and 9
Plateau growth phase: Days 12-14 and 19-21
d = the fraction of TA cells differentiating into post-mitotic cells
T_{pot} = potential doubling time
GF = estimated growth fraction

Table 6.8. Model B: Cell cycle kinetics of stem cells during different growth phases. Parameters calculated from the data generated by Staiano-Coico *et al.* (1986)

Stem Cell Parameters	**Growth Phase**		
	Initial	**Peak**	**Plateau**
T_{pot}	6.25 (150 hr)	4.1667 (100 hr)	10.4167 (250 hr)
T_{G1+G0}	2.0741 (49.78 hr)	1.5362 (36.87 hr)	1.7686 (42.44 hr)
T_S	0.1646 (3.95 hr)	0.5642 (13.54 hr)	0.3144 (7.54 hr)
T_{G2+M}	0.07481 (1.79 hr)	0.2134 (5.12 hr)	0.2308 (5.54 hr)
k_{G1}	0.4819	0.6505	0.5651
k_S	6.0385	1.7693	3.1698
k_{G2+M}	13.1879	4.6622	4.3129

Transit time (T) is expressed in days, and rate constants (k) are expressed in reciprocal days (day^{-1}). Cell cycle time (T_C) was estimated to be 2.314 days (55.54 hr) in stem cells.

Table 6.9. Model B: Cell cycle kinetics of transit-amplifying cells during different growth phases. Parameters calculated from the data generated by Staiano-Coico *et al.* (1986)

TA Cell Parameters	**Growth Phase**		
	Initial	**Peak**	**Plateau**
T_{pot}	1.458 (35 hr)	1.25 (30 hr)	1.667 (40 hr)
T_{G1+G0}	0.9659 (23.18 hr)	0.6104 (14.65 hr)	0.6243 (14.98 hr)
T_S	0.08731 (2.09 hr)	0.2915 (6.99 hr)	0.3145 (7.548 hr)
T_{G2+M}	0.1033 (2.48 hr)	0.2555 (6.13 hr)	0.2169 (5.21 hr)
k_{G1}	1.0342	1.6354	1.5991
k_S	11.3213	3.4177	3.1696
k_{G2+M}	9.5828	3.8986	4.5881

Transit time (T) is expressed in days, and rate constants (k) are expressed in reciprocal days (day^{-1}). Cell cycle time (T_C) was estimated to be 1.1567 days (27.76 hr) in TA cells.

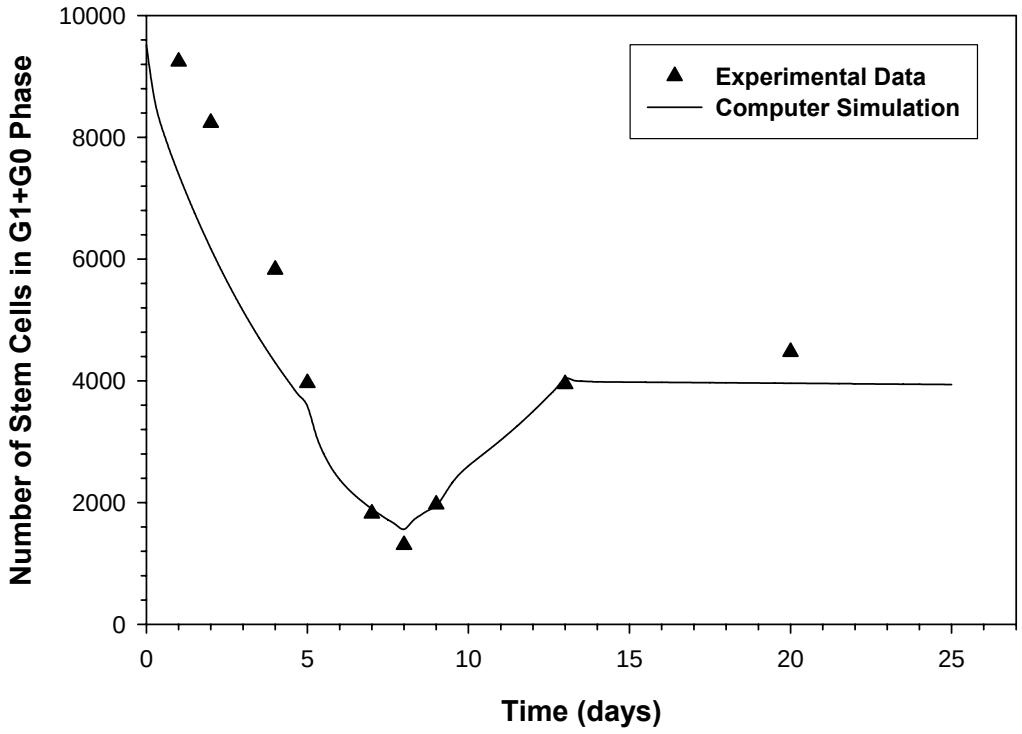

Figure 6.7. **Model B:** Cell kinetic characterization of NHEK stem cells within the G1+G0 phase of the cell cycle. This graph depicts the number of cells within this phase as a function of time measured in days. Symbols (▲) represent measured experimental data obtained from Staiano-Coico *et al.* (1986) and the solid line is the model simulation.

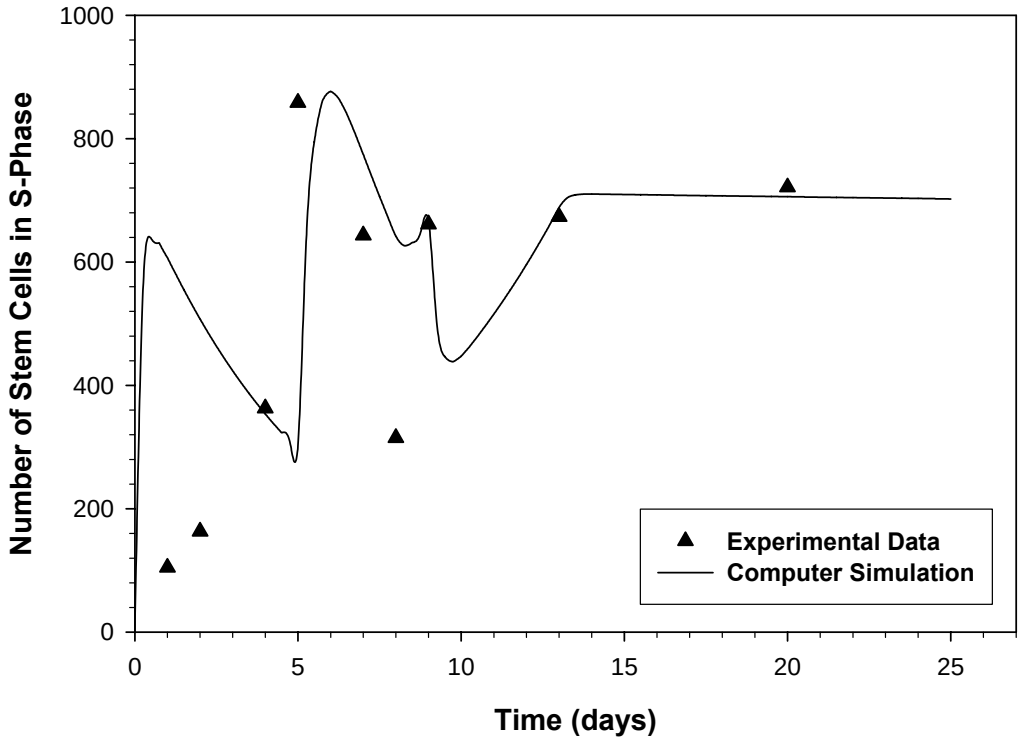

Figure 6.8. **Model B:** Cell kinetic characterization of NHEK stem cells within the S-phase of the cell cycle. This graph depicts the number of cells within this phase as a function of time measured in days. Symbols (▲) represent measured experimental data obtained from Staiano-Coico *et al.* (1986) and the solid line is the model simulation.

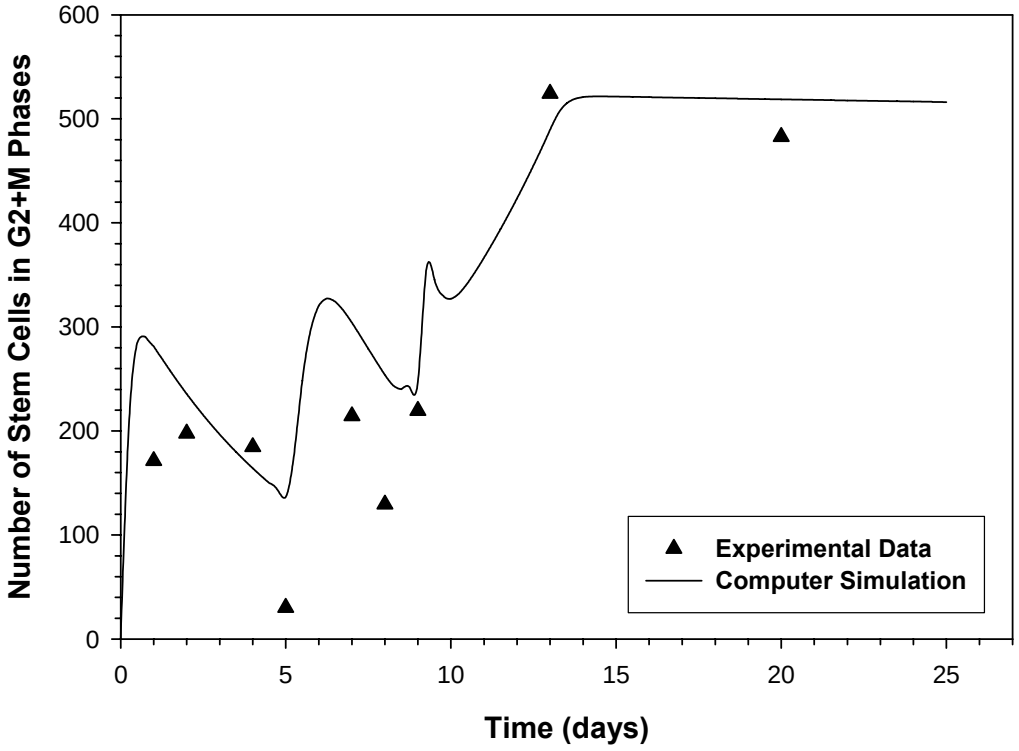

Figure 6.9. **Model B:** Cell kinetic characterization of NHEK stem cells within G2+M phases of the cell cycle. This graph depicts the number of cells within this phase as a function of time measured in days. Symbols (▲) represent measured experimental data obtained from Staiano-Coico *et al.* (1986) and the solid line is the model simulation.

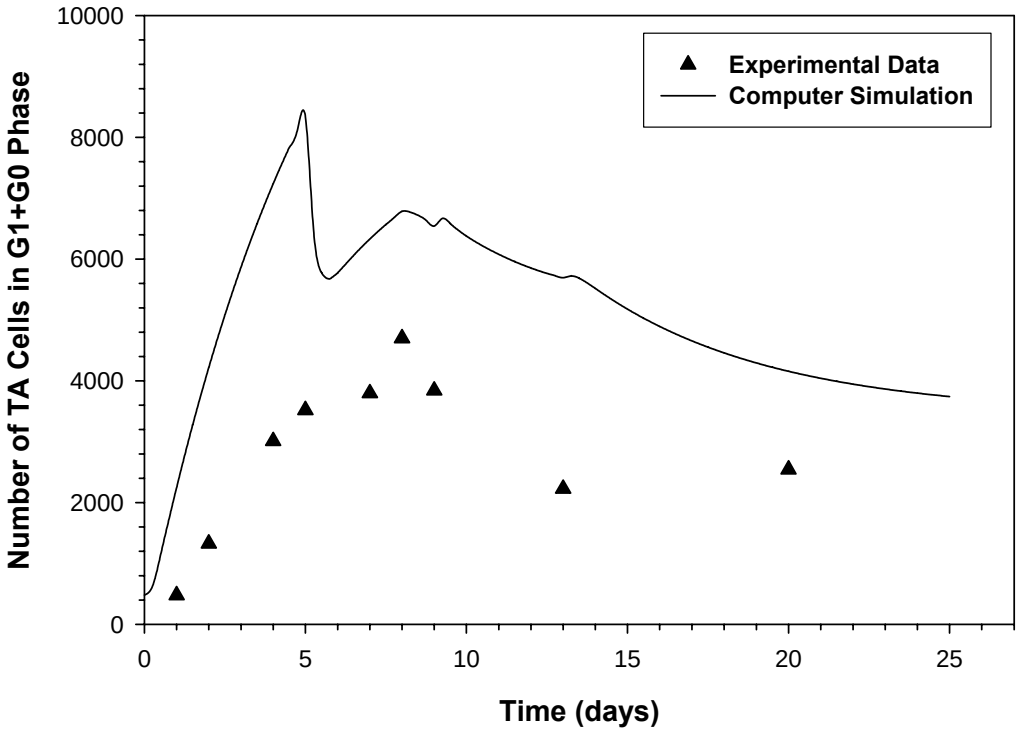

Figure 6.10. **Model B:** Cell kinetic characterization of NHEK TA cells within the G1+G0 phase of the cell cycle. This graph depicts the number of cells within this phase as a function of time measured in days. Symbols (▲) represent measured experimental data obtained from Staiano-Coico *et al.* (1986) and the solid line is the model simulation.

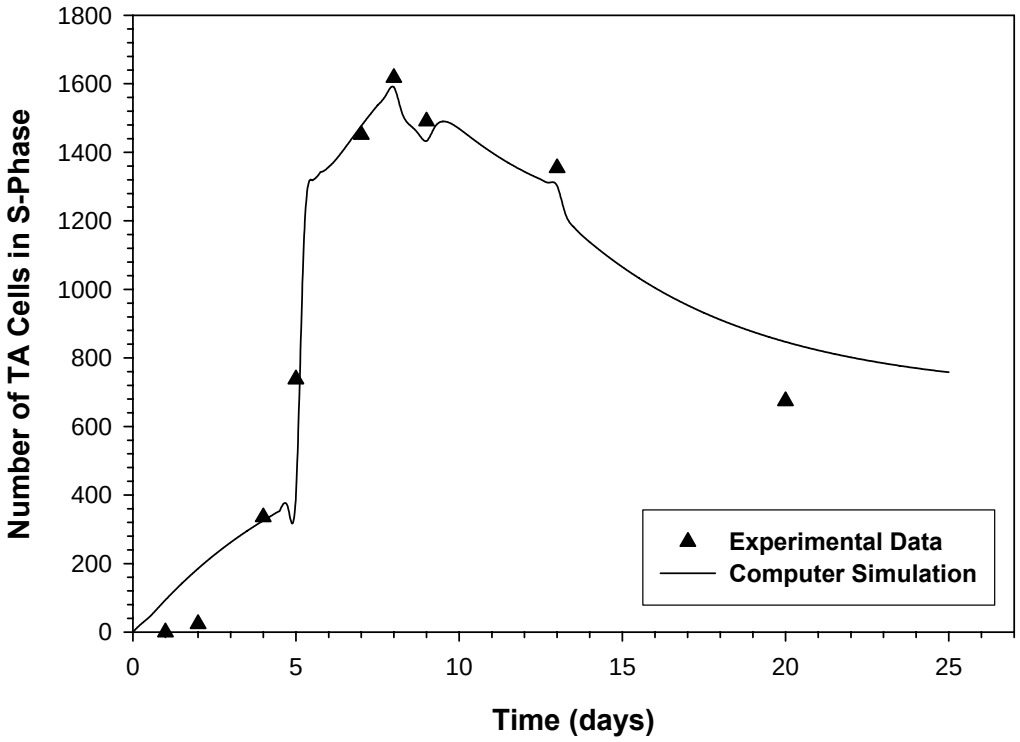

Figure 6.11. **Model B:** Cell kinetic characterization of NHEK TA cells within the S-phase of the cell cycle. This graph depicts the number of cells within this phase as a function of time measured in days. Symbols (▲) represent measured experimental data obtained from Staiano-Coico *et al.* (1986) and the solid line is the model simulation.

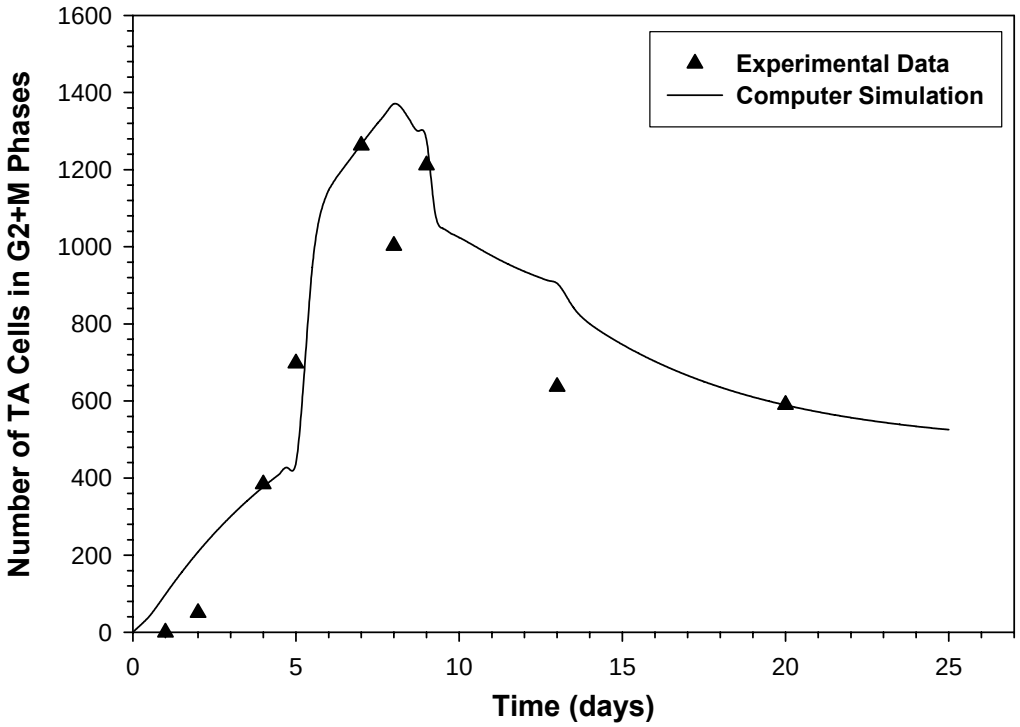

Figure 6.12. **Model B:** Cell kinetic characterization of NHEK TA cells within G2+M phases of the cell cycle. This graph depicts the number of cells within this phase as a function of time measured in days. Symbols (▲) represent measured experimental data obtained from Staiano-Coico *et al.* (1986) and the solid line is the model simulation.

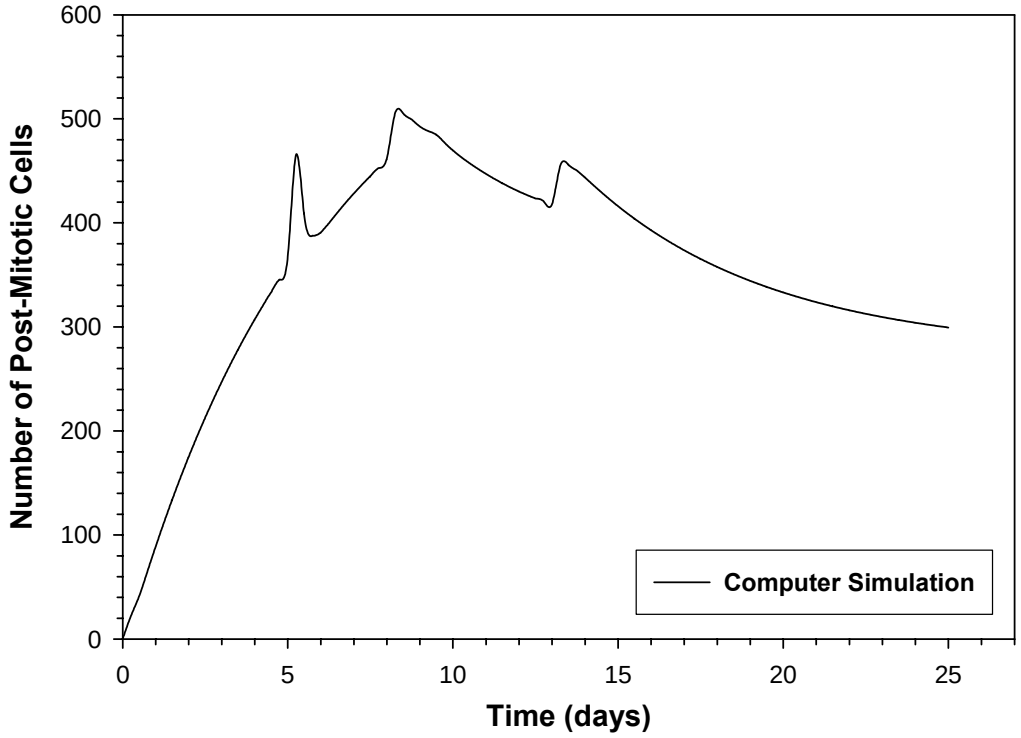

Figure 6.13. **Model B:** Cell kinetic characterization of NHEK TA cells that differentiate into PM cells. This graph depicts the number of PM cells as a function of time measured in days. The kinetics of PM cells was influence by the fraction of differentiating TA cells and the rate at which this fraction enters the PM compartment. This solid line represents the model simulation of PM cells.

Chapter 7

Conclusions and Future Directions

7.1. Introduction

In the end, the goal to characterize the effects of two mechanistically diverse skin carcinogens, benzo[*a*]pyrene and arsenic, on growth rate, cell cycle distribution, and squamous differentiation, and the examination of altered genes which may be involved in these cellular processes in human keratinocytes was very successful. In addition, the construction of the computational mathematical models will help aid in quantitative understanding of mechanisms involved in controlling cell cycle kinetic and differentiation events in keratinocytes. The following sections will briefly summarize the results gathered from experiments, present conclusions based on the data, and offer possible future directions to supplement the findings presented in this dissertation.

7.2. Overview of Results, Conclusions, and Future Directions

7.2.1. Cytotoxicity of Petroleum-Derived Hydrocarbons

The purpose of this study was to examine the individual toxicities of four prominent hydrocarbon derivatives found in petroleum-based chemical mixtures in primary epidermal keratinocytes *in vitro*. The four chemicals under investigation were benzo[*a*]pyrene (BaP), carbazole (CZ), dibenzothiophene (DBT), and isoquinoline (IQ).

Experiments using the MTT assay estimated the lethal concentration (LC) for BaP, CZ and DBT in normal human epidermal keratinocytes (NHEK). While IQ produced minimal toxicity in NHEK up to 200.0 μM, BaP ($LC_{50} \approx 2.0$ μM) proved to be 6-times and 14-times more toxic than CZ ($LC_{50} \approx 12.0$ μM) and DBT ($LC_{50} \approx 28.0$ μM), respectively. This trend is the same when the LC_{25} of each compound is examined. BaP ($LC_{25} \approx 0.5$ μM) is 8-times and 28-times more toxic than CZ ($LC_{25} \approx 4.0$ μM) and DBT ($LC_{25} \approx 14.0$ μM) respectively. However, this trend changes when one examines and compares the LC_{75s} of both CZ and DBT, while BaP remains the most toxic. At LC_{75}, BaP (5.0 μM) is 8.8-times and 8.4 times more toxic than CZ (44.0 μM) and DBT (42.0 μM) respectively, but now DBT is slightly more toxic than CZ.

Although subsequent research did not continue to investigate DBT-, CZ-, and IQ-mediated effects on keratinocyte growth and differentiation, these results provide valuable cytotoxicity information pertaining to each compound if further research is desired to study the effects of these chemicals in NHEK. These results are unique since they present, for the first time, the toxicity of DBT, CZ, and IQ in NHEK *in vitro*. As discussed in Chapter 3, various compounds which are structurally similar to these parental hydrocarbons were determined to be toxic and carcinogenic under some conditions. If derived compounds act in a similar manner to these hydrocarbons, then these hydrocarbons may not only be toxic, but potentially carcinogenic as well.

In general terms, the mechanisms of cell killing are well understood, however, death is the final outcome created by numerous pathological changes that occur within the cell. First, the toxicant is distributed to its cellular target(s), after which the ultimate toxicant interacts with endogenous target molecules, triggering changes in cell function

and/or structure, which initiate repair mechanisms at the molecular, cellular, and/or tissue levels. When these alterations exceed the repair capacity or when repair becomes malfunctional, toxicity occurs. Hence, the toxic endpoint affected by these hydrocarbons in NHEK is the resulting consequence of potentially numerous alterations produced at a cellular and molecular level. Further studies are necessary to investigate the mechanisms behind the toxicity created by these petroleum-derived hydrocarbons in NHEK.

These toxicity studies could potentially be utilized as a stepping stone for various types of future *in vitro* experimentation that focus on investigating toxic mechanisms. Future research could investigate chemical-induced effects of these compounds on crucial cellular processes such as differentiation, cell growth, and apoptosis. Studies examining these cellular processes would give clues to which mechanisms may be altered following chemical exposure. Once phenotypic changes are observed, gene or protein expression experiments could give detailed information pertaining to alterations of certain molecular pathways. Once altered signaling pathways are identified, one could start to piece together the mechanisms behind the toxicity produced in NHEK. These mechanistic studies could indicate that these compounds are potential carcinogens and may act as an initiator or promoting agent in NHEK, depending on the mechanisms affected during chemical exposure.

In addition, examining cellular effects produced by the alkylated derivatives or a mixture of these hydrocarbons would be highly informative and interesting. Studies centered on investigating the effects of various mixtures of these compounds would be enlightening due to possible synergistic or antagonistic effects induced by a mixture. Mixture- and BaP-induced effects could be compared to examine whether or not BaP is

an adequate indicator of toxicity or carcinogenesis within a petroleum mixture. Although BaP is often used to assess the carcinogenic and toxic risks of many petroleum products, by not considering the other compounds that may be contained within the mixture it becomes difficult to assess the actual risk of the petroleum product as a whole. The examination of the effects produced by chemical mixtures or alkylated derivatives would be very relevant in terms of real life exposures since, many times, these compounds and their alkylated derivatives reside in the same petroleum mixture. Thus, one could obtain a more realist viewpoint to how these compounds and their derivatives interact with each other when in a mixture.

7.2.2. Chemically-Induced Effects on Differentiation and Proliferation in NHEK

In this research the following hypothesis was tested: chemicals that alter or interfere in cellular differentiation will concomitantly induce growth perturbations and are, thus, potential carcinogens. To test this hypothesis, two known skin carcinogens, arsenic and BaP, became the main focus for these studies. The results demonstrated that BaP inhibits terminal differentiation in NHEK, as measured by cross-linked envelope (CLE) formation, by up to 5.8-fold in control and 1.7-fold in calcium (Ca^{2+})-treated cells. In comparison, arsenic decreased CLE formation by 20-fold in control cells and 5.5-fold in Ca^{2+}-treated NHEK. To characterize the effects of these agents on the growth rate and cell cycle distribution in NHEK, flow cytometric analysis was used. BaP at 2.0 μM increased proliferation rates by 29%. Altered cell-cycle distribution in BaP-treated cells indicated a more rapid progression through the cell cycle by a shortened G2 phase. In contrast, arsenic at 5.0 μM inhibited proliferation by 25% and seemed to block cycling

cells in G2 and possibly G1 since very few cells were detected in S-phase. Growth arrest (9%) was also observed in NHEK treated with 2.0 mM Ca^{2+}. These studies demonstrate that while the known human carcinogens, arsenic and BaP, are both effective inhibitors of differentiation in primary keratinocytes *in vitro,* they exert interesting, but opposite effects on cell growth.

The results presented in Chapter 4 demonstrate that, although both BaP and arsenic inhibit CLE production in NHEK, different mechanisms may be involved (since the magnitude of inhibition between the two carcinogens varied by almost 4-fold). Furthermore, opposite effects were observed on proliferation of NHEK; arsenic decreased cell division rates while BaP significantly increased proliferation rates. Again, since these chemical have opposite effects on cell cycle and growth properties, they are likely working through different mechanisms or are having opposite effects on similar regulators that are involved in controlling cell division in NHEK. As discussed in Chapter 2, altered differentiation in keratinocytes has been commonly observed to be a phenotypic change that occurs during the initial stages of carcinogenesis. BaP is a complete carcinogen and is thus capable, at certain doses, of impacting every stage of carcinogenesis. An increase in proliferation accompanied by inhibition of differentiation are typical phenotypic alterations noticed in initiated cell types. Therefore, it is possible these phenotypic changes indicate NHEK were initiated by BaP treatments. Alternatively, arsenic is only slightly mutagenic and acts as a co-carcinogen and progressing agent in most cell types including in the skin (Jha *et al.* 1992; Lee *et al.* 1988; Maier *et al.* 2002; Mure *et al.* 2003; Rossman 1981; Rossman *et al.* 1980; Rossman *et al.* 2001; Rudel *et al.* 1996). Arsenic was shown to have a very profound inhibitory effect on NHEK

differentiation; again typical of an initiated phenotype. However, decreased cell proliferation due to arsenic exposure is not representative of an initiated keratinocyte population. In contrast to BaP, Chapter 4 demonstrates the ability of arsenic to produce cell cycle blocks/delays and decreased cell division rates in NHEK. However, while high doses of arsenic inhibit cell growth, non-cytotoxic to slightly toxic concentrations of arsenic have been shown to increase cell proliferation (hormesis) (Chen *et al.* 2000; Liao *et al.* 2004; Styblo *et al.* 2002; Vega *et al.* 2001). From studies presented in Chapter 4, arsenic inhibited differentiation at very low, slightly toxic concentrations; however, this low arsenic concentration was not examined during flow cytometry experiments to investigate effects on cell growth rates. It would be interesting to see if low levels of arsenic could produce an initiated phenotype in keratinocytes as observed with relatively high BaP concentrations. If either of these chemicals actually created an initiated phenotype in NHEK, only a small portion of the cell population would contain initiated cells; therefore, one might not observe growth changes in the entire cell population.

The co-carcinogenic actions of arsenic affect cells in numerous ways. As mentioned in Chapter 2, potential carcinogenic actions for arsenic include oxidative stress, genotoxic damage, inhibition of DNA repair, epigenetic effects such as altered methylation, and activation of certain signal transduction pathways leading to aberrant gene expression. Thus, it is plausible that arsenic, in fact, altered epigenetic mechanisms that are involved in regulating the differentiation process in NHEK. Furthermore, since arsenic is known to cause substantial DNA damage (Mei *et al.* 2003; Shi *et al.* 2004), normal cells should easily recognize this damage, thus, sending signals to delay cell division in an attempt to repair DNA lesions. If the repair of damaged DNA is

unsuccessful, then cells will likely undergo programmed cell death (apoptosis) to make sure transcriptional mistakes are not inherited by daughter cells. Researchers have taken advantage of these anti-cancer effects on cell proliferation by using arsenic as a therapeutic agent in acute promyleocytic leukemia and ovarian carcinoma. Clearly, both BaP and arsenic have profound effects on the keratinocyte phenotype. In attempt to clarify and understand the mechanisms behind the chemically-mediated phenotypic alterations, studies presented in Chapter 5 attempt to identify chemical-specific gene targets which may be involved in the altered phenotypes observed in NHEK and are discussed in the next section.

The studies and results described in this section and in Chapter 4 provide a solid base and starting point for the possibility of future experimentation. For future research, more detailed studies would greatly aid in creating a more complete picture of chemically-mediated phenotypic changes in NHEK. It is highly important to conduct various time-course studies when examining chemical effects on NHEK differentiation. Quantifying cross-linked envelope (CLE) formation after chemical exposure on various days and at various chemical concentrations are required to investigate how BaP and arsenic might alter differentiation in a time- and dose-dependent manner. Since CLE quantification may be difficult in sub-confluent cultures, the possibility exists to examine the expression of cytokeratin markers in a time- and dose-dependent approach. Such experiments could provide information on the degree of differentiation as well as the rate at which differentiation occurs and how chemicals may alter these properties. In addition, studies could be conducted to examine chemically-altered differentiation at various passages which could provide information of how the differentiation process changes as

cells age. Furthermore, it would be interesting to examine the effectiveness of BaP and arsenic to inhibit differentiation when cells are exposed during an initial passage and then analyze chemically-induced effects again in a later passage.

The development of the S-35 radioactive isotope protocol to more accurately quantitate CLE formation could be an invaluable asset in future studies. I spent several months attempting to develop a variation of this previously published method with little success (Berkers *et al.* 1995; King *et al.* 1986). The radioactive isotope [^{35}S] methionine was intended to label detergent-insoluble proteins such as CLE. While attempting to quantify radiolabeled CLE using a scintillation counter, I also manually counted CLE under the microscope using a hemocytometer. When comparing the results from both methods the data never correlated well. The results from the S-35 assay appeared to produce non-specific labeling. The amount of S-35 labeling that was quantitated by the scintillation counter rarely coupled well with visual CLE numbers counted under a light microscope. If the S-35 labeled CLE method could be developed, it would save a substantial amount of time of tedious lab work and, in addition, could provide a more sensitive method to quantify the terminal differentiation of cultured NHEK.

Supplemental studies investigating chemically-altered growth properties, cell cycle distribution, and division rates could also be performed. In conjuncture with the purposed differentiation experiments mentioned above, detailed time- and dose-dependent studies of NHEK growth properties could provide interesting information and could be closely correlated with chemical-mediated effects on differentiation. Also, studies which examine chemically-induced alterations in NHEK growth at various confluence levels, cell passages, and/or in chemical mixtures could also be highly

informative. In light of previous research, it could be interesting to investigate how low arsenic concentrations effect NHEK growth, since previously published work displayed arsenic's ability to increase cell proliferation at non-cytotoxic to slightly toxic concentrations (Chen *et al.* 2000; Liao *et al.* 2004; Styblo *et al.* 2002; Vega *et al.* 2001). The construction of a mathematical model that describes the cell cycle kinetics and differentiation before conducting experiments would be extremely informative in terms of the types of experiments to be performed to gather all necessary data for the model. This issue will be addressed in a subsequent section dealing with the NHEK mathematical model. Many of the future experiment discussed above for examining differentiation could also apply when investigating chemically-mediated perturbations in NHEK growth properties.

A mixture experiment with both BaP and arsenic should also be considered since both chemicals are known to co-exist in the environment at hazardous waste sites (ATSDR 1999a, b, 2003a, b; Maier *et al.* 2002). It would be interesting to see whether mixture effects on NHEK differentiation and growth would be synergistic, antagonistic, or non-interactive. Also, since BaP is an excellent initiating agent and arsenic is a known co-carcinogen/progressing agent, it would be interesting to examine how BaP initiated cells react to succeeding arsenic exposure(s). This sequence of chemical exposure could produce phenotypic and genotypic alterations that could be extremely interesting. Although a very rare event in human cells, the sequential exposure to an initiator (BaP) and then to a co-carcinogen (arsenic) could potentially give rise to an immortalized/transformed clone.

7.2.3. Gene Expression Changes Associated with Chemically-Altered Growth and Differentiation

To identify molecular alterations that may be involved in chemically-induced phenotypic alterations previously discussed, microarray and real-time RT-PCR analysis was carried out on NHEK treated with equitoxic concentrations of BaP or arsenic. Results of the microarray experiments are as follows: 1) in total, 86 genes were induced and 17 genes were suppressed $\geq$2-fold by 2.0 μM BaP. 2) Arsenic (5.0 μM) induced 107 and suppressed 15 genes. Highly quantitative real-time PCR was subsequently used to confirm microarray findings on selected genes involved in keratinocyte growth and differentiation pathways. These studies confirmed induction in NHEK by BaP of α-integrin binding protein 63 (α-integrin-bp) (2.48-fold), retinoic acid- and interferon-inducible protein (RA-IFN) (2.74-fold), interleukin-1α (IL-1α) (2.64-fold), interleukin-1β (IL-1β) (2.84-fold) and Ras guanyl releasing protein 1 (Ras-GRP) (3.14-fold). Real-time PCR confirmed that arsenic induced the following genes: retinoblastoma 1 (Rb-1) (5.4-fold), retinoblastoma-binding protein 1 (Rb-bp1) (6.8-fold), transforming growth factor β-stimulated protein (TSC-22) (6.84-fold), MAX binding protein (MNT) (2.44-fold), and RAD50 (4.24-fold). Mechanistic studies with a subset of genes may allow one to correlate alterations in these molecular markers with chemical-specific blocks to differentiation in NHEK.

These results demonstrate that exposure to each chemical induced highly specific gene expression patterns in NHEK, implying that these chemicals target different steps in the pathways to growth and differentiation. The gene expression results also provide mechanistic clues towards understanding the chemically-mediated phenotypic changes

demonstrated in Chapter 4. BaP, which in previous studies increased NHEK proliferation while inhibiting differentiation, significantly altered the expression of genes involved in cell growth, RNA synthesis and/or processing, cell structure and adhesion, transcription regulation, cell cycle regulation, as well as inducing potential differentiation regulators (See Chapter 5 for details). Arsenic, which substantially inhibited differentiation and decreased proliferation rates in NHEK, altered the expression of cell cycle regulators, apoptotic genes, transcriptional repressors, tumor suppressors, an oncogene, DNA repair genes, regulators of growth and differentiation, cell structure and adhesion genes, and genes involved in chromatin structure and function (See Chapter 5 for details). Specifically, it is interesting to note that three *ras* genes and two *Rb* (retinoblastoma) genes were induced by BaP and arsenic respectively in NHEK. As presented in Chapter 2, both the *ras* oncogene and tumor suppressor *Rb*, when altered, play vital roles in skin carcinogenesis. In particular, the observed BaP-induced *ras* genes may provide evidence of NHEK initiation due to BaP exposure since mutated *ras* has been often observed in initiated cells as discussed in section 2.3.2 of Chapter 2.

Gene expression alterations induced by carcinogen exposure can be associated with influential consequences on signaling pathways involved in the regulation of cellular differentiation and cell cycle checkpoints. First, the overexpression of α-integrin-bp and IL-1α/β correlates with inhibited differentiation and increased cell proliferation, respectively, which are observed subsequent BaP exposure. The onset of keratinocyte differentiation can be triggered by detachment from the substratum together with loss of integrin expression (Figure 7.1). As discussed in Chapter 2 and 5, integrin gene expression levels are induced in non-differentiating keratinocytes. Therefore, α-integrin-

bp may be involved in the BaP-mediated inhibition of differentiation demonstrated in Chapter 4. Additionally, IL-1 signal transduction pathways in keratinocytes (Figure 7.2) interacts with TNFα receptor associated factor (TRAF)-6, which causes activation of protein kinases, TRAF associated kinase (TAK), IL-1 receptor associated factor (IRAK), and MKK1 (Freedberg *et al.* 2001). This results in activation of transcription factors, such as NFκB, C/EBPβ, ATF2, and AP-1 (Freedberg *et al.* 2001). Therefore, IL-1α and β induction may be playing a role in the increased growth rates observed following BaP treatment. Secondly, the induction of three *ras* genes by BaP may consequently affect pathways that drive cells to tranverse through the G1/S checkpoint (Figure 7.3). As discussed in Chapter 2, mutations in *ras* are common in initiated keratinocytes. Ras activation can initiate a signaling cascade that stimulates Myc via the Raf pathway. Myc can then activate cyclin D-cyclin dependent kinase (cdk) 4/6 complex directly or indirectly via Cdc25A phosphatase (Sears and Nevins 2002). Cyclin D-cdk 4/6 complex activation, along with cdk2, can lead to the hypophosphorylation of RB and dissociation of the RB-repressor complex. This dissociation allows for the accumulation of E2F which activate the transcription of numerous genes necessary for DNA replication as well as further cell cycle progression. In addition, Yaf2 expression was also altered in BaP treated NHEK. Yaf2 interacts with YY-1, which is only expressed in undifferentiated keratinocytes and also regulates Myc-mediated transactivation. It is not entirely clear the role of Yaf2 in keratinocytes, but it seems to be involved in regulating two genes (YY-1 and Myc) which can have influential effects on cellular differentiation and growth. All together, the induced genes mentioned above support the phenotypic alterations (inhibition of differentiation and increased proliferation rates) mediated by BaP

treatment. Therefore, phenotypic and gene changes produced by BaP indicate it is an initiator in NHEK.

Conversely, as discussed in Chapter 5, arsenic caused the overexpression of MNT, TSC-22, Rb-1, and Rb-bp1 which is indicative of G1 arrest (Figure 7.3). MNT interacts with Max to bind Myc-Max recognition sites which acts as a transcriptional repressor of growth. If Myc activation is suppressed by MNT, the cyclin D-cdk 4/6 complex may not be able phosphorylate RB. Moreover, TSC-22 is stimulated by TGFβ and is associated with Cdc25A (a phosphatase that activates the cyclin D-cdk 4/6 complex) inhibition. This event also indicates that the inactive cyclin D-cdk 4/6 complex is unable to phosphorylate RB. In addition, Rb-1 and Rb-bp1 expression levels were also induced by arsenic exposure. All together, these gene alterations indicate that RB will continue to bind to E2F, thus, preventing S-phase entry by causing cells to arrest in G1. Alterations in these genes support flow cytometry results from Chapter 4. DNA histograms show very few cells entering into S-phase, which is indicative of a G1 block most likely produced by MNT, TSC-22, Rb-1, and Rb-bp1. In addition, the G2/M phases in NHEK are also altered by arsenic exposure. The overexpression of a DNA repair gene, RAD50, is indicative of DNA damage produced during arsenic exposure. The G2/M DNA damage checkpoint prevents the cell from entering mitosis if the genome is damaged. DNA histograms presented in Chapter 4 display a substantial G2/M block, further supporting that DNA damage has occurred. From this evidence, it is apparent that arsenic induced DNA damage that caused both a G1 and G2/M block.

When comparing altered genes between the BaP and arsenic exposed cells, very few commonly affected genes were found. These results may imply that BaP and arsenic

target different steps in the pathways to growth and differentiation in NHEK. Theories concerning the alteration of individual genes and how these changes could be linked to altered growth and differentiation are discussed in Chapter 5.

At this stage one can only postulate that many of the gene expression changes are associated with phenotypic alterations in chemically exposed NHEK. With the present data, it is difficult to strongly link gene expression levels to phenotypic change. Thus, additional biochemical studies should be performed to demonstrate functional linkage between chemically-altered genotypes and changes in cell phenotypes. Examining genes which are mechanistically known to play a major role in differentiation or cell growth could be a starting point. Specifically, genes which could potentially induce a cell cycle block or inhibit differentiation could provide a better picture of the mechanisms involved in the altered growth/differentiation properties of NHEK. Also, investigating genes within a specific signaling pathway could provide information of the level at which chemicals are causing their effects. For example, in arsenic treated NHEK, MNT gene expression was induced but was this gene directly targeted by arsenic or did arsenic alter signals upstream from MNT that indirectly altered its expression? Also, how does alteration of MNT affect the genes it specifically interacts with and does gene expression alteration translate into protein changes? Clearly, it is also extremely important to examine any modification in the translated protein products of altered genes. Without this protein analysis it is impossible to clearly link a genotypic change to a phenotypic change. Therefore, future studies need to closely examine specific gene signaling pathways, as well as address protein modification to obtain a better mechanistic understanding. In addition, it would also be extremely informative to conduct time- and

dose-dependent gene expression experiments to display which concentration levels are affecting the expression of target genes and translated proteins. Time course studies would allow one to characterize a continuum of gene expression changes that may influence one another in a time-dependent manner. Molecular markers identified in these types of studies can potentially be incorporated into biologically-based pharmacodynamic models of the cancer process, adding predictive value in assessment of the carcinogenic potential of new and novel chemicals.

7.2.4. Mathematical Model of NHEK Cell Cycle Kinetics and Differentiation

I have successfully constructed two non-stathmokinetic mathematical models that describe the cell cycle kinetics and differentiation process in NHEK. Since the development of these computational models, several parameters have been discovered that are not obtainable from previous flow cytometric experiments (Chapter 4). Unfortunately, the NHEK differentiation model scheme was envisioned and developed after flow cytometry experiments were conducted. Otherwise, experiments would have been designed to gather necessary information to calculate required parameters in order to attempt to model NHEK as accurately as possible. Experiments conceived but not completed that would have added to the accuracy of the model are discussed later in this section. Nevertheless, several uncertain parameters were obtained from the literature in order to complete the models. Thus, simulations were produced from combining Chapter 4 results and data presented in the literature for Model A, and Model B was exclusively constructed based on information acquired from the literature.

The initial purpose of creating a mathematical model of NHEK was to improve our understanding of the differentiation process in keratinocytes and help predict chemically-induced cell kinetic changes due to carcinogen exposure. Developing models such as these force researchers to conceptualize all the factors which could play roles in regulating cellular processes involved in cell proliferation and differentiation. In studies presented in Chapter 6, by creating a homeostatic model (Model A) describing control NHEK, from optimizing growth fraction and differentiation parameters, I was able to easily switch control data with chemical treatment data and observe any chemical induced changes in the model simulations. It was interesting to see how data from chemically-exposed NHEK would drastically alter computer simulations; thus, correlating well with experimental results presented in Chapter 4. Model A, although a very simple model, presents a reasonable description of primary keratinocytes in culture and can be used to assess general changes in both the proliferative and differentiating compartments. In contrast, Model B is much more precise in regards to describing the compartments within the proliferating cell population. With all the necessary parameters in place and the capacity to accurately differentiate between stem and transit-amplifying (TA) cells in mixed populations, Model B has the potential to accurately illustrate NHEK growth kinetics and differentiation. Also, other biological effectors of these cellular processes, such as biochemical networks and other signaling events, could ultimately be incorporated into these models to more accurately portray the NHEK system. In due course, the purpose of creating this model is to aid in assessing and predicting chemical effects in the keratinocyte system without the use of extensive experimentation.

However, it is evident more information and possible model modifications are necessary in order for these mathematical models to have accurate predictive capabilities.

To obtain all required parameters for future studies, there are several experiments that are essential to perform. First, the determination of the NHEK growth fraction (GF), in stem and TA cell populations separately or together as a whole, would tremendously aid these modeling efforts since all subsequent calculations for transit times and rate constants are dependent upon T_C, which requires measurement of both GF and T_{pot} in order to be calculated. As stated in Chapter 2, GF measurement can be accomplished by labeling cells with Ki-67 (label only proliferating cells) and compare this number to the total number of cells in the population. Although these results would provide an accurate GF parameter for the cell population as a whole, it would not address individual GF values for both stem and transit-amplifying cell populations. To address this issue, GF can be calculated from directly measured T_{pot} and T_C values within each separate proliferative cell population. T_{pot} can be measured using BrdU procedures, as mentioned in Chapter 4, and T_C can be measured from percent labeled mitosis (PLM) curves as described previously (Aarnaes *et al.* 1993; Heenen *et al.* 1992; Loeffler *et al.* 1987). By obtaining both T_{pot} and T_C for each proliferative population, GF can be derived using Equations 6-20 and then by 6-3 from Chapter 6. Second, more time points would give us more data points to aid in model validation and provide more kinetic information. Initially, the objective was to calculate T_{pot} two and four hours after pulse-labeling with BrdU to examine proliferation changes due to chemical exposure. However, three time points, as measured in Chapter 4, is insufficient when comparing model simulations to experimental data. Thus, additional time points are necessary to acquire sufficient data in

order to perform model validations. Third, stathmokinetic experiments using a mitotic blocker would have made data analysis much simpler, in that, cell cycle kinetics could be measured without having to account for the production of new daughter cells produced from G2+M and entering into G1+G0. Fourth, death rate parameters in NHEK are another uncertain parameter. Death rate measurements could be conducted by staining cells with propidium iodide and subsequent flow cytometric analysis since this dye is taken up only by dead cells through damaged membranes and is excluded by live cells. This may be an important parameter to obtain since chemically-treated cells usually induce cell death via apoptotic pathways, thus, potentially impacting the kinetics of the model system. Fifth, as mentioned above, time course data examining CLE formation, both in control and chemically-treated NHEK, would provide information on the rate of terminal differentiation that could be used in the NHEK model. Sixth, performing experiments during varying cell ages or confluence levels would give us information of how these issues affect certain kinetic parameters over time. Finally, separating stem cells from transit-amplifying cells is another issue to manage. Sorting these two cell populations in keratinocytes can be done by analyzing RNA content levels or by using markers such as β_1 integrins as mentioned in Chapter 2. Conducting all of the experiments mention above would provide all the necessary data to calculate required parameters to develop a mathematical model that could accurately describe the cell kinetics and differentiation of cultured keratinocytes.

7.3. Final Comments

The research presented herein has provided data on: (1) the cytotoxicity of four petroleum derived hydrocarbons, (2) BaP- and arsenic-induced changes in cell

differentiation and growth, (3) chemically-induced gene expression alterations, and (4) mathematical models that describe the cell cycle kinetics and differentiation process in NHEK. It is clear that both BaP and arsenic produced phenotypic and genotypic changes in NHEK. These results are expected since both chemicals are human skin carcinogens. This research is unique in that it compares the effects produced by a polycyclic aromatic hydrocarbon and an inorganic metal in primary keratinocytes. Furthermore, it examines the general mechanistic effects that each carcinogen elicits in this cell system. The data gathered here will aid in the process of determining the cellular alterations created by both arsenic and BaP on differentiation and proliferation in a primary keratinocyte system. The chemically-induced effects produced in NHEK will aid in the understanding of how these chemicals effect a normal cell system, since a majority of *in vitro* research tends to focus on chemical effects in immortalized and transformed cells lines. Overall, a clearer understanding of cellular growth and differentiation, both from a normal standpoint and from alterations induced by chemical exposure, will greatly aid the risk assessment process for environmental contaminants. The results and data presented herein could potentially be used to assess the risk of skin exposure to both BaP and arsenic.

7.4. References

Aarnaes, E., Clausen, O. P., Kirkhus, B., and De Angelis, P. (1993). Heterogeneity in the mouse epidermal cell cycle analysed by computer simulations. *Cell Prolif.* **26**, 205-219.

ATSDR (1999a). Toxicological profile for arsenic. *Agency for Toxic Substance and Disease Registry* **Atlanta**.

ATSDR (1999b). Toxicological profile for polycyclic aromatic hydrocarbons (PAHs). *Agency for Toxic Substance and Disease Registry* **Atlanta**.

ATSDR (2003a). Toxicological profile for arsenic. *Agency for Toxic Substance and Disease Registry* **Atlanta**.

ATSDR (2003b). Toxicological profile for polycyclic aromatic hydrocarbons (PAHs). *Agency for Toxic Substance and Disease Registry* **Atlanta**.

Berkers, J. A. M., Hassing, I., Spenkelink, B., Brouwer, A., and Blaauboer, B. J. (1995). Interactive Effects of 2,3,7,8-tetrachlorodibenzo-*p*-dioxin and Retinoids on Proliferation and Differentiation in Cultured Human Keratinocytes: Quantification of Cross-Linked Envelope Formation. *Arch Toxicol* **69**, 368-378.

Chen, N. Y., Ma, W. Y., Yang, C. S., and Dong, Z. (2000). Inhibition of arsenite-induced apoptosis and AP-1 activity by epigallocatechin-3-gallate and theaflavins. *J.Environ.Pathol.Toxicol.Oncol.* **19**, 287-295.

Freedberg, I. M., Tomic-Canic, M., Komine, M., and Blumenberg, M. (2001). Keratins and the keratinocyte activation cycle. [Review] [180 refs]. *Journal of Investigative Dermatology* **116**, 633-640.

Heenen, M., De Graef, C., and Galand, P. (1992). Kinetics of the calcium induced stratification of human keratinocytes in vitro. *Cell Prolif.* **25**, 233-240.

Jha, A. N., Noditi, M., Nilsson, R., and Natarajan, A. T. (1992). Genotoxic effects of sodium arsenite on human cells. *Mutation Research* **284**, 215-221.

King, I., Mella, S. L., and Sartorelli, A. C. (1986). A sensitive method to quantify the terminal differentiation of cultured epidermal cells. *Exp Cell Res* **167**, 252-256.

Lee, T. C., Tanaka, N., Lamb, P. W., Gilmer, T. M., and Barrett, J. C. (1988). Induction of gene amplification by arsenic. *Science* **241**, 79-81.

Liao, W. T., Chang, K. L., Yu, C. L., Chen, G. S., Chang, L. W., and Yu, H. S. (2004). Arsenic induces human keratinocyte apoptosis by the FAS/FAS ligand pathway, which correlates with alterations in nuclear factor-kappa B and activator protein-1 activity. *J.Invest Dermatol.* **122**, 125-129.

Loeffler, M., Potten, C. S., and Wichmann, H. E. (1987). Epidermal Cell Proliferation: A Comprehensive Mathematical Model of Cell Proliferation and Migration in the Basal Layer predicts some Unusual Properties of Epidermal Stem Cells. *Virchows Arch B* **53**, 286-300.

Maier, A., Schumann, B. L., Chang, X., Talaska, G., and Puga, A. (2002). Arsenic co-exposure potentiates benzo[a]pyrene genotoxicity. *Mutat.Res.* **517**, 101-111.

Mei, N., Lee, J., Sun, X., Xing, J. Z., Hanson, J., Le, X. C., and Weinfeld, M. (2003). Genetic predisposition to the cytotoxicity of arsenic: the role of DNA damage and ATM. *FASEB J.* **17**, 2310-2312.

Mure, K., Uddin, A. N., Lopez, L. C., Styblo, M., and Rossman, T. G. (2003). Arsenite induces delayed mutagenesis and transformation in human osteosarcoma cells at extremely low concentrations. *Environ.Mol.Mutagen.* **41**, 322-331.

Rossman, T. G. (1981). Enhancement of UV-mutagenesis by low concentrations of arsenite in E. coli. *Mutat.Res.* **91**, 207-211.

Rossman, T. G., Stone, D., Molina, M., and Troll, W. (1980). Absence of arsenite mutagenicity in E coli and Chinese hamster cells. *Environ.Mutagen.* **2**, 371-379.

Rossman, T. G., Uddin, A. N., Burns, F. J., and Bosland, M. C. (2001). Arsenite is a cocarcinogen with solar ultraviolet radiation for mouse skin: an animal model for arsenic carcinogenesis. *Toxicol.Appl.Pharmacol.* **176**, 64-71.

Rudel, R., Slayton, T. M., and Beck, B. D. (1996). Implications of arsenic genotoxicity for dose response of carcinogenic effects. [Review] [55 refs]. *Regulatory Toxicology & Pharmacology* **23**, 87-105.

Sears, R. C., and Nevins, J. R. (2002). Signaling networks that link cell proliferation and cell fate. *J Biol Chem* **277**, 11617-11620.

Shi, H., Hudson, L. G., Ding, W., Wang, S., Cooper, K. L., Liu, S., Chen, Y., Shi, X., and Liu, K. J. (2004). Arsenite causes DNA damage in keratinocytes via generation of hydroxyl radicals. *Chem.Res.Toxicol.* **17**, 871-878.

Styblo, M., Drobna, Z., Jaspers, I., Lin, S., and Thomas, D. J. (2002). The role of biomethylation in toxicity and carcinogenicity of arsenic: a research update. *Environ.Health Perspect.* **110 Suppl 5**, 767-771.

Vega, L., Styblo, M., Patterson, R., Cullen, W., Wang, C., and Germolec, D. (2001). Differential effects of trivalent and pentavalent arsenicals on cell proliferation and cytokine secretion in normal human epidermal keratinocytes. *Toxicology & Applied Pharmacology* **172**, 225-232.

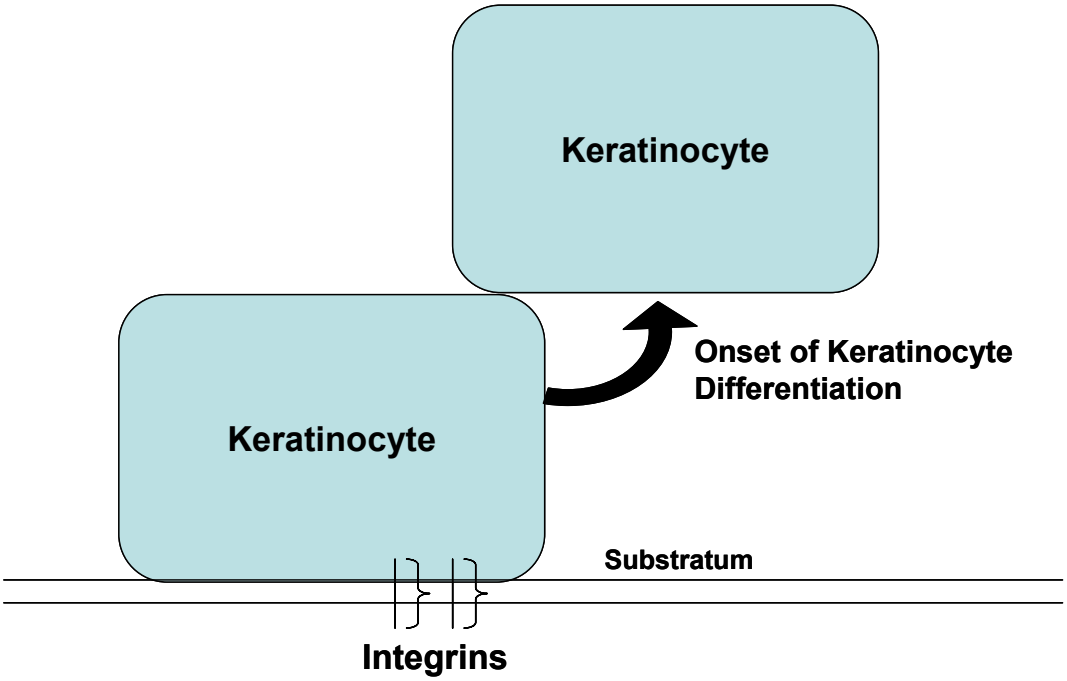

***Figure 7.1*. Integrin expression plays an essential role in controlling the switch between keratinocyte growth and differentiation.** The onset of differentiation can be triggered by the detachment of a keratinocyte from the substratum together with the loss of integrin expression. This mechanism is not exclusive but is involved in the establishment of the differentiated phenotype.

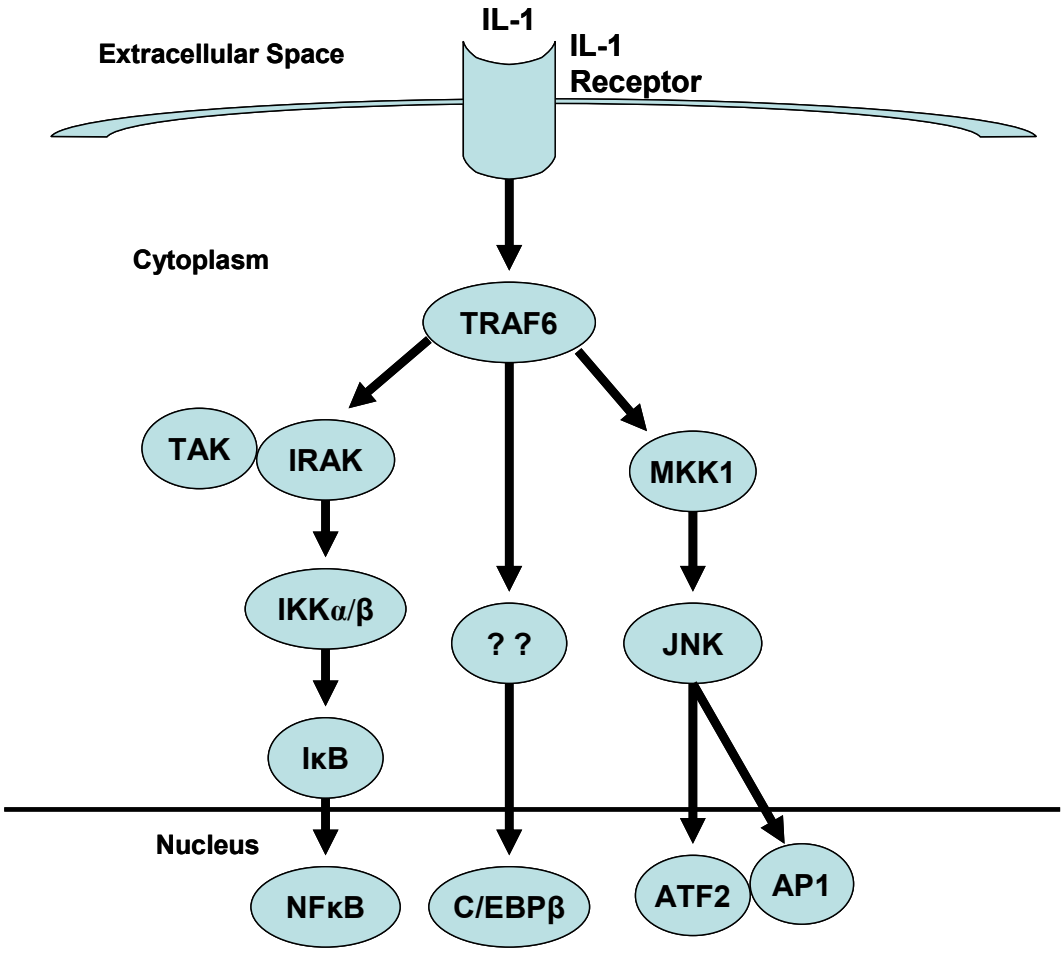

Figure 7.2. **The IL-1 signal transduction pathways in keratinocytes.** The receptor interacts with TRAF6, which causes activation of protein kinases TAK, IRAK, and MKK1. This results in activation of transcription factors, such as NFκB, C/EBPβ, ATF2, and AP-1.

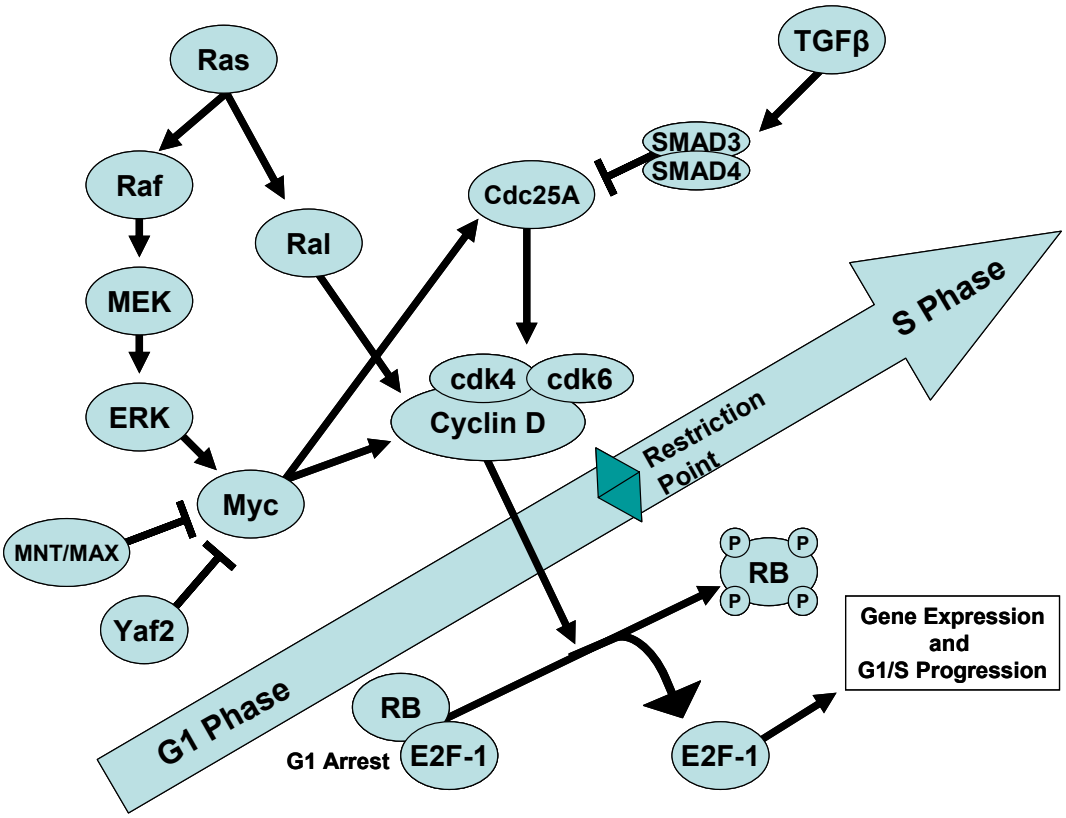

Figure 7.3. **G1/S checkpoint regulation.** Mitogen stimulation or oncogenic activation (due to point mutations that maintain Ras in the GTP-bound form) of Ras can (1) commence the Raf/MEK/ERK kinase cascade, primarily involved in plasma membrane to nucleus signaling and/or (2) initiate the Ral GTPase signaling pathway. Both pathways lead to cyclin D-cyclin dependent kinase (cdk) 4/6 complex activation. More specifically, Raf/MEK/ERK kinase cascade can induce Myc which activates the cyclin D-cdk 4/6 complex directly or indirectly via Cdc25A (a phosphatase that activates the cell cycle kinases). Cyclin D-cdk 4/6 complex activation, along with cdk2 (not shown) can lead to the hypophosphorylation of RB and dissociation of the RB-repressor complex. This dissociation allows the accumulation of E2F which activate the transcription of a large number of genes necessary for DNA replication as well as further cell cycle progression. The MNT/MAX complex and Yaf2 can block or regulate Myc activity, respectively, and both are involved in G1cell arrest. TGFβ inhibits the transcription of Cdc25A, also causing cells to arrest in G1.